UTS UNIVERSITY OF TECHNOLOGY SYDNEY

MODIFICATION OF MEMBRANES FOR TREATMENT OF CHALLENGING WATER AND NUTRIENT RECOVERY USING MEMBRANE DISTILLATION

by Morteza Afsari

Thesis submitted in fulfilment of the requirements for the degree of

Doctor of Philosophy

under the supervision of A/Prof. Leonard Tijing, and Prof. Hokyong Shon

University of Technology Sydney
Faculty of Engineering and Information Technology

January 2024

Certificate of Original Authorship

I, Morteza Afsari, declare that this thesis is submitted in fulfilment of the requirements for the award of Doctor of Philosophy, in the School of Civil and Environmental Engineering, Faculty of Engineering and Information Technology at the University of Technology Sydney. This thesis is wholly my own work unless otherwise referenced or acknowledged. In addition, I certify that all information sources and literature used are indicated in the thesis. This document has not been submitted for qualifications at any other academic institution. This research is supported by the Australian Government Research Training Program.

Signature:

Production Note:
Signature removed prior to publication.

Date:

2 January 2024

Acknowledgements

I would like to begin by expressing my deepest gratitude to my principal supervisor, Associate Professor Leonard Tijing. His unwavering support, guidance, and encouragement throughout my Ph.D. journey have been invaluable. I am truly thankful to him for providing me with this remarkable opportunity to undertake and complete this project and for imparting me with valuable insights every step of the way.

I am also indebted to my co-supervisor, Prof. Hokyong Shon, for his consistent support, invaluable guidance, and responsiveness to my research inquiries. His advice has been instrumental in shaping the course of my doctoral study, and I recognize that this journey would not have been the same without his wise supervision.

My heartfelt appreciation goes to the University of Technology Sydney (UTS) for awarding me the International Research Scholarship and the UTS President's Scholarship. These generous scholarships have enabled me to pursue my research. I am also grateful to the officials of the Environmental Engineering labs and school at UTS for their support, which has been instrumental in facilitating my research progress.

I want to convey my boundless love, immense gratitude, and profound thanks to my family. To my wife and daughter, Narges and Aida, without them, I would have made this stage sooner and better. Your love and encouragement have been my driving force, and for that, I am eternally grateful.

Arash, you have been not only my best friend but also an unwavering source of support throughout this challenging academic endeavour. Your friendship has been a constant source of inspiration.

Research Publications

Publications Related To Thesis:

- **M Afsari**, J Jiang, S Phuntsho, HK Shon, LD Tijing, Ammonia recovery from source-separated hydrolyzed urine via a dual-membrane distillation in-series process, Chemical Engineering Journal, 144215, **2023**
- **M Afsari**, MJ Park, NJ Kaleekkal, MM Motsa, HK Shon, L Tijing, Janus Distillation Membrane via Mussel-Inspired Inkjet Printing Modification for Anti-Oil Fouling Membrane Distillation, Membranes 13 (2), 191, **2023**
- **M Afsari**, Q Li, E Karbassiyazdi, HK Shon, A Razmjou, LD Tijing, Electrospun nanofiber composite membranes for geothermal brine treatment with lithium enrichment via membrane distillation, Chemosphere, 137902, **2023**
- **M Afsari**, HK Shon, LD Tijing, Characterization of nanofibers and nanofiber membranes, Elsevier, Electrospun and Nanofibrous Membranes, 295-322, **2023**
- **M Afsari**, AH Ghorbani, M Asghari, HK Shon, LD Tijing, Computational fluid dynamics simulation study of hypersaline water desalination via membrane distillation: Effect of membrane characteristics and operational parameters, Chemosphere 305, **2022**
- **M Afsari**, HK Shon, LD Tijing, Nanocomposite membranes for wastewater treatment via membrane distillation, Nano-Enabled Technologies for Water Remediation, **2022**
- **M Afsari**, HK Shon, LD Tijing, Janus membranes for membrane distillation: Recent advances and challenges, Advances in Colloid and Interface Science 289, **2022**
- M Toriello, **M Afsari**, HK Shon, LD Tijing, Progress on the Fabrication and Application of Electrospun Nanofiber Composites, Membranes 10 (9), 204, **2020**

Other Publications

- I Salahshoori, M Asghari, MN Jorabchi, S Wohlrab, M Rabiei, **M Afsari**, Methylene diisocyanate-aided tailoring of nanotitania for dispersion engineering through

polyurethane mixed matrix membranes: Experimental investigations, Arabian Journal of Chemistry 16 (6), 104792, **2023**

- HT Kim, **M Afsari**, NPB Tan, HK Shon, LD Tijing, Recent Progress on Passive, Thermally Localized Solar-Driven Multistage Water Evaporation, Membranes 13 (5), 460, **2023**
- Y Orooji, Z Nezafat, M Nasrollahzadeh, N Shafiei, **M Afsari**, K Pakzad, Recent advances in nanomaterial development for lithium ion-sieving technologies, Desalination 529, **2022**
- A Hosseinzadeh, JL Zhou, X Li, **M Afsari**, A Altaee, Techno-economic and environmental impact assessment of hydrogen production processes using bio-waste as renewable energy resource, Renewable and Sustainable Energy Reviews 156, 111991, **2022**
- M Asghari, S Saadatmandi, **M Afsari**, Graphene Oxide and its Derivatives for Gas Separation Membranes, ChemBioEng Reviews 8 (5), 490-516, **2021**
- I Ibrahim, V Bhoopal, DH Seo, **M Afsari**, HK Shon, LD Tijing, Biomass-based photothermal materials for interfacial solar steam generation: A review, Materials Today Energy 21, 100716, **2021**

List of Abbreviations

ALD	Atomic Laser Deposition
CNT	Carbon Nanotubes
DMF	N,N-dimethylformamide
DTAB	Dodecyl Trimethyl Ammonium Bromide
ENFM	Electrospun Nanofiber Membrane
FAS	(Heptadecafluoro-Tetradecyl) Trimethoxysilane
HLB	Hydrophilic–Lipophilic Balance
LEP	Liquid Entrance Pressure
LiCl	Lithium Chloride
MD	Membrane Distillation
NIPS	Nonsolvent Induced Phase Inversion
NP	Nanoparticle
OCA	Oil contact angle
PAN	polyacrilonitrile
PcH	Polyvinylidene fluoride-co-hexafluoropropylene)
PDA	Polydopamine
PDMS	Polydimethylsiloxane
PEG	Polyethylene Glycol
PEI	Polyethylenimine
PES	Polyethersulfone
PET	Polyethylene Terephthalate
PI	Polyimide
PP	Polypropylene
PS	Polystyrene
PTFE	Polytetrafluoroethylene
PVA	Polyvinyl Alcohol
PVDF	Polyvinylidene Difluoride
PVP-VTES	Polyvinylpyrrolidone triethoxyvinylsilane
SMM	Surface Modified Macromolecules
TGA	Thermogravimetric Analysis
TIPS	Temperature Induced Phase Inversion
WCA	Water Contact Angle

Table of Contents

List of Figures

List of Tables

Abstract

There has been a search for alternate methods for treating challenging water and wastewater. Membrane distillation (MD), which uses low-grade thermal energy to treat complex wastewater, has become more popular. In order to produce high-quality water, an MD membrane functions as a hydrophobic barrier that only permits water vapour to flow through. However, there are problems with existing membranes that MD must deal with, such as poor flux and wetting problems. MD's effectiveness is also hampered by contamination from elements such as oil droplets. By overcoming current obstacles, MD technology can significantly contribute to tackling freshwater production-related environmental issues and water scarcity in a variety of businesses. The Janus membrane, which has a hydrophilic/superhydrophobic or hydrophilic/omniphobic structure, is a viable solution. This design improves flux while lowering wetting and fouling tendencies, which improves MD's performance. In this research, the potential of MD as a hybrid separation technology to handle difficult water is examined. By modifying the membrane's physical and chemical properties, the study thoroughly analyses various fabrication and modification techniques for Janus membranes and assesses their effectiveness in desalination and wastewater treatment using MD.

The first research phase focuses on simulation-based optimisation of membrane characteristics for various feedwater conditions. The desalination of extremely saline liquids is made possible by the development of a novel triple-layer nanofibrous membrane. The next step involves combining inkjet printing techniques with catalytic reactions to improve membrane characteristics like resistance to fouling agents. The improved membranes are used to recover nutrients from landfill leachate and human

urine. The commercial membrane surfaces are modified using the layer-by-layer procedure by coating them with a thin layer of polymeric solutions while maintaining the membrane's overall hydrophobicity. Its flow can also be increased using suitable materials and lowering the membrane's heat conductivity. In treating severely polluted wastewater, such as human urine, landfill leachate, or oil field brine, the Janus membrane also protects against fouling chemicals. Further, a novel dual in-series MD configuration is suggested for effective ammonia extraction from human urine, adding to sustainable nutrient recovery methods. Overall, this research significantly improves resource use and MD-based separation approaches.

Chapter 1
Introduction

1.1 Background

Global water scarcity, driven by rapid urbanisation, population growth and climate change, is a critical issue nowadays and is expected to get worse in the next decade. As a result, alternative sources of fresh water, such as seawater and wastewater, are being sought. A huge amount of energy is spent on the production of fresh water. For example, the US government spends about 2% of their total used energy for the treatment and production of drinking water, which corresponds to about 40% of the total consumed energy in a metropolitan city [1-3]. The high production cost, besides the shortage of fresh water resources, convinced many countries to put high value on the research for contemporary and unconventional methods to decrease the cost and environmental problems of freshwater production [4-6].

The vast amounts of seawater available make desalination a viable option for freshwater extraction. However, the two most common desalination methods (i.e., thermal desalination and high pressure-driven RO) are still energy intensive. In addition, though state-of-the-art RO is widely used in many countries, it still has limitations in treating high-salinity brine. In recent years, the membrane distillation (MD) process has driven increased interest due to its ability to treat hypersaline solutions and even challenging wastewaters. MD is a thermal-based membrane separation system that benefits from low-grade thermal energy and is a brilliant candidate to treat a wide range of wastewater from common brackish and seawater to hypersaline RO retentate, shale-gas or coal-seam gas-produced water and highly polluted wastewaters [7, 8]. In this process, the membrane acts as a porous hydrophobic barrier with submicron-size pores, allowing only water vapour to pass through the membrane pores. The temperature

difference between the two sides of the membrane leads to a vapour pressure difference that acts as the driving force of the process. Thus, in theory, MD can reject 100% of non-volatile components and produce high-quality water at the permeate side that meets the water quality standards even for pharmaceuticals and semiconductor industries [9, 10]. It is necessary that the MD membrane should have a balance of high porosity for high water vapour permeation along with adequate thickness and low heat conductivity to have high energy efficiency as a result of limited heat losses [4, 11, 12]. As MD is driven by vapour pressure difference, the flux and quality of permeate are less likely affected by the concentration polarisation effect at the feed side. MD can work at ambient pressure, making it less costly in its material components and can be made modular and space-saving. It also has a decreased propensity to fouling, a major problem in other high-pressure-driven water treatment systems like reverse osmosis (RO). If low-grade heat is available, such as waste heat or renewable energy, the MD system is highly cost-effective and has less carbon footprint, especially for small-scale plants [4, 13].

Despite the many advantages of MD, industrial application is still limited due to low flux and wetting issues of currently used membranes. The currently used distillation membranes are based on microfiltration membranes made of PVDF, PP, and PTFE that are not designed mainly for the MD process. Thus, they result in low flux due to low porosity, inadequate membrane structure, and wetting problems. Wetting happens when liquid water overcomes the entry pressure of the membrane pores, starting from the largest pore size, thus penetrating and reaching the permeate side. This lowers the rejection performance and impedes the quality of the permeate. For long-term

operation, wetting in MD should be avoided. Wetting is exacerbated when dealing with challenging wastewaters that contain inorganic salts, humic acid and low surface tension components such as surfactants, oils, etc., that can adsorb and attach to the membrane surface and pores, leading to wetting and pore blockage. These materials, which commonly enter into the wastewater via domestic wastewater or chemical materials in industrial or shale gas wastewater, usually have two different structure sides: one hydrophobic side that can adhere to the hydrophobic surface of the membrane and one hydrophilic side that is exposed to the feed solution. This structure can change the hydrophobicity of the membrane surface to hydrophilic, which allows the transfer of liquid water across the membrane and can decrease liquid entry pressure (LEP) and cause wetting problems for the membrane. The wetting mechanism reduces the salt rejection of the membrane by directly transferring the feed water to the permeate side [9, 11]. However, though MD works in low pressure-driven conditions and has lower fouling problems compared to other common types of membrane process, it still deals with special fouling by clogging the membrane pores via large-size pollutants, oil or grease, which can adhere to membrane surface due to its hydrophobic-hydrophobic or electrostatic interaction and block the membrane pores and decrease the available area for vapour transport and, as a result, decrease the flux of the membrane [14, 15].

A proposal for tailoring this drawback is the fabrication of omniphobic membranes, which can repel both water and low-surface tension agents. This structure shows excellent wetting resistance against surfactants and can limit the wetting of MD membranes. These characteristics can usually be obtained by designing a hierarchical structure followed by coating with a low surface energy layer (generally fluorinated

compounds) [16, 17]. Nevertheless, due to oil droplets or other fouling materials, the omniphobic membrane cannot effectively address fouling issues. These materials can continuously attach to the membrane surface and foul the membrane [18-20]. In general, the underwater oleophobic surface is in-air hydrophilic. In other words, hydrophilic membranes have good oil droplet and fouling resistivity but low resistivity against wetting agents like water or low surface tension materials. Therefore, the best promising candidate as an MD membrane is one that simultaneously has both characteristics of omniphobic and hydrophilic membranes and uses their capability of repulsion of wetting and fouling agents. This can be done by coating one side of a hydrophobic or omniphobic MD membrane surface via a hydrophilic layer [16, 21, 22]. The hydrophilic layer repels the oil droplets, fouling materials, and other hydrophobic compounds and prevents their adhesion on the surface and blocking of the pores of the MD membrane, and the underlying hydrophobic or omniphobic layer mitigates the wetting problem. This design can give high flux and high rejection MD membrane for long-term application and offers bright prospects for MD to effectively overcome current industrial challenges in wastewater treatment to treat hypersaline and contaminated wastewater [9, 17].

Many recent studies have tried increasing the hydrophobicity of the membranes by designing re-entrant structures on the membrane surface. The rough surfaces can trap the air in the membrane surface and increase the membrane's slippery angle, which results in higher hydrophobicity. Different methods like nanoparticle (NP) coating [18, 23], co-extrusion [24, 25], co-spinning, electrospraying [21], grafting [20], and phase inversion technique [22, 26] have been used to increase the roughness of the surface.

Various kinds of NPs like oxides of Si [18], Al [27], Ti [28] have been widely incorporated or spread on the membrane and caused an increase in the surface roughness of prepared membranes. Furthermore, to diminish the membrane's surface energy, low-surface energy coatings are applied on the hierarchical surface to increase its hydrophobicity. For this purpose, different types of fluorinated materials are being used [17, 19, 29], resulting in superhydrophobic membranes with good wetting resistivity. Although the developed structure of the superhydrophobic membranes improved the wetting resistivity of the membrane against low surface energy components, its oleophilic characteristics lowered the durability of the membranes, and fouling was still a drastic problem [14, 30, 31].

Inspired by nature, especially sea species like clamshell and sharkskin, many groups worked towards using underwater oleophobic surfaces, dramatically decreasing the fouling problems made by microorganisms or organic fouling for MD application. Within the realm of suggested techniques, the Janus membrane, which encompasses a multilayer structure featuring hydrophilic/superhydrophobic or hydrophilic/omniphobic properties, emerges as a particularly promising choice for membrane distillation (MD) systems. Its potential applications span a range of industries, including food processing, leather and fabric manufacturing, shale gas well drilling, and treatment of human urine, leachate, and domestic sewage [32, 33]. Janus membranes are reported to increase the flux performance while reducing the propensity for wetting and fouling [16, 34]. In order to improve the driving force in MD and consequently have high permeate flux, membranes with low mass and high heat resistance are favourable. However, the thickness of the membrane plays a contradictory role in mass and heat transfer; both

mass and heat transfer increase with lower separation layer thickness, leading to increased flux and heat loss. As a result, membrane thickness in MD should be tuned via a trade-off; high thickness increases mass transfer resistance, and low thickness increases heat loss from the feed. A way to adjust this factor is by changing the porosity of the membrane; water vapour passes through the pores, whereas the membrane matrix carries out most heat loss. Therefore, a higher porosity membrane with a lower percentage of matrix is more efficient for MD separation. However, the high porosity membrane has low mechanical stability.

The preferable membrane for the MD process is a porous and low-thickness membrane. However, this feature dramatically decreases the strength of the membrane, especially at vacuum membrane distillation (VMD) modules. As a result, to overcome this problem, the best-suggested method is the fabrication of a Janus membrane to increase the thickness of the membrane without incrementing hydrophobic thickness [44]. Janus membranes have a special configuration that has an additional hydrophilic layer that acts as an additional heat barrier and decreases the total heat transfer without sacrificing the mass transfer coefficient [1, 41].

1.2 Research aim and objectives

1.2.1 Overall aim

This study aims to design, develop, and investigate the modified performance of the Janus membrane for treating challenging water, including desalination of seawater containing fouling and wetting agents and nutrient recovery from human urine and leachate.

1.2.2 Specific objectives

The specific objectives of this project are as follows:

- Evaluate the effectiveness of nanofiber-based Janus membranes and optimise their design and performance in treating hypersaline solutions via membrane distillation.
- Explore the feasibility of using ink-jet printing in modifying flat-sheet membranes towards Janus design for overcoming wetting and fouling challenges in MD.
- Investigate and explore the heat-transfer and mass-transfer performance of modified Janus membrane for MD application.
- Assess the performance of Janus membranes in the MD process for recovery of nutrients from human urine and leachate.

1.3 Contribution to knowledge

In this study, a thorough examination was carried out to examine various Janus membrane production, modification, and novel design approaches. Finding the correlation between the membrane's physical properties under different operational circumstances was the initial goal of this investigation. The goal was to use Comsol Software to determine the best values for factors like thickness, porosity, and other membrane characteristics across a broad range of feed salt concentrations, from seawater to RO brine and hypersaline feedwater.

A novel triple-layer membrane with a nanofibrous structure was developed to increase energy efficiency while maintaining high permeate flux and rejection capabilities for desalinating highly saline solutions after a thorough analysis of the performance of the MD system when dealing with challenging water. Three separate layers make up the

membrane structure: an upper hydrophobic layer, a middle thermal insulation layer, and a lower hydrophilic layer.

However, the electrospinning procedure exposed some imperfections in the homogeneity and construction of integrated Janus membranes. Therefore, the capacity to produce an integrated, thin, and uniform layer for depositing a hydrophilic substance onto the surface of a hydrophobic membrane was utilised via inkjet printing. This method created a Janus membrane with exceptional oil fouling resistance. The effect of including a hydrophilic layer on either one side or both sides of the membrane was investigated, along with the impact of the coated layer's thickness.

In order to change the membrane surface and produce a Janus membrane, this study used the inkjet printing technique. This was done since human urine causes fouling problems when it is treated using MD (membrane distillation). These altered membranes were then used to extract nutrients from human urine directly.

A ground-breaking dual in-series MD arrangement was subsequently developed to boost ammonia capture effectiveness from human urine. By preserving the proper pH range and reducing acid consumption, this creative design offers a viable method for the direct recovery of nutrients from human urine. This study represents an important step forward in the development of MD-based nutrient recovery technologies, which helps ensure the sustainable use of resources. The Inkjet-printed membrane was subsequently utilised in a dual-in series configuration for direct nutrient recovery from landfill leachate.

1.4 The organisation of the thesis

The thesis is organised into seven chapters, which are described below.

Chapter 1 introduces the research problem, aim and objectives, contributions to knowledge, and thesis organisation.

Chapter 2 presents the overview of the Janus membrane and its different configurations and fabrication and modification processes. In addition, the application of Janus membranes in the MD process has been studied.

Chapter 3 illustrates the modelling and analysis of transport in the membrane distillation process, and the performance of the membrane in the treatment of feedwater containing a wide range of salinities has been studied.

Chapter 4 explains the process for the fabrication of a triple-layer nanofiber membrane, and its application in the desalination of hypersaline water has been explored.

Chapter 5 describes the process for modification of the membranes to fabricate Janus membrane using inkjet-printing technology, and its performance in treating hypersaline water and human urine has been studied.

Chapter 6 provides the results describing the effectiveness of specially designed dual-in-series membranes for the recovery of nutrients from human urine and landfill leachate.

Chapter 7 outlines the procedure for adapting membranes to create Janus membranes using inkjet-printing technology, along with an evaluation of how these membranes extract nutrients from human urine and landfill leachate.

Chapter 8 summarises the key results from this study and proposes recommendations for future research.

Chapter 2
Literature Review

This Chapter is partially based on the following publications:

- **M Afsari**, HK Shon, LD Tijing, Janus membranes for membrane distillation: Recent advances and challenges, Advances in Colloid and Interface Science 289, **2021**
- M Toriello, **M Afsari**, HK Shon, LD Tijing, Progress on the Fabrication and Application of Electrospun Nanofiber Composites, Membranes 10 (9), 204, **2020**

2.1 Introduction

The rapidly diminishing sources of clean water pose a global risk, with estimates of nearly four billion people living in water scarcity in 2030. Rising population and urbanization, along with increasing pollution, threaten the water sources, the environment, and society. Thus, alternative water sources are being sought out to provide clean water, mainly from seawater or from wastewater. Desalination and wastewater treatment technologies have garnered increased use and attention in the past few decades. Though conventional treatment processes are still being used, membrane-based processes have exploded in utilization by industries due to their reliability and robustness, efficiency, and flexibility [1]. In most cases, membrane technology also saves huge amounts of space due to its compactness. Pressure-driven membrane processes such as reverse osmosis and nanofiltration are widely used in industries; however, they have high energy usage and operational and capital costs. In the last few decades, an emerging membrane technology called membrane distillation (MD) has garnered wide attention from researchers as a promising process for clean water production[2]. This is because MD is a nonpressure-driven process that instead utilizes the partial water vapour pressure difference (based on temperature difference, i.e., combining thermal and membrane processes) between the feed and permeate solution as the driving force. A hydrophobic membrane is essential as a barrier for the evaporation/condensation process to occur. In theory, the working mechanism of MD can result in 100% rejection of nonvolatile components. Though a large amount of energy is still required to heat the feedwater solution, this can be offset with the use of renewable energy or waste heat, making it an attractive, less costly process for clean water production [3].

However, MD has not enjoyed commercial success yet (though some pilot plants and small-scale modules exist), even though a huge amount of research has already been done on this area on the lab scale. One of the main reasons is the lack of suitable distillation membranes [4]. Hydrophobic polymeric membranes, such as those made of PVDF and PTFE that are commercially available, are commonly used. However, they usually have a lower flux rate and suffer from wetting, fouling, and scaling problems, which can negatively affect the long-term performance of MD. Thus, distillation membranes with added functionalities and new structures and morphologies have been developed to address the shortcomings of standard commercially available polymeric membranes that are not specifically designed for MD [5].

Breakthroughs in nanotechnology and nanomaterials have led to the improvement of membrane properties for MD, especially for manipulating the membrane structure and morphology, surface wettability, fouling resistance, and chemical and mechanical properties [6]. Nano-enabled polymeric membranes may be from nanoparticle incorporation or from nano-engineering of the surface structure and morphology and are considered one of the main ways to develop new distillation membranes. Nanocomposite membranes have been studied widely in the form of flat sheet, hollow fiber, and nanofiber membranes, mostly with results indicating improved flux and rejection performances [7]. This chapter will provide the developments, challenges, and opportunities in a special type of nanocomposite membrane fabrication and performance called Janus membrane, with particular emphasis on wastewater treatment via MD.

For MD to continuously work, especially when dealing with challenging waters and wastewater, one side of the membrane has to maintain its hydrophobic nature so as to avoid membrane wetting that can deteriorate the permeate quality (i.e., reduced salt rejection) and, ultimately, the overall MD process failure [8]. Thus, the wetting issue in MD is one of its biggest challenges. Wetting and fouling are very interrelated, whereby foulants may be organic, inorganic, or biological, which can lead to membrane wetting [9]. This is especially true when treating challenging wastewater containing various pollutants, including oil, surfactants, etc. Membrane wetting happens when hydrophilic components from the feedwater have attached to the membrane surface, lowering the overall hydrophobicity, thus allowing the penetration of feedwater to the permeate side instead of just allowing the water vapour [10]. The wetting of the membrane is affected by the membrane characteristics and process and feedwater conditions, which can be for long-term or short-term situations. On the other hand, the fouling and scaling can also lead to clogging of the membrane pores, resulting in a decrease in permeate flux [11]. Both fouling and wetting are dependent on time, and their long-term effects are not easily predicted.

There are many approaches to producing antiwetting membranes, as found in the literature [12]. These include fabrication and surface modification of membranes to improve their hydrophobicity or omniphobicity. Superhydrophobic membranes have been shown to be good at increasing flux performance and mitigating membrane scaling. However, they are not as robust for controlling organic and biofouling agents, major pollutants in wastewater. Omniphobic membranes were then designed to specifically address the limitations of hydrophobic and superhydrophobic membranes,

wherein organic contaminants are controlled to some degree [13]. Another approach is through the design of a Janus membrane, wherein there is asymmetric wettability of the two sides of the membrane [14, 15]. A study has found that when the feed-facing side of the membrane has a thin coating of a hydrophilic layer, it could minimize the effect of organic fouling, but it also risks wetting concerns in long-term operation. Controlling the wettability of the membrane surfaces is typically done by adding hydrophilic or hydrophobic nanoparticles in/on the membrane to provide the needed antiwetting properties and structure and morphology enhancements. Other methods include surface treatment such as plasma, etching, etc. Thus, nano-enabled membranes have seen wide interest in the production of MD membranes, especially in the past 2 decades.

2.2 Overview of Janus membranes

Janus is the name of the ancient Roman god that has two opposite faces; one looks to the past, and the other looks to the future [12, 35]. In the material science field, Janus was first used by De Gennes for the synthesis of particles that chemically have different hemispheres [36]. The first Janus materials have been composed of poly(methyl methacrylate) and polystyrene materials. Accordingly, materials with ambivalent properties are called Janus, like Janus particles, Janus nanosheets, and Janus membranes. The Janus membrane was first introduced by Cheng and Wiersma in 1982, and since then, the number of research focused on improvement methods of the Janus membrane has drastically increased [37]. Janus membrane is a new configuration that has asymmetric wettability on both sides. In other words, one side is hydrophilic, and the other side is hydrophobic or omniphobic [38]. Figure 2-1 shows a schematic of the

various designs of Janus membranes. As shown in this figure, the Janus membrane can be fabricated by coating a hydrophilic layer on top of a hydrophobic, superhydrophobic, or omniphobic base membrane. The superhydrophobic membrane is commonly fabricated by the incorporation of nanoparticles on a hydrophobic membrane to increase its surface roughness and consequently enhance its hydrophobicity. Omniphobic membrane is produced by forming re-entrant surface structures and the addition of low-surface-energy materials like fluorinated additives that enhance both repulsion of the membranes for many materials, especially low surface tension substances (e.g. surfactants). The fabricated Janus membrane can be used in both configurations, including the hydrophilic layer toward feed stream or vice versa.

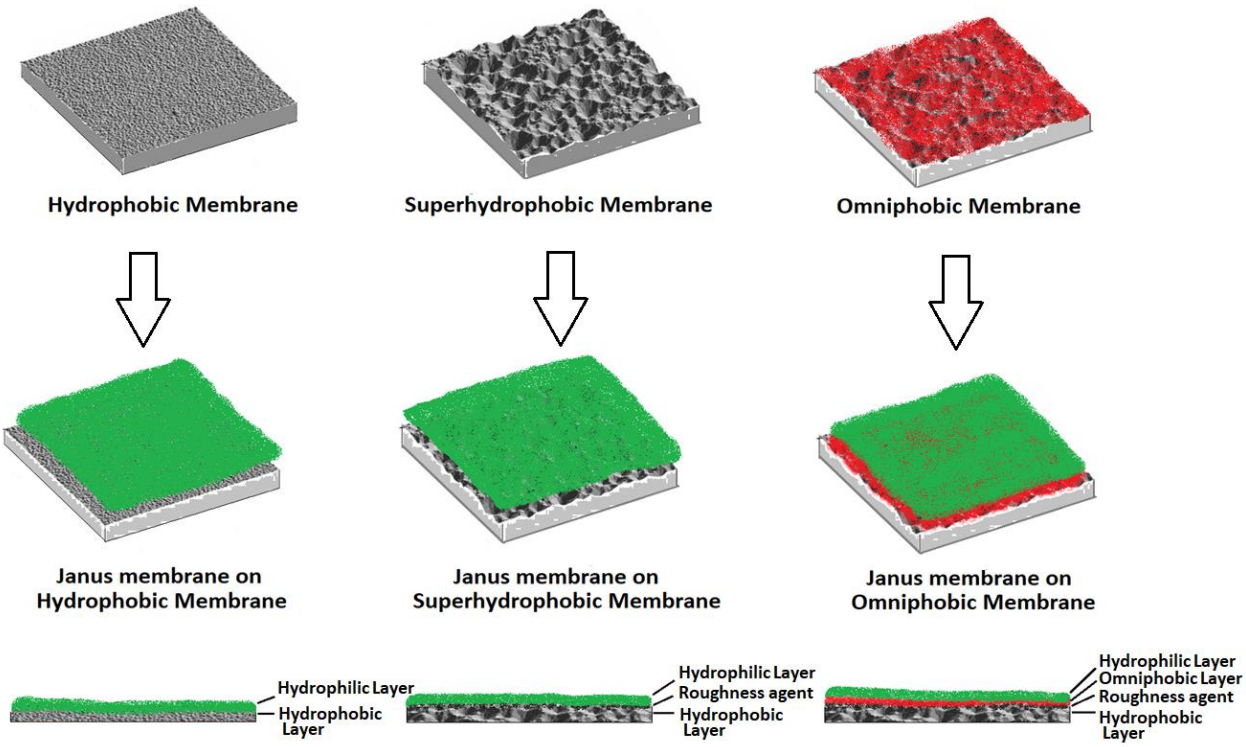

Figure 2-1. Different types of Janus membrane configurations.

According to the mass and heat transfer conflicts in MD systems, the optimum thickness can be approximately calculated using the pore size and heat conductivity coefficient. For the Janus membrane, the optimum thickness can also be designed accordingly. Reports indicated that the optimum thickness of the hydrophobic part (with porosity > 70%, thermal conductivity = 0.1-0.3 W/mK) should be in the range of 30-60 μm [24].

Hydrophobicity or hydrophilicity is a characteristic of the surface of materials that is related to its surface energy. This determines the tendency of the surface to adhere or repel the liquid materials. The wetting properties are dependent on the chemical structure of the surface and also on the roughness, pore size, and environmental condition. Empirical correlations can be used to predict the surface affinities of various liquids, but the easiest and most straightforward evaluation method is via measurement of liquid contact angle. In general, surfaces with a water contact angle (WCA) greater than 90^{o} are considered hydrophobic and less than 90^{o} are hydrophilic [7]. Different liquid types will have varying affinity to a particular material and surface. For membranes having rough and porous surfaces, the contact angle can be estimated using the Wenzel equation for homogenous and Cassie-Baxter for heterogeneous types. Figure 2-2 shows the transition lines for different wetting states versus the roughness of the surface [39].

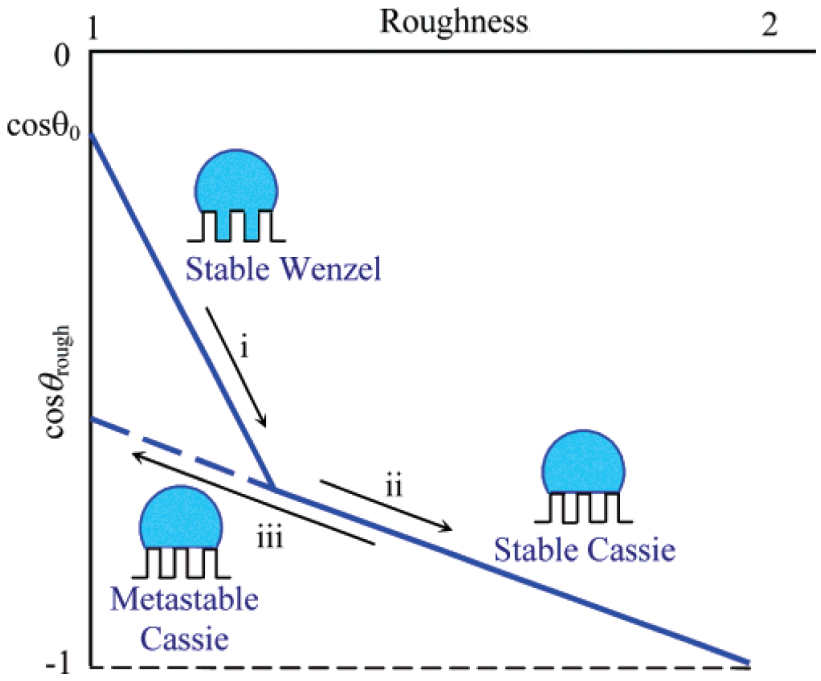

Figure 2-2. The transition line from the Cassie-Baxter regime to the Wenzel regime [39].

According to the physical and chemical properties of the surface and liquid, different states, from the Wenzel state to the metastable and stable Cassie-Baxter state, are formed. In order to increase the hydrophobicity and decrease the slippery angle of the membrane, especially for MD application, it is better to push the contact angle into the Cassie-Baxter regime. In this condition, upward capillary forces inhibit the intrusion of liquid into the grooves of the membrane surface and preserve the membrane from wetting [40, 41]. The addition of a hierarchical structure on the surface of the membrane can amplify the state of the membrane surface. In other words, as repeatedly performed on hydrophobic membranes, roughness increment can improve hydrophobicity and limit wetting, but for hydrophilic surfaces, roughness increment increases the hydrophilic affinity of the surface and decreases its WCA [29, 42]. For example, Chew et al. modified the hydrophilic layer of a Janus membrane by multilevel hierarchical structure using nanoparticle dispersion on the top surface, and the results proved

enhancement of its surface hydrophilicity and the top layer became super hydrophilic [43].

2.2.1 Anti-fouling and anti-wetting properties

Janus membranes, which possess opposite wettability at two sides of the membrane, can lead to wetting and fouling resistance if properly designed. The combination of two layers with distinct surface energy provides a specific wettability condition for Janus membranes [44]. When exposed to different types of liquids, including water, mineral oil, ethanol, or surfactant-rich water, Janus membranes can potentially limit their wicking into the membrane compared to other membranes. For example, superhydrophobic membranes are adequately resistant to high-surface tension liquids but are easily wetted by low-surface tension liquids [45, 46]. Omniphobic membranes are perhaps highly regarded for MD processes as they possess good resistivity against surfactants and wetting agents but still suffer from the fouling issue in oil-polluted wastewater [9, 16]. As Janus membranes have a thin hydrophilic layer on top of a hydrophobic/superhydrophobic or omniphobic membrane, this configuration simultaneously results in high flux and low fouling and wetting propensity. The top hydrophilic layer rejects the hydrophobic pollutants and allows water to penetrate, while the base hydrophobic membrane then resists the water from passing through and proceeds with water evaporation. This is particularly useful when dealing with challenging wastewater feeds. A high volume of oil-containing wastewater is produced during different food and shale gas drilling processes, making it crucial to find an effective and low-cost process for oil-water separation [47, 48]. Oil droplets in feed can lead to quick fouling of the membrane surface, resulting in a decrease in flux, clogging and wetting issues that affect its long-term operation. Thus, many groups have started

to design Janus membranes while utilizing the positive value of superhydrophobic or omniphobic substrates to deal with these issues.

Several studies have shown that hydrophobic and omniphobic membranes have less resistance to underwater oil droplets due to the hydrophobic-hydrophobic interaction between oil droplets and the membrane surface. Thus, oil can wick through the membrane and result in clogging, fouling, or eventually wetting of the membrane [20, 49]. But Janus membranes have thin hydrophilic layers that are hydrated with water, showing underwater oleophobicity, which can repel oil droplets and avoid oil fouling formation. Furthermore, according to Wenzel and Cassie theory, an increase in the roughness of the hydrophilic layer can lead to an increase in the area of the hydrated top layer and consequently enhance its oleophobicity. This was proven by a study by Huang et al., wherein the hydrophilic layer of the Janus membrane was coated with silica and chitosan to increase both the wettability and surface roughness of the membrane. This led to the reduction of fouling generated by oil droplets on the Janus membrane [46, 50]. Another study also demonstrated the effect of hydration of the hydrophilic layer on the repulsion of oil droplets from depositing on the surface [51]. They found that the adhesive force between the oil droplet and membrane surface for the hydrated top layer of the Janus membrane was less than 60 μN, while that of the hydrophobic PVDF membrane reached more than 300 μN (see Figure 2-3). This proportion shows a relatively high repulsive force of the Janus membrane for oil droplets. The receding curve also shows a dramatic decrease in a hydrophobic membrane (from about 300 to less than 200 μN), which reveals the presence of high adhesive interaction. In other words, the hydrophobic membrane attracted the oil droplets at the time of contact with

it and showed higher possibility of fouling, whereas the change in adhesive force for Janus membrane is zero, demonstrating that no interaction was formed during contacting and detachment [31, 51]. Also, DCMD test results revealed higher fouling resistivity of Janus membranes compared to hydrophobic or omniphobic membranes.

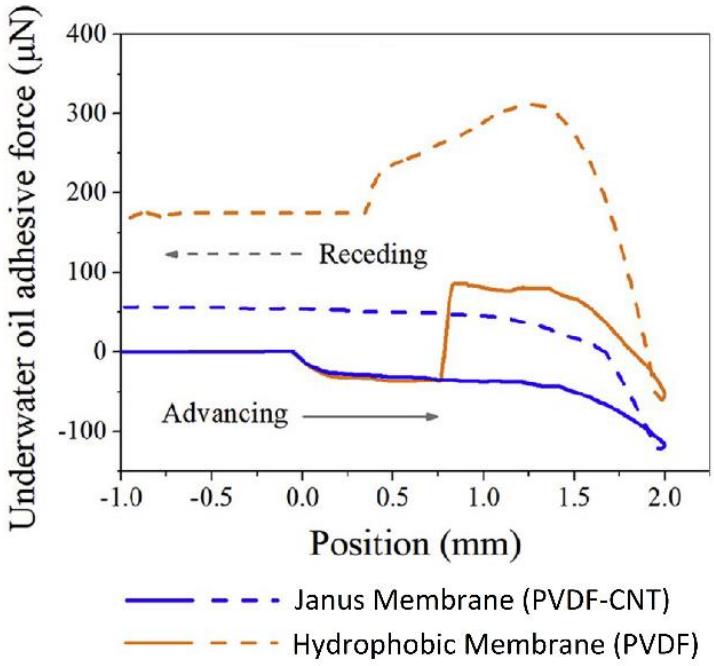

Figure 2-3. Force-distance curve for dynamic movement of oil droplet into contact of both Janus and hydrophobic membrane through advancing and receding movement [51]

In another study, the wettability performance of Janus membrane prepared by coating of PDA on omniphobic PTFE/PP-Teflon was compared by hydrophobic PTFE-PP membrane under various types of liquids. Results showed high interaction of hydrophobic membrane with low surface tension liquids but low interaction on Janus membranes. This low interaction is attributed to the presence of an omniphobic membrane substrate beneath the thin hydrophilic layer repelling the low surface tension liquids in the process. This exceptional behaviour helped the Janus membrane to work for long term MD operation with stable flux and salt rejection, while other

tested membranes showed reduction in performance after some hours of testing with contaminated and polluted feed water [52]. Li et al. also investigated the effect of coating a hydrophilic layer on the wettability of prepared membranes [16]. In their study, a hydrophobic membrane with WCA of 140° and omniphobic membrane with WCA of 151° was fabricated and Janus membranes were produced by coating of hydrophilic layer on top of both membranes. The formation of re-entrant and multilevel structure on omniphobic membrane improved its wettability compared to the hydrophobic membrane and placed it in Cassie-Baxter state for water. The Janus membrane that was formed on omniphobic substrate was wetted by all tested liquids but none of them could successfully penetrate into the permeate side of the Janus membrane, primarily due to the presence of the omniphobic substrate [16]. The results derived from this study also revealed that the hydrophobic membrane showed simultaneous increment of flux and decrement of salt rejection when the SDS concentration of the feed increased to 0.1 mM, indicating signs of severe wetting issues. The omniphobic and Janus membrane showed adequate performance even in higher SDS concentrations and lower feed surface tension for the wetting experiment. Additional fouling experiment was carried out using saline feed water containing surfactant-stabilized crude-oil (0.5 $g.L^{-1}$ crude oil, 0.03 $g.L^{-1}$ TWEEN 20, and 1 M NaCl). The emulsion contained all types of wetting and foulant agents to examine real performance of prepared membranes in harsh conditions. The hydrophobic membrane was fully wetted after only 40 minutes of operation, while the omniphobic membrane showed better separation performance with complete salt rejection after 4 hrs but with 30% flux decline, due to fouling problem. However, beyond 4 hr, the membrane rapidly wetted as indicated by the sharp increase in permeate conductivity. The Janus membrane on the other hand enjoyed a

near perfect salt rejection and constant flux during the full duration of test period, showing low fouling formation and stable long term MD performance. It is noted though that this study also demonstrated that the thickness of the hydrophilic layer can have dramatic effect on the fouling and wetting resistance of the omniphobic membrane, so care must be taken to come up with the optimum thickness [16].

Zhu et al. fabricated a Janus membrane by coating a hydrophilic PAN layer on F-SiO_2 @PVDF-HFP/PS omniphobic membrane. The hydrophilic PAN (4 wt%) solution was coated on the omniphobic membrane by electrospinning, and the formed structure resulted to a dramatic increase in underwater OCA to more than 164^o, proving underwater superoleophobicity of the Janus membrane [34]. Long term MD operation of the Janus membrane demonstrated a stable flux of 25 LMH and 100% salt rejection for 50 h continuous test, while hydrophobic PVDF and superhydrophobic PVDF NFM showed quick fouling after only half hour of test. The dynamic study of the fouling mechanism showed that oil droplets attached and fouled first on the other two membranes, but could not attach to hydrophilic PAN layer of Janus membrane. The unattached oil droplets were then aggregated on the surface of Janus membrane and formed bigger oil droplets and then left the Janus membrane surface without any fouling problem [34, 53]. The dynamic investigation of wetting and contact angle can determine the mechanism of fouling and wetting in the membrane and derived data are more helpful to assess the DCMD experimental results.

The effectiveness of Janus membrane for increasing the resistivity of membrane against fouling and wetting problems also depends on the composition of contaminants in the feed water. The structure and features of surfactants can change the fouling mechanism

in the Janus membranes. The ionic surfactants can adsorb on the membrane surface via the electrostatic or hydrophobic forces. Although the negative charge of a hydrophobic membrane (like PVDF membrane) repels the negative side of surfactants, it can interact with the other side of the surfactant and adsorb it. Therefore, the flux reduction in hydrophobic membrane could be attributed to this interaction. In this interaction, the hydrophobic to hydrophilic ratio of surfactants can determine the power of hydrophobic-hydrophobic interaction and, consequently the rate of surfactant adsorption [54]. In fact, the degree of hydrophobicity of the membrane surface needed in a MD membrane depends on the value of hydrophilic-lipophilic balance (HLB), which is defined as the proportion of polar to the non-polar segments of a surfactant. Whenever the HLB is lower, the surfactant is more hydrophobic. The surfactant adsorption changes the hydrophobic structure to hydrophilic ones and increases the wetting of the membrane. For Janus membranes, the hydrophobic interaction decreases, and electrostatic interaction plays the most important role. For example, in the case of the PDA-PEI/PVDF Janus membrane, the protonated amine functional group can make electrostatic interaction by sulphate groups of hydrophilic parts of surfactants and induce fouling for the membrane [16, 21, 22].

On the other hand, when Janus membrane deals with cationic surfactants like DTAB, the positive charges of protoned amine-functional groups in the membrane and quaternary ammonium heads of the DTAB repel each other and the intrinsic structure of Janus membrane keeps the membrane surface from surfactant fouling. In the case of hydrophobic membrane, like PVDF, the negative charge of the membrane surface can attract the positive parts of DTAB and make both electrostatic and hydrophobic

interaction and make wetting problem for hydrophobic membrane. In one fouling study, the surfactant-stabilized oil in water emulsion was prepared as the fouling agent. The oil droplets desire to have interaction with hydrophobic beneath layer but the surface tension force of water molecules with hydrophilic layer is stronger than adsorption force between oil droplets and hydrophobic membrane therefore the presence of the hydrophilic layer in Janus membrane makes a barrier against oil droplets and prevents the fouling of the membrane. Furthermore, the oil water emulsion has positive charge and is repelled by positive charge of protonated amine-functional groups on the Janus membranes and helps the hydrogen-bond in hydrated layer for prevention of oil fouling on the Janus membranes [20, 55, 56]. In general, the effectiveness of a modification should be investigated case by case and the moieties of the feed water and membrane structure should be recognised [55]

2.3 Janus membrane modification methods

2.3.1 Hydrophilic-hydrophobic configuration

The most common method for the production of Janus membrane, which has been widely used in many studies, is by deposition or incorporation of a hydrophilic layer on top of a hydrophobic or omniphobic membrane substrate [57]. This method has the advantage of being generally simple, straightforward, and is a step-wise process [58]. However, the modification methods in many cases compromise the quality of the substrate membrane by clogging the pores or changing the hydrophobicity of the membrane. Furthermore, stepwise preparation increases the material and fabrication costs and increases the delamination problems [4, 35]. Fabrication of new membranes is usually done by phase inversion, hollow fibre spinning or by electrospinning. However, these processes in many cases do not directly create the Janus membrane structure,

thus further modification processes are required. The modification processes include coating, incorporation of nanoparticles or surface modifying macromolecules, electrospinning or electrospraying of environmentally friendly hydrophilic materials like PEG, PDA, hydrogels, grafting of hydrophilic functional groups, and other ways of providing specific wettability and function to the membrane [49, 59, 60]. In other studies, before modification of the membrane surface, some chemical methods such as plasma treatment, were used to prepare the hydrophobic substrate to be more affinitive to the hydrophilic layer. This section presents the various ways to fabricate and modify Janus membranes with hydrophilic-hydrophobic structures.

2.3.1.1 Vacuum filtration

Vacuum filtration is a simple and straightforward method for coating of a hydrophilic top layer on hydrophobic or omniphobic base membrane. In this method, firstly a hydrophobic or omniphobic microporous flat sheet membrane is fabricated and then a hydrophilic layer is coated on the top layer using vacuum filtration of a solution containing desired hydrophilic nanoparticles (NPs). The size, dimension, and chemical structure of NPs are very important parameters in defining the efficiency of the Janus membrane. However, this method suffers from low stability and delamination problems. For example, one study covered the top layer of a PVDF membrane by vacuum filtration of solution containing Si NPs, which resulted in an increase in membrane surface roughness [61], while another study added CNT containing solutions, which led to a decrease in roughness for the same type of substrate [62, 63]. The explanation for this modification can be attributed to the size and shape of the nanoparticles and also the presence of a ridge-valley structure on the PVDF membrane

surface. This condition can cause a decrease in porosity, which can lead to diminished flux performance [51]. Even though the CNT-containing membrane decreased the pore size distribution of the Janus membrane by blocking or decreasing the effective area of some pores, its mechanical stability compared to the unmodified membrane increased. TGA data showed higher thermal stability and mechanical analysis of modified membrane revealed that imposing strains of PVDF-CNT membrane was about two-fold compared to unmodified PVDF membrane. However, the tensile strength obtained similar results to that of neat membrane [51]. The inorganic nature of CNTs and the functional groups present on their surface can have interaction with the substrate and other CNTs to make a strong deposited layer, having sufficient hydrophilic wettability [4, 11]. Generally, the physical and chemical structure of CNTs make possible rapid mass transfer of water molecules through outer and inner surface of CNTs via sequential sorption-desorption and can increase water transport to the membrane surface and simultaneously make a barrier against oil droplets for some special wastewater treatments like oil-emulsion treatment [51].

2.3.1.2 Coating via co-casting phase inversion

Co-casting is another method wherein both layers are subsequently cast and can be used to fabricate bilayer or multilayer materials, such as Janus membranes. One important factor in the investigation of the effect of a simple coating procedure is considering the structure of layers during coating. In phase inversion, the type of polymer, solvent, nonsolvent, and temperature are important factors of layering. The structure and morphology of the casted solution are formed according to the miscibility of the solvent and nonsolvent, and the difference in chemical and physical properties of

matrix polymer may cause delamination during coagulation process. Therefore, the thermodynamic properties of different mixtures should be considered to find the optimum type of solvent and nonsolvent [49, 64]. The ternary phase diagram should be used to determine the miscibility of polymers, solvents, and nonsolvent to estimate the optimum condition to fabricate an integrated multi-layer membrane. Figure 2-4 shows the change in structure of different dope solutions during phase inversion process in coagulation bath containing water [65]

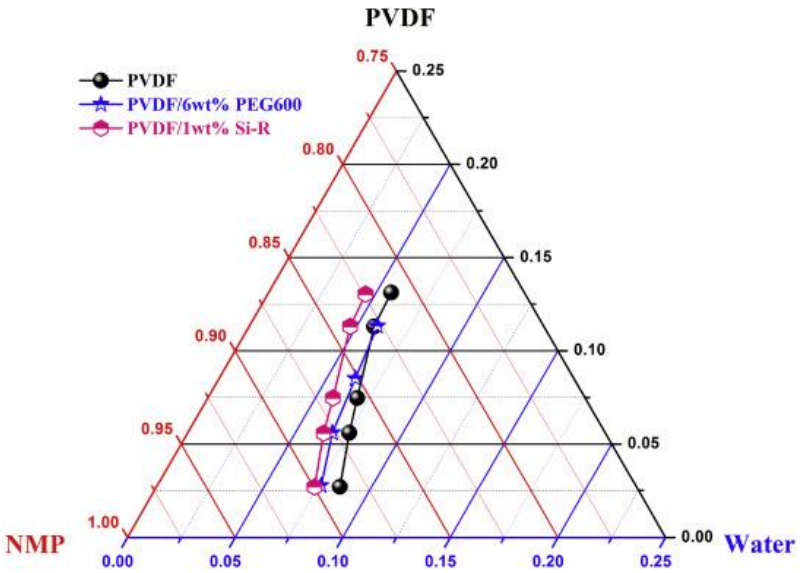

Figure 2-4. The Ternary diagram for coagulation of different types of PVDF/NMP solution in water bath *[65].*

For example, in the process of co-casting of PVDF-PVA as a hydrophilic layer and PVDF as a hydrophobic beneath layer, due to differences in solvent replacement, two distinct layers were formed (Figure 2-5). Differences in solvents and polymers resulted in the fabrication of asymmetric membrane with an obvious boundary between two layers. The difference in rate of miscibility of solvents in two phases into nonsolvent coagulant bath formed two distinct layers which increased the possibility of delamination [64]. In

general, slow dissolution of solvent in nonsolvent makes porous structure with small pore sizes, while rapid migration of solvents form finger-like structure with wide pore sizes [22, 64, 66]. Depending on the type of phase inversion process (TIPS or NIPS), the coagulation temperature also has direct influence on the structure of the Janus membrane. In TIPS membrane casting, higher coagulation temperature makes rougher top surface. Also, the pores are more blocked and the interconnectivities of the pores decrease. Generally, with temperature increments, the NIPS improve while TIPS weakens [64]. Also, molecular weight and concentration of polymer in dope solution impact the property of final membrane. Higher molecular weight or higher concentration of polymer in dope solution usually leads to the fabrication of membrane with smaller pore widths and shorter finger-like pores [66-68].

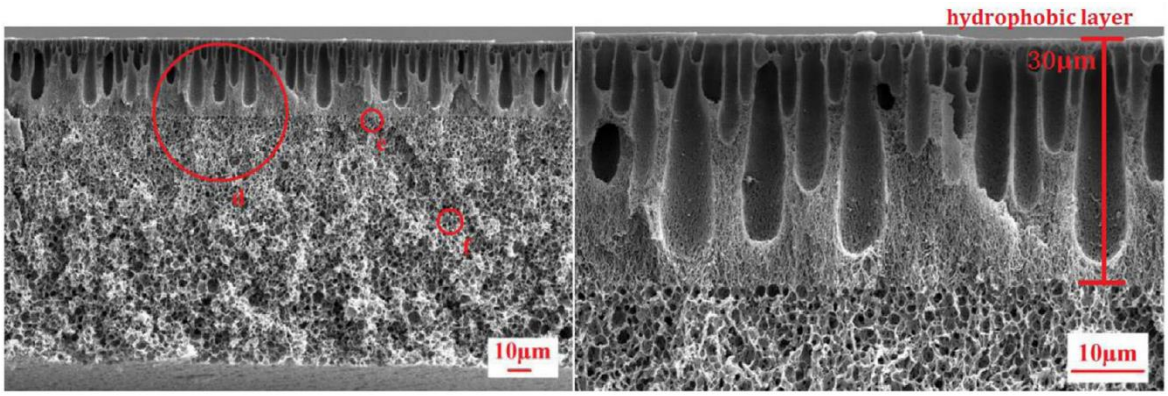

Figure 2-5. Cross section SEM image of flat sheet bilayer membrane fabricated by PVDF-PVA on PVDF [64]

2.3.1.3 Asymmetric fabrication

Asymmetric fabrication refers to the one-step fabrication of Janus membranes as opposed to symmetric fabrication, where a hydrophilic layer is subsequently coated on a hydrophobic or omniphobic layer. In the asymmetric method, usually the difference in solubility of materials is used to fabricate asymmetric structure. In brief, a dope solution

containing at least two distinct types of materials, like polymers or nanoparticles, is prepared and the dope solution is placed in a coagulant environment. Then, the asymmetric structures start to form due to difference in surface energy of materials and their tendency to reach the low-energy surface. Also in some cases, the difference in solubility of polymer composite in a coagulant liquid causes faster migration of polymer parts toward the outer surface and causes fabrication of a membrane with different wettability in both sides [32, 34, 69].

Additionally, it is possible to fabricate Janus membranes by internal migration of materials through the membrane matrix and make a polar hydrophilic structure. In this method, usually a dope solution containing both hydrophilic and hydrophobic materials is prepared and then the solution is placed in an asymmetric surface energy environment. In this condition, the macromolecules or monomers, which are not yet coagulated, tend to migrate to surfaces with lower energy, according to their chemical affinities. This movement usually occurs in phase inversion process. In this process, the nonsolvent tends to remove solvents and replace them, according to solvent-polymer-nonsolvent interaction in ternary phase diagram. In a heterogeneous polymer solution containing both hydrophilic and hydrophobic polymers, the polymer parts tend to migrate to the more-soluble nonsolvent due to their intrinsic interactions. For example, if the water is nonsolvent, the hydrophilic parts tend to migrate toward the outer surface and, as a result, can change the hydrophilicity of outer layers. In this method, an asymmetric membrane can be fabricated without delamination. For comparison, in a normal phase inversion, both top and bottom layers become similar in hydrophilicity due to the simultaneous migration of hydrophilic part of solution towards all sides. In

order to preserve the asymmetric style, novel methods like adhesion of an impermeable layer to one side of the casting surface should be used [22, 49]. Li et al. utilized glycerol to coat a nonwoven fabric, then a polymeric solution is casted on the fabric and then immersed in coagulation bath. As a result, a solution containing copolymer PVP-VTES and PVDF was prepared. The PVP-VTES has hydrophilic affinity and tends to interact with water to reach lower surface energy. Compared to PVDF, the PVP-VTES had a faster migration rate. Also due to the immiscibility of glycerol layer into water nonsolvent, the solvent cannot penetrate across the bottom layer of the membrane and the migration occurs only on one side of the casted layer and the difference in miscibility rate results in an asymmetric hydrophilic-hydrophobic structure [22].

The asymmetric modification of hydrophobic membranes to fabricate Janus membranes has various difficulties, such as wetting of the substrate pores via hydrophilic layer. The MD membranes have microporous structures, and the pores can usually be wetted due to capillary force and interactions between the bulk membrane and coating layer. As a result, if the modification method does not perform accurately, not only will the wetting and fouling not be hindered, but also the separation performance of the hydrophobic substrate decreases. Some methods have been suggested to enhance the modification process. One of these methods includes placing a separation interface to prevent the modification layer from intruding into the pores of the substrate. In this method, usually, a thin layer is coated on the surface of the hydrophobic membrane and then a hydrophilic layer is entangled with this intermediate top layer and two distinct regions are formed. The intermediate layer plays the role of making strong adhesion on both hydrophilic and hydrophobic layers and also prevents the pore clogging by the

hydrophilic layer. In another type of method, it is possible to adjust the reaction time of the polymeric dope solution to make a gradient reaction across the membrane width. In this method, the composition of dope solution is accurately selected to have different reaction rates and differences in reaction rate make an integrated asymmetric membrane with opposite wettability on both sides [11, 33, 70].

2.3.1.4 Two-phase interface method

One of the difficulties of Janus membrane fabrication is modification of only one side of the substrate. It is not so straightforward to modify only one side of a polymeric surface having only some micron thickness. Therefore, an applicable modification method should have capability of changing the wettability of one side of the membrane without changing the characteristics of the other side. The dilemma is the selection of proper solution. A wetting solution may intrude into the pores and decrease the efficiency of the MD process, while a non-wetting solution may not interact with the membrane substrate and may delaminate the top layer. Various methods have been proposed to modify the surface of hydrophobic membrane. Two phase interface method is a novel coating method that can be used to modify only one side of the membrane without affecting the other side. In this method the membrane substrate is soaked in the interface of two immiscible liquids so that one side of the membrane is in contact with the surface of the other liquid. Then, the desired layer reacts with the membrane substrate to form a layer on top of it [22, 58, 71]. For instance, Yang et al. have floated a PP membrane on a solution containing PDA/PEI. This resulted in a hydrophilic layer of PDA/PEI coated on the hydrophobic PP membrane and a Janus membrane was fabricated. In this method, it is essential to coat the membrane surface with high

viscosity solution to prevent intrusion of solution into the substrate pores via capillary force [71]. Similar method can also be applied by restricting one side of the membrane substrate by sticking an impermeable layer and then soaking the membrane inside a reaction liquid. In this way, the solution can react with only one side of the membrane and a hydrophilic layer is coated on the membrane substrate. The sticked layer preserves the other side of the substrate from solution reactants. After finishing the reaction, the impermeable coating is peeled-off and Janus membrane is fabricated. However, the peeling-off step, in most cases, destroys the beneath layer of the Janus membrane and may affect the performance of the membrane for application in DCMD [4, 72].

In another study carried out by Wang et al. [73], porous hydrophobic PET was covered with thin PTFE layer and then modified by tannic acid and diethylenetriamine coating to change the surface and pores of the composite to hydrophilic. After the drying process, the PTFE layer was peeled off and a Janus membrane with top-layer hydrophobic and hydrophilic substrate was formed. The WCAs on both sides were 110^{o} and 20^{o}, showing asymmetric characteristics. The thin hydrophobic and thick hydrophilic configuration makes great Laplace pressure and makes this membrane suitable for oil-water emulsion treatment. This method can also be used for the hydrophobization of a hydrophilic substrate to make a thin hydrophilic and thick hydrophobic membrane. The easy fabrication, wide range of available substrates, and grafting materials are some advantages of the potential for large-scale production of Janus membranes [73].

2.3.1.5 Surface modifying macromolecules

In general, Janus membranes can have two configurations: asymmetric wettability in a distinct layer or gradient wettability from top to bottom layer. The former type has a separating layer that connects the hydrophilic and hydrophobic layers together. The latter is usually formed by migration of materials having opposite wettability through the dope solution during coagulation or processing time and the concentration gradient makes the wettability gradient across the membrane. Application of surface modifying macromolecules (SMM) in the fabrication of the Janus membrane provides a gradient change in wettability across the membrane [74, 75]. SMMs are a group of active additives that tend to move toward the lower surface energy surfaces and can migrate in a non-solidified phase to reach to lower interfacial energy. In other words, the SMMs in a dope solution have the ability to move to sides to reach the surfaces and to have minimum interfacial energy. The small percentage of SMMs is sufficient to make a heterogeneous layer. Therefore, the application of SMMs has shown great potential for the fabrication of Janus membranes, especially for integrated membranes for MD application. The promising point of SMM is the possibility of one-step fabrication, which decreases commercial costs. SMMs are usually fluorinated polymer segments produced by fluorination of polymers like polyurethane, PVDF, and PES and are dissolved in a solution containing hydrophilic polymer solution. The dope solution is casted and placed in an air environment phase inversion process. The waiting time lets the SMMs to migrate toward the surface having low surface energy and make an asymmetric Janus membrane with a gradient wettability: hydrophobic top layer and hydrophilic bottom layer [76]. The type of blended polymer, SMM polymer and fluorocarbon, and dope solution solvent are important parameters affecting the mechanical, physical, and

chemical properties of Janus membrane. Zhang et al. reported the use of different types of solvents like $CHCl_3$, CH_3CN, THF, and acetone for the fabrication of SMM-based Janus membranes. Their results indicated that the best condition was achieved by using CH_3CN solvent, achieving the highest wettability difference between the two sides [76, 77].

The incorporation of SMM in hydrophilic membranes increases the chemical, mechanical, and thermal stability of the membranes and covers the delamination drawbacks for the application of Janus membrane in different wastewater treatment applications. One of the most important challenges is due to the all-directional movement of SMMs in dope solution, while the preferred movement direction is only one side migration. The derived membrane after the phase inversion process usually has a hydrophobic surface and hydrophilic bulk. In order to use the migration behaviour of SMM efficiently, the fabrication process needs to be modified using methods for controlling the directional migration. The covering of one side of the membrane is a possible method that has been used to direct the SMMs toward only one surface [22]. Before focusing on the application of SMMs in the Janus membrane, SMMs were used for enhancement of the hydrophobicity of the base membrane. In some research, the hydrophilic PEI membrane was modified with SMM to fabricate Janus membranes for MD application [76, 78]. Also, in a series of studies performed by Khayet's group, fluorinated SMMs were blended with hydrophilic PEI to enhance the LEP of the membrane. The derived composite membrane showed LEP greater than 2.9 bar. However, both liquid and gas flux of the membrane decreased due to lower pore sizes of the modified membrane. Also the DCMD results of Janus membranes prepared by PEI

and SMM in different studies showed equivalent or higher flux compared to commercial PTFE membranes [25, 79].

2.3.1.6 UV-mediated modification strategy

Another method for the fabrication of Janus membrane is treating one side of the membrane using photoreaction or photoresist materials. In this method, the membrane substrate can be soaked in a photoreactive or photoresist solution and then one side of the membrane is activated by irradiation of light. After the reaction is carried out, the remaining photoresist or photoreacted material is removed and a Janus membrane is fabricated. However, care must be taken to make sure that the photosensitive or photoreacted material must not affect the wettability of the membrane substrate after removal from the membrane surface. In a study performed by Lee et al., a Janus membrane was fabricated by firstly soaking porous hydrophilic alumina substrate in photoresist AZ 5214 and then etching one side of the membrane with air plasma. Afterwards, the etched surface was silanized using low surface energy perfluorodecyltrichlorosilane to make an omniphobic thin layer. The presence of photoresisted material makes a barrier against infiltration of the membrane pores with silane groups, preserving its hydrophilicity during the modification process. Afterwards, the remaining photoresist was washed out and removed. This fabrication procedure produced a Janus membrane with top hydrophobic coating and bottom substrate hydrophilic structure. This novel method also can be used for other modification techniques. After etching one side of the membrane, it is possible to coat-etch the surface of the substrate with other polymeric hydrophobic layers using methods like vapour deposition or interfacial layer deposition [4, 80].

UV-sensitive reactions are also good way to modify one side of the membranes. The thiol-ene click reaction is an example of reaction that is activated by UV light. This method has the benefits of rapid reaction rate, high yield, easy process, and controllable directional reaction. Li et al. modified different types of substrates by firstly coating of PDA, using mussel-inspired catechol chemistry, and then silanized it to produce superhydrophobic substrates. The polycondensation of Trichlorovinylsilane provides photosensitive functional groups. Afterwards, the superhydrophobic substrate was immersed in a thiol-ene click reaction solution and was irradiated by UV light, which renders one side of the membrane surface hydrophilic. This modification process makes a membrane with asymmetric wettability with a 140^{o} WCA difference between two sides of the membrane. According to the pore size distribution and thickness of the substrate, this membrane can be used for different water treatment applications like MD, oil-in-water emulsion, or water-in-oil emulsion separation [81].

2.3.1.7 Multi-step coating method

Wang et al. fabricated a Janus membrane using a multistep method to coat hydrophilic polyamine on one side and a hydrophobic polymer on the other side. In this study, cotton fabric was deposited by a compound of PDMS containing light-sensitive materials. Then one side of deposited cotton was irradiated to crosslink the light sensitive material and make a strong connection with the fibres. Afterwards, the remaining deposited material was washed using hot THF solvent. Then, the other side of the fibre was grafted by propyl methacrylate groups, using sol-gel method and a catalytic reaction, to increase the hydrophilicity of Janus membrane. Therefore, hydrophilic cotton fibres become hydrophobic/super hydrophilic Janus membranes

after these consecutive processes [82]. Furthermore, it is possible to combine the multi-effect of coated layer to enhance the effectiveness of the prepared Janus membrane for some special applications. For example, for the treatment of wastewaters with high bacterial activities, it is applicable to use some nanoparticles that have an antibacterial activity to simultaneously improve the separation performance of MD membrane and decrease bacterial growth on the surface of the membrane. In an experiment, the hydrophobic PVDF hollow fibre was coated by a hydrophilic PDA coating layer to fabricate the Janus membrane. Afterwards, silver nanoparticles were used in the top layer coating to increase the membrane's antibacterial activities and fouling resistivity. The experimental study on prepared membranes proved the lower adhesion of fouling agents on the membrane surface. Also, the proliferation of sulphur-containing proteins or thiol groups of enzymes was restrained in the silver-containing Janus membrane, which proves its antibacterial activities. Due to changes in structure of the hydrophilic layer during hydration process, the stability of coated layer is very challenging. In order to assess the stability and stiffness of the coated layer, especially for nanoparticle coating, the first step is to use an ultrasonic instrument. In this method, the loose bonding is detected and the applicability of the Janus membrane for long term operation is determined [55]. The stability of coated Ag nanoparticles was investigated by placing used membrane for one day and night in high-frequency ultrasonic bath, and results showed that about 85% of Ag nanoparticles remained on the surface after operation [9, 43].

Generally, the surface energy of PVDF is less than PTFE or PP, but it has been widely used for MD process due to its good compatibility with different polymers and solvents, low

cost, and adequate mechanical stability. Therefore, a wide range of polymers that are compatible with PVDF are used for the fabrication of bilayer or blended Janus membranes. In order to decrease delamination, it is better to choose polymers with close solubility parameters to make interactions during coating process. Although PVDF has been widely used as hydrophobic substrate for the MD process, it can be modified to become a hydrophilic or superhydrophilic substrate. In other words, its useful properties can be used in other side of technology to have high water wettability characteristics [14, 42, 83-85]. Zhou et al. fabricated a Janus membrane by changing a hydrophobic PVDF membrane to superhydrophilic membrane by initiation of vinyltriethoxysilane cross linking reaction that made it into a superhydrophilic PVDF substrate. The superhydrophilic PVDF was cast on a PET nonwoven fabric, and after coagulation, it was peeled off to generate micro and nano-size rough structures. Then, a superhydrophobic fluorinated silica nanoparticle solution was sprayed on these torn surfaces to coat the substrate and make a superhydrophobic layer. Regarding the degree of superhydrophobicity of the top layer, this Janus membrane can be used in different methods of water treatment, like forward osmosis or MD [86].

2.3.2 Hydrophobic-hydrophilic configuration

2.3.2.1 Liquid-liquid interface

Although most of the Janus membranes are fabricated by coating of hydrophilic layer on top of hydrophobic or superhydrophobic membrane, it is possible to do opposite fabrication method: coating of hydrophobic layer on top of hydrophilic layer [87]. In a novel method, liquid-liquid interface was used for the incorporation of a hydrophobic layer on top of a hydrophilic substrate. For this purpose, firstly the hydrophilic cotton membrane was soaked in dopamine solution for deposition of intermediate layer. Then

the DA-coated cotton membrane was floated on the water–dichloroethane–containing octadecylamine ($C_{18}NH_2$) two phase beaker. The membrane is placed at the liquid-liquid interface, according to a range of densities. The amine groups of C_{18}-NH_2 have hydrophilic tendency and stay orientated toward the water interface. Therefore, this intrinsic property caused the interaction of amine group with dopamine molecules deposited on the surface of cotton membrane. The deposition of PDA on the hydrophilic cotton fibre prepared the medium for attachment of C_{18}-NH_2 hydrophobic layers. The water-oil interface prepares the exchange area for this attachment. After interaction, the prepared Janus membrane has a relatively thin hydrophobic C_{18}-NH_2 layer beneath a thick hydrophilic layer [88]. However, this technique is only possible to perform on flat sheet membranes. In another study, Vanagamudi et al. have fabricated Janus membrane by casting a hydrophobic PVDF layer on the electrospun nanofibers made of hydrophilic nylon/chitosan blend. The presence of hydroxyl and amine functional groups gives high hydrophilicity to the electrospun nanofiber. Although the Janus membrane showed reduced pore size, the flux and rejection increased compared to neat PVDF membrane [89].

2.3.2.2 Electrospinning deposition

Yan et al. have used a novel method by deposition of hydrophobic electrospun nanofiber on superhydrophilic non-polymeric substrate. The substrate was constructed from porous copper mesh with nanosized needles. This substrate was prepared by immersion of smooth copper mesh into NaOH solution having $(NH_4)_2S_2O_8$ [77, 90]. This process changed the wettability of the substrate from hydrophobic to super hydrophilic feature (WCA changes from 114^o to 0^o). The nanosized needles can intrude into the deposited

nanofibers and enhance coating interaction and decrease the possibility of delamination and, in general, increased the entanglement of deposited hydrophobic layer with the substrate. Furthermore, the formed interface roughness increases the hydrophobicity and hydrophilicity of Janus membrane. The top layer was deposited using electrospinning of polymer solution containing different PVDF concentrations. The change in the concentration of the PVDF solution changed the properties of nanofibers. While beads were formed on the nanofibers fabricated at lower concentrations, the beads disappeared at higher PVDF concentrations. Also, Tijing et al. have fabricated a dual-layer membrane for DCMD application by electrospinning of PVDF-HFP on PAN microfibers. In this method, the PAN nanofibers firstly were electrospun on the drum, and then the PVD-HFP nanofibers were electrospun on the PAN substrate. The prepared membrane showed superb porosity of 90% and WCA of 150^{o} at the feed side, flux of 45 LMH, and complete salt rejection, completely suitable for DCMD application [91].

2.3.2.3 Other methods

Other researchers also have used hydrophilic porous substrates like cellulose acetate or cellulose nitrate and coated hydrophobic layers like styrene or vinyltrimethylsilicon compounds to fabricate bilayer Janus membranes. However, these researchers have used radiation graft or plasma polymerization methods that are relatively complicated and expensive for large-scale fabrication [24, 92]. Also, most of the studies were performed in flat sheet module and more research on other commercial modules like hollow fibre is necessary.

Perfluoropolyether (PFPE) compounds, like PTFE, are polymeric materials that have high content of fluorine in its structure. The fluorine content increases the chemical and

thermal resistivity of the polymers and forms a superhydrophobic compound. Beside these outstanding properties, the fabrication of porous PTFE membrane is complicated and expensive. On the other side, PVDF, a fluorine-containing polymer that is being used as MD membrane, has lower hydrophobicity compared to PTFE. Therefore, applying novel methods to use the benefits of PTFE and decreasing the complicity and cost of the process for MD application is favourable [2-4]. In a study performed by Figoli et al., a UV-sensitive PTFE layer was coated on commercial hydrophilic polyamide membrane. In this work, commercial microfiltration PI membrane was dip coated in PTFE oligomer solution, and then one side of coated layer was cured by UV light. The UV process stabilized PTFE on one side of the PI membrane and the remaining PTFE from other side was washed out to produce a Janus membrane. The derived membrane had high hydrophobicity, owing to the PTFE layer, and was fabricated simpler than commercial PTFE microporous membranes. Additionally, it had the advantage of being a Janus membrane. The fabricated Janus membrane showed LEP of about 3.5 bar and obtained a flux of 8 LMH at 40^{o}C temperature difference in DCMD module system. However, the porosity of the membrane showed a little reduction compared to the substrate [87].

2.4 Surface modification strategies towards Janus membrane fabrication

2.4.1 Plasma treatment

Gas plasma technology is a chemical-energy modification method that changes the structure of the material to the phase other than three regular solid, liquid, and gas phases. In this technology, usually high voltage is applied to the materials to ionize them and the materials are brought to the plasma phase. In this phase, a controlled reaction on a narrow and thin layer can be performed according to the properties of used gas and the substrate surface. Plasma technology is widely used in membrane technology

to change the properties of the surface layer to desired property, mostly to prepare surface for adopting a coating layer [93]. Plasma etching can scratch a very thin layer of the membrane substrate and prepare conditions for making interaction with coating layer [94, 95].

For a Janus membrane, the membrane substrate has hydrophobic or omniphobic properties and the top layer has hydrophilic wettability. The opposite wettability characteristics of these layers make challenges in the adhesion process. Therefore, gas plasma method can be used to ionise the hydrophobic or omniphobic substrate surface and change the structure for hydrophilic attachment. For example, Li et al. treated the surface of PP substrate via plasma for two minutes (at 200 W) to coat a hydrophilic top layer. The treated surface effectively accepted the coating of a Teflon layer for increasing hydrophobicity of the substrate and also attachment of hydrophilic PDA layer [52]. Zuo et al. have used plasma technology to modify the surface of PEG and TiO_2-coated PVDF membrane. The etching technique modified the surface of a hydrophobic PVDF membrane to graft with PEG functional groups. The FTIR spectrum showed a decrease in both asymmetrical and symmetrical stretching bond of CF_2 at 1178 and 1275 cm^{-1} and increase in OH stretching bond at 3400 cm^{-1}, which is a sign of a successful modification process. This grafting process caused a change in the wettability of the membrane to hydrophilic and fabrication of Janus membrane. However, the grafting approximately halved the average pore size of the membrane, which is beneficial for decreasing the wettability but also decreases the flux of the membrane.

2.4.2 Nanoseeding technique

Nanoseeding is a novel technology for changing the structure of the surface by increasing the surface roughness and its physical and chemical characteristics. In this method, first, the nanoseeds are stabilized on the substrate surface and then the nanorods are grown on the activated sites of the substrate. This modification method also can be used to increase the hydrophobicity of the substrate by growing of hydrophobic nanorods. Furthermore, due to barbed morphology of the surface, it is possible to immobilize a layer containing opposite wettability to fabricate Janus membrane. The combination of bumped rods with chemical interaction provided by thermal and mechanical treatment can fix the top layer on the superhydrophobic substrate [96, 97]. In a study, ZnO nanorods were grown on a hydrophilic cellulose acetate fibre in arrays and then superhydrophobic layer was made by immersion in sodium laurate solution. Afterwards, hydrophilic MnO_2 nanowires were coated on one side of the substrate via vacuum filtration and hydrothermal treatment. The modified membrane has shown superb properties like high porosity, asymmetric wettability and highly stabilized coated layer. The substrate showed superhydrophobic characteristics with WCA of 153^o and sliding angle of 3^o. However, the OCA of the substrate is 0^o that shows oleophilicity of the substrate, which indicates that it is susceptible to rapid fouling. The asymmetric modification process makes a surface oleophobic and substrate hydrophobic that provides condition for treatment of foulant-rich contaminated wastewater, using MD method. Additionally, the stability of the coated layer was tested by immersion of the membrane in a hot water/ethanol solution. This solution swells both layers and provides maximum layer stress. The results showed no detachment of MnO_2 nanowires that proves high interaction of coated layer [92].

2.4.3 Atomic layer deposition method

Layering technology can also be used to fabricate a Janus membrane via atomic layer deposition (ALD) method (see Figure 2-6). ALD is a precise technique used in the semiconductor fabrication process for layer-by-layer conformal growth. In this method, a metal oxide layer having a molecular-sized thickness is deposited on the desired surface without changing the structure of the pores. Therefore, this method can be used to precisely coat an oxide metal having hydrophilic features on the surfaces of hydrophobic or superhydrophobic substrate. Waldman et al. have modified the surface of hydrophobic PP membrane by deposition of hydrophilic aluminium oxides to fabricate Janus membranes. The results demonstrated that Janus membrane, having high wettability difference, was fabricated without considerable change in porosity and pore size distribution of the substrate. Also, it was revealed that the coating depth and degree of hydrophilicity can be tuned by controlling the exposure dose and time of the process. Also, the molecular precision of ALD makes it possible to provide sharp wettability differences across a narrow line on one side of the substrate. [57]

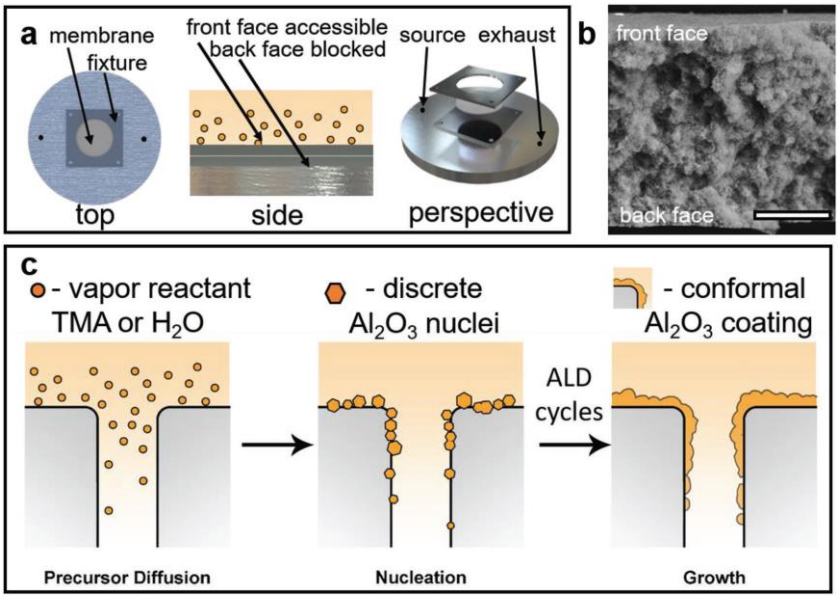

Figure 2-6. Atomic Layering Deposition Technique used for changing the characteristics of top Layer [57]

2.4.4 Other methods

Other novel methods like laser modification are also possible for surface modification and fabrication of Janus membrane. However, these methods are expensive and time-consuming and only has justification in some special applications. In this method, both sides of hydrophilic substrate are roughened and coated with low surface energy material to produce superhydrophobic membrane. Then, one side of the surface is treated with laser to scratch fluorinated or low surface energy coating [70].

In one study, Ghaleni et al. modified PVDF flat sheet membrane with concentrated KOH to graft hydrophilic functional groups on the membrane surface. During the reaction, the high alkaline condition breaks the carbon-hydrogen and carbon-fluorine bonds and generates carbon hydroxyl bonds. The zeta potential analysis performed on the modified membrane showed that the surface became more negatively charged, compared to unmodified membrane, owing to its hydrophilic structure that adsorbs more anions like OH- or Cl- from the electrolyte [49]. Some studies also used facile

fabrication of Janus membrane by simply putting hydrophobic mesh filters on top of hydrophilic substrates, usually hydrophilic fabrics like cotton. This method can be used for special applications like fog harvesting, but due to low adhesion interaction and large pore sizes of hydrophobic meshes cannot be used for applications like MD or oil-water separation [33]. Also, it is possible to premodify the membrane surface to increase the efficiency of prepared Janus membrane. For instance, The Si nanoparticles, which have been widely used to increase the roughness of the membrane, have negative charges and the membrane surface should have positive charge to make possibility of interaction of Si NPs with membrane surface. Therefore, charge modifiers like TEOS or CTAB can be used to change the charge of the membrane surface to positive. After deposition of roughening materials like silica nanoparticles, the surface of rough membrane is coated with low surface energy coating like fluorine materials to make in air omniphobic membrane. Now, the hydrophilic layer like composition of Si NP/chitosan/ perfluorooctanoate can be coated to make superb Janus membranes. If the attachment process is carried out perfectly, a high performance Janus membrane is achieved with mentioned layer characteristic [46].

2.5 Configurations of Janus membranes

2.5.1 Flat sheet Janus membrane

The easiest structure to prepare for MD application is flat sheet membranes. Although flat sheet has a low area to volume ratio and is not a favourable module for commercialization, fabrication of flat sheet membrane is useful for understanding of fundamentals of water or vapour transport phenomena of membranes. The one-dimensional structure that brings one direction mass and heat makes it easy to interpret any physical or chemical changes performed on the membrane. Therefore, it is possible

to easily understand the effect of any changes in membrane structures like thickness change, addition of nanoparticles or any additives, thermal condition of test, on the performance of MD modules. Flat sheet membranes are widely fabricated to investigate the performance of various Janus membranes [11].

Delamination is a major problem of Janus membranes fabricated through coating procedures. The solvent and nonsolvent types are important factors affecting the uniformity and integrity of the two layers. Therefore, flat sheet membranes are used for determining the effect of these parameters. In a study, the effect of changing the solvent of PVDF-based membrane on delamination was investigated. ε-Caprolactam was used as solvent for both flat sheet PVDF hydrophobic substrate layer and PVDF-PVA hydrophilic top layer. The results demonstrated that using water-soluble solvent improved the fabrication of delamination-free Janus membrane for MD application. The presence of same solvent and PVDF polymer in both hydrophobic and hydrophilic layer and also the solubility of ε-Caprolactam in the water resulted in the fabrication of an integrated Janus membrane [22, 64]. Li et al. also fabricated a flat sheet Janus membrane comprising of an omniphobic layer composed of PVDF-silica NPs coated with FDTES low surface energy as substrate and hydrophilic layer by coating of atom-transfer radical-polymerization (ATRP) on the plasma-etched substrate. The flat sheet structures helped in the investigation of the effect of the low-thickness coating of the hydrophilic layer on both the foulant and wetting resistivity of the prepared Janus membrane. Also, the effect of operating condition on flux and salt rejection was easily studied [16].

In general, the layer deposition is the simplest modification method for fabrication of Janus membrane. In this method, which is commonly applicable for flat sheet

membranes, a thin layer of desired coating solution is coated on the surface of the substrate. Due to low viscosity of the solution at the time of casting, pore wetting may be an issue for this method. Also, high viscosity solution may clog the pores of the membrane. The interaction of coating layer with the membrane substrate also is another important factor that affects the performance of the membrane for long term operation. In a study, the glutaraldehyde-PVA solution was prepared, coated, and incubated on the surface of PVDF membrane. The substrate pores were preserved from wetting by controlling the physical condition of the solution. The derived flat sheet membrane showed good coating with low pore wetting and high water productivity [98]. In some studies, before coating the main hydrophilic layer, the top surface of the membrane is pre-treated to prepare conditions for strong interaction of hydrophilic layer with the substrate. Plasma etching or coating with intermediate polymer solutions like PDA are some examples of this intervention. Although some of these methods showed superb layer interactions and great separation performance, the applicability of the suggested method for large-scale and commercial systems is not satisfied. In general, flat sheet membrane is generally thought of as not a favourable module for industrial application. Furthermore, multi-step fabrication technique increases the cost of the membrane and decreases its commercialization potential[98].

2.5.2 Hollow fibre Janus membrane

One of the most optimum modules for commercialization of water treatment application is hollow fibre membranes. This structure has a relatively high aspect ratio and low facility volume per volume of produced permeate water. Although its fabrication on a lab scale is more difficult than flat sheet membranes, it is favourable for industrial and large-scale production. Therefore, the most facile and straightforward

modification methods should be applied to hollow fibre membranes to find a shortcut path for commercialization [99]. A negative point of the hollow fibre membranes is having high pressure drop along the membrane that increases the working pressure of membrane and as a result, the wetting possibility of the membrane. Furthermore, due to the exponential correlation of vapour pressure with temperature, temperature decrease in the module and as a result, the flux dramatically decreases at the end of the membrane. Therefore, the optimum condition is to have a low length hollow fibre membrane with feed inlet through the shell side with higher contact surface area and permeate gathered through the lumen side of the membrane [24, 100-103].

Regarding high promising potential of hollow fibre membrane for wastewater treatment applications, different studies have focused on modifying or fabricate hollow fibre Janus membrane. Various types of methods have been proposed, including vapour deposition, lumen coating, outer surface coating, and co-extrusion. Among these methods, coating process is simplest method, but the homogeneity and lamination are two main problems during fabrication and operation of this type of Janus membrane. The one-step fabrication of Janus membrane is desirable to simultaneously save the time and cost. For this purpose, it is possible to use triple orifice spinneret to co-extrusion of two polymeric solution with opposite wettability characteristics. From large-scale production point of view, the co-extrusion is most efficient and applicable method for production of membrane modules. With respect to other modification methods, co-extrusion method decreases the possibility of delamination of distinct layers. However, the proper selection of dope solution and coagulant bath conditions are crucial sections of production process. The type and category of solvents used for the preparation of

both dope solutions and their interaction during extrusion and coagulation are determining the quality of the hollow fibres and the possibility of delamination. Therefore, the co-extrusion has shown great flexibility through dope preparation and fabrication process [25, 79]. Zou et al. fabricated Janus hallow fibre membrane by co-extrusion of PVDF/PEG and PVDF Si-R dope solution and NMP/water as bore fluid. One advantage of this method is the use of NMP as solvent for both dope solutions. Therefore, the unique solvent helped in the preparation of integrated membrane without separable layer. The presence of Si nanoparticles also increased the roughness of the outer hydrophobic layer, and PEG increased the hydrophilicity of the inner layer. As depicted in Figure 2-7, the composition difference makes two different morphologies for inner and outer parts of the membrane; PVDF-Si NP formed a thin hydrophobic outer surface with WCA of 137^{o} and PVDF-PEG formed thick hydrophilic inner layer with WCA of 56^{o} [101]. This difference can be attributed to the difference in inner and outer coagulation bath condition and difference in dissolving rate of polymers in coagulant solution. The presence of NMP in the bore fluid decreases the exchange rate of solvent-nonsolvent and produces porous structure with small pore sizes, whereas the pure water coagulant bath in outer surface prepared high dissolution rate and finger-like structure during phase inversion process is formed. The superhydrophobicity properties of Si-R was also effective on formation of such configuration, which prevent extensive distribution of water molecules through dope solution for NMP-water exchanging. As a result, instead of liquid-liquid mixing, solid-liquid mixing occurred and porous and triangle structure is formed. The interface of two dope solution is obvious in the SEM images (Fig 7), however the similar solvent make strong uniformity between two phases and decreased the possibility of delamination.

Although these studies proved the benefits of co-extrusion process, it has some limitations in the selection of polymer and solvent and the tolerance in the degree of hydrophilicity and hydrophobicity of Janus membrane layers. In other words, co-extrusion method compromises the wettability difference between the top and bottom layers to overcome the delamination challenge.

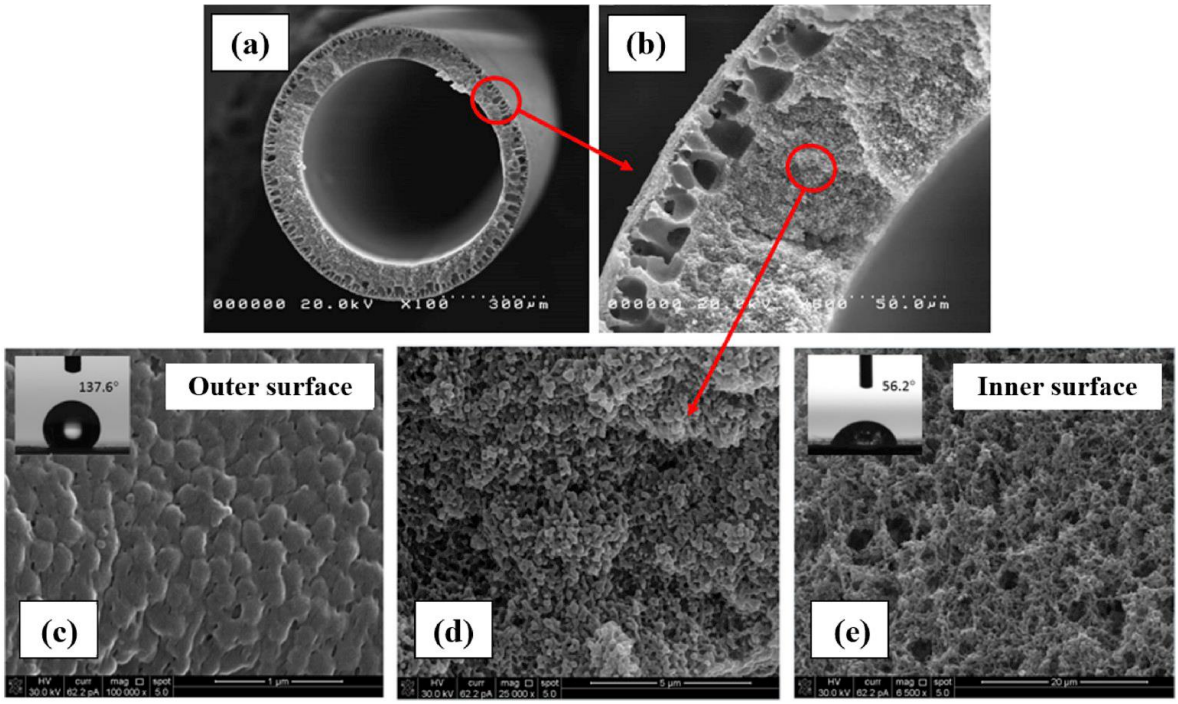

Figure 2-7. SEM images of Janus membrane fabricated using co-extrusion technique (a, b)and the inner and outer morphology and their surface WCA (c, d, e)[١٠١]

The surface modification of hollow fibre membrane is another attractive method for modification of currently industrialised hollow fibre membranes. The advantage of this method is on the modification of a standard hollow fibre membrane that have uniform and applicable substrate structure. However, the drawbacks of coating procedures are still challenging for this modification process. One of the commonly used procedures is using mussel-inspired technique to adhere hydrophilic layer in inner or outer surface of hydrophobic hollow fibre membrane. However, the modification of lumen is more

straightforward. For example, Yang et al. have modified the lumen side of PP hollow fibre membrane by coating of PDA/PEI dope solution. In this method, the dope solution is stepwise intruded through the pores of the substrate and changes the wettability of inner layer to hydrophilic ones. The thickness of hydrophilic layer can be adjusted by changing deposition time. The presence of dopamine in the coating dope made a tough and strong hydrophobic adhesion by substrate and a uniform structure was formed. The depth of penetration and thickness of hydrophilic layer of Janus membrane are measured by using an EDX scan. PDA can chelate silver ions and make bonds via its catechol groups. Therefore, Ag solution was circulated through the lumen of hollow fibre and after chelating, EDX scan was taken from the cross section of membrane to evaluate the terrace of silver ions, which is equivalent to thickness of hydrophilic layer. The results showed that about 20% of thickness of hydrophobic membrane was coated by hydrophilic layer (about 90 µm out of 450 µm) [100]. In another study, Zuo et al. focused on fabricating a Janus hollow fibre membrane by co-extrusion of PVDF and Ultem dope solutions. The bilayer Janus membrane showed more than four times higher tensile strength and 45 LMH flux than conventional one-layer PVDF membrane [104]. Polyetherimide is also a good substrate for dual layer Janus membrane fabrication for MD application, owing to its mechanical strength, hydrophilicity, and compatibility with PVDF. Even though the Polyetherimide Ultem is immiscible with PVDF, the solubility parameters of both are so close, which can make tough molecular interaction between two connected layers.

Another important point in the fabrication of bilayer Janus membrane is the concentration of polymers in dope solution. Regarding the fact that after the coating

process, the dope solutions start to shrink, the inner and outer layer's relative concentration directly influences the quality of the interface layer. In hollow fibre membranes, the shrinkage direction is towards the centre. Therefore, if the concentration of outer layer is less than the thinner layer, the shrinkage process causes the outer polymer solution to be firm around the lumen polymer solution. This transition makes a tough and tight interface layer. However, the physical properties of both layers can improve this adherence. More integrated polymeric bilayer is achieved in the case of choosing polymers with high mechanical strength for inner layer and polymer with high stretching property for outer layer. This combination stretches the outer layer on the tough support surface [65, 105, 106].

The porosity of both layers is a crucial point for fabrication of a high flux Janus membrane. Due to the fact that most polymeric layers are fabricated through phase inversion process, the coagulation bath condition is the most important parameter for adjusting the porosity of the membrane. In this state, the composition of coagulation bath, its distance from the spinneret, and also its temperature should be properly adjusted to an optimum value. Coagulation bath containing a mixture of nonsolvent (water) and polymer solvent reduces the rate of phase inversion and directs the transition phase towards more porous structure. However, very slow phase inversion causes more dense structure in inner sides of the polymer layer and achieves opposite result.

Bonyadi et al. fabricated a Janus membrane by co-extrusion of PVDF and PAN solution in the outer and inner orifice layers, respectively of hollow fibre spinneret without any defects in the layering and morphology, but the difference in expansion coefficient and

also loosing of interactions after swelling of both layer, the layers were delaminated during the DCMD test and separation process was interrupted. In another attempt to modify this drawback, they fabricated a bilayer Janus hollow fibre membrane by using PVDF as main polymer and hydrophobic and hydrophilic clays in both dope solutions. In this study, PVDF solution containing hydrophobic cloisite nanoparticles have been used as outer layer and PVDF-PAN dope solution containing hydrophilic cloisite NA as the inner solution. The presence of PVDF in both layers caused strong adhesion through co-extruding process. In this study the effect of coagulant bath composition was studied and results demonstrated that a dense and smooth surface is obtained by using a nonsolvent with strong exchange rate, like water. But using a moderate coagulant bath like mixture of methanol and water made a rough membrane with more porous membrane structure. The optimum membrane porosity was achieved for coagulant bath comprising water/methanol with concentration of 20/80 wt%, having contact angle of 140^{o} and 50^{o} for two sides [24].

2.5.3 Electrospun Janus nanofiber membrane

Electrospinning is a nanofiber fabrication method that uses electrostatic forces to produce ultrafine nanofibers with high tolerance in tunability of the structure of produced mat [107, 108]. Also, the process can be easily controlled and different polymeric solutions or compositions can be used for the process. Having these features and also advantages of fast laboratory fabrication that increases the rate of optimising of the effective parameters made electrospinning and electrospraying attractive methods for the fabrication of membranes. A bilayer electrospun Janus membrane can be fabricated by consecutive electrospinning of the substrate and top layer. In this type of membrane, the special structure and morphology of electrospun membrane make

good entanglement of electrospun nanofiber mats and produce a tough and strong bilayer composite [109]. It should be noticed that the composition of both substrate and top layer should be accurately chosen to find the highest available interaction during layering and decreasing the possibility of delamination [110].

Some studies were performed using this method, and usually a similar type of polymer for both layers is used. In other words, prepared composite dope solution for both layers have at least one similar polymer in its composition. Yue et al. fabricated a bilayer electrospun nanofiber firstly by electrospinning of PVDF-PVAc as hydrophilic substrate and then coated with electrospun PVDF nanofibers containing SiO_2 nanoparticles modified by hexamethyl disilazane, as hydrophobic layer. In the prepared membrane, the presence of modified SiO_2 enhanced the hydrophobicity of the coated layer but decreased the interaction of ENFs with the substrate layer. Therefore, in order to increase the layer interaction, it is possible to stepwise increase the concentration of modified SiO_2. At first dope solution having lower nanoparticle percentage makes stronger interaction with substrate and then dope solution having higher percentage of nanoparticles is electrospun, which increases the hydrophobicity of outer surface. Membrane analysis showed WCA increment to 170^o and a sliding angle decrement to 3^o by increase in nanoparticle concentration to 2 wt% [110]. The advantage of electrospun nanofibers is their intrinsic surface roughness that formed due to the cylindrical shape of nanofibers and multilevel structures of mats. This structure naturally increases the resistivity of the membrane against wetting problem by decreasing the interaction area and transferring the wettability state of the membrane toward the Cassie-Baxter state. Furthermore, coating of the membrane surface by nanoparticles can enhance its

roughness by the formation of a multilevel re-entrant geometry and, decreases the wetting challenge and makes electrospun nanofibers a good candidate for MD process [111].

Electrospinning is a conventional fibre fabrication technique with significant aspect ratio advantages. The nanofibers' nanoscale diameter increases the fibres' processibility for various applications. This feature makes it possible to adjust the pore size of the produced mat for special applications. Due to the micron-size pores of fabricated mats, electrospun nanofibers can be used in MD applications. Also, the layer by layer fabrication process increases the roughness of produced mats, which is highly favourable for fouling and wetting resistivity of the membranes in MD operation. This configuration can be effectively applied in fabrication of Janus membrane. The electrospinning process gives the option to coat hydrophilic electrospun nanofiber on top of superhydrophobic substrate. Also, by changing the applied voltage and physical condition of solution, it is possible to electrospray the solution on top of the membrane substrate. Electrospraying can also produce a uniform, stable, and tough covering layer and it can be used for the implantation of microsphere structures on the surface of membranes to increase their roughness to produce omniphobic or superhydrophobic membranes. Electrospinning or electrospraying can also cover a uniform and even coating on the membrane surface and decrease the presence of defects on the membrane surface. These defects are places for intrusion of oil pollutants or surfactants that decrease the efficiency of the membrane for long term operation. Regarding these privileges, electrospinning and electrospraying have been widely used for fabrication of Janus membrane for water treatment application [97, 112-114].

Zhu et al. used both electrospinning and electrospraying methods for the fabrication of breathable asymmetric Janus membrane for MD application [34]. In his study, PVDF nanofibers were first spun as membrane substrate and then Si and low surface energy agent (FAS) were added to the solution containing PVDF and polystyrene and electrosprayed to transfer the omniphobicity to the membrane surface. Afterwards, SiO_2-PAN solution was electrospray on the omniphobic substrate to fabricate Janus membrane. Proper selection of solution mixtures is an important aspect of this method. The microspheres coated for increment of roughness and decreasing of surface energy in first electrospraying step and coating of hydrophilic layer in second electrospraying stage should have adequate adhesion and durability. The attachment of polymer on top of solid polymeric layer is not very strong and it needs to consider the process of adhesion of coating layer on membrane substrate. The type of solvent used on the dope solution and its interaction with substrate polymer are important factors for increasing the stability of the coated layer. The solvent should have the ability to make a medium for interaction of quest polymer with substrate polymer. Furthermore, as much as the produced microspheres are smaller, the stability, robustness, and roughness of the coating layer are higher. Therefore, when electrospraying technique is used for membrane fabrication, the process is affected by polymeric dope composition, applied voltage, tip-substrate distance, and other operational parameters that should be adequately adjusted to produce smaller-sized microstructures. Studies revealed that the addition of nano or micro size particles can break up the production of larger-size microspheres during electrospraying process [115]. In an example, aerogel was added to the PVDF dope solution for electrospraying process. The hydrogel particles in high voltage electrospraying conditions can disrupt the PVDF solution and distribute through

the solution and make nano-sized spheres sprayed on the surface of substrate. Lower weight and higher contact area of sprayed microspheres helped increasing the interaction with substrate and enhanced durability and roughness of produced membranes.

Therefore, some additives or a mixture of some polymers should be used to simultaneously attain the desired property and strong adhesion and long durability. For example, LiCl was added to the PVDF solution of substrate to increase its conductivity that ease facile fabrication of electrospun nanofibers. Also, polystyrene has been added to PVDF-HFP-Si NPs to produce fibres having stabilized microsphere shape beads [115]. In a study, Wu et al. used subsequent electrospinning method for fabrication of Janus membrane by deposition of hydrophilic PVA on PU substrate. PVA has the hydrophilic nature and PU has hydrophobic and their combination resulted to a high performing Janus membrane with 120^{o} contact angle difference between the two sides. The processibility of electrospinning can also give the option to analyse the performance of Janus membrane having different coating thickness, by changing deposition time [116, 117].

2.6 MD performance of Janus membranes

2.6.1 Hydrophilic-hydrophobic or hydrophilic-omniphobic Janus membrane configuration

In general, higher concentration of the coating layer can block the pores and decrease the flux of membranes [9, 64]. The blockage of the pores by top layer should be recognised on the reasons for flux decrement. For example, in one study, the flux of the

fabricated membrane decreased from 29 LMH to 17.5 LMH by covering of the hydrophobic membrane by a hydrophilic layer. Though the permeate conductivity of the Janus membrane remained constant during the 600 min test, the hydrophobic membrane lost its salt rejection performance and permeate conductivity reached from zero to 200 μS/cm [16]. However, the comparison of different experimental studies have demonstrated that the value of flux decreasing is dependent on the coating procedure and also the type of used materials and in some cases the flux of Janus membrane has enhanced [32, 34, 52]. Zhu et al. have shown that while the flux of the Janus membrane is relatively equal to the hydrophobic ENF PVDF (28 LMH), its salt rejection is stable for long term application and permeate conductivity remained approximately zero during 50 hrs test experiment. This value for hydrophobic ENF PVDF reached to 75 μS/cm after 50 hrs [34].

Generally, the explanation of any process for fabrication of Janus membrane should be assessed case by case. Although the presence of thin hydrophilic layer can improve the thermal efficiency of the MD module, increment of the hydrophilic layer thickness above an optimum value can have the opposite influence. In this case, temperature polarization worsens and thick solid layer decreases the rate of water passage and, as a result, the flux decreases. Furthermore, the heat from the feed side cannot be easily transferred to the boundary layer of evaporation, and this barrier decreases the driving force of vapour transport. In general, the degree of hydrophilicity of the top layer is an important factor for the determination of the influence of the Janus membrane in separation of wastewater. Hydrophilic layer of Janus membranes with lower hydrophilic affinity has less feed transport rate and consequently the amount of water reached to

the surface of hydrophobic layer for vaporization decreases and the flux of the membrane decreases. Therefore, the selection of top layer with high wettability is desired. Also, the saturation time for the top layer is an important factor during lab work and the experimental data should be reported after saturation of top layer [4, 48]. In this way, during recent years, various materials have been used in different studies and a broad experimental data of the performance of fabricated Janus membranes was obtained. A general comparison of different studies performed by different coating materials showed relatively higher effectiveness of zwitterionic hydrophilic layers for decreasing of fouling problem and increasing separation performance. In other words, the zwitterionic made strong adhesion on omniphobic membrane without compromising the omniphobicity of substrate layer [16]. A brief comparison of different Janus membrane fabricated for MD application is shown in Table 1.

Table 2-1. Comparison of different membrane optimization methods in terms of MD permeate flux.

Hydrophilic layer	Substrate	Hydrophobic Layer	Method	ΔT	Flux LMH	Advantages	Dis-advantages	Module	WCA Hydrophobic	WCA Hydrophilic	ref
CTAB/PVDF-HFP	Nano fibre	SiNP/CTS /PFO Spray	ENF/Dip coating	50				DCMD	150	10	[46]
Dopamine -self polymerization (L)	FLAT SHEET	PTFE/PP (B)	Dip coating	50	20	Long term performance	Fabrication difficulty (3 step)	DCMD	128	30	[61]
Zwitterionic	HOLLOW fibre	Omniphobiced Quartz fibre		40	15.5	High antifouling and antiwetting	Fabrication difficulty (3 step)	DCMD	121	25	[16]
SiO_2/PAN	Nano fibre	PVDF ENF (F:SiO2/PAN, M: SiNP FAS PVDF PS, P: PVDF-HFP)	Elstrospinning Electrospraying	40	25	excellent breathability high antifouling	Low mechanical	DCMD	170	10	[34]
PDA-$AgNO_3$	HOLLOW fibre	PDA-AgNPs	HF-Coating	40	17	Antibacterial Long term	Presence of Ag in permete	DCMD	109	7.6	[43]

PVA-CNT	FLAT SHEET	PVDF	spraying	40		High fouling resistence	CNT stability	DCMD	115	33	[51]
PVA-GA	FLAT SHEET	PVDF	Dip Coating	40	25	Anti-Scaling characteristic	lower flux	DCMD	151	56	[98]
PDA-PEI	HOLLOW fibre	PVDF	Dip Coating	40	15	one-step fabrication	pore blockage	DCMD	109	25	[55]
PI	FLAT SHEET	PTFE	Dip Coating	40	8	low cost, one step,	Low Flux	DCMD	145	45	[87]
KOH-Modification	FLAT SHEET	PVDF	grafting	50	45	Simple Process	low durability	DCMD	150	62	[49]
Cotton Fabric	FLAT SHEET	PDMS	grafting			high wettability	complicated process		153		[86]
PVDF-PAN-Cloisite	HOLLOW fibre	PVDF-cloisite	CO-extrusion	90	55	High Flux		DCMD	50	140	[24]
Hydrogel	FLAT SHEET	Teflon (PTFE)	Coating	40	30	High wetting resistivity	Low stability	DCMD			[54]
PDADMAC/PAA	FLAT SHEET	PVDF		45	5	long-term robustness	Low flux	DCMD	125	50	[60]
DA	FLAT SHEET	PTFE		50	89	High flux, Antifouling		VMD	134	59	[118]
cellulose acetate	FLAT SHEET	PTFE	Electrospinning	40	20	Antifouling, Mechanical		DCMD	135	39	[119]

graphene oxide	FLAT SHEET	PVDF	dip-coating	40	25	Antifouling and	Low stability	DCMD	145		[120]
PU	FLAT SHEET	PTFE	Dip coating	40	23	Antifouling and		DCMD	130	15	[121]
EDA/PEI	FLAT SHEET	PVDF	Electrospinning and dip-coating	35	5	High oil-fouling	Low flux		127	40	[72]

Always, nature is the best reference for the production of most optimum and environmental friendly materials and instruments. Mussels have the ability to make a strong, rapid and tough adhesion to different underwater places and preserve themselves from high pressure water forces. This tough adhesive that has the ability to adhere to various surfaces has dopamine-based structure and as a result, mussels as inspired from nature have been utilized for the fabrication of materials to render attachment of different surfaces having opposite wettability tendency. In fact, dopamine has the ability to be used as an interface for attachment of hydrophilic layer on top of hydrophobic membrane substrates [32, 100]. Polydopamine is a biological adhesive inspired from mussels and formed through self-polymerization of dopamine at room condition via autoxidation in an aqueous media containing dissolved oxygen [58, 122]. The presence of catechol, quinone and amine functional groups gives hydrophilic nature to dopamine and also make it possible to make various types of interaction, including hydrogen bond, covalent bond, pi-interaction, charge transfer interaction and metal chelation, with substrate materials. This wide range of interactions made dopamine an attractive material for adhesion to substrates having various conditions like wet, dry, organic, or inorganic. This ability caused PDA to play the role of primary or intermediate layer for covering the top layer of hydrophobic, superhydrophobic, or omniphobic membranes for fabrication of Janus membranes in MD applications [18, 58, 122]. For example, Chew et al. co-deposited a hydrophilic layer of PDA/PEI on the outer surface of the PVDF hydrophobic substrate. The novelty of this work is in the co-deposition of hydrophilic layer on top of hydrophobic substrate. The hydrophilic layer made strong bond with water molecules and become hydrated and this hydrated layer

prevent membrane fouling and enhance the separation performance of the membrane [55]. In this work, the permeate flux for the Janus membrane (11 LMH) was slightly lower than hydrophobic ones (4 LMH). However, the permeate conductivity for Janus membrane was close to zero during 80 hr test (~100 % rejection). For hydrophobic membrane it stepwise increased until it reached to more than 1000 µS/cm after 20 hrs.

In another study, Wu et al also deposited PDA/PEI on the surface of PP membrane. In this work, Janus membrane was fabricated by floating of a PP membrane on solution containing dopamine and PEI. As a result, the hydrophilic layer was deposited on the substrate using mussel-inspired catechol groups of dopamine. This asymmetric configuration obtained 130^{o} wettability difference between two sides of the membrane [58]. The SEM images proved the presence of microchannels, which helped transport water molecules using hydrophilic moieties and capillary forces. Also, the MD experimental results showed that while the pore size of the outer surface of the Janus membrane compared to the neat hydrophobic membrane decreased, the flux did not decrease. This result proved that the proper selection of type and method of the top hydrophilic layer can cover its drawbacks. Also, long-term experimental results in high SDS feed water better determined the effectiveness of the prepared Janus membrane. While the neat hydrophobic PVDF membrane encountered severe wetting and fouling by increment in permeate conductivity and decrement in flux after 90 h of test, the Janus membrane still continued its good flux and salt rejection. This result demonstrated that the grafted hydrophilic layer can positively prevent the importation of surfactant and oil droplets and can prevent the Janus membrane from fouling and wetting [58].

2.6.2 Hydrophobic-hydrophilic Janus membrane configuration

Though most of research on Janus membrane was performed to investigate the effect of hydrophilic layer on feed side of the MD system, some studies have investigated the impact of hydrophilic layer on permeate side of the MD modules. In these works, the hydrophilic face of the Janus membrane was placed toward permeate side. In a study performed by Zou et al, a hydrophilic layer containing PEG was coated on hydrophobic substrate and separation and energy performance of prepared Janus membrane was investigated by placing its hydrophilic side toward permeate side of the module, while the feed side of the membrane was hydrophobic. The change in energy performance of the Janus membrane was compared to neat hydrophobic membrane and results proved that co-extruding of a thin PVDF/PEG hydrophilic layer on the PVDF hollow fibre substrate enhanced the energy efficiency of the membrane from 55% to 72%. This increase can be attributed to the presence of highly porous and hydrophilic layer on permeate side that improves the condensation rate of the evaporation layer. Also, the hydrophilic layer prevents the intrusion of permeate water into the pores and decreases the wetting possibility. Experimental results revealed that the salt rejection, flux and heat efficiency of the membrane have decreased in long-term tests, and wetting problem occurred after 200 h of operation [65]. In general, in this type of Janus membranes, the bottom layer should have high heat conductivity to easily transfer the released heat of condensation and maintain the driving force of water transport [4, 90, 123].

2.7 Challenges facing Janus membranes in MD

Regardless of the type of method used for fabrication, Janus membranes have encountered two main challenges, which cause problems in the way of their performance and potential commercialization. First, due to different chemical structure of hydrophobic and hydrophilic layers, Janus layers have weak interaction with each other and have been delaminated after a period of time of operation. This poor compatibility is a crucial point for long term application of Janus membranes. Second, only the hydrophilic layer can repel hydrophobic foulant and low surface compounds, like surfactants, and if these foulant can pass through the hydrophilic layer, they can cause wetting of the hydrophobic layer beneath [22, 32, 34, 65].

2.7.1 Delamination

Delamination is one of the main issues facing the use of Janus membranes. As per design structure of a Janus membrane, it consists of two layers with opposing wettability, which means that the layers could be made of different materials that are not affinitive with each other without proper modification. For example, in general Janus membrane fabrication, the hydrophobic substrate is firstly modified to form re-entrant structure on the surface and coated with low surface energy materials converting it into omniphobic membrane. The omniphobic membrane then becomes the substrate to coat a hydrophilic layer on top to form the Janus membrane, but the low surface energy coating on the omniphobic membranes decreases the interaction of coated hydrophilic layer and a weak adhesion is formed that making it less robust and stable. This problem is exacerbated during the water treatment process when the top layer becomes hydrated. Due to the difference in

wettability of the contacted layer, the swelling of hydrophilic layer increases interaction conflicts and may cause membrane delamination problems. Therefore, high attention should be paid to simultaneously improve layer adhesion and separation performance of Janus membrane [9, 12, 35]. The schematic of the delamination process is shown in Figure 2-8.

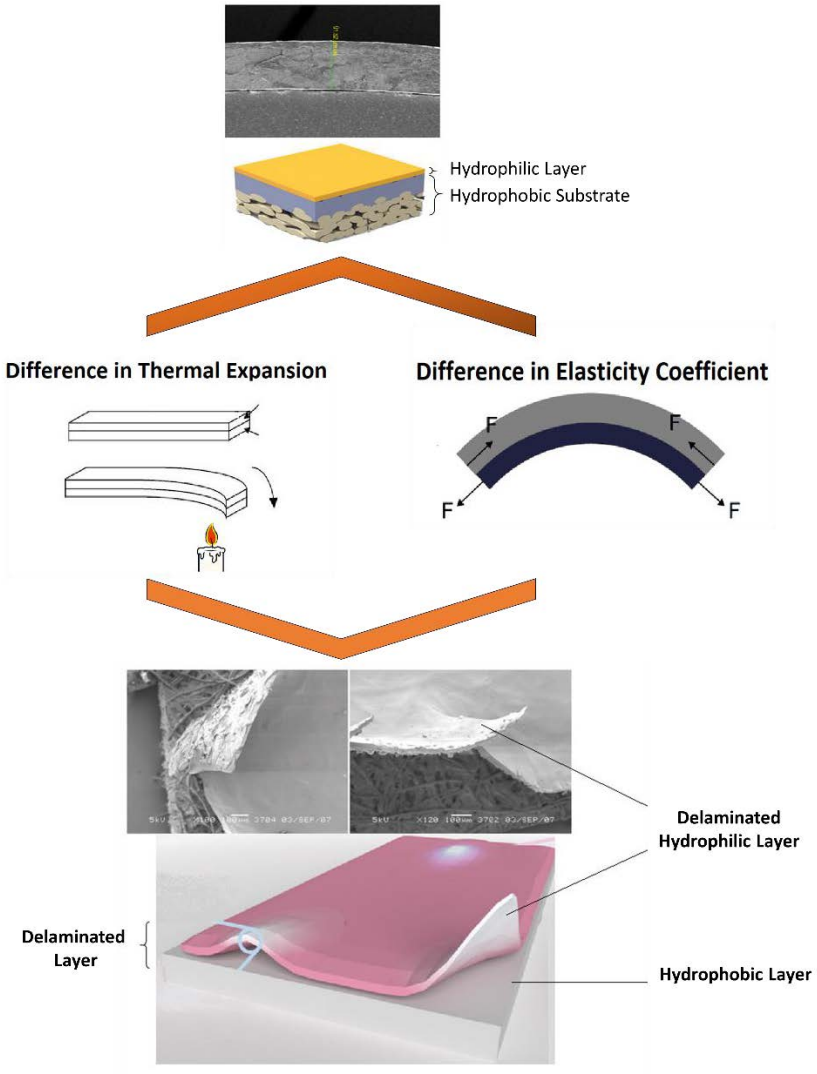

Figure 2-8. The schematic of delamination process for Janus membrane

Although the fabrication of multi-layer polymers has been widely progressed in recent years, delamination still remains as an issue in this process. In general, the difference in physical and chemical properties of both layers make it a balancing challenge between attachment and detachment forces. Also in some studies, in order to increase the accuracy and quality of the top layer, the hydrophilic layer was coated using layer-by-layer method and through some steps. This layering coating causes distribution of exerted stress across the coated layer and, in real operational condition, sequential detachment takes place for a multilayer surface (as shown in Figure 2-8). The delamination in coating process generally refers back to one of following two mechanisms: (1) difference in phase inversion process during coagulation step, and (2) difference in shrinkage coefficient of layers in both sides of coating layer. In order to decrease the delamination, the best choice is by selecting dope solution coming from similar solvents and/or the same polymer family. Using similar solvent helps adhesion of distinct layers to form an integrated coating. However some studies have indicated that using similar solvents caused achievement of good attachment of coated layer on the substrate to form Janus membrane, MD test results indicated that this method compromised the wettability of coated or substrate layers. As a result, the separation performance is lower compared to Janus membranes which have high wettability difference between two layers.

Another issue during phase inversion process of Janus membranes is that the structure and phases of layers can change. If the two layers are formed with different coagulation rates, two separate layers are formed that have low attachment with each other. Therefore, besides the selection of dope compositions and their compatibility, the ternary phase

inversion of both layers should be compared to find the difference in phase inversion rates. Furthermore, Janus membranes operated in temperatures below or beyond the ambient temperature has led to shrinkage or expansion during the process. This indicates that one has to consider the differences in shrinkage coefficient that can amplify the stress and strains on the polymers and on the coated layer further exacerbate layering and delamination problem [38, 124]. To address this drawback, many groups have used various new fabrication techniques, like co-extrusion for hollow fibre membranes, co-casting for flat sheet membranes, addition of diluents or additives, and proper selection of polymers according to their phase diagram [27, 125-127].

In general, the quality and robustness of coated layers to avoid delamination problem are tested via exposing them to harsh conditions. One way is by immersing the membrane in an ultrasonic bath for a long time, which exposes it to constant stress and strain from ultrasonic waves. Analysis is then carried out to determine the condition and amount of the coated layer with respect to its previous condition. One study utilized FTIR to determine the functional groups on a coated PVDF Janus membrane after exposing it to ultrasonication for 10 minutes. The results showed the presence of functional groups that make strong attachments between layers, which were corroborated by the EDX and DCMD results [9, 43].

To enable good interaction of the hydrophilic layer with the substrate for strong adhesion, some groups used a pre-treatment process to prepare an omniphobic substrate for strong coating step [43, 58]. Studies have shown that a hydrophilic dope solution needs active sites

on the omniphobic layer to attach to it. Direct coating of top hydrophilic layer will not render it effective due to the absence of active sites on the previously generated omniphobic surface. This is because omniphobic substrates naturally repel almost all types of liquid and do not let the solvents make active sites. Forming fluorocarbon sites on the omniphobic surface is a good strategy but it needs high activation energy, equivalent to a temperature of 90^{o}C. The plasma etching technique is a good pre-treatment method to effectively produce active sites on the omniphobic surface prior to coating of hydrophilic layer. A study has utilized such a pre-treatment strategy and strong interaction between the coating layer and the omniphobic layer was observed, and no delamination was found after DCMD test. Compared to other fabricating techniques of Janus membranes, high and stable MD separation performance was observed for this Janus membrane [69].

2.7.2 Reduced vapour transport

Another challenge for Janus membranes, which usually comes along with a delamination problem, is dense interface morphology issue that provides resistance against vapour transport across the membrane for MD application. The compactness at the interface of coating layer generally decreases the effective surface area, and as a result decreases the flux of the membrane. For example, Lin et al. coated a porous hydrophobic PTFE membrane by hydrophilic hydrogel to enhance its antifouling and anti-wetting performance, but the compactness and blockage of the pores decreased the flux of the membrane for DCMD application from 30 LMH to 23 LMH [54]. In another study, Wang et al. utilized chitosan to modify hydrophilic PVDF membrane and results showed 15% flux decline with respect to neat PVDF membrane (reached 26 LMH from 31 LMH) [3]. However, the modified

membranes showed significantly better antifouling and antiwetting performance. One potential way to address both delamination and dense interface morphology problems is by manipulation of the concentration and composition of dope solution and fabrication using the co-extrusion method. Zuo et al. have used this method and fabricated a membrane with different dope compositions to find the most optimum point for decreasing the delamination [104]. The dense interface morphology was overcome by the addition of alumina nanoparticles to the inner layer of the co-extruded orifice. In this condition, alumina nanoparticles made some defects on the polymeric matrix layer and increased the porosity and, consequently, decreased the dense morphology. This resulted to enhanced flux performance. However, overuse of nanoparticles also decreased the mechanical strength, the separation performance, and the top-layer attachment to the membrane [104]. Thus, balance must be performed when designing a Janus membrane material with regards to the structure of the coating layer while maintaining strong adhesion to the substrate material.

2.7.3 Scaling problem in Janus membrane

In the DCMD process, during water vaporization and vapour transport across the pores, the salt concentration in the membrane-feed water interface increases. Additionally, due to heat loss through the membrane matrix and also latent heat conversion, the temperature of feed layer close to the surface decreases and is lower than the temperature of the bulk. This situation transfers concentrated water into supersaturated zone and prepares condition for formation of mineral scaling by deposition of excess minerals at the interface layer. Therefore, due to intrinsic hydrophilicity of the formed scales, the hydrophobicity of

the membrane surface decreases, which can increase the probability of wetting and diminish LEP of the membrane. Also, further increase in scales can block the membrane pores and simultaneously decrease the flux of the membrane. Therefore, scale formation, which has separate characteristics from fouling problem, should be noticed for long-term operation of the MD membranes [65, 128]. One of the commonly used methods for cleaning the scaling on the surface of the membranes is membrane regeneration. In this method, the scales are physically or chemically removed from the membrane surface after a period of time. Although membrane regeneration increases the applicability of the membrane, in general, due to potential changes in the physical and chemical structure of the membrane pores, the performance of the regenerated membrane is not similar to that of the neat membrane. All in all, the most cost-effective method is preventing the formation of scales on the membrane surface [65].

Due to high salinity and contamination of feed water in MD process, the scaling is highly susceptible to form and is one of the major problems of MD modules. According to nature of feed water, different types of scales may be formed. The most common types of MD scales are calcite, gypsum, and silica. The gypsum and NaCl scales form through crystallization mechanism, while silica scale is formed by polymerization of silica acid, a non-crystallization method. Anti-scalants are widely used to mitigate the crystallization and formation of scales, but due to amorphous structure of silica minerals, most of used anti-scalants showed weak performance for decreasing silica scale formation [4, 129]. The presence of silica scales has been reported in long-term application of MD for treatment of RO, Brackish, and shale gas wastewaters [130, 131].

In general, the scaling can be formed through two pathways: homogenous or heterogeneous nucleation. In homogenous nucleation scaling, by supersaturating of minerals in small liquid parts, the scale particles spontaneously formed in that place. By increasing the concentration of minerals by evaporation of liquids, homogenous scaling continues to form, and scales are formed and deposited on the surface of membranes. Heterogeneous scaling is another type of scale that is formed at the liquid-solid interface. In this type of scaling, the interaction between dissolved minerals and membrane surface plays the main role in scale formation. Therefore, the physical and chemical characteristics of the membrane surface determine the level of scaling [56, 132].

Until now, different studies have focused on mitigation of fouling and wetting in MD process, usually by organising roughness of the surfaces and coating them with low surface energy materials. Though these modification methods could effectively diminish fouling and wetting problems, the scaling challenges still need additional attention for the commercialization of MD membranes [98, 132]. In order for deep investigation of the scaling issue, the composition of fresh and used membranes should be analysed by EDX to investigate the type of crystals formed on the surface of the membrane after wastewater treatment by MD. In a study performed by Zou et al., the new peaks were observed in the used membrane, which were relevant to the oxygen, irons, calcium, and magnesium. The results demonstrated that sulphate, carbonate, and hydroxide scales are formed on the membrane surface. Comparison of the intensity of the peaks revealed that the calcium carbonate is one of the main scales formed on the surface of membrane. However, the membrane used for treatment of RO brine usually has large proportion of sodium chloride

scales, and the composition of wastewater determines the most dominant scales formed on the membrane surface [65, 133].

Additionally, silica formation is another major scaling problem in the application of MD process. Although the formation of homogenous nucleation depends on the characteristics of feed water, the main challenge of scaling is formation of heterogonous nucleation that attach to the membrane surface, gathers homogenous silica scales and increases the volume of scales on the surface. For this reason, different studies were carried out to decrease the side effect of scale formation by enhancement of membrane surface geometry and structure to decrease slippery angle of the membrane, which directly causes a decrease in formation and attachment of heterogeneous nucleation on the membrane surface [134, 135]. In a study, Yin et al. performed a DCMD test to investigate the behaviour of Janus and hydrophobic membranes during scale formation in a high SDS feed water. The feed solution containing different concentrations of amorphous silica, NaCl, and gypsum scales was prepared and the test was performed on three different membranes: hydrophobic PVDF membrane, PVDF-SiNP-FAS superhydrophobic, and PVA/PVDF-SiNP-FAS Janus membrane. The sliding test was performed on the membranes and results show that while hydrophobic membrane showed high WCA, the water droplet didn't slide from the membrane surface. Furthermore, water droplet starts to slide at sliding angle of 17^{o} for superhydrophobic membrane [98].

Also, dynamic light scattering (DLS) test was used to determine the hydrodynamic diameters of the scales formed during the MD test. All membranes showed perfect

separation performance during DCMD test for feed water with initial saturation index of -0.82. In this condition, only small heterogeneous silica scales were formed on the membrane surface, without affecting the performances of the membranes and structures of the pores. For the feed water with silica saturation index of 0.55, gel-like silica scales with the size of 100-200 nm were formed in all membranes and the flux decreased for all of them, but Janus membrane experienced lower decrease in performance. In this condition, due to high concentration of silica, the homogenous nucleation of silica particles can react with silica acids and form a cross-linked structures which can attach to the membrane surfaces. Continuous formation and attachment of this particles can clog the membrane pores and also change the wettability of the membrane surface. As a result of this silica-silica interaction and formation of both heterogeneous and homogenous silica nucleation, the flux of the membrane decreased and the conductivity of permeate increased. The results of this experiments showed that the formation of scales decreased the flux of Janus membrane, similar to hydrophobic and superhydrophobic ones, by clogging the membrane pores. Even though the scale formation changed the wettability of the hydrophobic or superhydrophobic membranes, it did not change the wettability of the Janus membranes [49, 98]. All in all, the flux decline in superhydrophobic membrane was less than others, but the Janus membrane derived the highest water productivity. In order to remove the formed scales on the membrane surface, the Janus membrane can be regenerated using custom backwashing method. Zou et al regenerated the Janus membrane and then analysed the membranes for evaluation of its performance. The experimental results showed that after 16 h of test, the water recovery of the membrane became about half of the fresh membrane

after three days of continuous test. This result proved that the formation of scales on the Janus membrane deformed the structure of the pores and the stability and the shape of the membrane changed and lost its high salt rejection and water recovery in long term operation [65].

2.7.4 Formation of microdefects on hydrophilic layer

Besides the delamination problem, the coating of a hydrophilic layer on top of an omniphobic or a hydrophobic layer can face another challenge: the formation of microdefects during formation or polymerization of hydrophilic layer, which can produce microchannels, resulting to a decrease in salt rejection of the membrane. To address this challenge, the coated hydrophilic layer using common methods is usually exposed to drying and hydration steps before their application in real wastewater treatment. Also, sometimes during the real test, the membrane may go to a recovery or maintenance mode and get dried. The changes in hydration (consecutive drying and wetting) can affect the structure of the hydrophilic layer and produce some defects that decrease the performance of the membrane. To cover this deficiency, in some studies production of multilevel structure was suggested. Also according to Wenzel theory, similar to hydrophobic surfaces that higher roughness increases hydrophobicity of the membrane, roughness increment in hydrophilic layer can increase the hydrophilicity of the top layer. For example, Chew et al. fabricated a Janus membrane by coating of self-polymerized PDA layer on top of PVDF porous hydrophobic substrate. The wetting and fouling tests on the prepared membrane was carried out using 500 mg/L Tween 20-stabilized petroleum-in-water emulsions and results showed better performance for Janus membrane with respect to neat PVDF membrane.

The neat PVDF membrane encountered severe wetting and fouling after 20 h operation, but the Janus membranes showed slight wetting and fouling after 50 h of experimental test. The analysis was carried out to determine the source of decrease in the efficiency of Janus membrane and, in this way, the SEM images showed presence of microvoids that work like channels to transmit fouling and wetting agents to the hydrophobic layer beneath hydrophilic top layer and, therefore, decrease in the performance of the membrane can be attributed to these voids.

In order to heal these features, Janus membrane can be coated with nanoparticles to cover the formed microchannels or prevent the formation of these microvoids during hydration stresses. In a study, the surface of hydrophilic layer was coated with Ag nanoparticles using immersion techniques (Figure 2-9). The experimental DCMD results showed perfect performance even after 96 hr test without compromising the flux or salt rejection. The Ag nanoparticles could effectively cover the microchannels and prevent the entrance of low surface energy compounds or oil droplets, even in high oil and surfactant-contaminated feed water [43].

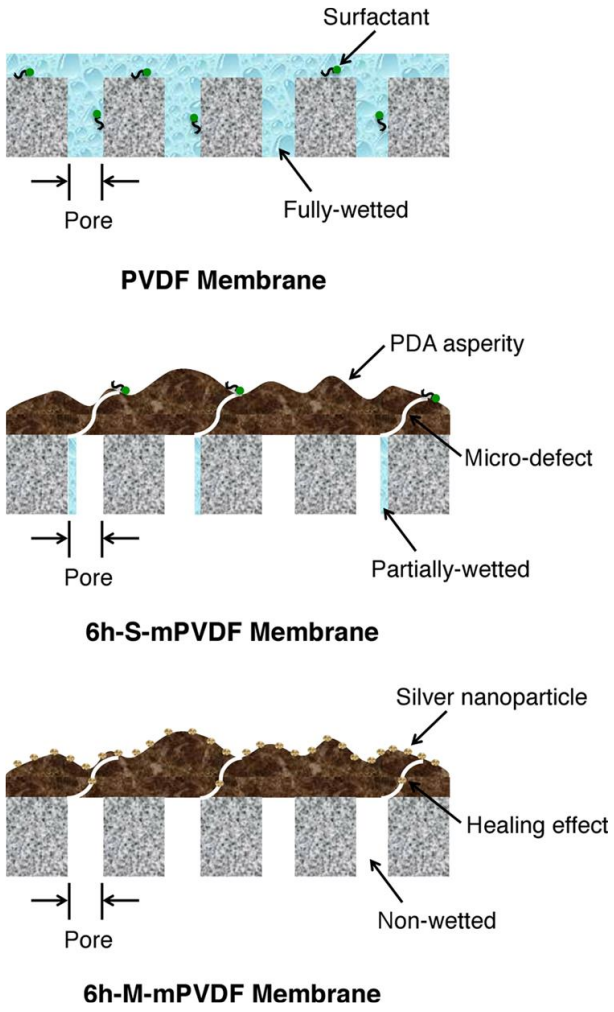

Figure 2-9. the effect of dispersion of silver NPs on the wetting resistance of Janus membrane [43]

2.8 Applications of Janus membrane in MD process

Membrane distillation (MD) is a promising technology with various applications, including the desalination of hypersaline water, treatment of challenging water, and nutrient recovery from human urine or leachate. Hypersaline water refers to water sources that have extremely high salinity levels, often exceeding the salinity of seawater. Desalination of hypersaline water and challenging water is particularly challenging due to the high

concentration of dissolved solids, such as salts and minerals [136]. Therefore, special technology is required to treat these challenging waters. MD process utilizes low-grade thermal energy to increase the vapour pressure of the feed side and make a driving force over two sides of the membrane. Compared to other methods for the treatment of challenging water, the advantage of the MD process is that its separation performance has a low dependency on the concentration of the impurities in the feed stream [137].

On the other hand, the consumption trend of nitrogen-based fertilizers worldwide has shown consistent growth over the past few decades. Nitrogen is a vital nutrient for plant growth, and nitrogen-based fertilizers are widely used in agriculture to enhance crop productivity. The global consumption of nitrogen-based fertilizers has witnessed a steady increase, driven by various factors. Population growth, urbanization, and changing dietary patterns have led to a rising demand for food. This, in turn, has increased the need for nitrogen fertilizers to support higher crop yields and ensure food security [138, 139].

The consumption of nitrogen-based fertilizers varies across regions. Developing countries, particularly in Asia, have grown substantially in fertilizer consumption. Countries like China and India, with large agricultural sectors and increasing populations, have significantly increased their use of nitrogen fertilizers. In contrast, developed regions like North America and Europe have relatively stable or slightly declining consumption trends due to factors such as improved fertilizer application practices and environmental regulations [140, 141].

The intensive use of nitrogen-based fertilizers has raised concerns regarding environmental sustainability. Excessive fertilizer application or improper management can lead to nutrient

runoff, water pollution, and greenhouse gas emissions. There has been a growing emphasis on adopting sustainable nutrient management practices, optimizing fertilizer application rates, and promoting nutrient stewardship to minimize environmental impact.

Ongoing research and innovation efforts focus on developing nitrogen-efficient crop varieties, enhancing fertilizer formulations, and exploring alternative sources of nitrogen. These include bio-based fertilizers, organic amendments, and biological nitrogen fixation methods, which aim to reduce dependence on synthetic nitrogen fertilizers and minimize environmental risks [138, 140].

Nutrient recovery from human urine and leachate is of significant importance for several reasons. Urine and leachate contain valuable nutrients essential for plant growth. By recovering these nutrients, we can minimize the use of synthetic fertilizers and promote sustainable agricultural practices. When urine and leachate are not properly managed, they can contribute to water pollution. Excess nutrients, such as nitrogen and phosphorus, can leach into water bodies, leading to eutrophication, harmful algal blooms, and degradation of aquatic ecosystems. By recovering these nutrients, we can prevent their release into the environment and mitigate these negative impacts. Moreover, nutrient recovery from urine and leachate is a part of a circular economy. Rather than treating these waste streams as pollutants, we can transform them into valuable resources. The recovered nutrients can be used as fertilizers or processed into other products, closing the nutrient loop and reducing waste generation [142-144].

However, due to hazardous chemicals like pharmaceuticals or heavy metal ions in human urine or leachate, it is essential to focus on the production of reliable fertilizers and prevent the side effects of hazardous substances on fertilisers. MD process is a reliable method that can be used to separate the ammonia to produce hazardous-free nitrogen-based fertilizer effectively directly. This section explains the application of the MD process and Janus membrane in the treatment of hypersaline water and nutrient recovery from human urine and leachate.

2.8.1 Treatment of Hypersaline water

Membrane distillation offers a potential solution to overcome the treatment of hypersaline water. It operates on the principle of selective vaporization and condensation. The process involves the use of a hydrophobic membrane that acts as a barrier, allowing only water vapour to pass through while rejecting dissolved solids.

The advantages of membrane distillation for hypersaline water desalination include high salt rejection, tolerance to feedwater salinity, low fouling potential, and low-grade heat utilisation. The hydrophobic membrane selectively allows water vapour to pass through, leaving behind the dissolved salts and impurities. This leads to high salt rejection rates, enabling the production of high-quality freshwater. In addition, MD exhibits high tolerance to hypersaline feedwater, making it suitable for treating water with extreme salinity levels. It can handle brines, produced water from oil and gas operations, and other highly concentrated saline solutions. Furthermore, the hydrophobic nature of the membrane

reduces the likelihood of fouling due to mineral scaling or organic fouling. This allows for more prolonged operation without frequent cleaning or maintenance, resulting in higher system efficiency and reduced operating costs. MD can additionally be driven by low-grade heat sources, such as waste heat from industrial processes or solar energy, making it an energy-efficient desalination option [145-147].

The application of Janus membranes in membrane distillation for the desalination of hypersaline water is an emerging area of research and innovation. In the context of membrane distillation, Janus membranes offer several advantages and enhanced capabilities compared to conventional membranes. Janus membranes have different surface properties on each side. One side is typically hydrophilic, promoting water vapour transport, while the other side is hydrophobic, preventing the passage of liquid water. This design enables a more efficient separation between the feedwater and the condensing side [148, 149].

In addition, the asymmetric nature of Janus membranes allows for improved heat transfer during membrane distillation. The hydrophilic side enhances the absorption and transport of heat, facilitating the vaporization of water on the feed side, while the hydrophobic side aids in the condensation process on the permeate side.

Wetting occurs when liquid water penetrates the membrane pores, impeding vapour transport and reducing the overall efficiency of the process. By incorporating a hydrophobic surface on one side of the membrane, Janus membranes exhibit reduced wetting

tendencies, minimizing the negative impact on performance and prolonging the membrane's operational lifespan.

The dual functionality of Janus membranes allows for better control over the transport of dissolved salts. The hydrophilic side selectively transports water vapour while rejecting salts, ensuring a higher salt rejection rate and producing purer water on the permeate side [90, 101].

In a study carried out by Li et al., neat hydrophobic and Janus membranes were fabricated and their performance was compared. While Janus membranes with hydrophobic PVDF substrate showed the highest flux, their salt rejection was lower than Janus membranes with omniphobic substrate. The covering of the PVDF substrate with fluorinated layer enhanced the salt rejection of the Janus membrane. Also, the comparison of the flux of Janus membranes with hydrophobic and omniphobic membrane showed that the Janus membrane has higher separation performance for both flux and salt rejection [52]. Experimental results showed that while the flux of hydrophobic membrane was 15 LMH and it decreased to 14 LMH for omniphobic membrane, the Janus membrane showed flux of about 20 LMH without compromising the salt rejection. These characteristics can be attributed to the presence of hydrophilic layer, which helps bring the hot feed water into the pores of the omniphobic membrane substrate for evaporation. Furthermore, in the case of using low concentration of hydrophilic solution, these materials can intrude into the beneath pores without blocking of the pores and decrease the thickness of hydrophobic or omniphobic layer and therefore increase the mass transfer ratio.

In addition, Janus membranes can exhibit improved fouling resistance compared to conventional membranes. The hydrophobic side repels organic compounds, minerals, and other fouling agents, reducing the likelihood of fouling and enabling longer operation times before cleaning is required. Janus membranes offer the flexibility to tailor the membrane design based on specific application requirements. By adjusting the composition and properties of each side, researchers can optimize the membrane for hypersaline water desalination, enhancing performance and efficiency.

In a study, Tang et al. have fabricated a anti-wetting and anti-fouling multifunctional Janus membrane by optimization of reentrant structure size and hydrophilic layer position [150]. They have utilized a straightforward approach to fabricate a dual-layer bioinspired membrane using a two-step electrospray technique. The resulting composite structure exhibited exceptional properties, including high omniphobicity (WCA= 159°) and underwater superoleophobicity (underwater oil contact angle of the hydrophilic top surface measured at 152 °). Additionally, the fabricated Janus membrane demonstrated robust wettability across a broad pH range of 1–14. In continuous MD treatment of emulsified oily hypersaline solutions, the Janus membrane displayed stable permeate flux and excellent salt rejection (approximately 100%). These impressive performances were attributed to the combined effects of the hydration properties of the hydrophilic top layer and the cavitation and slip boundary effects of the reentrant structure. The Janus membrane's anti-wetting and anti-fouling characteristics remained robust throughout the treatment process. The novel bioinspired Janus membrane holds promise for the treatment of challenging wastewaters, such as shale oil produced-water [150].

It's important to note that the application of Janus membranes in membrane distillation is still an active area of research, and further development is needed to optimize their performance, durability, and scalability. Nonetheless, their unique characteristics hold promise for addressing the challenges associated with the desalination of hypersaline water.

2.8.2 Nutrient Recovery from Landfill Leachate

Leachate, a liquid that emerges from landfills and other waste disposal sites, contains a diverse range of contaminants, including nutrients. These nutrients, if not properly managed, can contribute to environmental pollution and pose a risk to ecosystems. However, in recent years, there has been growing interest in developing technologies and strategies to recover valuable nutrients from leachate, turning it into a potential resource for sustainable nutrient management [142, 150, 151]. There are some methods of nutrient recovery from leachate that are generally categorised as follows [151-153]:

Chemical Precipitation: One common method for nutrient recovery from leachate is chemical precipitation. This technique involves adding specific chemicals to leachate, causing the precipitation of nutrients such as phosphorus in the form of struvite. Struvite can be further processed and used as a slow-release fertilizer in agriculture.

Biological Processes: Various biological processes, such as anaerobic digestion and microbial transformations, have shown promise in nutrient recovery from leachate. Anaerobic digestion can convert organic matter in leachate into biogas while also facilitating

nutrient recovery. Microbial transformations, including denitrification and nitrification, can convert nitrogen compounds in leachate into forms suitable for nutrient reuse.

Membrane Filtration: Membrane filtration techniques, such as reverse osmosis and nanofiltration, can be employed to separate and concentrate nutrients from leachate. These processes use semi-permeable membranes to selectively remove contaminants, leaving behind a nutrient-rich concentrate that can be further processed.

However, these methods encounter with some challenges and need some considerations. The composition of leachate can vary significantly depending on the waste type, age of the landfill, and environmental conditions. This variability presents challenges in designing nutrient recovery processes that can effectively handle the diverse characteristics of leachate. Moreover, the leachate often contains high concentrations of various contaminants, including heavy metals and organic pollutants. These contaminants can interfere with nutrient recovery processes, affecting their efficiency and the quality of the recovered nutrients. Therefore, appropriate pre-treatment steps may be required to remove or mitigate the effects of these contaminants. Additionally, implementing nutrient recovery technologies for leachate can be technically complex and expensive. The selection and optimization of appropriate recovery processes, along with the necessary infrastructure and operational costs, pose challenges for large-scale implementation [138, 153].

The application of Janus membranes in membrane distillation for nutrient recovery from leachate is an innovative approach that shows potential in addressing the challenges associated with treating leachate and extracting valuable nutrients from wastewater

streams. Leachate refers to the liquid that drains or leaches from landfill sites, containing various organic and inorganic contaminants, including nutrients. Janus membranes can be designed to transport certain components selectively while rejecting others. In the case of leachate treatment, the hydrophilic side of the Janus membrane can facilitate the transport of water vapour, while selectively allowing the passage of dissolved nutrients such as nitrogen and phosphorus. By leveraging this selective transport property, Janus membranes enable the recovery of valuable nutrients from leachate, which can be used for various purposes, such as agricultural fertilizers or nutrient-rich solutions for hydroponics.

The asymmetric nature of Janus membranes provides enhanced separation efficiency in the membrane distillation process for nutrient recovery. The hydrophobic side of the membrane repels liquid water and contaminants, allowing only water vapour and ammonia gas to pass through. This design minimizes fouling and enhances the purity of the recovered nutrient stream.

Recovering nutrients from leachate using Janus membranes aligns with the principles of resource conservation and environmental sustainability. By extracting valuable nutrients from leachate, the process reduces the environmental impact of landfill sites and provides a potential source of nutrients that can be recycled and reused, mitigating the need for synthetic fertilizers and minimizing nutrient pollution in water bodies [153, 154].

While the application of Janus membranes in membrane distillation for nutrient recovery from leachate shows promise, it is important to note that further research and development are needed to optimize membrane performance, ensure long-term durability, and address

scalability and cost-effectiveness considerations. Nonetheless, this approach represents a potential solution for sustainable nutrient management and resource recovery from wastewater streams, contributing to the circular economy and environmental stewardship.

Recovered nutrients from leachate can be utilized as fertilizers in agriculture, reducing the dependency on synthetic fertilizers and closing the nutrient loop. In addition, nutrient recovery from leachate is a part of circular economy, as it transforms waste into valuable resources. By recovering nutrients, we can conserve natural resources and reduce the environmental impacts associated with conventional nutrient extraction and production methods.

Certain nutrient recovery processes, such as anaerobic digestion, can generate biogas as a byproduct. This biogas can be utilized for energy generation, reducing the reliance on fossil fuels and contributing to renewable energy production [154, 155].

Nutrient recovery from leachate presents a promising approach to transform a waste stream into a valuable resource for sustainable nutrient management. Various methods have shown potential for recovering nutrients from leachate. However, challenges related to leachate variability, contaminant interference, and technological complexity need to be addressed for successful implementation.

2.8.3 Nutrient recovery from Human urine

The recovery of nutrients from human urine has gained significant attention in recent years due to its potential to address environmental and resource challenges.

Human urine is a valuable source of essential nutrients, including nitrogen, phosphorus, and potassium, as well as trace elements and organic matter. Traditional wastewater treatment systems fail to harness the potential of urine as a resource, resulting in the loss of valuable nutrients and the contamination of water bodies. Nutrient recovery from urine not only reduces pollution but also provides an opportunity for sustainable resource management [156, 157].

Nutrient recovery from human urine is an innovative and environmentally sustainable approach that aims to harness the valuable resources present in our everyday waste. Human urine, often considered a waste product, contains significant amounts of essential nutrients, which are vital for plant growth and soil fertility. Instead of letting these valuable nutrients go to waste, various methods and technologies have been developed to recover and recycle them, turning urine into a valuable resource for sustainable agriculture and nutrient management [139].

Nitrogen is an essential element for life, and its concentration in human urine presents an intriguing opportunity for nutrient recovery and sustainable resource management. Human urine contains a significant amount of nitrogen in the form of urea, a compound excreted by the body as a waste product of protein metabolism. The conversion process of urea to ammonia, known as hydrolysis, plays a crucial role in the release and subsequent recovery of nitrogen from urine. Understanding the concentration of nitrogen in human urine and the hydrolysis process is vital for harnessing this valuable resource and promoting its utilization in various applications [158, 159].

The concentration of nitrogen in human urine can vary depending on factors such as diet, age, and overall health. Human urine contains approximately 9 grams of nitrogen per liter, making it a concentrated source of this essential nutrient [156]. Harnessing and recovering this nitrogen not only has implications for sustainable agriculture but also offers opportunities in industries such as wastewater treatment, bioenergy production, and environmental remediation.

The hydrolysis of urea to ammonia is a chemical reaction that occurs naturally in urine, facilitated by the enzyme urease. Urease catalyzes the conversion of urea, a relatively stable compound, into ammonia (NH_3) and carbon dioxide (CO_2). This process is influenced by various factors such as temperature, pH, and the presence of urease-producing microorganisms. Hydrolysis is an important step in the nutrient recovery process, as it transforms urea, a form of nitrogen that is not readily available for plants, into ammonia, which can be utilized by plants as a nitrogen source [139, 156, 160].

The conversion of urea to ammonia holds great significance in agricultural practices. Ammonia is a crucial component in the production of nitrogen-based fertilizers. Through the hydrolysis of urea, ammonia can be captured, processed, and transformed into a usable form for agricultural applications. This sustainable approach reduces the reliance on synthetic fertilizers derived from non-renewable resources and minimizes the environmental impact associated with their production and use.

Moreover, the hydrolysis process of urea to ammonia also plays a role in wastewater treatment. In wastewater treatment plants, the hydrolysis of urea helps in breaking down

organic nitrogen compounds, reducing their potential harmful effects on the environment. The generated ammonia can then be further processed to remove it from wastewater, preventing nitrogen pollution in water bodies and promoting cleaner water management practices [139, 156].

The concept of urine nutrient recovery aligns with the principles of the circular economy, where waste is considered a valuable input for another process. By recovering nutrients from urine, we can reduce the dependency on synthetic fertilizers, which require extensive energy and resource inputs for production. Additionally, the recovery process reduces the environmental impact associated with nutrient pollution from conventional wastewater treatment plants, where urine is typically diluted and mixed with other wastewaters, leading to excessive nutrient discharges into water bodies.

Moreover, urine-derived nutrients can play a crucial role in addressing global challenges such as food security, water scarcity, and climate change. As the world's population continues to grow, there is an increasing need for sustainable agricultural practices that minimize the use of non-renewable resources. Nutrient recovery from urine presents an opportunity to close the nutrient loop and establish a more circular and sustainable approach to agriculture.

In recent years, several innovative technologies have emerged for urine nutrient recovery. These technologies range from simple and low-cost solutions suitable for developing countries to advanced processes applicable in urban settings. Common methods include struvite precipitation, which converts urine phosphorus into a slow-release fertilizer, and

nitrification-denitrification, which converts urine nitrogen into gaseous forms that can be captured and used as a fertilizer [139].

Janus membranes can be engineered to have distinct surface properties on each side. In the case of urine treatment, the hydrophilic side of the Janus membrane allows for the transport of water vapour , while selectively permitting the passage of dissolved nutrients present in the urine and decrease the susceptibility of fouling and scaling. This selective transport enables the recovery of valuable nutrients while retaining other undesirable components.

The asymmetric nature of Janus membranes provides enhanced separation efficiency in membrane distillation for nutrient recovery. Moreover, recovering nutrients from human urine using Janus membranes aligns with the principles of sustainable nutrient management. It reduces the reliance on synthetic fertilizers, which have environmental impacts associated with their production and use [161, 162].

While the application of Janus membranes in membrane distillation for nutrient recovery from human urine shows promise, further research and development are needed to optimize membrane performance, ensure long-term durability, and address scalability and cost-effectiveness considerations. Additionally, the implementation of such systems requires proper consideration of hygiene, safety, and public acceptance factors. Nonetheless, this approach represents a sustainable and resource-efficient solution for nutrient recovery from urine, contributing to a more circular and environmentally friendly approach to wastewater management.

Furthermore, the benefits of urine nutrient recovery extend beyond agriculture. The captured nutrients can also find applications in the production of biofuels, bioplastics, and other value-added products, contributing to the development of a bio-based economy [163].

nutrient recovery from human urine presents a promising solution to address the challenges of resource scarcity, environmental pollution, and sustainable agriculture. By recognizing the value of urine as a nutrient-rich resource and implementing appropriate recovery technologies, we can create a more efficient and sustainable approach to managing our waste and resources while simultaneously supporting global food production and environmental stewardship.

Recovering nutrients from urine allows for the production of sustainable fertilizers, reducing the dependence on energy-intensive and environmentally harmful conventional fertilizer production. By separating urine from wastewater streams, water consumption in sanitation systems can be significantly reduced. This separation not only conserves freshwater resources but also minimizes the energy requirements associated with wastewater treatment processes, leading to a more sustainable water management approach.

Urine collection and handling raise concerns about hygiene, privacy, and social acceptance. Overcoming these challenges requires effective communication, education, and the development of appropriate infrastructure to ensure the safe and comfortable collection of urine.

Various technological approaches have been proposed for urine nutrient recovery, including struvite precipitation, ion exchange, electrochemical processes, and biological treatment methods. However, these technologies often face limitations in terms of scalability, cost-effectiveness, and operational complexity. Ongoing research and development efforts are necessary to improve the efficiency and practicality of urine nutrient recovery technologies.

Struvite precipitation is a widely studied method for phosphorus recovery from urine. It involves the addition of magnesium or calcium to form struvite crystals, which can be used as a slow-release fertilizer [161, 162].

Electrochemical technologies, such as electrocoagulation and electrooxidation, show promise in urine nutrient recovery. These processes can effectively remove contaminants and recover valuable resources, but further research is needed to optimize their efficiency and cost-effectiveness.

Chapter 3

Computational Fluid Dynamics Simulation Study of Hypersaline Desalination via Membrane Distillation

This Chapter is partially based on the following publication:

- **M Afsari**, AH Ghorbani, M Asghari, HK Shon, LD Tijing, Computational fluid dynamics simulation study of hypersaline water desalination via membrane distillation: Effect of membrane characteristics and operational parameters, Chemosphere 305, 135294, **2022**

3.1 Introduction

Water scarcity is one of the grand challenges faced by many countries around the world. The United Nations has predicted that about half of the world's population will experience a degree of water scarcity by 2050. Efforts have been directed in the use of unconventional sources of water such as seawater to produce drinkable or usable water for agriculture [138, 164]. Seawater desalination is one of the attractive methods with high potential for large-scale investment because of the unlimited availability of seawater source [165]. Reverse osmosis (RO) is a mature membrane technology that is considered the state-of-the-art desalination process, which is utilized around the world due to its high efficiency and high purity water production. However, RO has limitations in treating hypersaline and challenging wastewater solutions. Membrane distillation (MD) is a hybrid method with thermal and membrane technology advantages. When cheap, low-grade energy source is available, it can present good economic and operation privileges like low fouling susceptibility and low working pressure compared to RO, and low working temperature compared to thermal methods [166, 167].

Recently, many studies have investigated the performance of the MD system in different operational conditions and in improving the overall efficiency. Most of the recent studies have been on the development of new distillation membranes. Since MD is a simultaneous process involving heat and mass transfer, a deep understanding of the mechanism of simultaneous heat, mass, and momentum transfer of the MD system in both liquid and vapour phase is necessary to make the process more efficient [168]. Experiments are usually done to understand the mechanisms involved, however, performing a wide range of

experiments that need to change most of the characteristics of the membrane and module in different operating and material conditions is very time-consuming and not economical [169, 170]. For this purpose, numerical method can be used to simulate the process to simultaneously evaluate the heat and mass transfer through the channels and membrane pores [66, 171].

In the MD system, temperature and concentration polarisation (TP and CP) are two main challenges that decrease the separation performance of the process [172]. In TP, due to evaporation of the water on the surface of the membrane and condensation on permeate side, the temperature on the surface of the membrane on the hot and cold side are lower and higher than the bulk temperature, respectively, which causes a decrease in temperature difference and driving force. However, the experimental evaluation of TP and CP is complicated and inaccurate [173]. Therefore, the need to use the modelling and simulation technique to analyse the behaviour in a direct contact MD (DCMD) as a model configuration is essential. Until now, some studies have focused on modelling the DCMD system to predict its behaviour in different conditions. In these studies, empirical correlations were used to evaluate the performance of the membranes [174, 175]. Recently, advances in computational fluid dynamics (CFD) techniques have increased the attention of scholars to use the CFD method to simulate the performance of the MD process, and some researchers have used CFD for modelling of MD system [176, 177].

Different studies have been performed to model the performance of the DCMD systems; however, some of them have relied on correlations or assumptions that are not clear or

accurate. CFD offers a comprehensive and more accurate transport field, including full momentum, mass and heat transfer profiles throughout the system [147, 178]. The simultaneous evaluation of temperature, velocity, and concentration brings the advantage of easily identifying the bottlenecks of the process and optimization of the system that are too complex via experiments [178-180]. Moreover, many studies that used 2 and 3 dimensional CFD simulation for DCMD modelling just focused on coupling of mass and heat transfer without investigation of hypersaline feed salt concentration and mostly focused on up to 3.5 wt% salt concentration [181-189]. Other studies investigated the salt concentration without a deep study of temperature distribution and polarization and optimum physical parameters of the membrane in different feed-side salt concentrations [174, 190-193].

Therefore, there is a lack of understanding of the effect of feedwater salinity on the operation of the MD system and the optimum physical values of the membrane for efficient treatment of hypersaline feed water. This study has focused on deriving the dependency of the physical parameters of the membrane in different operation conditions and has focussed on driving the optimum values of thickness, porosity and other membrane parameters in a wide range of feed salt concentrations (from seawater to RO brine and hypersaline feedwater range). This study aims to comprehensively simulate the effect of changing various types of parameters, including temperature difference, flow velocity, membrane conductivity, porosity, length, and thickness, on the behaviour of the DCMD system using Comsol Software. Here, the temperature and concentration profile in the hot channel, cold channel, and membrane were drawn, and accordingly, the flux of the system

was evaluated. This study uses the continuity, Navier-Stocks, and diffusion correlations to solve the finite-elements equations and find the steady-state profiles of temperature, vapour pressure, velocity, and concentration. In addition, feedwater containing a wide range of salinity (up to hypersaline) was used to simulate the separation performance of the DCMD process. The simulation results were first validated using experimental data, and then the developed method was used to evaluate the effect of different changes in parameters.

3.2 Methods

3.2.1 Geometry and governing equations

A 2-dimensional flat-sheet membrane was used as the basis for both experiments and modelling. The schematic of the designed system is shown in Figure 3-1. The feed solution containing different NaCl concentrations at various feed velocities enters the module with inlet feed temperature of $T_{f,in}$ and concentration of $C_{f,in}$. On the other side of the membrane, the distillate water is passed over the permeate channel with an inlet temperature of $T_{p,}$. The feed and permeate velocities were varied to evaluate the effect of different velocities on the system performance in the experiment and simulation. The modelling was performed based on experimental data obtained from a study by Eykens et al. [53]. In the referenced study, the experiments were carried out and MATLAB was used for modelling of some of the processes. In this study, COMSOL software was used to carry out a comprehensive modelling of the MD process and to derive the optimum characteristic of the membrane for treatment of feedwater containing a wide range of salinity. The

characteristics of the membrane used in the experiment and operational condition are shown in Table 3-1. In this study, the transfer phenomena (mass, heat, and momentum) in a counter-current DCMD system were investigated. Additionally, both conductive and convective terms were considered. The mathematical study of the system was divided into three parts: the feed side of DCMD where hot saline water enters, the hydrophobic porous membrane through which the water vapour passes, and the permeate side of the membrane where water vapour condenses at the cold side of the system. From a molecular point of view, the water molecules are evaporated on the contact area of the feed-side membrane surface due to the hot temperature of the feed, then pass through the membrane pores and are condensed on the contact area of the permeate side surface of the membrane. The water flux is directed according to the vapour pressure gradient over the membrane surfaces. Therefore, the process of MD desalination can be divided into three main resistances including water evaporation in the feed side (R1), vapour transport through the pores (Rm), and condensation in the permeate side (R2) [176, 178].

Figure 3-1 illustrates the geometry and the direction of mass, heat, and momentum transfer. In this study, four physical phenomena were applied on the setup to run the model according to the following criteria: Firstly, the flow was assumed laminar in both upside and downside of the channel. Then, heat transfer was assumed to occur on all areas of the hot channel, membrane, and cold channel to accurately evaluate the heat transfer phenomena in the system. In addition, the mass transfer occurs at the feed side, and a concentration distribution is formed on the feed side. The permeate side was assumed to be pure water,

i.e., without zero NaCl concentration, thus, there was no concentration distribution on the cold channel profile. Lastly, the mass passes through the membrane pores.

Table 3-1 Membrane characteristics (values used are based from Eykens et al. [53]) and MD operational conditions

Characteristics/ Parameter	Details/Values
Membrane material	Polypropylene (PP)
Membrane type	Flat sheet (unsupported)
Membrane porosity	83%
Membrane average pore size	0.5 µm
Membrane liquid entry pressure (LEP)	2.5 ×10^5 Pa (2.5 bar)
Membrane tortuosity	1.28
Membrane thickness	188 µm
Membrane conductivity	0.12, 0.2 W/m K
Membrane length *	5, 10, 50, 100 cm
Feed solution concentration	0, 12, 22 g/L
Inlet feed and permeate velocity	0.28, 0.13, 0.04 m/s
Feed/permeate inlet temperature (Temperature difference)	62.5/42.5 (ΔT=20 °C), 60/45 (ΔT=15 °C), 55.5/49.5 (ΔT=6 °C) [°C/°C]

** The modelling and study of the effect of length of the membrane was performed just in this study and the reference paper didn't study the effect of length*

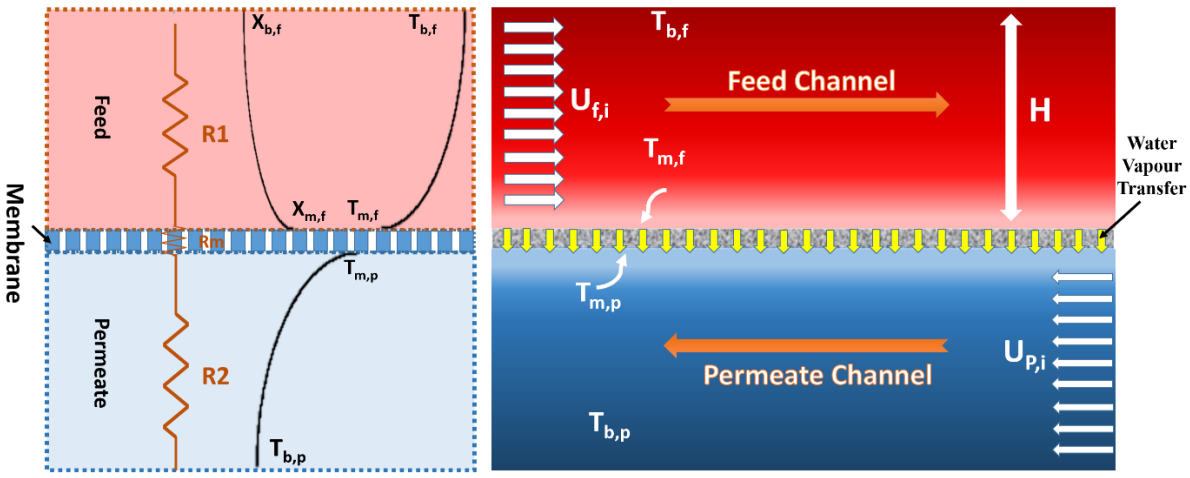

Figure 3-1 Schematic of the module for MD system showing the mass and heat transfer resistance (left) and direction of liquid and vapour transfer (right) across the membrane

Some additional assumptions were made to simplify the iteration process in this model. The operation was assumed steady-state, and the stream flows on both sides were laminar. Also, the heat loss of the module to the environment was ignored, and heat was just transferred through the membrane. The mass transfer through the pores of the membranes was assumed to be a combination of molecular diffusion and Knudsen, and the convective mass transfer was neglected inside the pores (the diameter of the pores was not in the Darcy flow, and no convective momentum was inside the pores). In addition, the membrane characteristics like porosity, pore size, and conductivity were assumed constant during the test at different operating temperatures.

3.2.2 Transmembrane mass transport

Mass transfer of water vapour through the membrane is obtained by the following equation:

$$J = J_v + J_d \tag{3-1}$$

Overall flux through the membrane was equal to the viscous and diffusion mass transfers. The Dusty Gas Model (DGM) has been applied herein to evaluate the flux passing through the porous membrane. DGM considers three transport mechanisms through a membrane: molecular diffusion, viscous flow, and Knudsen. The effectiveness of each mechanism depends on the physical and chemical properties of the porous media. Knudsen's number can determine which mechanism is dominant. In the membrane with micron size structure, the viscous flow has a negligible impact on the overall flux [178].

The flux in the membrane directly depends on the difference in vapour pressure over the membrane, which is the driving force of the process. Therefore, the mass transfer can be determined according to the following formula [194]:

$$J_i = -D_{eff}(P^i_{T_f} - P^i_{T_p}) \quad (3\text{-}2)$$

where I is the membrane flux, D_{eff} is the local mass transfer coefficient, calculated using the DGM. $P^i_{T_f}$ and $P^i_{T_p}$ are local water vapour pressure on the feed and permeate sides, respectively, which are derived from Antoine's equation.

According to Antoine's correlation, the vapour pressure of the feed and permeate are directly dependent on the temperature expressed as:

$$P^{sat} = \exp\left(23.238 - \frac{3841}{T_m - 45}\right) \quad (3\text{-}3)$$

However, when the non-volatile components are dissolved in water, the vapour pressure can be measured using a modified correlation [179, 195]:

$$P_m = a_w P^{sat}, \quad a_w = 1 - 0.03112b - 0.001482b^2 \quad (3\text{-}4)$$

where, b is NaCl molality (mol/kg), P^{sat} is saturation pressure of the fluid, T_m is the membrane surface temperature, a_w is activity of the fluid, and P_m is the vapour pressure of the liquid at that point.

The flux passing through the membrane is controlled by Knudsen diffusion and molecular diffusion and can be calculated according to the following correlations [195]:

$$1/D_{eff} = \frac{1}{D_v} + \frac{1}{D_{Kn}} \quad (3\text{-}5)$$

$$D_v = {}^{\varepsilon\mu_v}/_{\tau\rho_v} \quad (3\text{-}6)$$

$$D_{Kn} = \frac{2\varepsilon}{3\tau} d_p \sqrt{\frac{2RT}{\pi M_w}} \quad (3\text{-}7)$$

where, ε and τ and μ_v are porosity, tortuosity, and viscosity of water vapour, respectively and d_p is the average pore size of the membrane. D_{eff} and D_{kn} are effective and Knudsen diffusivities, respectively and D_v is ficks diffusion (Dv) [196].

3.3 Thermal conductivity of the membrane

The mass transfer in MD process is composed of three steps: evaporation of the water on the feed side, water vapour passing through the membrane, and condensation of the water vapour to water on the permeate side [149, 197]. Regarding the porous structure of the membrane, the overall heat transfer (q) through the membrane is carried out in two ways: heat conduction (q_c) through the matrix of the membrane, and the heat transferred via the evaporated water (q_v) that condenses on the other side of the membrane as represented by the following equation:

$$q = q_c + q_v \quad (3\text{-}8)$$

Due to the temperature difference between the two sides of the membrane, which induces the evaporation, passing, and condensation of the water vapour, heat transfer therefore plays the main role in determining the efficiency of MD systems. For MD membranes, thermal conductivity is measured according to the porosity of the membrane, which includes both the thermal conductivities of the membrane matrix and those of the water vapour and air inside

the pores. Considering the potential changes in the polymer chains due to temperature change effect which can affect the thermal conductivity of the polymer, a variable thermal conductivity for the membrane was used in this model. Different models correlate the thermal dependence of the thermal conductivity like isostress, flux law, or even isostrain [198]. However, each of these models has their own errors, affecting the final deviation of modelling results compared to the experimental data. In this study, the isostrain model was selected for the measurement of the average thermal conductivity of the membrane, and the equations are as follow [199-201]:

$$k_s(\mathrm{T}) = 0.253 + 4.86 \times 10^{-4}\mathrm{T} \quad (3\text{-}9)$$

$$k_g = 1.5 \times 10^{-3}\sqrt{T} \quad (3\text{-}10)$$

$$k_m = (1-\varepsilon)k_s + \varepsilon k_g \quad (Isostrain\ Model) \quad (3\text{-}11)$$

where k_s is the thermal conductivity of the solid matrix, k_g is the pore thermal conductivity, and k_m is the average thermal conductivity of the membrane.

Therefore, the heat flux via conduction and convection through the membrane is calculated according to the following equation:

$$q = \frac{k_m}{\delta}\left(T_m^f - T_m^p\right) + J\lambda \quad (3\text{-}12)$$

where the T_m^f and T_m^p are the temperatures on the surface of the membrane facing the feed and permeate sides, respectively, δ is membrane thickness, J is mass flux and λ is the specific latent heat of water [202].

3.4 Governing equations for the channel flows

In MD, the vapour pressure gradient induced by the temperature difference is the main driving force, thus, energy conservation equations are written to explore the temperature gradient over the hot and cold channels and the membrane. By considering the temperature gradient of the MD module, it is possible to obtain the thermal efficiency of the system. The energy conservation equation in the MD channel includes both conduction and convection terms and is expressed as follows:

$$\frac{\partial^2(kT)}{\partial x^2} + \frac{\partial^2(kT)}{\partial y^2} - \frac{\partial(\rho C_P UT)}{\partial x} = 0 \quad (3\text{-}13)$$

where ρ is density, C_P is heat capacity, U is flow velocity in the x-direction, k is thermal conductivity coefficient, and T is temperature [203].

Furthermore, the fluid flow in both feed and permeate sides follow the Navier-Stokes correlation with the terms used for incompressible Newtonian fluids [204]. The general form of the equation is as follows:

$$\frac{\partial(\rho V)}{\partial t} - \nabla.(\eta(\nabla V + (\nabla V)^T) + V.\nabla(\rho V) + \nabla p = F \quad (3\text{-}14)$$

where, η is dynamic viscosity, V is y-direction velocity, P is pressure, and F is body force. In addition, the continuity equation is given as:

$$\frac{\partial(\rho U)}{\partial x} + \frac{\partial(\rho V)}{\partial y} = 0 \quad (3\text{-}15)$$

To increase the accuracy of the model, the density and viscosity of fluid are considered to change by temperature and concentration [205, 206]. Furthermore, the concentration profile in hot channel can be expressed using the following mass transfer equation:

$$\frac{\partial C_w}{\partial t} = -(\nabla \mathrm{U} C_w) - \nabla . \mathrm{j}_w + R_w \quad (3\text{-}16)$$

where, C_w is concentration, U is flow velocity in x-direction, j is flux, R is chemical reaction rate (zero in MD process), and t is time. The steady-state mass transfer correlation is simplified as:

$$\left[\frac{\partial^2 (D_w C_w)}{\partial x^2} + \frac{\partial^2 (D_w C_w)}{\partial y^2}\right] = \frac{\partial (C_w U)}{\partial x} \quad (3\text{-}17)$$

3.5 Results and discussion

3.5.1 Model validation

In this study, the experimental data reported by Eykens et al. [53] was used for validation and comparison of the model data obtained using Comsol software. Firstly, the process was modelled by Comsol and then was verified by experimental results, and the deviation in different conditions was reported. The operation of the membrane in various temperature differences, feed velocities, and salinities was investigated and modelled. Afterwards, the model was used for evaluation of the behaviour of the membrane in DCMD process in different operational conditions and membrane characteristics. The comparison of the model and experimental results is shown in Table 3-2. The results demonstrated that most of the errors were less than 3%, proving the accuracy of the simulation results.

To show the operation condition of the process, $dT_xV_yS_z$ coding was applied, so that dT shows the temperature difference between feed and permeate, V is the inlet velocity of feed and permeate, and S is the salinity of the process. Also, x, y, and z are the values of dT, V, and S, respectively. For example, $dT_{20}V_{28}S_{22}$ represents that the process is operated in temperature difference of 20 C, flow velocity of 0.28 m/s, and feed salinity of 22 wt%

In the first step, the setup configuration was designed. The system concentration, temperature, and vaporization pressure profiles in all hot and cold channels and membranes were derived.

Table 3-2 Comparison of experimental and modelling flux in different conditions

	Material	dT (°C)	flow velocity m/s	Salinity g/l	Experimental Flux (LMH) [53]	Modelling flux (LMH)	Error %
1	PP	20	0.13	0	24.5	24.9	1.6
2	PP	20	0.13	12	19.5	21.0	7.7
3	PP	20	0.13	21	17.2	17.3	0.6
4	PP	20	0.13	22	16.2	16.4	1.2
5	PP	15	0.13	0	19	19.0	0.1
6	PP	15	0.13	3	18.3	18.5	1.1
7	PP	15	0.13	12	16.5	16.7	1.2
8	PP	15	0.13	14	15.8	16	1.3
9	PP	15	0.13	22	12.2	12.3	0.8
10	PP	15	0.13	23	11.7	11.6	0.9
11	PP	6	0.13	0	9.5	8.9	6.3
12	PP	6	0.13	3	8.4	8.2	2.4
13	PP	6	0.13	12	5	5.8	16
14	PP	15	0.28	0	21.3	21.8	2.3
15	PP	15	0.28	12	18.6	21	12.9
16	PP	15	0.28	22	12	14	16.7
17	PP	15	0.13	0	19	18.98	0.1
18	PP	15	0.13	12	15.9	16	0.6
19	PP	15	0.13	22	12.1	12.3	1.7
20	PP	15	0.04	0	12.4	12.6	1.6
21	PP	15	0.04	15	10	11	10.0
22	PP	15	0.04	22	8.5	8.4	1.2

3.5.2 Temperature, vapour pressure and concentration distribution profiles in the DCMD module

The temperature and vapour pressure distribution profiles of the counter-current DCMD process derived by the model are shown in Figure 3-2. The modelling was carried out in feed and permeate inlet temperatures of 60 ^{o}C and 20 ^{o}C, respectively, feed salinity of 200 g/l, and membrane length of 5 cm to show the trends of the temperature, velocity, and concentration profiles. The distributions of both feed and permeate side over the channels show the direction and rate of heat transfer. As water evaporation and heat transfer are dependent on the temperature difference between both sides of the membrane, investigations on the temperature variation over the membrane is of utmost importance. The average temperature difference through the membrane length is clearly shown in Figure 3-2a. Hot and cold water enters the module at 60^{o}C and 20 ^{o}C, respectively, and shows a temperature contour in the hot channel, wherein the contour increases its distance from the membrane surface with the growth of the thermal boundary layer. For the membrane length of 5 cm, the outlet temperature profile in hot side varies from about 40 ^{o}C on the membrane surface up to 60 ^{o}C on the bulk of system. The counter-current direction of the flow between the hot and cold sides helps to maintain a low driving force tolerance over the membrane length. However, the membrane performance directly is generally known to be affected by the velocity of the flow and the characteristics of the membrane.

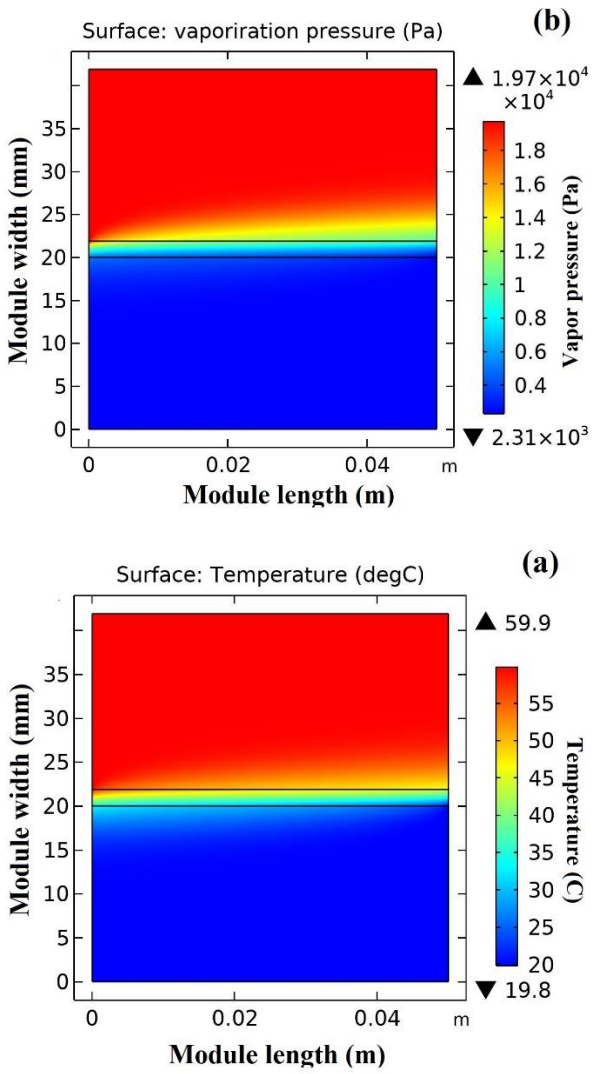

Figure 3-2 The simulated distribution profiles in the DCMD module with membrane length of 5 cm: (a) temperature (b) vapour pressure, and (c) concentration. Inlet feed and permeate temperature: 60/20^{o}C; Feed and permeate velocity of 0.13 m/s in hot and cold channel

The distribution of the contours of vapour pressure, which have been derived using the temperature and concentration corrections is shown in Figure 3-2b. Vapour pressure is a function of temperature and concentration. The most important section for evaluating vapour pressure is on the membrane surface and inside the membrane pores. The rate of variation in vapour pressure in this section determines the velocity and flux of water vapour

through the membrane. As seen in the figure, the isochromatic lines for both temperature and vapour pressure are nonlinear and have a semi-cubic function that the value of line slope in the middle is minimum. This trend proves the moderate change in temperature in the middle of the membrane, which causes a decrease in driving force in the middle of the membrane. The simulation results proved that the minimum velocity of the water vapour inside the membrane pores takes place in the middle of the membrane[176, 178, 207]. In DCMD, the temperature distribution depends directly on the porosity, thickness, thermal conductivity and pore size distribution of the membrane as well as the flow velocities on both channels, which have been considered in this study [53, 175, 178, 180, 208].

Figure 3-3 shows the temperature and vapour pressure distributions on the membrane feed side surface for a MD system with a membrane length of 10 cm, feed and permeate side temperatures of 60 and 45 ^{o}C, respectively, feed stream velocity of 0.28 m/s, and salinities of 0 and 22 wt%. The results reveal that while the outlet temperature on the membrane surface for hypersaline feed stream (22 wt% salinity) is greater than freshwater feed stream (0 wt% salinity), its vapour pressure is lower, which resulted in a decreased driving force and subsequently, lower flux.

The results demonstrated that the higher activity of saline water dramatically reduces its vapour pressure and the system with higher salinity achieve lower flux due to lower deriving force. Therefore, the rate of evaporation and heat transfer in this system is lower and as a result, the temperature drop across the membrane surface is lower and the outlet

temperature on the membrane surface for system working with higher salinity is greater. Other studies also derived the same results [146, 147, 178, 209].

The NaCl concentration profile in the feed side shows the value and direction of mass transfer in the hot channel. The concentration distribution can estimate the concentration polarisation in the DCMD process. Furthermore, the value of concentration and temperature on the liquid-vapour interface determines the vapour pressure and driving force of the process [210]. For this reason, the mass and momentum transfer correlations are used to model and simulate the NaCl concentration distribution on the feed side [178].

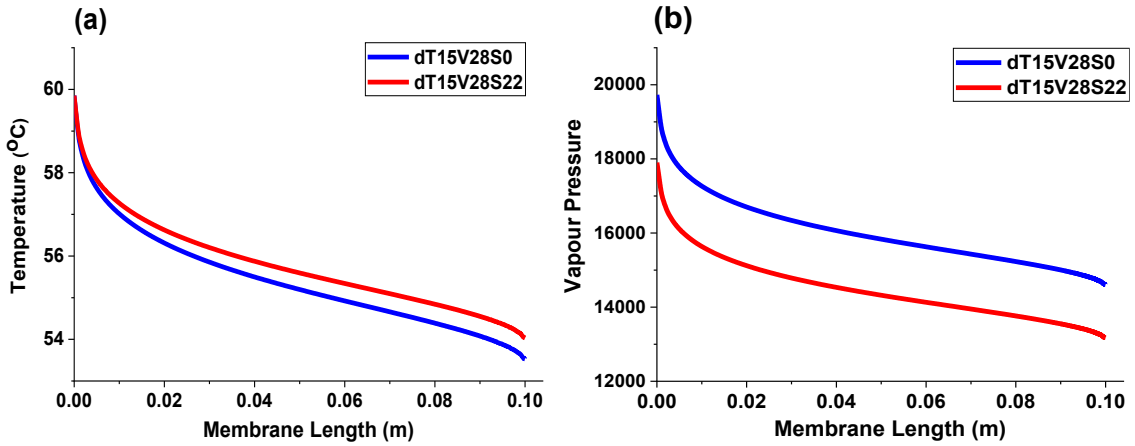

Figure 3-3 The vapour pressure (left) and temperature (right) changes along the membrane length (10 cm) for feedwater having feed velocity of 0.28 m/s and salinity of 0 and 22 wt%. Although the outlet temperature of hypersaline feedwater is greater than freshwater (left), the vapour pressure of freshwater is higher than saline water (right). The blue line is data for feedwater with 0 wt% salinity, and the red line is for feedwater with 22 wt% salinity.

Figure 3-1 shows a steady-state concentration field on the hot side of the membrane. The temperature and concentration fields derived using the simulation model show that the concentration boundary layer is narrower than the temperature boundary layer. This difference can be attributed to the differences in temperature and mass diffusivity

coefficients. In general, in aqueous solutions, the thermal diffusivity (α) is significantly greater than the mass diffusivity (D), which causes thinner concentration boundary layer compared to the temperature one so that Le number (= α/D) is usually greater than 40 [178]. In addition, the complete salt rejection is assumed for the MD membranes and therefore, concentration distribution profiles are just formed in hot channel and the NaCl concentration throughout the membrane and permeate side is zero.

3.5.3 Velocity distribution profile in DCMD

The velocity profiles in the feed and permeate channels and in the membrane are shown in Figure 3-4, which are obtained by solving the mass, heat and momentum transfer (Navier-Stocks) correlations over the channels and pores using the simulation software. As shown in the figure, the velocity profile forms just after the fluid entrance. The velocity was maximum in the middle of the channels and minimum in the sides.

In this study, the velocity distribution through the channels in the middle of the module (0.5L) was considered for different inlet velocities and the results are shown in Figure 3-4**b**. At various velocities (0.04, 0.13 and 0.28 m/s), a laminar pattern was formed with a parabolic velocity profile through the channels (Figure 3-4**b**). A comparison of the velocity profiles for the three velocities indicate that an increase in the velocity changes the graphs parabolicity. The higher velocity decreases the boundary layer and improves the rate of change of the velocity in the y-direction, which has a positive effect on the mass transfer in the feed side [211]. In addition, the fluid velocities in the feed and permeate sides show

that the maximum velocity that occurs at the middle of the channel in the feed side is slightly greater (about 2%) than that in the permeate side.

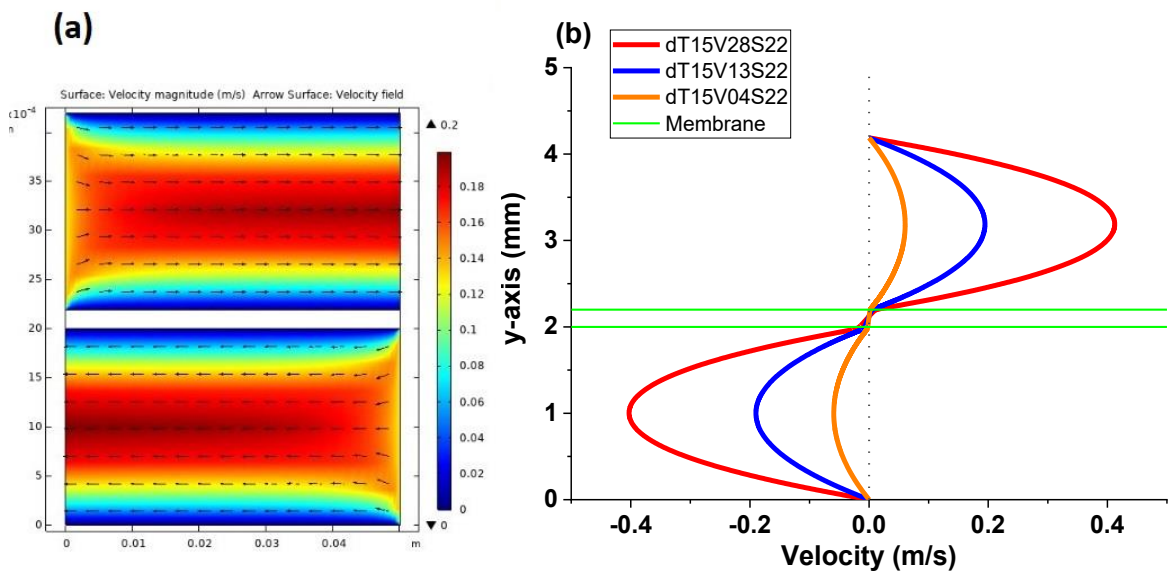

Figure 3-4. (a) The velocity profiles through the hot and cold channels of the membrane, and the (b) profiles in different inlet velocities (0.28, 0.13, 0.04 m/s).

3.5.4 Effect of velocity on flux and temperature profile

Figure 3-5 shows the temperature and vapour pressure profiles on the membrane feed side surface versus the membrane length at different feed velocities. From Figure 3-5**a** and **b**, it can be seen that the outlet temperature increases with the increase in velocity, which can be attributed to the shorter residence time of the feed in the hot channels. By increasing the velocity, the residence time of the feed in the hot channels decreases. So, the heat has less time to transfer through each feed element. As a result, the temperature drop across the membrane length decreases. This change causes greater vapour pressure for feed-stream with higher velocity and results in greater driving force and flux.

The outlet temperatures in both hot and cold channels in different velocities and feed salinity are shown in Figure 3-5**c**. The velocity was observed to increase the hot channel outlet temperature while it decreased the temperature of the cold channels. In addition, the salinity has a similar effect on the outlet temperature. While salinity increases, the outlet temperature increases in hot channels and decreases in cold channels. This figure clearly shows a lower driving force for the system with lower velocity.

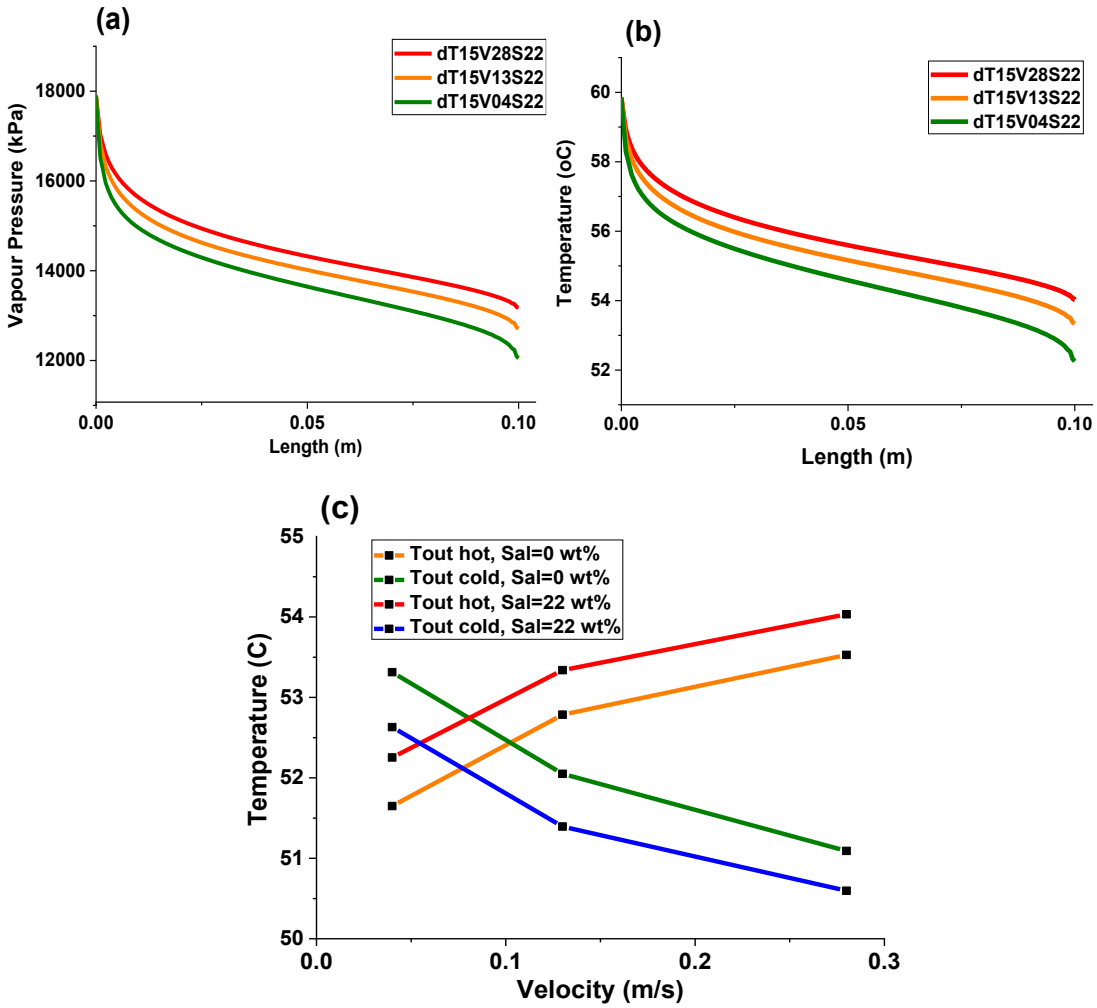

Figure 3-5. The temperature and vapour pressure profiles in the feed (hot) channel at different velocities (a, b). The increase in velocity increases the outlet temperature and

vapour pressure. Also, the outlet temperature in the hot channel increases by velocity, and the outlet temperature of cold channel decreases by velocity (c).

The effect of the velocity on DCMD performance has been experimentally investigated previously [53]. The study demonstrated that changes in the velocity change all mass, momentum, and heat transfer through the membrane and directly affect the outlet temperature and salt concentration and the fluid and energy efficiency of the membrane.

In the present simulation study, the vertical temperature profile of the fluids in hot and cold channels and the membrane in the middle of the module is shown in Figure 3-6a. In this simulation, the inlet temperatures of feed and permeate sides were fixed at 60 and 45 ^{o}C, respectively, and the flow velocity was set at 0.28, 0.13, and 0.04 m/s for desalination of a feedwater containing 22 wt% NaCl. The temperature profile shows that higher velocity tends to have a sharper temperature profile. This difference provides higher driving force for mass transfer in feed and permeate sides and lower R1 (feed side) and R2 (permeate side) resistivities. Furthermore, the temperature of a system with a high velocity on the membrane surfaces on the hot and cold sides is higher and lower, respectively, showing a greater driving force across the membrane and lower Rm resistivity. Overall, in the velocity range studied in this work, all resistivities (R1, Rm and R2 - see Figure 3-1) for a high velocity MD system are lower than for a low velocity one [176].

The experimental results showed that an increase in velocity enhanced the membrane flux, and the trend was preserved for different feed salinities up to 22 wt% [53]. The model prediction is consistent with the trend of the experimental results from a previous study (Figure 3-6**b**). The increase in velocity generally improved the system performance.

However, the membrane flux decreases with the increase in salinity due to the decrease of the feed stream vapour pressure. The effect of the velocity on the flux can be interpreted according to the heat, mass, and momentum transport phenomena [176, 208]. On one hand, the liquid residence time in the channels of the high velocity system is lower. Therefore, the mass and heat have short time to transfer over the membrane, leading to the increase in the feed temperature and concentration with velocity. Thus, higher velocities cause higher outlet temperature, resulting in greater temperature difference along the membrane and higher driving force across the membrane, enhancing the overall driving force and improving the flux. On the other hand, higher velocity decreases the thickness of the sublaminar stream on the membrane surface, causing a decrease in the concentration polarisation of the membrane [212, 213]. Also, the temperature distribution of the membrane becomes more homogenous in higher feed velocity and diminish the temperature polarisation over the membrane feed side. These two effects enhance the DCMD performance and increase the flux.

The comparison of model predictions with the experimental data shows that the simulated model results are more consistent with experimental data in lower velocity conditions. An increase in feed stream velocity increases the deviation of the model.

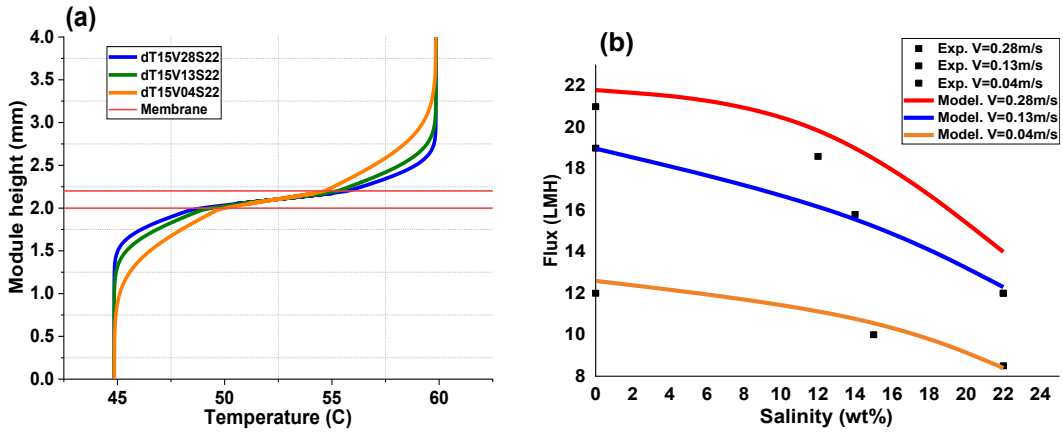

Figure 3-6. (a) Temperature profiles of the feed (hot) channel, membrane, and cold channel in the middle of the module, and the experimental (dots, based from [53]) and modelling (line) results of DCMD flux vs salinity (b) at various velocities. The flux decreases with the increase in salinity and a decrease in flow velocity.

3.5.5 Effect of channel length

Membrane length is one of the important parameters in determining the DCMD efficiency. There is an optimum length for the system to have high mass transfer and low heat loss. Therefore, a dimensional optimization should be carried out before running the experiments. Numerical modelling is the best and cheapest method for evaluating the system performance before sorting out the experiments. Therefore, the DCMD performance has been simulated for the systems with different lengths. Accordingly, after validating the simulation predictions with experimental data, the proven models and coefficients were used to estimate the temperature and flux profiles of the DCMD module.

The overall flux of the membrane in unit length of the membranes with different lengths are shown in Figure 3-7. The simulation results prove that longer membrane gives lower flux and the operation efficiency of the membrane decreases with length. In addition, desalination of hypersaline feedwater dramatically decreases the flux, and the rate of drop

in flux in the longer membrane is higher. For the 5 cm length membrane, desalination of feedwater containing 100 g/l NaCl drops the membrane flux from 22 to 17 L/m^{2}h (LMH) (25% drop) while for the 50 and 100 cm length membranes, the flux drop reaches more than 50%. This result suggests that in order to have higher average flux through the membrane, it is more efficient to use multiple series of low length modules. However, cost analysis should be carried out to obtain the optimum length of the membrane to have both efficient cost and operation performance. Similar results were also achieved by a previous study, which shows high temperature depreciation with length of the membrane that caused decrease in flux and thermal efficiency of the system [171].

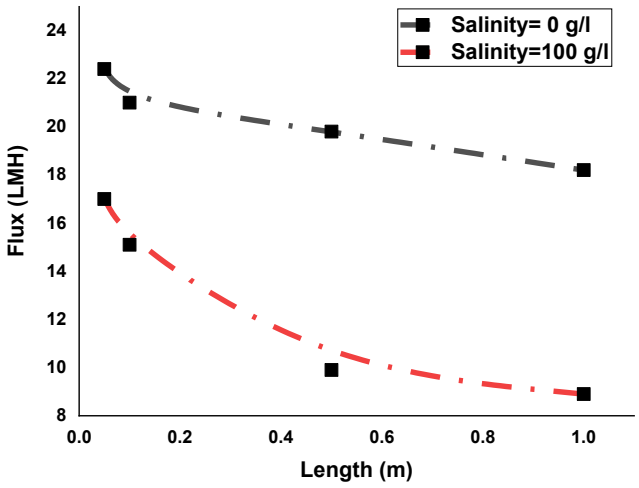

Figure 3-7. MD membrane flux vs module length in different feed salinity.

3.5.6 Effect of membrane thickness

The mass transfer resistance directly relates to the membrane thickness, i.e., the thinner the membrane, the less the resistance. In contrast, the heat loss has opposite relation with thickness so thinner membranes loss more heat. Temperature polarisation is exacerbated by heat loss across the membrane and changes both R1 and R2 resistances, lowering the

driving force across the membrane and decreasing the flux of the system. Despite the importance of evaluating the effect of the thickness, few studies are focusing on MD membranes thickness [169, 214].

In the current DCMD system study, the concentration is assumed to be constant in R2 and Rm regions but variable in the hot channel, and R1 is exponentially changed by concentration. It demonstrates that the rate of change in vapour pressure directly depends on the salinity; higher vapour pressure changes in high salinity feedwater than low salinity feedwater. Therefore, in high salinities, the driving force exponentially decreases and rate of decrease in flux is higher.

By decreasing the membrane thickness, both mass and heat transfers are developed, having a counterbalance effect on flux. Therefore, the effect of each resistance should be considered separately [214]. The model predicted fluxes of the feedwaters with different salinities are shown in Figure 3-8. As demonstrated, the membrane thickness decreases the flux of the feedwater at 0 wt% salinity. In fact, while decreasing the thickness, the mass transfer resistivity (Rm) decreases and the flux increases. However, higher heat loss for thinner membrane intensifies the temperature polarisation by decreasing the membrane surface in the hot side and increasing the membrane surface on the cold side. Therefore, heat loss negatively affects the flux by increasing the R1 and R2, but the effect of improvement in permeability is more dominant. However, an increase in the salinity of the feedwater declines the feedwater vapour pressure [215]. Therefore, the effect of the heat loss and temperature polarisation across the membrane, which led to a decline in vapour

pressure difference and driving force, becomes more pronounced in saline water: the more saline feedwater, the more decrease in driving force. As a result, by decreasing the thickness, the power of temperature polarisation outweighs the power of permeability and a decrease in thickness causes a drop in flux [53, 214, 215]. Therefore, there is an optimum thickness for the desalination of saline water in the DCMD [53, 214]. The results shown in Figure 3-8 and Table 3-3 prove that the optimum thickness for desalination of saline water increases with salinity. However, the maximum flux derived for more saline water is lower, mainly due to the effect of saline water activity in the vapour pressure of feedwater that diminishes the driving force. In this study, the salinity of feedwater changes from 0 to 22 wt% and the results show that the optimum thickness change from as low as possible for freshwater to 120 μm for hypersaline feedwater.

Temperature and concentration polarisations are two main challenges in DCMD systems, which decrease the MD efficiency. An increase in heat transfer through the membrane intensifies the temperature polarization (TP) and concentration polarization (CP), reducing the DCMD efficiency.

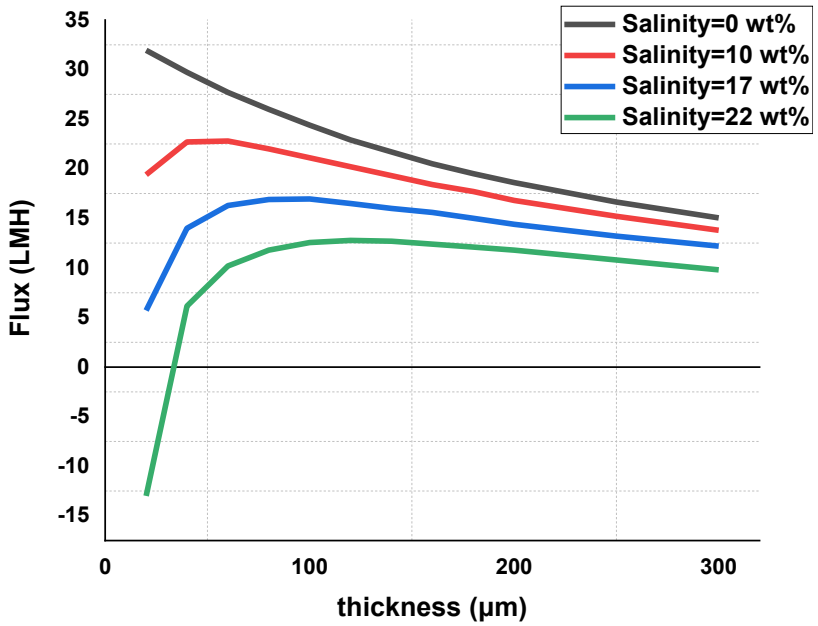

Figure 3-8. Flux versus the membrane thickness in different feedwater salinities.

Table 3-3 The optimum thickness, deriving maximum flux in different feedwater salinities

Salinity (wt%)	Optimum thickness (µm)	Flux (LMH)
0	<<1	>32
10	50	22.8
17	100	17
22	120	12.8

Additionally, the effect of other parameters like membrane porosity, temperature difference, conductivity, and velocity on the membrane with different thicknesses was investigated in this study. The results of the effect of *membrane* porosity on the membrane performance in different thicknesses are shown in Figure 3-9. As demonstrated, the porosity has no impact on the optimum thickness of the membrane [214, 215] . However, the membrane flux with higher porosity is greater, due to the higher available surface area for vapour transport.

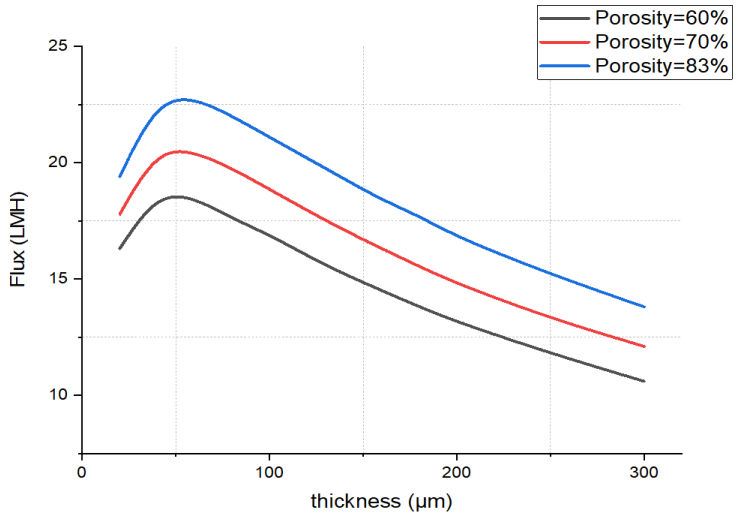

Figure 3-9. The change of flux vs thickness for membranes with different porosity on the performance of the MD setup

3.5.7 Effect of membrane conductivity and temperature difference

The membrane in the MD process contains a matrix that plays a role in heat loss from hot channels to cold channels, and the pores play the main role in transferring the water vapour. The membrane characteristics play a major role in determining the performance of the DCMD system.

The heat loss through the membrane by conduction is the main obstacle to having a high flux and low energy-demanding MD system. The heat transfer through the membrane is carried out via vapour transfer through the membrane pores as well as conduction through the membrane matrix. Therefore, the membrane conductivity has an important role in determining the heat loss through the membrane. Changing the characteristic of the membrane and using polymers with lower conductivity can change the thermal behaviour of MD system [216].

The effect of conductivity on the performance of the membranes with various thickness is considered and shown in Figure 3-10a and b. For feedwater at 0 wt% salinity, the flux decreases by thickness. Although there is an optimum thickness for desalination of hypersaline feedwater (22 wt% NaCl), its value depends on the membrane conductivity. The fluxes of the membranes with three different conductivities of 0.06, 0.12 and 0.25 W/mK show that the highest thickness of the membrane with conductivity of 0.12 W/mK is 120 µm with a flux of about 13 LMH, while for the membrane with conductivity of 0.25 W/mK, the maximum flux is 8.1 LMH occurring at a thickness of 200 µm. Fabrication of membrane with lower thermal conductivity dramatically decreases the heat loss through the membrane and diminishes the MD temperature polarisation [216, 217]. Therefore, by fabrication of a low thermal conductivity membrane, the higher flux can be achieved in lower thickness.

The effect of temperature difference over the membranes with different thicknesses was also evaluated, and the results are shown in Figure 3-10**c and d**. As seen, the flux decreases with salinity and higher temperature difference results in higher flux. This trend is also similar for treating hypersaline feedwater, but there is an optimum thickness that gives the highest flux. In addition, the system working in a higher temperature difference achieves maximum flux in a thinner membrane. The system working at the temperature difference of 20 ^{o}C can achieve the flux of about 19 LMH with the 100 µm thickness. While at the temperature difference of 15 ^{o}C, the maximum flux is less than 13 LMH for the 120 µm thick membrane, and so on.

The simulation predicts negative values for too thin membranes fluxes. In fact, when the membrane is very thin, the heat loss causes extra temperature polarisation and decreases the temperature difference across the membrane. In this condition, for high salinity of feedwater, the vapour pressure sharply drops to lower than that on the membrane surface at permeate side. Therefore, the flux direction reverses from permeate towards the feed. Further decrease in temperature difference or membrane thickness exacerbates the condition and increases the reverse flux, as the negative flux. As a result, higher flux can be achieved by applying higher temperature difference and thinner membrane [217].

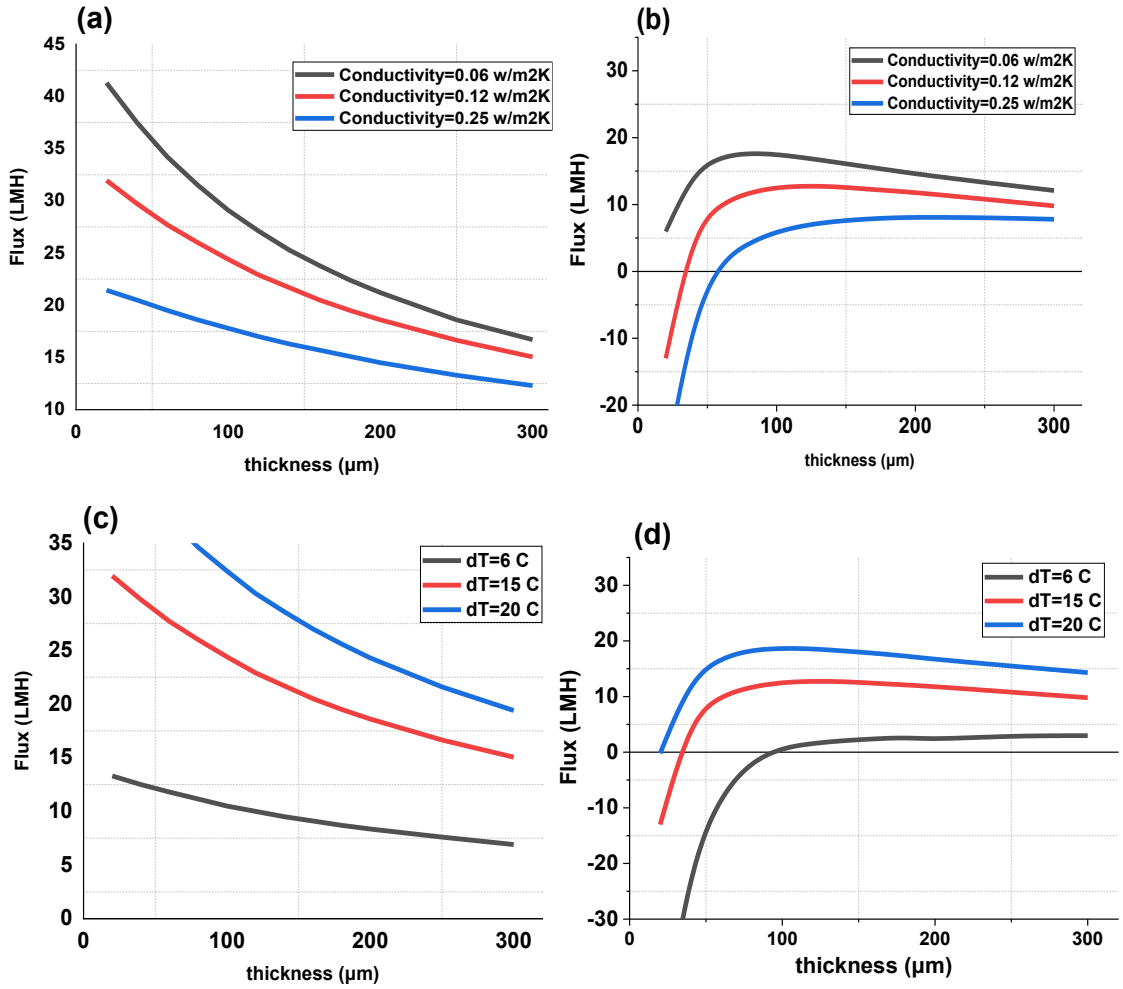

Figure 3-10. The flux versus membrane thickness for feedwater without salinity (left) and feedwater with 22 wt% salinity (right) for DCMDs with different conductivities (a, b), different temperature differences (c, d), and different feed velocities (e, f)

3.6 Conclusion

In this study, Computational Fluid Dynamics (CFD) was used to simulate the behaviour of a DCMD process in different operational conditions and experimental data was used for the validation of the simulation. The effect of feed velocity and salinity, as well as feed and permeate temperatures on the flux of the membrane, was investigated by evaluating the

temperature, concentration, and vapour pressure profiles across the membrane and within the module. The optimum membrane thickness was also predicted for a salinity range of upto 22 wt.%, velocity (0.04-0.28 m/s) and temperature difference (6-20 ^{o}C). The results demonstrated that the salinity decreases the vapour pressure of the feedwater and causes a decrease in the flux. The modelling results showed that a decline in flux for hypersaline feedwater could be compensated by a decrease in thermal conductivity, whereby the flux increased to over 32 LMH using a membrane with a four times lower thermal conductivity.

Moreover, the results proved that optimum thickness is directly related to the salinity and thicker membrane are more suitable for treatment of hypersaline feedwater, mainly due to lower thermal conduction through the membrane. The optimum thickness in this study for the treatment of feedwater containing 10 wt% and 22 wt% NaCl is 50 µm and 120 µm, respectively. However, the maximum flux decreases with salinity and changed from 32 LMH to less than 13 LMH by increasing salinity of up to 22 wt%. The results demonstrated that a thinner membrane is operationally more proper for the treatment of low saline feedwaters, while for hypersaline desalination (HSD), the thicker membranes give higher fluxes and thermal efficiencies. In addition, simulation results showed that the maximum driving force and flux are achieved in both sides of the module and the flux and thermal efficiency of the system decrease with the length of the module.

Chapter 4

Desalination of Challenging Water Using Modified ENF-Based Janus Membranes

This Chapter is partially based on the following publication:

- **M Afsari,** MM Shirazi, AH Ghorbani, M Asghari, HK Shon, LD Tijing, Triple-layer nanofiber membrane with improved energy efficiency for treatment of hypersaline solution via membrane distillation, Journal of Environmental and Chemical Engineering, **2023**

4.1 Introduction

In a direct contact MD (DCMD) process, which is the simplest and most studied configuration, both sides of the membrane are in direct contact with the feed and permeate streams in the liquid form, under warm/hot and cool/cold temperature conditions, respectively. Under this circumstance, the temperature on the membrane surfaces (heat transfer boundary layers on the membrane surface) in the feed and permeate channels are lower and higher than the bulk temperatures, respectively. This temperature difference can cause temperature polarization, which can severely limit the permeate flux. This is mainly due to the heat transfer, in particular the vaporization heat transfer, the latent heat transfer (both are considered the heat transfer via the permeate flux), and the heat loss via the thermal conduction through the membrane structure, from the feed channel towards the permeate channel [137, 218]. The heat transfer via vaporization and latent heat is inevitable, as the vapour molecules transfer from the feed channel with higher temperature towards the permeate channel with the lower temperature. Although the DCMD process is versatile, simple to operate, and beneficial for water treatment purposes, the heat loss via the membrane thermal conduction can be considered a major bottleneck for this MD configuration, which can seriously limit the permeate flux, productivity, and energy efficiency [219]. To overcome this challenge, other configurations have been introduced, where in all of them, the negative effect of heat loss through the membrane thermal conduction is considerably reduced. However, each one presents new challenges, such as a considerable mass transfer resistance in air-gap MD (AGMD) and need to an external

condenser and a blower or vacuum pump to produce the permeate stream in the liquid form in sweeping gas and vacuum MDs (SGMD and VMD, respectively) [220]. However, suppose the challenge of thermal conduction for the used membrane in the DCMD process can be overcome. In that case, DCMD is still the most promising MD configuration due to its advantages, simplicity, ease of operation, compact system, internal condensation of vapour molecules, etc. [149, 221, 222]. Therefore, one innovative approach can be fabricating a specially designed membrane for the DCMD process, which can minimise heat loss via thermal conduction in the membrane. The main novelty of the present research relies on fabricating and developing a thermally insulated membrane for water recovery from high salinity brine.

Recently, electrospun nanofiber membranes (ENMs) have been introduced to the MD technology and their unique characteristics could make them a promising option in this field [223]. The nanofibrous structure can provide a highly porous membrane with interconnected pores and high surface hydrophobicity. All these as well as the simplicity of the electrospinning technique and lower polymer/chemical solvent consumption, have made ENMs a promising alternative for fabricating somewhat greener MD membranes [224]. ENMs can consist of single-layer, double-layer or even multi-layer structures. Generally, for feedwater with salinities less than 35 g/L, thinner ENMs can provide higher permeate flux. According to the discussion, thicker membrane samples performed better with higher permeate flux for higher salt concentration in the feed stream than in the literature [225]. Moreover, the modification of the membranes showed promising results to enhance the performance of DCMD. In a series of studies, superhydrophobic carbon

nanotubes have been used to increase the hydrophobicity of membranes without sacrificing the porosity to modify the membranes and improve the flux in desalination of high-salinity feed water in DCMD [226-228]

Although the obtained results in all these works as well as other published results on the application of ENMs for DCMD were promising [107], the performances of the single layer nanofiber membranes could still suffer from improper mechanical strength and low permeate flux when high salinity feed is introduced to the DCMD system. To enhance the permeate flux and improve the mechanical strength of ENMs, double- and triple-layer membranes with a composite structure were suggested. Various polymers have been investigated for electrospinning of the bottom, hydrophilic layer, such as nylon-6 (N6), polyvinyl alcohol (PVA), and polyacrylonitrile (PAN) [109], as well as commercial hydrophilic nonwoven substrates [229]. Despite efforts to improve multilayer membranes, delamination remains a major obstacle. Delamination can occur due to several reasons, such as poor adhesion between layers, mechanical stress, and chemical degradation [166]. In addition to that, mixed matrix ENMs have been developed as effective membranes for desalination and removing ions from saline solutions. However, the drawbacks of these ENMs often include particle agglomeration, high cost, and surface defects [230]. Furthermore, while dual-layer structured ENMs and nanoparticle incorporation in the ENMs structure have the potential to improve the permeate flux, the issue of heat loss through membrane heat conduction remains a challenge.

The permeate flux and energy efficiency are two important parameters that should be concomitantly optimized to improve the general performance of DCMD. These two parameters are directly proportional to the operating conditions (e.g., the feed and permeate temperatures, flow velocity in channels, and the salinity) and the membrane characterization (e.g., pore size, conductivity, thickness, porosity, etc.). Therefore, a simultaneous heat, mass, and momentum transfer simulation should be investigated to understand the influence of each parameter and find the most optimum operational condition. Moreover, the temperature and concentration polarizations (TP and CP, respectively) are two of the most important factors that hinder the operation of DCMD and decrease its efficiency. These two parameters are highly proportional to the properties of the membrane and the operational condition. Therefore, a deep understanding the effect of each parameter is highly recommended to modify the system accordingly. Computational fluid dynamics (CFD) is a powerful tool for modelling and simulating MD systems to demonstrate fluid behaviour during desalination. However, only a few studies have reported the CFD simulation of ENMs in the DCMD-based desalination [220].

Different studies have been performed to model the performance of the DCMD systems; however, some of them have relied on correlations or assumptions that are not clear or accurate. CFD offers a comprehensive and more accurate transport field, including full momentum, mass and heat transfer profiles throughout the system [147, 178]. The simultaneous evaluation of temperature, velocity, and concentration brings the advantage of easily identifying the bottlenecks of the process and optimization of the system that are too complex via experiments [178-180]. Moreover, many studies that used 2 and 3

dimensional CFD simulation for DCMD modelling just focused on coupling of mass and heat transfer without investigation of hypersaline feed salt concentration and mostly focused on up to 3.5 wt% salt concentration [181-189]. Other studies investigated the salt concentration without a deep study of temperature distribution and polarization and optimum physical parameters of the membrane in different feed-side salt concentrations [174, 190-193].

In this work, a triple-layer Janus membrane with nanofibrous structure was developed to enhance the energy efficiency and to maintain the high permeate flux and rejection for desalination of high salinity solutions. The membrane structure consists of three layers, including a top hydrophobic layer, a middle thermal insulation layer, and a bottom hydrophilic layer. The membrane was characterized comprehensively and their performance in DCMD was evaluated. The membrane performance was also compared with a single and a dual layer ENM for better understanding of the role of the middle insulation layer on enhancing the energy efficiency. The salinity of feedwater was varied to derive the trend of different parameters in various concentrations of NaCl and find the optimum operational condition for DCMD.

4.2 Materials and methods

4.2.1 Materials

PcH (Mw~400,000 $gmol^{-1}$), PAN (Mw~150,000 $gmol^{-1}$), and PS (Mw=35,000 $gmol^{-1}$) were used as raw polymers for the fabrication of nanofibers. DMF (99.8% purity), acetone (ACS reagent, >99.8%) as well as the LiCl salt (purity>99%), were used as solvent and co-solvent, respectively. All above materials were purchased from Sigma Aldrich. Deionized water and

commercial NaCl were used for the preparation of the saline solution for MD experiments. A commercial PVDF membrane with a pore size of 0.22 µm was purchased from Millipore (USA) and was used for comparison. All materials were used as received, without any further purification.

4.2.2 Electrospinning

Figure 4-1 shows a schematic of the electrospinning system used in this study. Details of the electrospinning setup can be found in our previous work [231]. To fabricate the nanofiber samples, various optimum solutions of each polymer were first prepared and used for electrospinning to obtain bead-less and uniform nanofibers. The electrospinning conditions and compositions of the dope solutions are presented in Table 4-1. For the preparation of 10 wt% PAN solution, 20 mg of LiCl was added to 14.4 mL of DMF and after dissolution, 1.5 g PAN was added to the solution. LiCl addition can enhance the electrospinnability of the dope solution. The dope solution was then stirred (150 rpm) overnight at 70 ^{o}C. After preparation of the solution, it was cooled down and degassed. To prepare a 15 wt% PcH solution, 3.3 mL of acetone was added to10.9 mL of DMF to control the rate of evaporation of solvent through the electrospinning process and fabrication of nanofibers having desirable morphology. Then, 0.1 wt% of LiCl was added to the mixture of solvents, followed by adding 2.25 g of PcH to the mixture at room temperature. Moreover, to prepare an 11 wt% PS solution, 1.65 g of PS was added to 14.2 mL DMF and stirred overnight, then followed by degassing step.

To fabricate the single layer ENM, the PcH solution was placed into a 10 mL syringe and electrospinning was performed. For the dual layer ENM (i.e., PAN/PcH), first the PAN solution was electrospun and then followed by electrospinning of PcH solution. It should be noted that the electrospinning of PcH solution was started 5 min before completion of the PAN electrospinning. This simultaneous electrospinning could help provide the entanglement of the PAN and PcH nanofibers. As a result, a delamination-free multiple layer membrane could be fabricated. In the case of the triple layer ENM, PAN was first electrospun, then followed by PS solution and then finally by PcH solution. For every layer change, the two interconnecting layers are simultaneously electrospun for 5 min to produce entanglement of each different layer [231].

Table 4-1. Electrospinning conditions for each fabricated layer.

Solution	C_P	C_{DMF}	$C_{acetone}$	Q_d (mL/h)	HV (kV)	L (cm)	T(^oC)	RH (%)
PcH	15 wt%	68 wt%	17 wt%	0.5	18	15	21	69
PAN	10 wt%	90 wt%	0	1	15	12	21	71
PS	11 wt%	89 wt%	0	1	15	12	23	65

C_p: polymer concentration
C_{DMF}: DMF concentration
$C_{acetone}$: Acetone concentration
Q_d: Injection rate for the dope solution
HV: Applied high voltage
L: Tip-to-collector distance
T: Electrospinning temperature
RH: Relative humidity

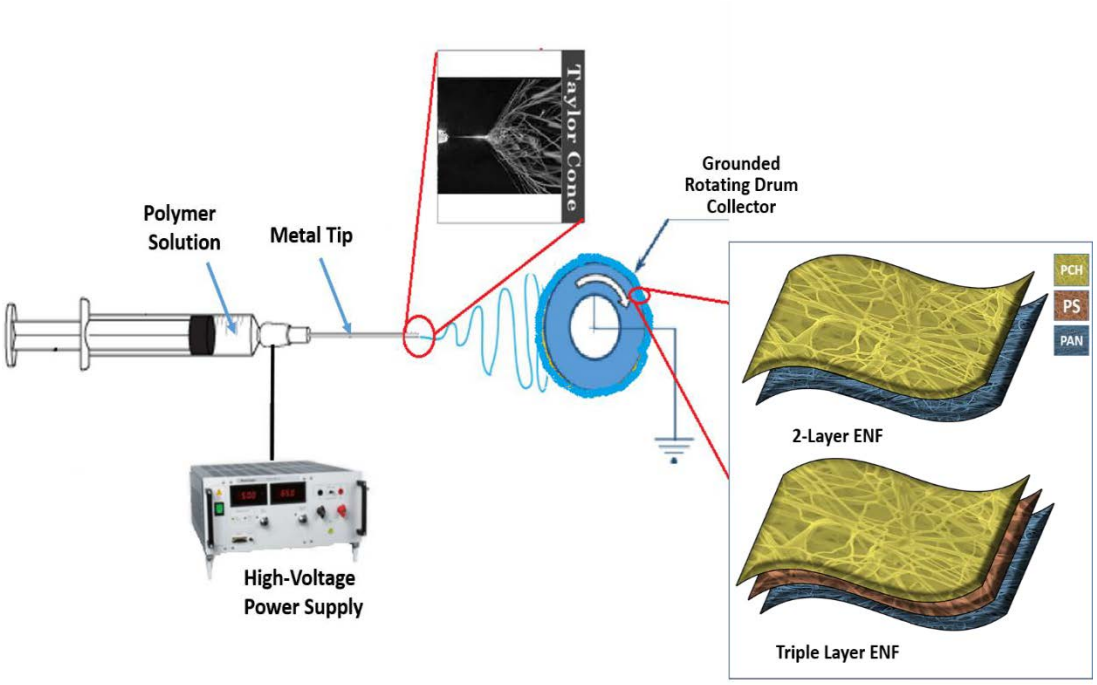

Figure 4-1 Schematic of the electrospinning system used in the present study. The process includes sequential electrospinning of different solutions to fabricate multilayer ENFs. For example, for the triple layer nanofiber membrane, the support PAN layer was first electrospun, then followed by the PS nanofiber on top of PAN layer, and then finally the PcH nanofiber on top of PS layer.

Two samples of triple-layer Janus ENMs having different thicknesses of the middle layer (insulation layer made of PS) were fabricated to study its effect on the overall energy efficiency and MD performance. To change the thickness, we varied the electrospun solution amount in the middle PS layer: one at 2 mL (PS20 sample) and one at 4 mL (PS40 sample). After the preparation of the membrane samples, the ENMs were exposed to a heat pressing step. This could enhance the integrity and reduce the delamination risk for the multi-layer membrane samples. The heat press conditions were well explained in our previous work [231]. Afterwards, the membranes were placed into an oven for complete drying and evaporation of the remaining solvents.

4.2.3 Membrane characterization

FESEM

The nanofiber membrane samples were firstly cut and coated with Au/Pd prior to analysis. An accelerating voltage of 10 kV was applied, and images at different magnifications were taken. The pore size, fibre diameter, and fibre diameter distribution were measured using the ImageJ software (FIJI) by analyzing at least 100 counts based from the SEM images.

Gravimetric method

A sample of the nanofiber membrane was dried, weighed, and then immersed into isopropanol for 10 minutes to ensure complete wetting of the entire membrane structure. Afterwards, the membrane sample was taken out and surface liquid was wiped out, then it was weighed. The porosity of the ENM sample was measured according to the physical properties of the polymer and the weight change of the sample, using the following equation:

$$\varepsilon = \frac{(W_1 - W_2)/\rho_e}{[(W_1 - W_2)/\rho_e] + W_2/\rho_p} \quad (4\text{-}1)$$

where, W_1 and W_2 are the weights of the sample in wet and dry conditions (g), and ρ_e and ρ_e are the densities of the wetting liquid (isopropanol) and polymer ($g.cm^{-3}$), respectively.

Thermal Conductivity Measurement

In this study, thin film module of the Hot Disk TPS 2500S was used to measure thermal conductivity of electrospun nanofibers following the ISO standard 22007-2 (TPS 2500S, Hot Disk ab, Gothenburg, Sweden). The experimental procedure involved placing two nanofiber samples on either side of a nickel double coil equipped with a temperature sensor. The samples were subjected to heating by applying power, while simultaneously monitoring the temperature changes in the nanofibers over time. Thermal conductivity was subsequently calculated by analyzing the resistance exhibited by the samples in response to the applied heat.

4.2.4 DCMD tests

The desalination performance of the fabricated membrane samples was tested via DCMD (Figure 4-2). The membrane sample was placed into a lab-scale DCMD module with a 26 cm^2 effective membrane area. The feed and permeate flowrates were both set at 400 cm^3min^{-1}. The permeate temperature was kept constant at 20 ^oC for all tests, while the feed temperature was varied at 50, 60, and 70 ^oC to evaluate the performance of the membranes at different temperatures. Different salinities in the range of 0-200 gL^{-1} were investigated to explore the effectiveness of the newly developed membranes for desalination of hypersaline feedwater.

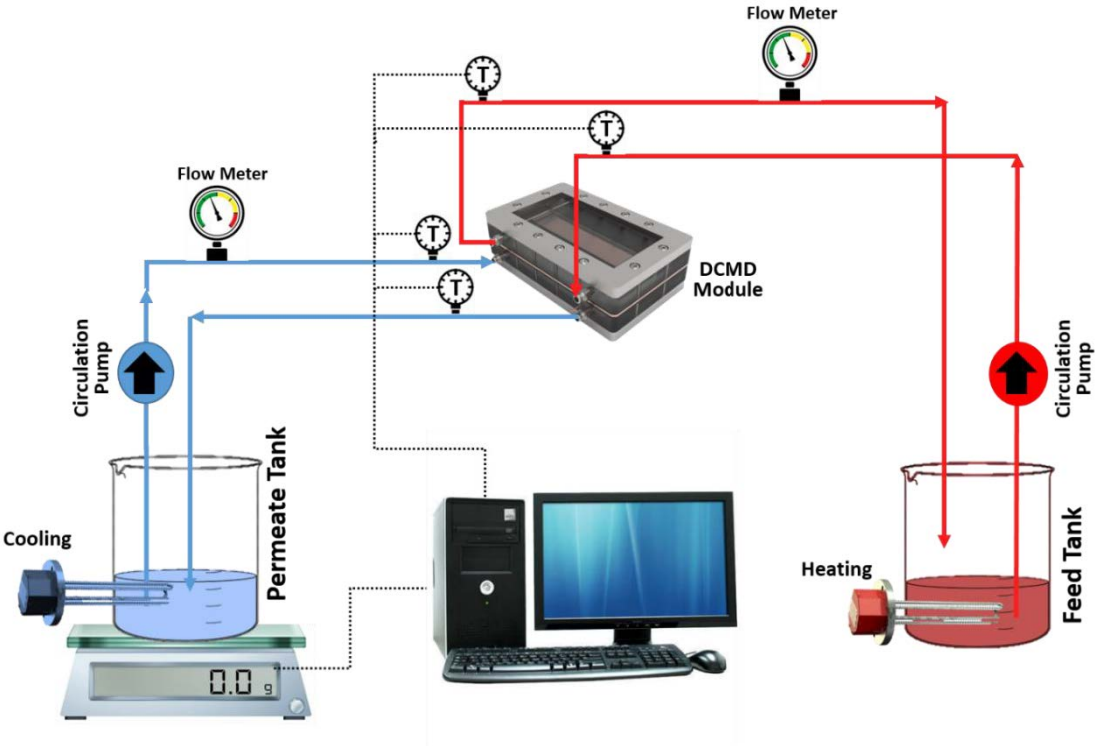

Figure 4-2. Schematic of the present DCMD experimental setup. The system is composed of a hot feed NaCl solution in one side of the membrane and a cold DI water solution on other side of the membrane.

The permeate flux and the salt rejection of the membranes were calculated using the following equations:

$$J = \frac{\Delta m}{A \times \Delta t} \tag{4-2}$$

$$R(\%) = \frac{C_f - C_p}{C_f} \times 100 \tag{4-3}$$

where *Δm* and *Δt* are the mass of the water accumulated in the permeate side (g) and time (s), respectively, and *J* represents the permeate flux of the system ($Lm^{-2}h^{-1}$ or LMH). For salt rejection, *C* (ppm) refers to the concentration of the salt on the feed side (f) and the recovered water in the permeate side (p). A conductivity meter (HQ40d, Hach) was used to

measure the electrical conductivity of the solution, which was used to check the intrusion of feed solution into the membrane pores and membrane wetting.

4.2.5 Energy efficiency measurement

The energy efficiency (EE) of the MD membranes is the ratio of the heat transfer via the evaporation of the water that provides the permeate flux to the total heat transfer through the membrane [23]. The EE is evaluated according to the following correlations:

$$EE(\%) = \frac{Q_{flux}}{Q_{flux}+Q_{conduction}} = \frac{Q_{flux}}{Q_{overall}} \quad (4\text{-}4)$$

where,

$$Q_{flux} = J.\Delta H \quad (4\text{-}5)$$

and

$$Q_{overall} = \frac{\dot{m}C_P(T_{in}-T_{out})}{A} \quad (4\text{-}6)$$

In these equations, Q_{flux} is measured by multiplying the permeate flux (J) in LMH to the enthalpy of evaporation (ΔH) in Jkg^{-1}. $Q_{conduction}$ is calculated by using $\dot{m}$ as the feed flowrate (kgs^{-1}), A as the membrane surface area (m^2), C_p as the specific heat capacity of the feed solution ($Jkg^{-1}C^{-1}$), and T_{in} and T_{out} as the inlet and outlet temperatures (^oC) of the bulk, respectively.

4.3 Simulation

4.3.1 Governing equations

This study focuses on the three-layer nanofiber membrane to improve the efficiency and flux rate of DCMD. The three layers are composed of a hydrophobic membrane layer (PcH), another thin hydrophobic layer (PS) with high thermal insulation and low

conductivity, and the third layer is a hydrophilic membrane (PAN) as support. A two-dimensional flat-sheet membrane was used as the basis for both experiments and modelling. Experiments and modelling were based on feed and permeate temperatures of 60 ^{o}C and 20 ^{o}C, respectively with DI water as permeate and NaCl solution at various salinities as feedwater. Table 4-2 presents the membrane characteristics that were used to simulate the DCMD process using COMSOL. The transport phenomena were simulated for flat sheet membranes in a counter-current flow across the membrane, considering both conductive and convective terms. The system is divided into three sections: the feed (hot) side containing saline water, the multilayer applied membranes, and the permeate (cold) side containing fresh water with no salinity. Moreover, it was considered that water evapour ated in the feed-membrane interface using the available thermal energy, passing through the first membrane pores then in the first-two interface membranes water molecules diffuse in the second hydrophobic membrane and finally in the last membrane interface water vapour is condensed due to the hydrophilicity of third layer and water passes through membrane to reach the permeate-membrane interface.

The following assumptions have been made to simplify the simulation. The flow streams have been assumed to be laminar and fully developed inlets, and the heat and mass transfer properties are considered homogenous through the membranes [175, 232]. Moreover, each membrane pore size has been assumed to be identical, and the flow regime in first two layers was assumed to be a combination of molecular diffusion and Knudsen diffusion and the third layer was assumed to be molecular diffusion [221, 233]. The heat transfer in membrane layers occurs by conduction and convection simultaneously. Modified

saturation pressure was applied in the saline water interface for driving force. The convective mass transfer was neglected inside the pores (the diameter of the pores was not in the range for the Darcy flow, and no convective momentum was inside the pores) [202]. Furthermore, the flow was assumed to reach its steady-state condition, and the heat loss to the environment has been neglected. All membrane properties were assumed to be constant during the test [200, 201]. The Transmembrane mass transport, Energy equations for the membrane, thermal conductivity measurement, and equations for the channel flows have been described in Chapter 3.

4.4 Results and discussion

4.4.1 Morphology

The SEM images of different electrospun nanofibrous layers at various magnifications are shown in Figure 4-3. As could be observed, bead-less nanofibers were fabricated for all layers with different polymers. The incorporation of an appropriate amount of LiCl to the dope solution, and the presence of the co-solvent (acetone) could facilitate the formation of smooth fibres. This can be attributed to the enhancement of the electrical conductivity and reduction of the viscosity of the dope solution, leading to more stretching and whipping of nanofibers [234, 235]. Moreover, a net-like structure for all nanofibrous layers was achieved. This highly porous structure with inter-connected pores can increase the void volume for the vapour molecules transferring from the feed channel to the permeate side, which can lead to an increased permeate flux. The mean diameters of PcH, PS, and PAN nanofibers were measured to be 200±4 nm, 120±12 nm, and 170±48 nm, respectively. This

is in good agreement with the published results in the literature for the electrospun nanofibers made of similar polymers [236, 237]. Moreover, the applied heat-press post-treatment did not affect the nanofiber diameters.

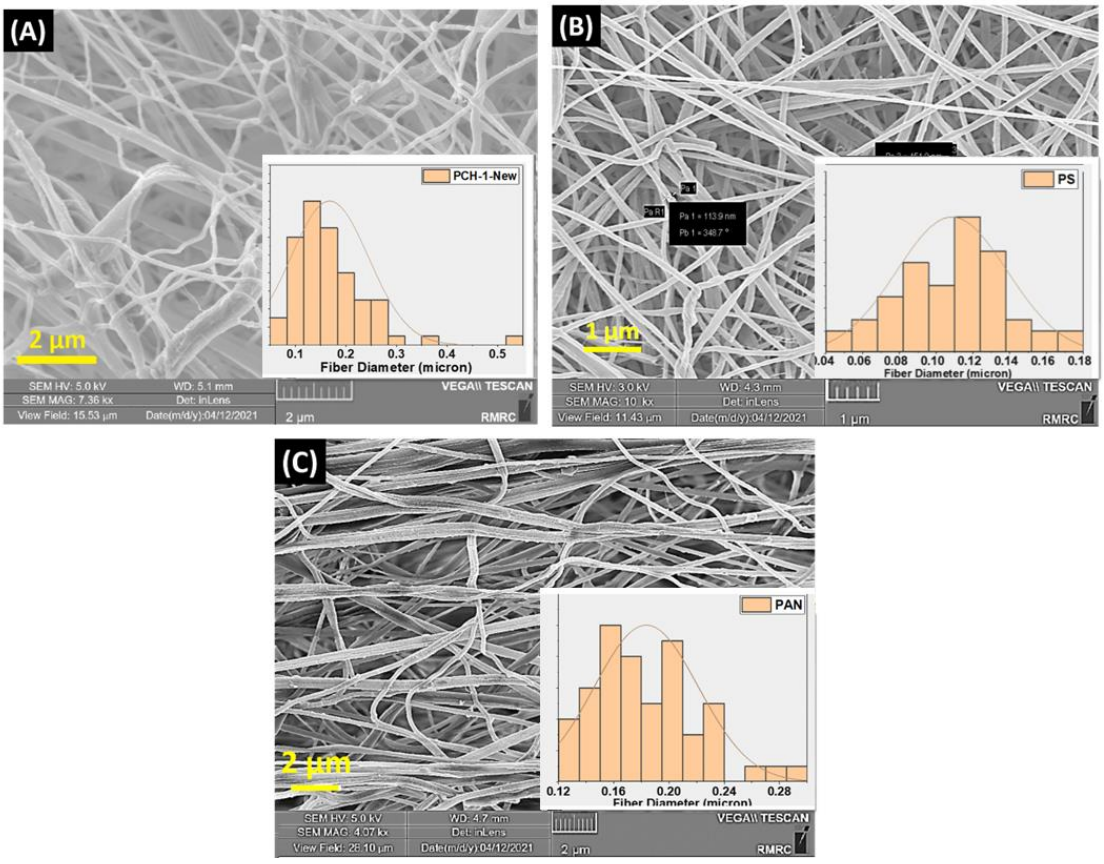

Figure 4-3. SEM images of (A) PcH, (B) PS, and (C) PAN nanofiber layers, and their corresponding fibre diameter distribution.

4.4.2 Membrane characteristics

Table 4-2 presents the characteristics of the fabricated membrane for each layer, namely PcH layer, PAN layer, PS20 layer (triple layer), and PS40 layer (triple layer). As could be observed, the PcH and PAN single-layer nanofiber samples possess a mean pore size of 0.24±0.07 and 0.18±0.03 µm, respectively, while the PS nanofiber sample had 0.35±0.01 and 0.28±0.01 µm for PS20 and PS40, respectively. The reduction in the pore size of the PS40 sample can be attributed to the higher fibre density with longer spinning time. This agrees with the reported results on the effect of the electrospinning time on ENM properties, in particular the mean pore size [217, 225].

Table 4-2. Characteristics of various single and multilayer nanofiber membranes used in this study.

Membrane code	Mean pore size (µm)	Mean fibre Diameter (µm)	Thickness (µm)	Porosity (%)	WCA (degree)	LEP (kPa)	Thermal Conductivity ($Wm^{-1}K^{-1}$)
PcH layer	0.24±0.07	0.20±0.04	108-117±2.1	79±1.0 [a]	135±1.5	96±6	0.107±0.008
PAN Layer	0.18±0.03	0.17±0.02	117-123±1.9	75±1.7 [a]	90±6.5	-	0.149±0.005
PS20 Layer	0.35±0.01	0.13±0.02	18±0.4	83±1.3 [a]	118±1.1	-	-
PS40 Layer	0.28±0.01	0.12±0.03	45±0.7	84±1.2 [a]	115±1.2	-	-
PCH/PAN Membrane	-	-	230±2.5	78±0.7 [b]	-	94±4	0.121±0.011
PS20 Membrane	-	-	246±0.9	82±1.2[b]	-	203±9	0.093±0.007
PS40 Membrane	-	-	272±1.1	83±1.4[b]	-	219±8	0.074±0.009
Commercial PVDF	0.22	-	110	75%	122	204	0.131±0.003

[a] measured by ImageJ software analysis
[b] measured by gravimetric method

The PS nanofiber layers possess higher porosity in comparison with other nanofiber samples (83 and 84% for PS20 and PS40, respectively). Meanwhile, the PcH nanofiber layer showed higher surface hydrophobicity with a water contact angle (WCA) of 135°, while it was measured at about 118 and 115° for the PS20 and PS40 nanofiber layers, respectively. The PAN layer was quite hydrophilic, thus, the water droplet could easily wick into the membrane, providing very low WCA.

Moreover, to assess the impact of the middle layer on the thermal resistance of the membranes, the thermal conductivity of single, double, and triple layer membranes was measured. The results, presented in Table 4-2. Characteristics of various single and multilayer nanofiber membranes used in this study., provide insights into this effect. The thermal conductivity of the PCH/PAN ENF membrane was 0.121 W/m.K. However, upon electrospinning the PS ENF layer (PS20), the thermal conductivity decreased to 0.093 W/m.K. Furthermore, an increase in the thickness of the middle layer resulted in a more significant reduction in thermal conductivity, with the PS40 membrane exhibiting a thermal conductivity of 0.074 W/m.K. These findings clearly demonstrate that the incorporation of PS ENFs leads to a substantial decrease in the thermal conductivity of the membranes.

The LEP test is performed to study the tolerability of the membrane against the intrusion of the saline solution into the pores. The LEP values for the single, dual, and triple-layer Janus nanofiber membranes are also shown in Table 4-2. As could be observed, the single-layer PcH membrane possesses an LEP of 96 kPa, which is not high enough to guaranty the anti-wetting performance of an MD membrane. The LEP value for the dual-layer PcH-PAN

membrane also returned similar value at 94 kPa which is maybe due to the intrusion of the PAN layer into the PcH layer during the electrospinning, that causes the reduction in the effective hydrophobic layer thickness. The LEP values for the triple-layer Janus ENM samples, however, increased up to 203 and 219 kPa for the PS20 and PS40 membranes, respectively. This can be attributed to the thicker structure of the hydrophobic layers as well as the overall thickness of these membranes. The triple-layer ENMs consist of two hydrophobic layers on the top of the PAN nanofiber layer, which could potentially enhance the LEP of the membrane. It should be noted that the higher the LEP value, the lower the pore wetting risk. Therefore, more stable DCMD performance with a better anti-wetting behaviour can be expected for membranes with higher LEP values, i.e., the triple-layer ENMs in this work (Table 4-2). This was also evaluated experimentally and is discussed in the next section.

4.4.3 Desalination performance using the DCMD process

4.4.4 Model validation

The results of the simulation were validated using the experimental data at similar operating conditions. The simulation study was performed by using COMSOL Multiphysics to derive the trend of various profiles and to deeply understand the transport phenomena in the DCMD process for the ENMs. The validated data was then used to obtain the performance of the membrane in various operational conditions and membrane characteristics. Table 4-3 compares the experimental and simulation results of the triple-layer membranes.

Table 4-3. Comparison of the experimental and simulation results of the triple layer membranes.

No.	Material	dT (°C)	Salinity (g/L)	Exp Flux (LMH)	Modelling Flux (LMH)	Error (%)	EE Exp	EE Modelling	Error (%)
1	PS20	40	0	19.5	19.13	1.9	83	87	4.8
2	PS20	40	50	17.5	17.6	0.6	81	86	6.2
3	PS20	40	100	15.8	16.12	2.0	75	80	6.7
4	PS20	40	150	14.3	14.6	2.1	71	76	7.0
5	PS20	40	200	12.5	13	4.0	66	69	4.5
6	PS20	30	200	6.1	7.1	16.4	57	60	5.3
7	PS20	30	0	11.5	9.5	17.4	70	74	5.7
8	PS20	50	200	22.7	22	3.1	78	80	2.6
9	PS20	50	0	34	33.6	1.2	91	94	3.3
10	PS40	40	0	15.8	15.95	0.9	88	93	5.7
11	PS40	40	50	15.1	15.1	0.0	84	87	3.6
12	PS40	40	100	14.3	14.15	1.0	80	85	6.3
13	PS40	40	150	13.2	13.2	0.0	76	82	7.9
14	PS40	40	200	12.5	12.2	2.4	71	74	4.2
15	PS40	30	0	9.5	6.85	27.9	70	73	4.3
16	PS40	30	200	7.3	5.15	29.5	61	63	3.3
17	PS40	50	0	31	32.5	4.8	91	95	4.4
18	PS40	50	200	24	24.6	2.5	85	89	4.7

As the vapour pressure difference is the main driving force in the DCMD process, the simulation process was used for drawing the temperature and vapour pressure profiles of

different layers of triple-layer ENM samples to understand the rate of temperature and vapour pressure change along the membrane module as well as on various layer interfaces. The results in Table 4-3 show errors to be within 5% indicating the accuracy and good agreement of the experimental and simulation results. Vapour pressure depends on the temperature and concentration of non-volatile particles. The relevant equations have been used to simulate and derive the local values of temperature, concentration, and velocity to derive the flux of the membrane.

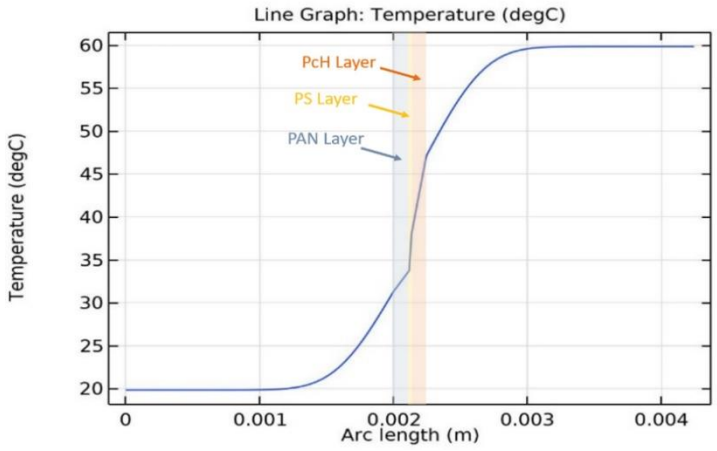

Figure 4-4. the temperature distribution along an imaginary line at the midpoint of the membrane module, progressing from the feed channel to the permeate channel - The graph depicts the difference in rate of heat transfer attributed to the thermal conductivity of the nanofiber layers.

Figure 4-4 shows the temperature profile in an imaginary line in the middle of the membrane module, from the feed channel towards the permeate channel. The feed and permeate bulk temperatures are equal to the inlet temperatures. The trend of change in the temperature in different layers is also shown in the figure. The results revealed that the rate of drop in temperature for the PcH layer (top layer) is lower than the PS layer (the middle layer). This variation occurs due to changes in thermal conductivity and porosity of

the layers, which affect the rate of temperature drop [39, 46, 47]. The PS layer plays the role of an insulator and prevents the heat loss through the heat conduction of the bulk membrane. Therefore, as shown in Figure 4-4, the temperature difference per unit thickness across the PS layer is more significant than that of the PcH layer (PcH layer has over 100 μm thickness while the PS layer has 20 μm thickness). The vapour molecules condense and form a liquid phase in the PAN layer (bottom support layer). This could cause the difference in the trend of temperature distribution compared to the vapour phase.

4.4.5 DCMD performance

Figure 4-5 a illustrates the effect of feed salinity, i.e., the concentration of salt in the feed stream and in the permeate flux, obtained via the experiments. As could be observed, the permeate flux decreased for all membrane samples with higher concentration of salt in the feed solution. It is well-known that the driving force for DCMD is the difference in the vapour pressure, which is caused by the temperature difference between the two sides of the used microporous membrane [48]. As could be observed in Figure 4-5, among the tested membrane samples, the PcH-PAN dual-layer membrane showed the highest experimental permeate flux (22 $kgm^{-2}h^{-1}$) at 0 g/L salt concentration. This can be attributed to the zero-salt content in the feed solution and the composite structure of the membrane, which consists of a top hydrophobic layer and a bottom hydrophilic layer, and a thinner thickness. While the hydrophobicity of the top layer can prevent the feed from intrusion into the pores, the hydrophilicity of the bottom layer can help to extract out the permeated vapour molecules. This facilitated mass transfer mechanism agrees well with the reported results

in the literature [2]. However, the permeate flux decreased to 10.7 $kgm^{-2}h^{-1}$ at 200 gL^{-1} salt concentration, which is mainly due to the lower water activity and higher temperature polarization at this salt concentration in the membrane module. Compared with all the tested membrane samples, the PS40 triple-layer membrane showed the lowest flux decline. This can be attributed to the lower effect of concentration polarization for thicker membranes at high salinity as well as higher energy efficiency of this membrane compared to other samples, due to the incorporation of the middle-insulated layer. Moreover, the sharpest flux decline was observed for the single-layer PcH membrane. The commercial PVDF membrane, however, possessed the weakest performance in terms of the permeate flux with a considerable decline at higher salt concentration in the feed stream. From Figure 4-5, the simulation results (solid lines) showed adequate agreement with the experimental data. This could also prove the accuracy of the validated model. The values of both experimental and simulation as well as error values are shown in Table 4-3. In addition, the values of flux of the different types of membranes and relevant thickness and porosity are shown in Table 4-4. The result reveals that the flux is inversely related to the salinity and thickness of the hydrophobic layers. However, the thickness of membranes shown in Table 4-4 for PS20, PS40, and PCH/PAN membrane is a combination of both hydrophobic and hydrophilic parts. Regarding the fabrication process, the findings indicate that an increase in the thickness of hydrophobic layers leads to a decrease in flux at lower salinities. However, at higher salinities, the thermal properties of the layers have a more significant impact on flux.

Table 4-4 The value of flux of different membranes in a wide range of salinities from 0 to 200 g/L and value of porosity and thickness of membranes

Salinity (g/L)	Flux				
	PS20	PS40	PcH/PAN	PcH	Commercial
0	19.13	15.8	23	22	15
50	17.6	15.1	20.7	19	12.9
100	16.12	14.3	17.9	15.8	10
150	14.6	13.2	14.2	12.6	8
200	13	12.5	10.7	7.8	5.6
Thickness (µm)	246	272	230	112	110
Porosity %	82	83	78	79	75

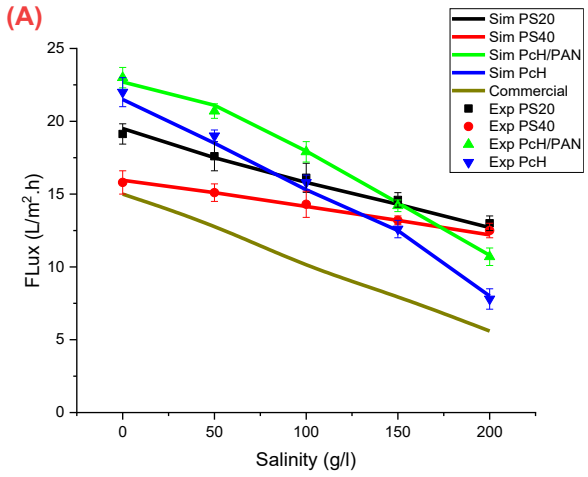

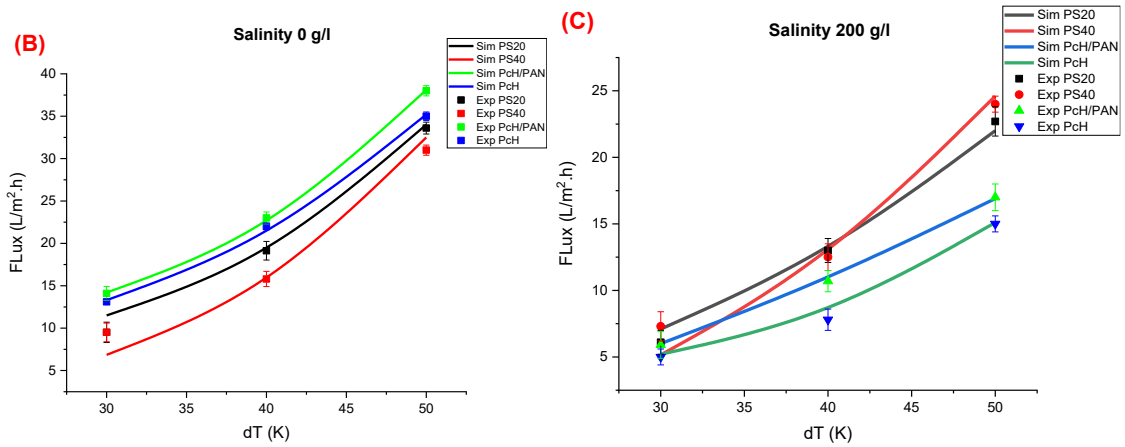

Figure 4-5. (A) Effect of feed salinity on the permeate flux for different membrane samples (feed and permeate flowrates of 400 cm^3min^{-1}, feed and permeate temperature of 60 and 20 ^oC, respectively, salinity from 0-200 gL^{-1}), and the effect of temperature difference on the permeate flux at different salinities of (B) 0 gL^{-1} and (C) 200 gL^{-1}, respectively (feed and permeate flowrates of 400 cm^3min^{-1}, permeate temperature of 20 ^oC, and feed temperature: 30, 40, and 50 ^oC).

Figure 4-5 B and C illustrate the permeate flux variation versus the feed temperature at the lower and upper bounds of the investigated feed salinities, i.e., 0 and 200 gL^{-1}. As could be observed, when distilled water was introduced to DCMD, the permeate flux increased with the increment in the temperature difference in the order of PcH-PAN>PcH>PS20>PS40>PVDF. This can be attributed to the structure and thickness of the membranes when they are used for desalination experiment in the presence of 0 gL^{-1} salinity. When the solute concentration in the feed stream is quite low, the thinner the membrane, the higher the permeate flux. This is the main reason for observing higher permeate flux for single and dual-layered membranes. Moreover, the hydrophobic-hydrophilic structure of the PcH-PAN membrane could facilitate the higher permeate flux at 0 gL^{-1} salt concentration in the feed solution. This is in good agreement with the literature [10, 49]. However, one may ask about the better performance of the PcH-PAN membrane

in comparison with the single-layer PcH one. Dual-layer ENMs consist of a hydrophobic top layer, which is in direct contact with the hot feed stream, and a hydrophilic or less hydrophobic bottom layer, which is in direct contact with the permeate stream. In this structure, each layer has its own contribution to the membrane performance. While the thinner top layer can prevent the pore wetting by repelling the process liquid from entering the pores, the bottom hydrophilic layer can extract the vapour molecules and enhance the permeate flux, considerably. Moreover, better mechanical strength can be achieved using this structure. However, in the presence of zero or a very low solute concentration in the feed stream, the thinner structure can provide higher permeate flux due to the lower mass transfer resistance from the feed channel towards the permeate channel through the membrane pores. This is in good agreement with those reported in literature [23]. On the other hand, different membrane performance regarding the permeate flux was observed when a higher salt concentration (200 gL^{-1}) was introduced to the feed stream. As could be observed in Figure 4-5 C, the PS40 membrane with triple layer structure could provide higher permeate flux in comparison with others. This can be attributed to the thicker structure, as thick membranes are less sensitive to the temperature polarization compared to thin membranes [50]. The middle layer made of PS could also insulate and further reduce the effect of temperature polarization via lower heat loss through the membrane thermal conduction.

In this study, a thin insulator layer of PS nanofiber is placed between the top and bottom layers. Moreover, the high porosity of PS nanofiber layer, which is over 80%, can further reduce the thermal conductivity of the middle layer. The thermal conductivity results

obtained for membranes (as shown in Table 4-2. Characteristics of various single and multilayer nanofiber membranes used in this study.) proof that embedding a thin layer of PS nanofibers drops the thermal conductivity of membrane and enhance its thermal resistivity. Therefore, the presence of the PS nanofiber layer can considerably decrease the heat loss through the polymer matrix. Although increasing the membrane thickness is another obstacle in an efficient MD process, the experimental results demonstrated that for the treatment of hypersaline water, having low conductivity and an optimum thickness is preferable. Therefore, the middle layer can play two positive roles in the desalination of high salinity water: it decreases the conductivity and increases the thickness to reach the optimum thickness for increasing the permeate flux. Figure 4-6 illustrates the cross-section SEM image of the triple-layers nanofibrous membrane (PS40) sample in this work. Here, the middle-layer made of PS polymer can insulate the membrane and reduce the heat transfer from the feed channel with higher temperature towards the permeate channel with lower temperature. As a result, lower heat loss through the membrane conduction would be expected. This discussion was also proved experimentally in this research.

On the other hand, one may ask about the increase in the membrane thickness, which can impose a considerable mass transfer resistance. This can be explained according to the DCMD membrane performance when high salinity solutions are processed for water and salt recovery. In fact, thicker membranes can perform better in processing of high salinity brines in comparison with thinner membranes. This is due to the lower effect of the temperature polarization of thicker membranes ($\delta \geq 180$ μm) for processing of solutions with high salt content (>150 g/L) [50]. In other words, at high salinity, the positive influence of

lower temperature polarization can overcome the negative effect of the mass transfer resistance for thicker membranes. This can also be further enhanced when the membrane is thermally insulated, as the obtained results experimentally proved. Therefore, our results indicated that the membrane performance for high salinity range (200 $g.L^{-1}$) at different temperature differences is in the order of PS40>PS20>PcH-PAN>PcH>PVDF (Figure 4-5 C).

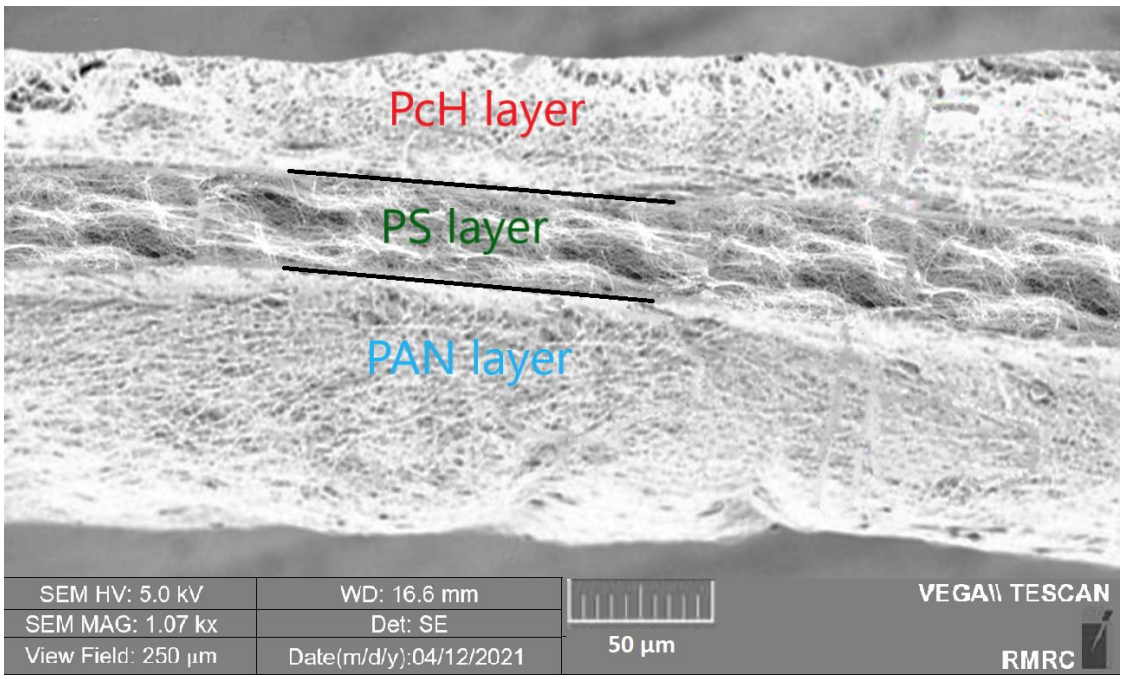

Figure 4-6. Cross-section SEM for structural observation of the triple-layers (PcH-PS-PAN) electrospun nanofiber membrane sample (PS40). The SEM image clearly shows difference in properties of the fabricated layers.

4.4.6 Energy efficiency

In the DCMD process, the heat transfer through the membrane includes two main mechanisms, i.e., heat transfer provided by the permeate flux (transferring by the vapour

molecules from the feed side towards the permeate side through the membrane pores) and heat transfer due to conduction through the bulk membrane. The latter is considered as a bottleneck in DCMD, i.e., heat loss, as it can cause the temperature polarization, resulting in considerable flux decline. As mentioned earlier, energy efficiency (EE) is defined as the ratio of the efficient heat transfer due to the permeate flux and the total heat transported through the membrane [50]. Figure 4-7 illustrates the effect of feed salinity as well as the effect of feed temperature difference at various salinities (0 and 200 $g.L^{-1}$) on the energy efficiency of the fabricated membranes. As could be observed, the energy efficiency decreased with increasing the salinity for all tested membrane samples. Among them, the sharpest decrease was observed for the commercial PVDF membrane. However, the highest energy efficiency was observed for the triple-layer ENM with the thicker PS middle layer (i.e., PS40). For this membrane, EE was measured at 71% at the highest tested feed salinity (200 $g.L^{-1}$). According to the obtained results, the order of membranes performance in terms of EE is as follows: PS40>PS20>PcH-PAN>PcH>PVDF indicating that the incorporation of the insulated middle layer could considerably enhance the energy efficiency of the DCMD membrane, even at high salt concentration.

The simulation process has been used to evaluate the inlet and outlet temperature of the feed stream to evaluate the energy efficiency of the DCMD process. In this study the average inlet and outlet values driven by the simulation were placed in the energy efficiency equation to obtain EE values and results are shown in Figure 4-7. The results revealed that EE obtained by simulation is higher than experimental values. This trend can be mainly attributed to this point that the data acquired by simulation are for the exact inlet and outlet

points of the membrane module. Thus, the simulation data for outlet temperature of feed stream is higher than experimental value which was obtained by the utilized thermal sensors placed in the outlet of the module. Furthermore, in the simulation, the heat loss through the module was ignored, while in experiment the heat loss to the environment could affect the outlet temperature of the feed stream. Thus, the outlet temperature could be lower than the inlet one. As a result, the inlet and outlet temperature difference of the simulation data is lower than the experimental data. That is why the derived EE of simulation is higher than experimental result.

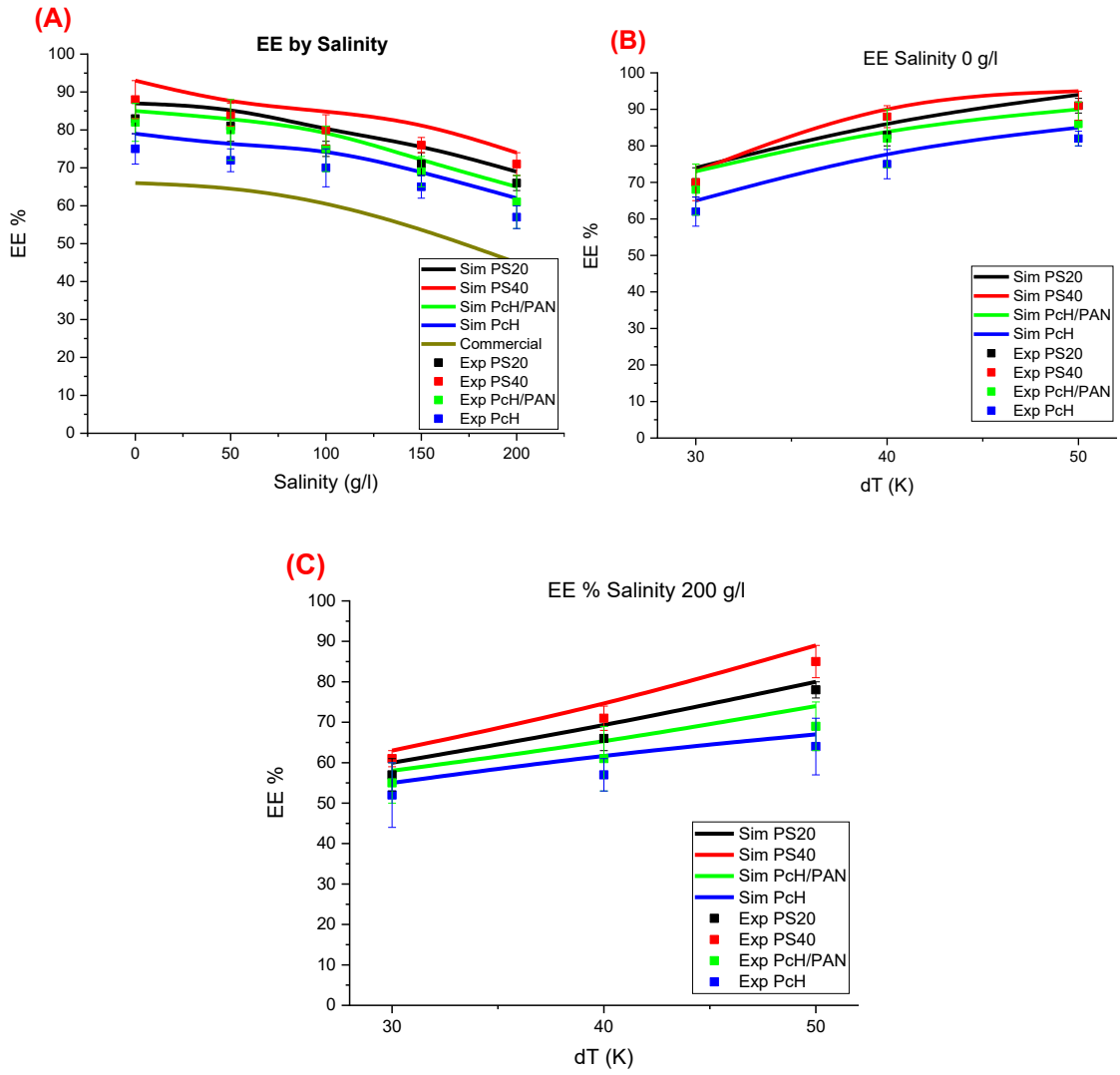

Figure 4-7. (A) Effect of feed salinity on the energy efficiency (EE) for different membrane samples (The feed and permeate flowrates of 400 $cm^3.min^{-1}$, feed and permeate temperature was set at 60 and 20 °C, different salinities in the range of 0-200 $g.L^{-1}$), and the effect of temperature difference on EE at different salinity, (B) 0 $g.L^{-1}$ and (C) 200 $g.L^{-1}$, respectively (The feed and permeate flowrates of 400 $cm^3.min^{-1}$, permeate temperature was set at 20 °C, and feed temperature was set at 30, 40, and 50 °C).

As could be observed in Figure 4-7, despite decreasing EE with increasing salt concentration (Figure 4-7 a), the energy efficiency increased for the triple-layer membranes at higher operating temperatures for both 0 and 200 $g.L^{-1}$ feed concentrations. This supports the

increment of the permeate flux for the same membrane samples. At higher salt concentrations, this can be attributed to the lower negative effect of the temperature polarization on the permeate flux and EE. In particular, while the permeate flux is reduced at higher salt concentrations, the driving force for the mass transfer is not affected by the heat loss due to conduction.

The highest energy efficiency was observed for the PS40 membrane, even at high salt content in the feed solution. Figure 4-8 schematically illustrates the concept of the heat loss and energy efficiency for the newly developed triple-layer membrane in comparison with the conventional membranes with single or dual-layer structures. As could be observed, the incorporation of the PS nanofibrous layer into the membrane structure could considerably reduce the temperature polarization and heat loss effects. This discussion was proved by the experimental results presented in Figure 4-6 and Figure 4-7. Therefore, it can be concluded that at high salt concentrations in the feed stream, the energy efficiency of the newly developed membrane is less affected by salinity and the temperature polarization, while a severe reduction of EE and the permeate flux was observed for the commercial PVDF membrane as well as the typical single and dual-layer membranes.

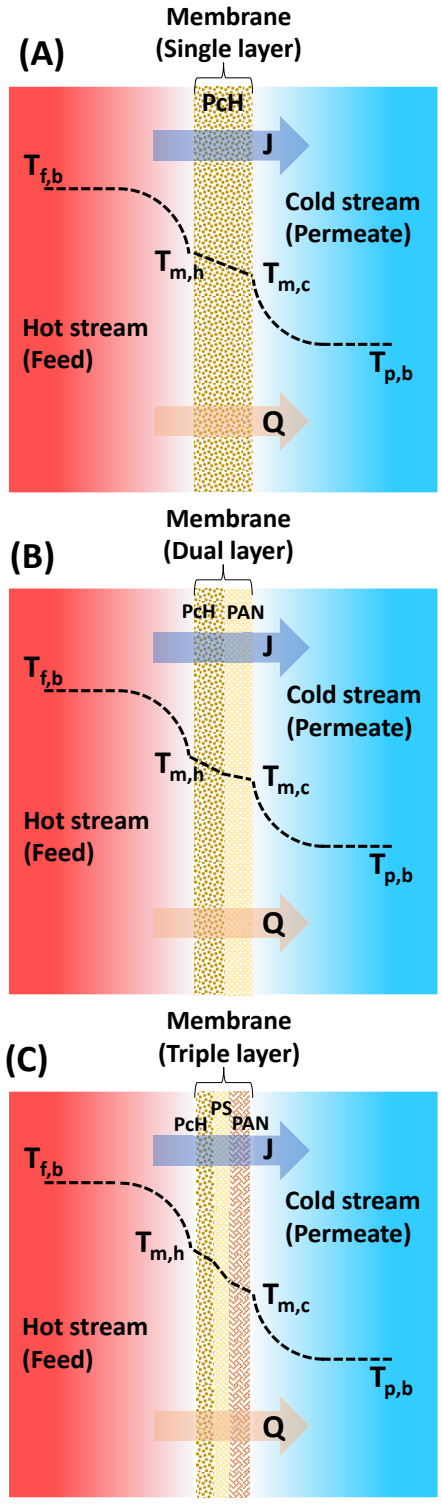

Figure 4-8. Schematic of the thermal isolation concept of the newly developed, triple-layer ENM for desalination of highly saline solution using the DCMD process. These images

show the temperature profile across the single layer, dual layer, and triple layer membranes.

Table 4-5 also compares the reported results in the literature with the obtained ones in this work, in terms of energy efficiency and the permeate flux. As could be observed, the developed triple-layer membranes could provide comparable EE and permeate flux with the previously investigated ones. Moreover, it should be mentioned that in all experiments conducted, the salt rejection of >99% was achieved for all membranes.

Table 4-5. Comparison of the obtained results in this work with the literature in terms of the permeate flux and energy efficiency

Year	Membrane						Process						Ref.
	Material	r (µm)	ε (%)	δ (µm)	WCA (°)	LEP (kPa)	Feed	T_h (°C)	T_c (°C)	F (kg.m^{-2}.h^{-1})	R (%)	EE (%)	
2016	PVDF	1.77	80	13.9	123	64	NaCl 50 g/l	60	20	12	>99	55	[51]
2016	PVDF	1.07	82	15.5	135	65	NaCl 50 g/l	60	20	20	99.8	67	[51]
2016	PVDF	0.92	85	22.6	129	66	NaCl 50 g/l	60	20	16	99.7	70	[51]
2017	Polyurethane	0.22	70	74	127	57	NaCl 100 g/l	50-60	20	5	>99	74	[52]
2017	Polyurethane	0.27	70	148	132	68	NaCl 100 g/l	50-60	20	6	>99	63	[52]
2013	PVDF	1.3	85	144	139	63	NaCl 60 g/l	40–80	20	9	99.39%	89	[39]
2013	PVDF	1	89	1206	141	93	NaCl 60 g/l	40–80	20	3.3	99.5	86	[39]
2013	PVDF	1.1	93	1529	139	110	NaCl 60 g/l	40–80	20	3	99.9	85	[39]
2022	PS20	0.4	83	250	135	203	NaCl up to 200 g/l	50-70	20	17.5	>99	81	This work
2022	PS40	0.3	84	270	135	219	NaCl up to 200 g/l	50-70	20	15.1	>99	84	This work

4.5 Conclusions

In this study, triple-layer Janus-like electrospun nanofiber membranes were successfully fabricated and used for desalination of hypersaline feedwater. The consequence of nanofiber layers was chosen to have high hydrophobicity and low thermal conductivity simultaneously. Incorporation of the PS middle layer, which its conductivity is one-fifth of PVDF and has higher porosity, could decrease the heat loss through the thermal conductivity of the membrane and consequently enhance the energy efficiency by about 20%. The effect of the middle-layer was more obvious in the desalination of high-salinity feedwater, in which lower conductivity and higher thickness improved both the permeate flux and the energy efficiency of membrane by diminishing heat loss. This could be achieved by controlling the temperature polarisation and improving the driving force, especially in the treatment of highly saline solutions. Furthermore, CFD was used to simulate the trends of mass, heat, and momentum transfer for the triple-layer membrane and was validated by experimental results. The results proved that high salinity decreased the driving force in the membrane-liquid interfaces and improved in energy efficiency to compensate the effect of salinity on the permeate flux. The results also revealed that the triple-layer membrane with a Janus structure is suitable for treating the feedwater of up to 200 g/L salinity.

The optimum membrane thickness was also predicted for a wide range of salinity (0-22 wt.%), velocity (0.04-0.28 m/s) and temperature difference (6-20 ^{o}C). The results demonstrated that the salinity decreases the vapour pressure of the feedwater and causes a decrease in the flux. The flux of the MD system experienced about 50% decrease by an increase of the salinity up to 200 g/l. The modelling results showed that

decline in flux for hypersaline feedwater can be compensated by a decrease in the thermal conductivity, whereby the flux increased to over 32 LMH by using a membrane having four times lower thermal conductivity.

Moreover, the results proved that optimum thickness is directly related to the salinity and thicker membranes are more suitable for the treatment of hypersaline feedwater, mainly due to lower thermal conduction through the membrane. The optimum thickness in this study for the treatment of feedwater containing 10 wt% and 22 wt% NaCl is 50 µm and 120 µm, respectively. However, the maximum flux decreases with salinity and changes from 32 LMH to less than 13 LMH by increasing salinity of up to 22 wt%. The results demonstrated that a thinner membrane is operationally more proper for the treatment of low saline feedwaters, while for hypersaline desalination (HSD), the thicker membranes give higher fluxes and thermal efficiencies. In addition, simulation results showed that the maximum driving force and flux are achieved in both sides of the module and the flux and thermal efficiency of the system decreases with the length of the module.

Chapter 5

Developing an Anti-Oil Fouling MD System Using Inkjet-Printed Janus Membrane

This Chapter is based on the following publication:

- **M Afsari**, MJ Park, NJ Kaleekkal, MM Motsa, HK Shon, L Tijing, Janus Distillation Membrane via Mussel-Inspired Inkjet Printing Modification for Anti-Oil Fouling Membrane Distillation, Membranes 13 (2), 191, **2023**

5.1 Introduction

In MD, a hydrophobic membrane is used to separate a hot feed and a cool permeate, wherein the difference in vapour pressure induced by temperature gradient is the driving force. Some studies have also indicated the high potential of MD to treat challenging wastewaters containing surfactants and oil, such as those from coal seam or shale gas-produced water. However, the hydrophobic nature of the MD membranes makes them susceptible to the attachment of hydrophobic fouling agents to the surface of the membrane [238, 239]. The presence of some hydrocarbon pollutants in wastewater can cause hydrophobic-hydrophobic adherence and quick fouling and wetting of the membrane [130, 166]. Previous studies have shown that providing an asymmetric wettability on the membrane, as a Janus structure, such as adding a thin hydrophilic layer on top of the hydrophobic membrane, could help alleviate the effect of oil fouling formation [9, 240]. Various approaches have been carried out to provide a thin hydrophilic layer, such as vacuum filtration, layer-by-layer assembly, electrospinning, co-casting phase inversion, and electrospraying. Although these techniques have improved performance, most of these processes face challenges regarding non-uniform deposition, less precise coating, thickness control is not easy, and more materials being consumed or wasted. Thus, the fabrication of a homogenous and thin hydrophilic layer, which is strongly integrated into the support layer, is the main challenge in the fabrication of a Janus membrane. The intrusion of the hydrophilic layer into the channels of the microporous hydrophobic membrane can accelerate the wetting of the membrane. In the previous chapter, we employed the electrospinning technique to manufacture the Janus membrane. Despite observing enhanced separation efficacy in the MD process through experimental outcomes, particularly when dealing

with hypersaline feedwater, the evaluation exposed certain constraints associated with modifying the membrane via electrospinning. These limitations impede its viability for extensive production, notably due to issues like membrane delamination and non-uniformity of characteristics across different membrane sections. The divergent properties of the modified layer across various areas of the membrane pose a significant obstacle to the creation of membranes suitable for commercial production. To address these challenges, our approach is to use an inkjet printing technique to modify a hydrophobic membrane and print a very thin hydrophilic layer, providing a Janus property.

Inkjet printing is a commonly used printing method wherein small ink droplets are dropped onto a flat printing surface and produce a thin and homogenous printed coating layer [240]. This technology has many advantages, such as being simple and fast, it is widely available and cheap in production, efficient in using materials, thereby limiting waste, and is highly scalable technology [241, 242]. In fact, inkjet printing has been used in many applications such as electronics, catalysts, biological cells, and sensors. The unique and simple working strategy of inkjet printing has received increasing interest towards the deposition of particles on the surface of materials. Zhang et al. have used inkjet printing to enhance the hydrophobicity of the surface of a paper [243]. In recent years, inkjet printing has also found its way to application in the membrane technology field. For example, a study by Park et al. has inkjet-printed a thin layer of carbon nanotubes as an interlayer to enable a high-performance thin film composite nanofiltration membrane [244, 245]. In another study, graphene oxide together with dopamine was used to coat a nanofiltration membrane via inkjet printing to add

antifouling and chlorine resistance properties. However, so far, there is no study carried out on the modification of a hydrophobic membrane via inkjet printing for membrane distillation applications especially dealing with oily feedwater.

In this study, the capability of inkjet printing to make an integrated, thin and homogenous layer was used for the deposition of a thin layer of hydrophilic materials on the surface of a hydrophobic membrane to fabricate Janus membrane with high anti-oil fouling resistivity. We used dopamine as a hydrophilic polymer and binder on the surface of the membrane. Dopamine is a mussel-inspired material that has the ability to self-polymerise on both organic and inorganic surfaces without any damage to the surface and provide functional groups for grafting of other polymers or nanoparticles [32]. Therefore, polydopamine (PDA) acts as a powerful binding agent between membrane and polyethyleneimine (PEI). PEI has the ability to bond with both primary and secondary amine groups. Therefore, it can covalently graft with quinone functional groups of dopamine and attach to the surface of the membrane. The other amine functional groups of the PEI can enhance the hydrophilic characteristic of the surface and make a hydrophilic layer [15]. The effect of the thickness of the coated layer was investigated, including the effect of the addition of a hydrophilic layer on one side or on both sides of the membrane. The anti-oil fouling performance for membrane distillation was studied by using feedwater containing different concentrations of mineral oil and NaCl solutions. The results demonstrated that the application of inkjet printing technology is highly interesting for the facile modification of membranes with robust properties for water treatment and desalination applications.

5.2 Materials and Methods

5.2.1 Materials

A commercial PVDF membrane with a pore size of 0.22 µm was purchased from Millipore (USA). Dopamine hydrochloride (MW = 189 g/mol), polyethyleneimine (PEI) (MW = 2500), and tris(hydroxymethyl) aminomethane hydrochloride (Tris-HCl), which was used for the polymerisation of dopamine solution, were all bought from Sigma-Aldrich. Sodium chloride (NaCl) and mineral oil were bought from local markets. All chemicals were used as received without any further purification. Deionised (DI) water was produced by a Millipore Milli-Q water system. The printing procedure was performed using a portable Deskjet 2130 HP printer.

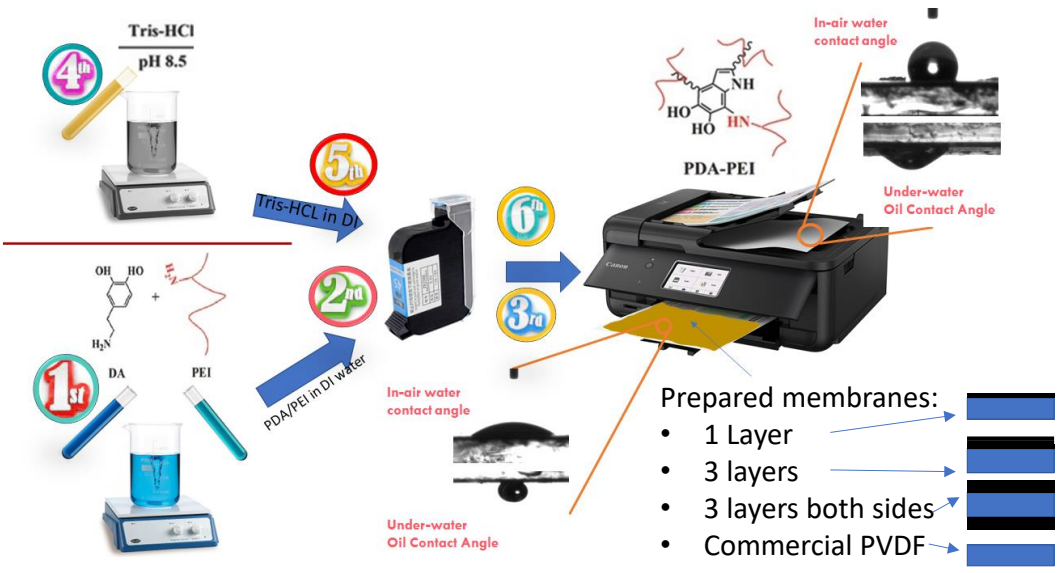

Figure 5-1 Schematic of the solution preparation and procedure for inkjet printing modification of a commercial hydrophobic membrane. The lower right figures show the schematic of the prepared membranes.

5.2.2 Inkjet printing modification

Two different solutions were first prepared: a dopamine/PEI solution and a Tris-HCl solution. In the first solution, 0.7 g dopamine and 0.7 g PEI were added to 50 mL DI water

and stirred for 4 h at room temperature to make a homogenous solution of PDA/PEI. The colour of the solution after mixing turned dark brown. Tris-HCl powder was poured into the DI water in another beaker to produce 50 mM Tris-HCl solution. The pH of the solution was adjusted to 8.5 by using 1 M HCl solution. Afterwards, a 4 cm x 6 cm black pattern was drawn in PowerPoint software and printed on A4-sized paper to run the print order exactly on the membrane sample. Then, A4-sized PET film was placed on the printed paper and the commercial membrane cut in 4 cm x 6 cm size was taped on the PET film, accurately aligning on the previously printed pattern. Printing resolution was set to a maximum (1200 x 1200 dpi) with glossy paper as the paper type. Then the prepared solutions were poured into clean and dried cartridges. In order to have a homogenous printing, the printing order was placed for multiple times to get high-quality print on the A4 paper. Then, the membrane taped on the PET film was loaded into the printer and printing order was placed to print the DA/PEI solution on the membrane. Afterwards, another cartridge containing Tris-HCl was loaded and printed on one side of the membrane to accelerate dopamine polymerization. This process was repeated three times on another membrane to have 1-time and 3-times coated membranes. For the fabrication of double-sided modified membranes, the printing procedure was performed three times on both sides of the membrane. Thus, three layers of DA/PEI and Tris-HCl were subsequently printed on one side and after one day of drying the membrane at room temperature, the other side was taped on the PET film, and the printing procedure was performed three times on other side of the membrane. Finally, there are four types of membrane labelled as 1-P (one side and one layer), 3-P (one side and three layer), D-P (double-side printed), and Com-PVDF (commercial PVDF membrane).

5.3 Membrane characterization

The membrane surfaces of both commercial and modified membranes were characterized by attenuated total reflectance Fourier transform infrared (ATR-FTIR, Affinity-1 Shimadzu) spectrometer to check the functional groups on the surface. These functional groups can determine the interaction of the fouling material with the membrane. Furthermore, the functional groups can ensure the completion of the polymerization of the dopamine as well as the interaction of the coated layer with the membrane surface.

The membrane surface was characterized using scanning electron microscopy (SEM, Zeiss Supra 55VP, Carl Zeiss AG). Furthermore, the EDS mapping was taken using SEM instrument to analyse the distribution of elements on the membrane. The changes in wettability of the membranes surface were characterized by measurement of contact angle using Theta Kite 100, Biolin Scientific goniometer via a sessile drop method. The measurements and analysis were repeated at least three times to ensure their repeatability, and the average was reported [246].

The porosity of the membrane was measured using a gravimetric method. In this method, the membrane sample was dried, weighed, and then immersed in a wetting liquid. Then, the two sides of the membranes were gently wiped using an adsorbent tissue to remove excess wetting liquid. The change in weight of dry and wet samples was used for the measurement of the porosity of the membrane. The membrane porosity is calculated as equation (3-1) [247]:

The liquid entry pressure (LEP) determines the wetting resistivity of the hydrophobic membranes [231]. Higher LEP indicates good wetting resistance. LEP was measured

using a lab-made setup composed of a cell filled with DI water, and the membrane sample was placed and tightened on top of the water. Then, water pressure is step-wise increased using compressed air. An increase in pressure causes the penetration of DI water into the pores of the membrane and finally can wet it. The minimum pressure that water passes through the membrane and water liquid is observed on the other side of the membrane is the LEP of the membrane.

5.4 Membrane distillation and oil fouling tests

To determine both the fouling and wetting resistivity of the membranes, direct contact membrane distillation (DCMD) test was performed in a lab-scale DCMD, as shown in Figure 4-2. In this system, the membrane sample wherein the modified hydrophilic layer faces the feed solution is placed in a MD module with an effective surface area of 9 cm^2. The feed water at 60^oC was passed through the feed side of the membrane, and on the other side, DI water as permeate cooled by a chiller and maintained at 20^oC was passed in a counterflow set-up. Feed and permeate flow rates were maintained at 400 and 350 cm^3/min, respectively. The flow rate of the feed was set slightly higher than the permeate to increase the hydraulic pressure of the feed side and help in the fast detection of wetting.

The performance of the membranes was evaluated by testing at different salinities (0, 35, 50, and 70 g/L) of the feed solution, with and without oil contaminant. During the MD tests, oil was introduced into the feedwater every 3 h, and the salt rejection and flux of the membranes were measured to evaluate the separation performance of the membranes. The hydrophobic PVDF membrane is oleophilic and has tendency to adsorb mineral oil and showed potential for rapid fouling for the mineral oil. The oily feedwater

was prepared by adding appropriate amounts of mineral oil into the NaCl solution and vigorously stirred using a laboratory mixer at 2000 rpm for 30 min. The prepared oil concentrations in the feedwater were 0.001 v/v% (8 mg/L) 0.005 v/v% (40 mg/L), and 0.01 v/v% (80 mg/L). These values were selected to simulate the oil in a shale gas produced water. For more homogenous mixing, the solution was heated to 50^{o}C and a 0.5 wt% of non-anionic surfactant (Tween80) was added to produce an emulsion. The concentration of tween80 was optimized to make a homogenous emulsion. The concentration of the NaCl was adjusted to 0, 35, 50, and 70 g/l to simulate the effectiveness of the membranes in harsh conditions.

5.5 Results and discussion

5.5.1 Morphology and physical characterization

In order to investigate the effect of the modification process on the morphology of the membrane as well as on the change in physical properties of the membranes, SEM images were taken and compared. Figure 5-2 shows the SEM images of the top surface and cross-section of the commercial and modified membranes and the corresponding FTIR spectra. Furthermore, the modification of membranes via the inkjet printing method causes the penetration of a thin layer of hydrophilic solution into the hydrophobic pores. Therefore, the SEM images cannot solely determine the effective thickness of the membrane. For this purpose, the EDS results of cross-sectional images were taken to provide important data about the effective thickness of the Janus membranes. The commercial membrane (Figure 5-2a) showed highly microporous surface with interconnected pores. The cross-sectional image (Figure 5-2b) proves the

symmetric structure of the membrane, which provides homogenous distribution of the porosity through the depth of the membrane. After inkjet modification, a homogenous layer was seen to cover the membrane surface and did not affect much of the bulk PVDF substrate. At one-layer coating, the surface pores of the commercial membrane started to diminish, with only small pores left visible. It is indicated that one-layer coating was insufficient for homogeneous coverage of the pristine membrane surface, with some parts showing defects. The cross-section showed an asymmetric structure composed of a thin hydrophilic coating and a thick hydrophobic pristine PVDF membrane. While the three-layer printing showed a much more uniform and homogenous coating over the surface of the membrane, with much fewer visible pores left. This indicates better coating at a higher number of printing layers. The cross-sectional images (Figure 5-2 e and f) confirm the presence of the printed layers on top of the membrane surface, with the 3 layers showing a bit thicker coating (4-5 µm compared to 2 µm for 1-layer). There is also a partial penetration of the top layer coating to the pristine base membrane, providing a good anchor to the base membrane. To ensure the actual thickness of the coated layer and determination of the amount of penetration of the solution, the membranes used for the NaCl test were dried. Then EDS mapping was taken to measure the amount of sodium on the membrane. Regarding the presence of Na on the top layer (hydrophilic layer), the thickness of the layer containing Na represents the thickness of the hydrophilic layer. This method was used to measure the actual thickness of the hydrophobic layer, which plays the primary role in the MD system. The EDS results are shown in Figure 5-2 g and h. The EDS results proved that the thickness of the hydrophilic layer in 1-P is around 2 µm and for 3-P is 5 µm.

Further confirming the successful printing of the hydrophilic layer is through ATR-FTIR analyses of the membranes. Figure 5-2 i shows new peaks for the inkjet-printed membrane (3-layers) in comparison to the unmodified commercial PVDF membrane at around 3,300 cm^{-1}, which is attributed to the presence of PDA relating to N−H and O−H stretching vibrations, verifying the polymerisation of DA on the surface of the membrane. Furthermore, the peak at around 1648 cm^{-1} corresponding to the stretching vibration of C=N bonds indicates the presence of PEI, which provide amine functional groups for hydrogen bonding and added hydrophilic property.

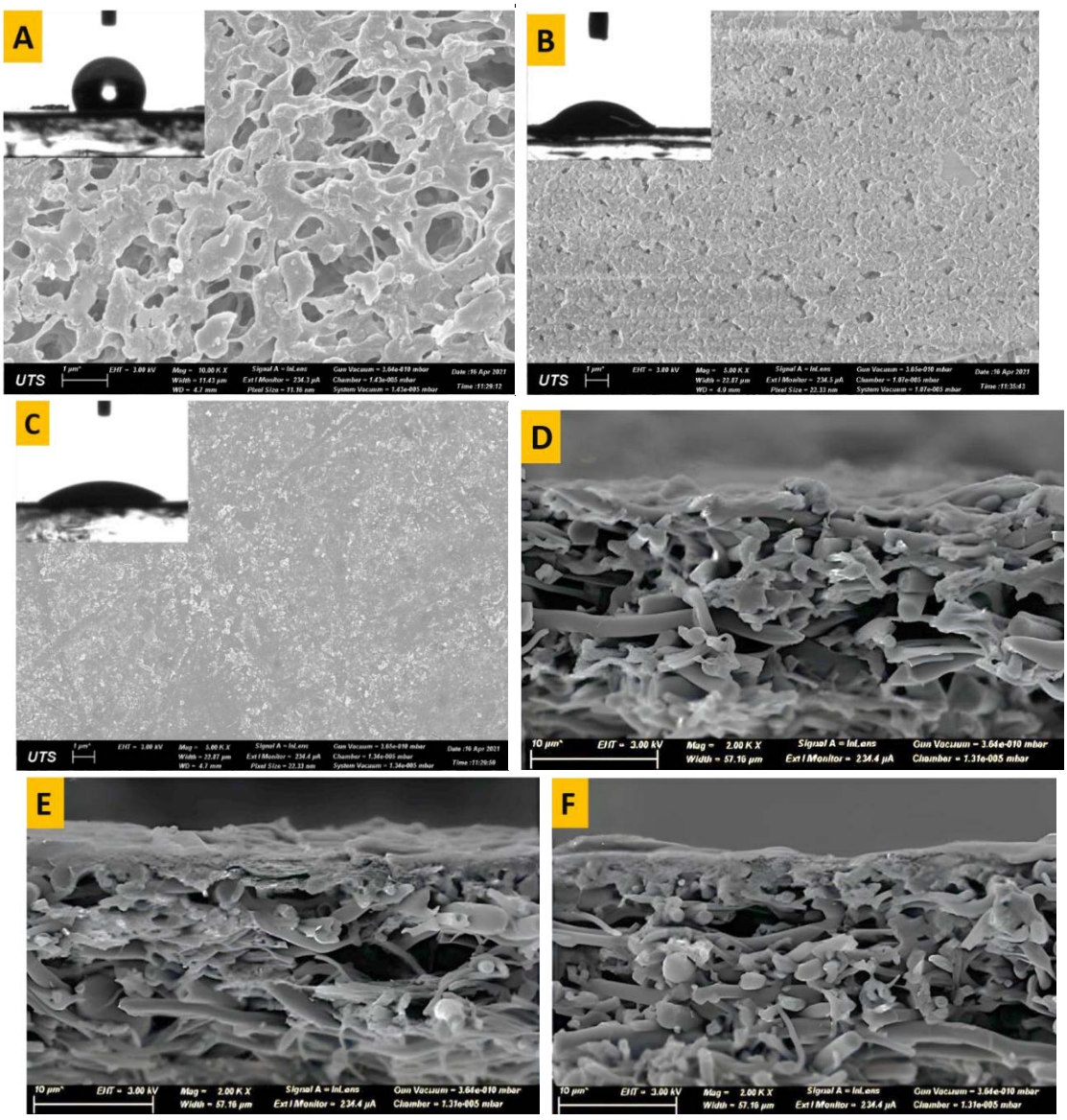

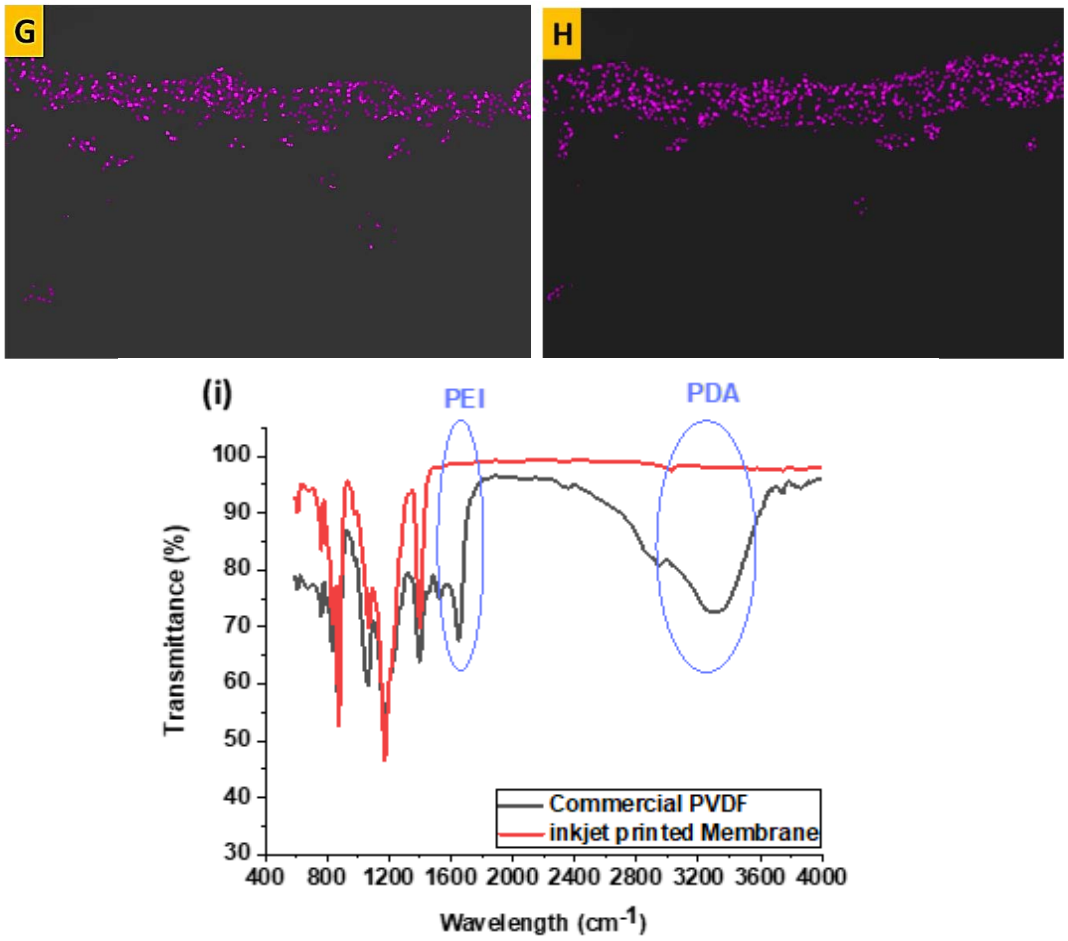

Figure 5-2 SEM images of the top (a-c) and cross-sectional (d-f) surfaces of the (a,d) commercial PVDF membrane, (b, e) 1-P membrane, and (c, f) 3-P membrane. Inset images also show the corresponding water contact angles of the membranes; (g, h) the EDS of Na for 1-P and 3-P membranes, (i) FTIR spectra of the commercial PVDF and inkjet-modified membrane (3-layers).

Table 5-1 shows the various physical characteristics of the commercial and modified membranes. As shown in the table, the overall porosity of the membrane showed only a slight decrease with the addition of very thin hydrophilic coating layers. The thickness of the hydrophilic layer is too thin that when compared to the bulk membrane thickness, it is just too small, as seen in the thickness measurement results. This results indicate that the negligible PDA-PEI hydrophilic thickness did not alter much of the membrane porosity.

Table 5-1 Physical characteristics of the inkjet-modified and commercial membranes. LEP: Liquid entry pressure; WCA: In-air Water contact angle; OCA: Oil contact angle

Sample	LEP (kPa)	Membrane thickness (µm)	Porosity (%)	WCA (deg)	In-air OCA (deg)	Underwater OCA (deg)
C-PVDF	225	112 ± 1.40	75 ± 0.86	117	10	0
1-P	215	113 ± 1.23	73 ± 0.65	34	51	93
3-P	214	114 ± 1.55	73 ± 0.91	26	85	152
D-P	205	115 ± 1.85	72 ± 0.74	26	85	152

5.5.2 Contact angle (CA)

The water and oil wettability of the surface of commercial and modified membranes were analyzed by a sessile drop method to measure the contact angles. The insets of Figure 5-2 present the corresponding in-air water contact angles (WCA). The pristine PVDF membrane showed a WCA of 117°., indicating a hydrophobic surface. However, after inkjet printing modification, the WCA of 1-P membrane was decreased to 34°, while for 3-P membrane, it further reduced to WCA of 26°. Both printed membranes indicated hydrophilic surface modification, which confirms the presence of the successful coating of the hydrophilic layers. The better hydrophilicity of 3-P membrane can be due to a more uniform and homogenous coating along the surface of the membrane. This change in wettability enables the membrane to resist hydrophobic interaction with hydrophobic foulants such as oil *[248, 249]*.

We further tested the membrane for its in-air oil wettability, using a similar procedure for WCA measurement but using mineral oil. The commercial membrane showed quite in-air oleophilic behaviour, continuously decreasing the CA of oil droplets to less than 10°, while the 1-P membrane showed in-air OCA of 51° and revealed higher repulsion than the commercial membrane. The in-air OCA for the 3-P membrane was even higher,

almost reaching hydrophobic behaviour (85^{o}). However, for the membrane to have an anti-oil fouling effect, the membrane needs to have underwater oleophobicity. Thus, we tested our modified membranes for their oil contact angle underwater (last column in Table 5-1). The underwater OCA was measured by immersion of membranes in DI water and placement of oil drops on the membrane. The underwater OCA results showed that the oil droplet directly spread on the commercial membrane, showing high oleophilicity of the membrane, in underwater condition. However, the inkjet-modified membranes showed a different behaviour, with underwater OCA for 1-P and 3-P membrane reaching to 93^{o} and 152^{o}, respectively. This result shows acceptable oleophobicity of the modified membrane. This result is attributed to the formation of a hydration layer due to the presence of the thin hydrophilic layer. In other words, the hydrophilic characteristic of coated layer increases the interaction of water and membrane and can prevent the attachment of oil droplets into the membrane surface. This interaction was derived due to the presence of hydrophilic functional groups like amine, which provides strong hydrogen bonding with water droplets forming an interfacial hydration layer *[250]* and increases the oleophobicity of the modified surface, especially at increasing thickness of the printed layer. The hydrogen bonding is vital and needs high energy demand to destruct, and oil cannot afford this energy value to adsorb on the surface and cause fouling on the embrane.

5.5.3 Liquid entry pressure (LEP)

LEP, which is the minimum transmembrane pressure needed for a liquid to penetrate the largest pore of the membrane, is an important parameter for the long-term performance of MD. LEP is measured based on the Young-Laplace equation, which is a function of the geomertic pore coefficient, the surface tension of the liquid, the

wettability of the surface, and is inversely proportional to the maximum pore size. The LEP results (see Table 5-1) indicated that the commercial membrane had the highest LEP at 225 kPa, while the inkjet-modified membranes had slightly lower LEPs. This is interesting as even though a hydrophilic layer was added, there was not much reduction in the LEP of the modified membrane in the range of 205-215 kPa. The LEP values for 1-P and 3-P membranes were approximately similar. Other studies have also observed similar results where the addition of a thin hydrophilic layer barely influenced the LEP of the membrane *[3]*. The small reduction in LEP may be due to minimal penetration of the hydrophilic coating layer into the membrane, wherein the total length of the hydrophobic membrane base is slightly changed. But for D-P, wherein the two sides have been inkjet print-coated, there must be an added penetration at the other side of the membrane where there is a bigger pore size; thus, this penetration has resulted in lowering of the effective thickness of the pristine hydrophobic base membrane. In other words, the inkjet printing provided a homogenous and thin-thickness layer that prevented the high intrusion of coating solution into the membrane's pores and limited the decrease in the membrane's LEP. As the inkjet printing did not really affect the pore size and porosity much (as presented in Table 5-1), the membranes still maintained their intrinsic characteristics, making them attractive for MD application.

5.5.4 DCMD and anti-oil fouling test

Figure 5-3 presents the results for DCMD tests at a feed solution of 35 g/L NaCl and at feed and permeate inlet temperatures of 60 ^{o}C and 20 ^{o}C, respectively. During the tests, the first three hours was only 35 g/L NaCl solution without oil addition, after which various oil emulsion concentrations (0.001, 0.005, and 0.01 v/v% of oil) were added to the feed solution at 3 h intervals. The oil emulsion was first prepared by dispersing oil in

water, and a small amount of Tween 80 as a surfactant was added and stirred using a high-speed mechanical mixer. From Figure 5-3 a, the commercial membrane showed a constant flux of 15 LMH for the first 3 h, and then after adding 0.001 v/v% mineral oil, the flux started to decrease, but salt rejection remained stable and constant (100%). This indicated that the mineral oil has high tendency to adhere to hydrophobic membrane and gradually fouled the membrane covering the pores because of the long-range hydrophobic-hydrophobic interaction *[251]*, thus declining the flux. However, the rejection still remained high for quite some time and started to decrease after more than 2 h of additional operation. But at a point where 0.005 v/v% was added, the flux started to increase, indicating that wetting has slowly occurred and the rejection further reduced. This could be attributed to the bridging effect when some salts penetrate with the oil filling the pores, resulting in some water molecules bridging to the other side of the membrane to start wetting. This result shows a very weak performance of commercial membranes in oil-containing feedwater.

On the other hand, the test using 1-P membrane showed a slightly higher flux at 18 LMH in the first few hours, which showed small enhancement compared to a commercial PVDF membrane. This slight increase can be attributed to the potentially decreased thickness of the hydrophobic layer due to the small penetration of the hydrophilic coated layer that improved the mass transfer coefficient. The addition of 0.001 and 0.005 v/v% led to a gradual decrease in flux, indicating partial fouling formation. The salt rejection in the first steps remained constant. Afterwards, at 0.01 v/v% oil addition, the flux started to increase along with the decrease in salt rejection, indicating that wetting of the membrane has started to occur at this high oil concentration.

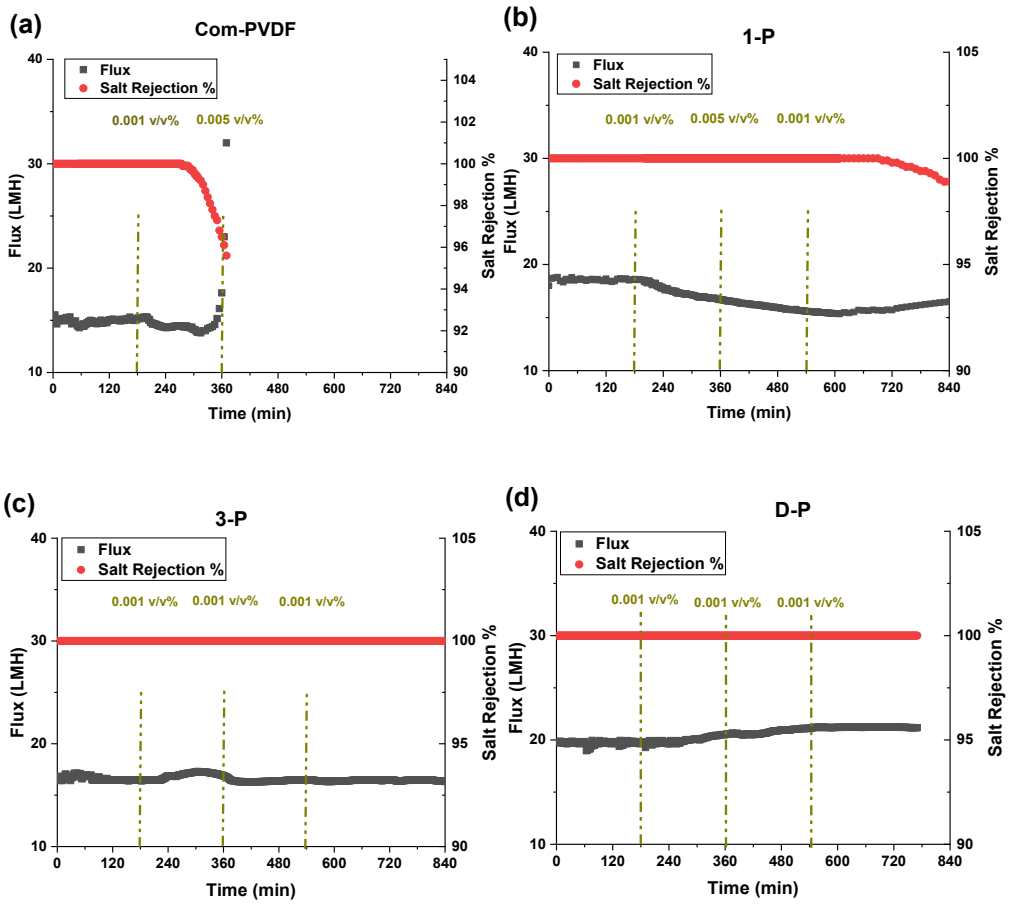

Figure 5-3 DCMD and anti-oil fouling performance showing flux and rejection for the commercial and the inkjet modified membranes: (a) Commercial PVDF membrane, (b) 1-P (1 layer inkjet coating), (c) 3-P (3-layer inkjet coating), and (d) D-P (double-sded 3-layer inkjet coating). The DCMD test was carried out at feed/permeate inlet temperatures of 60/20^{o}C and using 35 g/L NaCL solution with and without mineral addition of 0.001, 0.005 and 0.01 v/v% at 3 h intervals.

The 3-P membrane (Figure 5-3 c) showed lower flux than the 1-P membrane but was still higher than the commercial membrane. This could be due to the way the inkjet printing process for the second and third printing was done. In printing the first layer, the solution tends to intrude in the top part of the membrane and slightly decreases the bulk hydrophobic layer thickness, which could have caused an increase in the flux. After completion of the polymerization step, the first layer acts as a barrier against intrusion of the second and third layer printed solution onto the membrane. Therefore, further printing just makes a barrier against water transmission to the hydrophobic layer that

can slightly decrease the flux. Even at increasing oil concentration in the feed, the flux and salt rejection remained constant throughout the test, which indicated that no fouling or wetting occurred during the test. This could be due to the interaction between the water molecules and the hydrophilic layer that maintains a hydration layer that prevents oil from attaching to the surface [252]. This makes the 3-P membrane an attractive membrane with oil-fouling resistivity in MD. With this positive enhancement of oil resistivity, we also prepared a membrane with 3-layer printing, but this time, at both sides of the membrane (D-P membrane). It is interesting to see from Figure 5-3 d that the D-P membrane obtained the highest flux among the prepared membranes, at 20 LMH, which is 30% higher than the commercial membrane. This enhancement in the flux is attributed to the decrease in the hydrophobic membrane bulk thickness due to the slight penetration of the hydrophilic inkjet coating on both sides of the membrane, which reduces the mass transfer resistance and accelerates the condensation process. The presence of a hydrophilic layer on the permeate side does not have an influence on the anti-oil fouling performance of the membrane but can accelerate the condensation of the water vapour as well as help the mechanical stability of the hydrophobic membranes with lower thicknesses. The combination of an oil-barrier layer on the feed side and a hydrophilic layer on the permeate side enhanced the flux without sacrificing the salt rejection performance of the membrane. The membrane showed approximately stable performance throughout the test with complete salt rejection. This result implies that the use of inkjet printing as a coating technique is a good approach for uniform and homogenous coating of the hydrophilic layer to the membrane surface only, without compromising the hydrophobicity of the pristine PVDF base membrane material that maintains high rejection, and therefore improved MD performance. This approach of

providing both hydrophilicity and oleophobicity on the membrane, rather than just hydrophilicity for fouling control, has also been reported in the literature [3, 253].

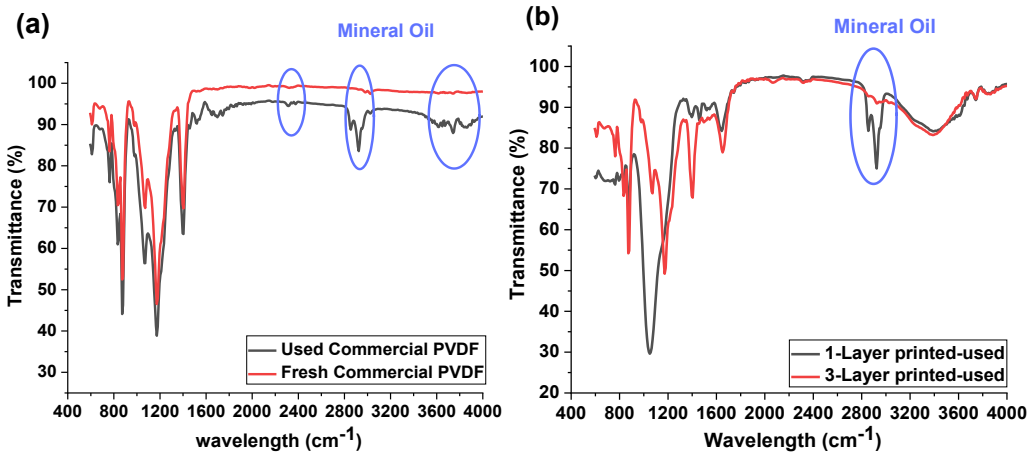

Figure 5-4 FTIR spectra of the various membranes: (a) Commercial PVDF membrane before and after oil-fouling test, (b) 1-P and 3-P membrane after oil-fouling test.

Figure 5-4 shows the ATR-FTIR spectra of the commercial and inkjet-printed membranes before and after the oil-fouling test. FTIR analysis can be used to determine the attachment of fouling agents on the membranes *[254]*. After the test, the FTIR results showed the presence of peaks in wavelength around 2900, 2300, and 3700 cm^{-1}, which is attributed to the mineral oil and proves the fouling of the membrane (Figure 5-4 a). This confirms that oil has adhered to the commercial membrane surface. Similarly, for the 1-P membrane, the same peaks for mineral oil appeared on its FTIR data (Figure 5-4 b). This also corroborates the result of flux performance with the decrease in flux data for the 1-P membrane due to the formation of an oil-fouling layer on the membrane. Furthermore, the peaks around 1700 cm^{-1} show the presence of PEI, which provides amine functional groups for hydrogen bonding and hydrophilic behaviour.

However, the membrane coated with three-layer hydrophilic material (3-P) showed no mineral oil peaks and revealed high membrane resistivity against the fouling. This result

proves the lower interaction of mineral oil and hydrophobic membrane in higher thickness of the hydrophilic layer that directed to no fouling membrane, while 1-P membrane still retains the mineral oil-hydrophobic interaction, which in the long term caused fouling of the membrane.

Furthermore, we also investigated the effect of salinity with and without oil contaminant on the DCMD performance of the unmodified commercial PVDF and the inkjet-modified Janus membranes. As shown in Figure 5-5 a, the flux of all the membranes decreased with the increase in salinity. In general, the flux in MD systems depends on the driving force provided by the difference in vapour pressure of the liquids on both sides of the membrane. According to the thermodynamic correlations, the vapour pressure of the liquids directly depends on the temperature. Therefore, the temperature difference between the two sides of the membrane makes a vapour pressure gradient and is the main source of the driving force of MD. However, the temperature difference is not the only influential parameter and the driving force also depends on other factors like salinity. In fact, the vapour pressure of the feedwater is affected by the activity of the water on the surface, which is measured according to the molality of the feedwater [255]. The results prove that the flux of the membrane decrease by about 20% with an increment of the salinity from 0 to 75 g/L. The experiments took 4 hrs for each step. The pristine membrane dealt with wetting in the last step (salinity of 75 g/L), mainly caused by clogging of the pores and changing in the wettability of the membrane surface that caused the formation of the water channels on the membrane. However, the modified membrane showed better resistivity during the test and could retain its salt rejection throughout the DCMD test. The flux for D-P was higher than other membranes in

different salinity ranges, but it dealt with the decrease in flux with the increase in salinity. In general, the salinity affected the vapour pressure of the feed water and decreased the derived flux of membranes.

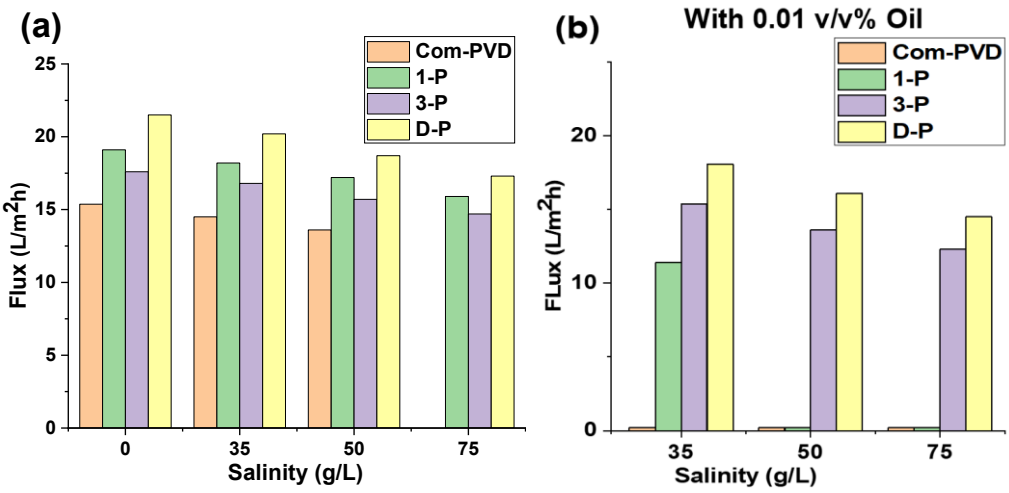

Figure 5-5 Effect of salinity on the performance of the different membrane in this study. Flux performance (a) without oil contaminant in feed, and (b) with 0.01 v/v% mineral oil in feed solution.

We then tested the membranes at various feedwater salinities containing 0.01 v/v% mineral oil (Figure 5-5 b). Similar to the previous observation, the increase in salinity has also led to a decrease in the driving force, resulting in lower flux. In some cases, the presence of oil in feedwater accelerated the pore blocking of the membranes. The commercial membrane had its pores blocked with oil, leading to low flux. The 1-P membrane also was partially blocked after 8 h of test caused by mineral oil fouling. Although the 1-P membrane showed less than 5% decrease in flux in feedwater with no oil, the oily saline water dramatically decreased the flux of the 1-P membrane. In this case, the flux showed 40% decline compared to the initial flux. Afterwards, the membrane started to increase in flux sharply and blocked. However, one-layer coating

caused more tolerability compared to the commercial membrane. The 3-P and D-P membranes could retain their complete salt rejection performance even in oily and high salinity feedwater, but their flux was stepwise decreased by an average of 30% flux decline compared to their initial fluxes. The results show that the decline in flux for oily feedwater is higher than for no-oil feedwater. The average flux decline in each step for membranes was less than 7% with total flux decrease of less than 20% for the DCMD test by feedwater containing no oil. These values for the treatment of feedwater containing 0.01 v/v% (80 mg/L) mineral oil were more than 10% for each step and about 30% for the total period of the test. The higher decrease in flux for oily feedwater can be attributed to the change in vapour pressure of the feedwater. The presence of any impurity can affect the vapour pressure of the water. The boiling point of mineral oil is higher than 300 ^{o}C, and the dispersed oil can decline the evaporation rate of water and consequently decrease the vapour pressure and driving force of the MD process *[3, 55]*.

5.6 Conclusion

In this study, we have tested the feasibility of using inkjet printing as a coating approach to producing a Janus membrane with a commercial PVDF membrane as a pristine base membrane for membrane distillation application. The printing process was performed on a commercial membrane to print one to three layers of a hydrophilic solution containing DA and PEI. Then Tris-HCl solution was printed to complete the dopamine polymerization and make an integrated hydrophilic layer. The effect of printing layer thickness on its desalination and anti-oil fouling performance was investigated. The FTIR spectra proved the completion of the polymerization of dopamine, and oil/water contact angle data revealed a change in the wettability of the membrane after the

modification process. The membranes were tested to analyze their antifouling resistivity, and experiments showed that commercial membranes showed high susceptibility to mineral oil fouling, while the Janus membrane could tolerate fouling. The thicker (3 layers) hydrophilic layer provided higher fouling resistivity even at oil concentrations up to 0.01 v/v%. 3-P and D-P membranes showed the highest fluxes (17-20 LMH) and maintained a high rejection rate (>99.9%) compared to commercial and 1-P membranes. This study signified the potential of a facile inkjet printing coating method to produce a Janus membrane that can withstand oil fouling for membrane distillation. This opens up further exploration of such an approach for the preparation of functional membranes suitable for challenging wastewater treatment and desalination.

Chapter 6

Ammonia recovery from source-separated hydrolysed urine via a dual-membrane distillation in-series process

This Chapter is based on the following publication:

- **M Afsari**, J Jiang, S Phuntsho, HK Shon, LD Tijing, Ammonia recovery from source-separated hydrolyzed urine via a dual-membrane distillation in-series process, Chemical Engineering Journal, 144215, **2023**

6.1 Introduction

The release of nutrients and other urine-based micropollutants is highly detrimental to the environment. Nutrient overabundance in water ignites the eutrophication process, which causes the growth and spread of algae. Wastewater treatment plants (WWTPs) are specially designed to remove nutrients, which exposes a significant cost to the treatment process [140, 256]. Human urine is the primary source of nutrients and pharmaceuticals in wastewater treatment plants [257], which comprises about one percent of domestic wastewater by volume while contributing over 50% of the nitrogen and 60% phosphorous in the sewerage system.

The nutrients in wastewater are harmful to the environment. However, they are also a precious source for plants' growth and are the main components of agricultural fertilizers [140, 258, 259] in the form of nitrogen (N) and phosphorous (P) [139, 257]. Nutrient recovery from source-separated human urine is a contemporary circular economy technique for separately collecting human urine via dry toilets and treating it for concentrated nutrient recovery and direct fertilizer production [144, 160, 260]. Human urine is a diluted solution containing urea, creatinine and organic salt and is an enriched source of nitrogen, phosphorous and potassium. Many studies revealed that by maximizing nutrient recovery from human urine, there is a potential to reproduce about 13% of agriculture fertilizer demand with over $14 billion annual potential revenue [139, 156, 261].

Recent studies have focused on different methods like distillation, forward osmosis (FO), reverse osmosis (RO), freeze-thaw, membrane distillation (MD), membrane-based technology, etc., for dewatering of urine for fertilizer production [142, 262, 263]. MD is

a membrane-based method that uses a low-grade waste energy and a microporous hydrophobic membrane to separate volatile compounds from non-volatile components driven by vapour pressure difference, which makes it a promising technology for nutrient treatment and recovery from human urine by separating nitrogen-based compounds from other parts and producing N, P, and K-based fertilizers separately [166, 238, 264]. In the MD system, the gaseous ammonia passes through the microporous MD membrane and is then harvested on the permeate side of the membrane [265]. The harvesting process can be carried out using an acid collector system composed of an acid solution that quickly reacts with ammonia forming nitrogenous-enriched compounds, which in most of cases can be directly used as liquid fertilizer. Although the MD process attracted attention as an efficient method for nutrient recovery, it still suffers from some challenges [143, 265, 266]. In the MD process, the permeate is affected by a simultaneous transfer of water and ammonia, which dilutes the permeate and the pH [267, 268].

The pH value in the permeate acid collector is one of the main parameters to control the rate of ammonia capture. Ammonium sulphate is a commercial fertilizer that can be used directly in agriculture. At pH around 3, sulphuric acid molecules have the ability to capture two molecules of ammonia, while at the lower pH range, a part of the reaction is directed towards the formation of NH_4HSO_4, which has lower fertilizer property and takes just one ammonium per sulphate molecule and decreases the process efficiency [269]. Therefore, the persistence of the permeate pH at stable pH of around 3 is highly desirable. Additionally, higher pH represents a lower concentration of sulphuric acid that can contribute to a drop in capturing agents and, consequently, in ammonia

capture. Therefore, designing a setup that could retain the pH at a constant level for a prolonged period is highly essential.

The production of ammonia in the urine solution increases the pH of the solution. Therefore, with the progress of the hydrolysis process and decomposition of urea, more ammonia is produced, which causes an increase in the pH of urea from 4 (fresh urine) to over 9 (hydrolyzed urine). Transferring produced ammonia into the permeate solution consumes available hydrogen ions in the acid collector and increases its pH. This process causes a decrease in the efficiency of fertilizer production and a drop in the rate of ammonia capture and fertilizer production [143].

The utilization of MD for harvesting ammonia from urine samples faces a significant challenge in controlling the permeate pH. Several studies have attempted to address this obstacle by renewing the permeate solution with fresh acid, thereby maintaining the desired pH range, dramatically increasing the acid consumption [270]. Additionally, some experiments have been limited to shorter durations to prevent the pH from increasing over time and halting the process [271]. The control of permeate pH has emerged as a key bottleneck in MD for nutrient recovery from urine. By addressing this challenge, the MD process can take a significant step forward in direct nutrient recovery from human urine.

In this study, a novel dual in-series MD setup was designed and used to preserve the acid collector pH at an optimum value to increase the fertilizer production rate in a competitive in-series reaction, simultaneously enhancing the ammonia-capturing efficiency. This innovative design not only preserves the desired pH range but also minimizes the amount of acid consumed, making it a promising approach for direct

nutrient recovery from human urine. The performance of the system in different feed pH and feed temperature was evaluated and compared with a single MD module as a benchmark process. In this study, the waste heat from the feed bath was used to warm up the acid collector to lower the consumed energy. Furthermore, higher feed temperatures were studied to evaluate the effect of feed temperature on the ammonia flux and obtain the optimum operational condition. This research represents a significant step forward in advancing MD-based nutrient recovery technologies for sustainable resource utilization.

6.2 Experimental

6.2.1 Materials

A commercial flat sheet polyvinylidene fluoride (PVDF) membrane (0.22 µm pore size, 100 µm thickness), was supplied by Millipore (USA). Sodium hydroxide (NaOH), sulphuric acid (H_2SO_4), and hydrochloric acid (HCl) solutions were sourced from Sigma Aldrich Australia. The hydrolyzed urine was used as a feed solution for undertaking the experiments. Hydrolyzed urine was collected from the basement of the University of Technology Sydney (UTS) Building 11. In this 15-storey building, the nutrient recovery pilot facility in the basement collects all male human urine from each storey using waterless male urinals. The urine is stored in tanks to complete the hydrolysis process.

6.2.2 Membrane distillation tests

The schematic diagrams of both single and dual in-series DCMD setups are shown in Figure 6-1. The experimental procedure for both setups was identical. The regular single MD setup was named Single MD, and the designed dual-MD module was named dual

In-series MD. A commercial PVDF membrane with an effective surface area of 26 cm2 was used for the tests. The hydrolyzed urine as feed is heated up to the desired temperature and fed from a feed tank placed inside a water bath (WiseCircu, Digital Circulated Water Bath) into the DCMD module using a gear pump (Cole-Parmer Instrument, USA). The effect of feed temperature (T_f) on the system performance was studied by setting feed temperatures at 40, 50, 60, and 70 ^oC. The permeate of the 1st MD module was collected in an acid collector filled with 1 mL/L sulphuric acid solution. The acid collector is heated using a heat exchanger utilizing the waste heat from the feed tank. The permeate of the 2nd MD module was collected in a deionized (DI) water tank. The electric cooler was used to cool the permeate tank. The acid collector temperature was set at 40 ^oC, and the DI permeate water was set at 20 ^oC. In the single MD setup, the feed temperature was set at 40, 50, 60, and 70 ^oC and the permeate acid collector temperature was set at 40 ^oC.

All flow rates were adjusted to 400 mL/min using a gear pump and measured by a rotameter. The inlet temperatures to the module for both feed and permeates were recorded using a digital thermometer (Vernier Go Temp USB Temperature Thermometer Probe). The permeate is weighed using an electronic balance (ADAM PGL 8001) to evaluate the membrane flux. In addition, each bottle was sampled in regular intervals to assess the ammonia concentration. The pH and conductivity of feed, and 1st and 2nd stage permeates were continuously monitored and recorded using pH meter (Tris-Compatible Flat pH Sensor) and conductivity meter probes (HQ40d Portable Conductivity Meter).

In the single MD configuration (Figure 6-1B), hydrolyzed urine as the feed solution is circulated over a commercial PVDF membrane at desired conditions, with the permeate solution (either as DI water or sulphuric acid) collected on the opposite side of the membrane. In the Dual In-series MD setup (Figure 6-1A), the hydrolyzed urine is first fed through the first MD module, while the permeate is made of an acid solution. This acid solution then flows through as the feed solution for the second MD module, where dewatering happens with DI water as the permeate solution.

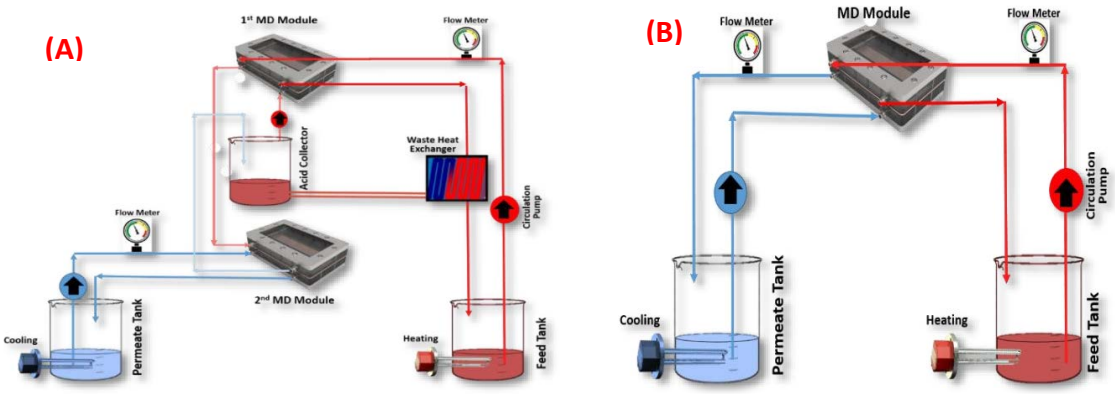

Figure 6-1. Schematic of (A) a dual, in-series MD module and (B) a single MD module for ammonia from hydrolyzed human urine.

The effect of feed pH on the performance of the setups has been studied. For this purpose, the feed pH has been controlled by adding 10 M NaOH solution or 11.3 M HCl solution in the pH range of 6 to over 13, whereas the acid collector and permeate tank pH were initially 3 and 7, respectively. In the last part, the effect of feed flow rate on the membranes was studied. In this step, the circulating feed flow rate was adjusted from 100 to 400 mL/min, and the behaviour of the dual in-series MD module was investigated. The operating condition of the process is shown in Table 6-1.

Table 6-1. Experimental parameters and conditions for both single and dual in-series MD setups in the present study.

	Dual in-series MD			Single MD	
Effect of temperature	**Feed temp (°C)**	**Permeate 1 temp (°C)**	**Permeate 2 temp (°C)**	**Feed temp (°C)**	**Permeate temp (°C)**
	40	40	20	40	40
	50	40	20	50	40
	60	40	20	60	40
	70	40	20	70	40
Effect of pH	**Feed pH**	**Permeate 1 pH**	**Permeate 2 pH**	**Feed pH**	**Permeate pH**
	6	3	7	6	3
	8	3	7	8	3
	9.5	3	7	9.5	3
	10.5	3	7	10.5	3
	12	3	7	12	3
	13.2	3	7	13.2	3
Effect of flow rate	**Feed flow rate (mL/min)**	**Permeate 1 flow rate (mL/min)**	**Permeate 1 flow rate (mL/min)**		
	100	400	400		
	200	400	400		
	300	400	400		
	400	400	400		

6.2.3 Characterisation and measurements

Samples were regularly taken from the first permeate tank at 15-minute intervals through a sampling valve to measure the change in ammonia concentration. The concentration of ammonia was measured using a spectrophotometer (Spectroquant NOVA 60; Merck KGaA, Darmstadt, Germany). In this method, the samples were diluted using Milli-Q water (20-100 times), and then standardized parts were added to prepare the solution. The additives change the colour of the solution. The prepared sample is placed in the spectrophotometer to compare its colour and transparency with another standard solution to evaluate the ammonia concentration. Human urine is subject to hydrolysis and conversion of its complex compounds to smaller parts. In the hydrolysis process, the primary nitrogen sources are converted to ammonium and other ions. The produced ammonium (NH_4^+) is in equilibrium with dissolved ammonia:

$$NH_4 + OH^- \leftrightarrow NH_3(aq) + H_2O \quad (6\text{-}1)$$

The progress of this reaction directly depends on the temperature and pH. The dissolved ammonia is in equilibrium with gaseous ammonia:

$$NH_3(aq) \leftrightarrow NH_3(g) \quad (6\text{-}2)$$

This equation demonstrates the equilibrium between ammonium ions and free ammonia gas, in which the rate of ammonia gas (free ammonia) production directly depends on pH and temperature, as shown in the following equation, where higher free ammonia gas is produced by increasing pH and temperature [272].

$$\mathrm{FA} = [\mathrm{TAN}] \times \frac{10^{\mathrm{pH}}}{e^{\frac{6344}{273+\mathrm{T}}}+10^{\mathrm{pH}}} \quad (6\text{-}3)$$

In this equation, TAN is Total Ammonia Nitrogen measured by the spectroscopic method, and FA is Free Ammonia gas.

In the MD process, water and ammonia could transfer through the membrane pores, whereas the operational condition determines the passing competition. In this study, water and ammonia flux is calculated to demonstrate the influence of operating conditions on the performance of the process. The flux of membranes is calculated using the equation (3-2).

The accumulated weight of water is measured using a digital balance and is normalized to take into account the accumulated weight of absorbed ammonia, which is measured after analyzing the permeate samples.

Ammonia flux is an important factor in the nutrient recovery process, as it shows nitrogen transport between wastewater and permeate. Understanding ammonia flux is essential for optimizing the efficiency of nutrient recovery systems and minimizing the

environmental impact of waste streams from domestic, agricultural, and industrial processes. The ammonia transmembrane flux is the rate of ammonia transferred through the membrane pores during nutrient recovery via the MD process, which shows the process efficiency. Ammonia flux (J_A, g/m^{2}h) can be determined by dividing the ammonia capture ratio (CR) over the membrane surface area (A). CR (g/h) is the slope of the linear line fitted on the amount of ammonia captured in the acid collector versus time [272].

$$J_A = \frac{CR}{A} \tag{6-4}$$

Moreover, the ammonia concentration profile in the acid collector was used to measure the Specific Ammonia Transfer (SAT), which shows the competition of water and ammonia in the MD process:

$$SAT = \frac{Transferred\ Ammonia\ (g)}{Transferred\ Water\ (g)} \tag{6-5}$$

In this equation, transferred ammonia is the amount of ammoniacal nitrogen transferred through the membrane pores, and transferred water is the weight of accumulated water in the permeate that passes through the pores. The SAT value is a precise ratio to measure the competency of the process for nutrient recovery. A higher SAT is favourable in the MD process, which shows selective transportation of ammonia.

The availability of sulphuric acid in the permeate is a crucial parameter determining the driving force for capturing the ammonia and evaluating the ammonia transfer rate. The ammonia transfer in the presence of sulphuric acid in the permeate causes the following reaction:

$$NH_3 + H_2SO_4 \leftrightarrow NH_4HSO_4 \,/\, (NH_4)_2SO_4 \tag{6-6}$$

In pH<1, mostly NH_4HSO_4 is produced, and with pH rise, the ratio of $(NH_4)_2SO_4$ to NH_4HSO_4 increases. pH around 3 is the optimum point to produce a higher percentage of ammonium sulphate $(NH_4)_2SO_4$ as suitable fertilizer [271]. Therefore, the reaction of ammonia and sulphuric acid directly depends on the permeate pH [269].

The mass transfer coefficient was utilized to objectively evaluate and compare the impact of different operational conditions on the efficiency of ammonia removal. The overall mass transfer coefficient (K_{ov}) was determined by analysing the time-dependent variation in ammonia concentration, employing the following calculation.

$$K_{OV} = \frac{V_o}{A\Delta t} \ln\left(\frac{C_0}{C_t}\right) \quad (6\text{-}7)$$

In the equation, C_0 represents the initial total ammonia concentration, Δt signifies the time, V_o represents the total volume of ammonia solution, and A represents the area per volume, respectively.

Based on the pore size dimension, the movement of ammonia gas through the porous membrane follows to the dusty gas model, which comprises Knudsen and viscous diffusions in a sequential network. The passage of ammonia across the membrane can be described as a resistances-in-series model. The comprehensive mass transfer coefficient, Kov, can be represented as the summation of mass transfer coefficients on the aqueous feed side, membrane, and receiving solution side, respectively.

Furthermore, ammonia is assumed to be in thermodynamic equilibrium with its vapour at the liquid-membrane interfaces and the reaction between ammonia and sulphuric acid is regarded as instantaneous. Consequently, Henry's law can be applied at these interfaces, and laminar conditions are considered for the flat sheet membrane module.

Equation (8) was derived from mass balances of the permeate and the feed solution, assuming that the acid collector tank is sufficiently large to capture all the ammonia [273-275].

6.3 Results and discussion

6.3.1 DCMD performance

Permeate pH is one of the influential parameters affecting the performance of the gas stripping process [271]. The acid solution's effect on ammonia capture has been studied in this work. In the first step, a single MD module was used to treat the hydrolysed urine, and DI water or sulphuric acid solution was used on the permeate side. The trend of pH change in the permeate is shown in Figure 6-2, and results show that the pH rises rapidly and reaches above 9 in the case of DI water as the permeate. Consumption of hydrogen ions during ammonia harvesting increases the pH over time. However, the rate of the pH increase around pH = 7 is higher, mostly due to the logarithmic effect of hydrogen concentration on pH values. This result complies with the relationship between hydrogen ions concentration and pH [276].

On the other hand, the rate of increase in pH for the acid collector is dramatically lower than DI water in the first hours. The permeate pH in the acid collector reached from 3 to 4 during the first 2 hours, while for the DI water, it rose from 6.5 to over 9. This signifies that the presence of hydrogen ions and cations that absorb ammonia gas decreases the pH rise rate. In addition, the results show that the conductivity of the DI water increases with time and reaches over 1500 µS/cm, which reveals the ammonia transfer from the feed to the permeate. In contrast to the normal MD system, wherein

a conductivity increase with time is a sign of wetting, in urine recovery, it is a sign of ammonia transfer.

The conductivity trend in the acid collector system is different, and the acid solution showed high conductivity. The acid-ammonia reaction takes place by transferring ammonia, and NH_4SO_4, which has lower conductivity than the reactants, is formed [271]. Therefore, with the progress of the process, more ammonia was transferred, and the conductivity continuously dropped from 6200 µS/cm of initial conductivity to around 1700 µS/cm. However, the trends depict that after a while, the conductivity gradually rose with time and reached around 2700 µS/cm. The turning of the trend is mainly attributed to the dilution of the acid solution in which some transferred ammonia is absorbed by water without any reaction in the permeate. Therefore, there is a competition between the reacted ammonia (which decreases the conductivity) and absorbed ammonia (which increases the conductivity), and the first part is more dominant in the first hours of the process.

Several studies [143, 271, 275, 277] have investigated nutrient recovery using an acid collector system, and the results consistently demonstrate that ammonia transfer to the permeate leads to an increase in pH and a decrease in conductivity of the acid solution. The rate of change in pH and conductivity is directly influenced by the rate of ammonia transfer and the reaction between ammonia and the acid solution, with specific conditions observed for each type of acid. The composition of the acid solution and its reaction after ammonia transfer play a crucial role in determining the quality of the produced fertilizer. Notably, sulphuric acid, known for its strong acidity characteristics,

exhibits a higher ammonia capture capacity and yields a desirable final product for fertilizer production [143, 271, 275, 277].

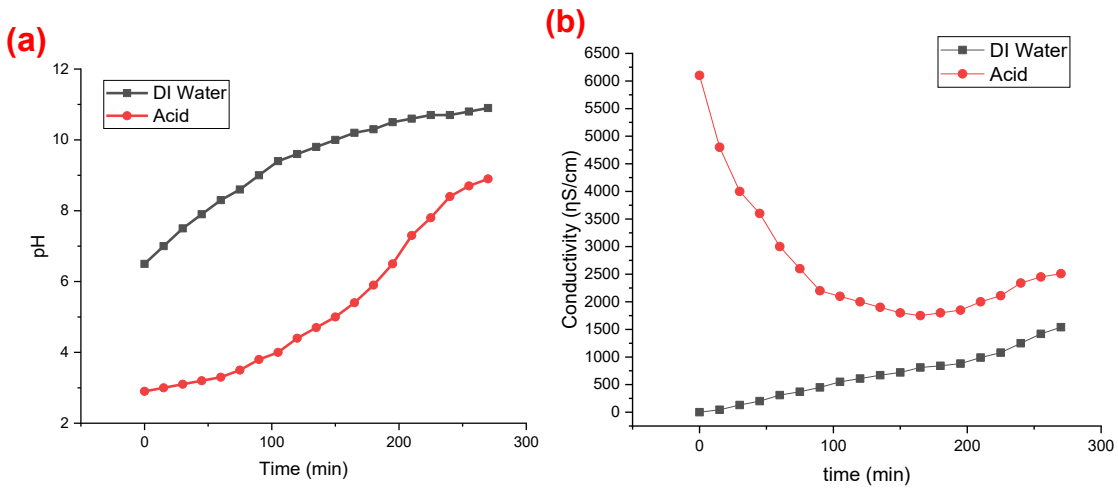

Figure 6-2. Changes in the pH (a), and conductivity (b) of the permeate with time for a single MD setup using either DI water only or with sulphuric acid in the permeate (Feed temperature = 60 °C, Permeate temperature = 40 °C, feed pH = 12, acid collector pH = 3 and DI water collector pH = 7, Feed and permeate flow rate = 400 mL/min).

In the next step, the dual in-series MD module was used to study the effect of various parameters on the performance of the designed module. The result of the pH change in the acid collector for both setups is shown in Figure 6-3. The result shows that the pH in the dual in-series MD setup is constant during the test, while the single MD setup showed an increase in pH after the first hour of testing and quickly reached over pH 8 after 5 h of the test. The ability of the MD process to remove volatile compounds, dewater the permeate and preserve other parts leads to an increase in the concentration of the sulphuric acid solution, thereby maintaining the pH and compensating for a part of the pH increase by ammonia transfer. The single setup MD dealt with pH increase, sourced from ammonia transfer and ion consumption, while the in-series MD showed constant pH in early time and a slight pH decrease with time. The

captured ammonia (NH_3) in the acid collector reacts with the hydrogen ions (H^+) converting into stable ammonium due to low pH. Therefore, only water is transferred to the permeate side in the second module and collected in the tank. The water transfer causes an increase in the concentration of H^+ ions and helps to preserve the first permeate pH as well as increase the concentration of the potentially produced fertilizer.

In addition, membrane fouling is one of the main issues in treating hydrolyzed urine. In the dual in-series setup, the first membrane deals with hydrolyzed urine containing fouling agents, while the second membrane does not involve fouling agents. Therefore, the net permeate flux that entered the first collector decreased with time, while the output flux was almost constant. This negative net flux causes an increase in the H^+ ion concentration in the acid collector and, consequently, drops the pH or helps maintain almost constant pH values in the acid collector.

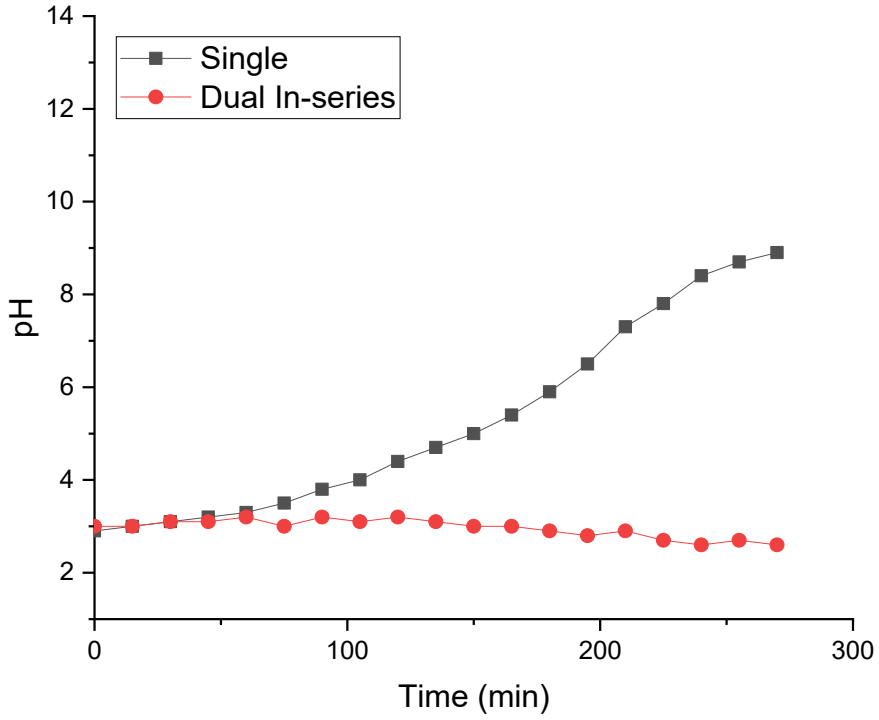

Figure 6-3. Change in permeate pH (acid collector) with time for both single and dual in-series MD modules (Single MD: Feed temperature = 60 °C, Permeate temperature =

40 °C, Acid collector initial pH = 3, feed pH = 12, feed and permeate flow rate = 400 mL/min. Dual in-series MD: Feed temperature = 60 °C, Permeate temperature = 40 °C, feed pH = 12, acid collector initial pH = 3, Feed and permeate flow rate = 400 mL/min, DI water collector pH = 7, DI water collector temperature = 20 °C).

Figure 6-4 shows the net accumulated water flux of the membranes in single and in-series MD setups (for 1st MD module as shown in Figure 6-1). The results show that the net water flux for both membranes is approximately similar during the test. However, fouling caused a slight decrease in flux over time, and dropped from about 5 LMH to 4.5 LMH

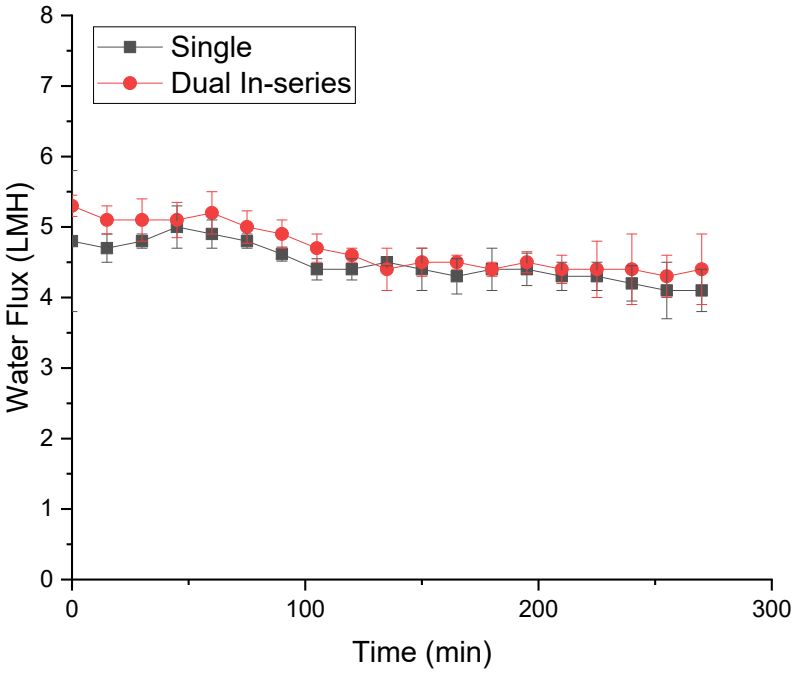

Figure 6-4. Water flux for both single and dual in-series MD systems (flux of 1st MD Module as shown in Fig. 1) (Single MD: Feed temperature = 60 °C, Permeate temperature = 40 °C, feed pH = 12, acid collector initial pH = 3, feed and permeate flow rate = 400 mL/min. Dual in-series MD: feed temperature = 60 °C, permeate temperature = 40 °C, DI water collector temperature = 20 °C, feed pH = 12, acid collector initial pH = 3, DI water collector pH = 7, Feed and permeate flow rate = 400 mL/min).

The change of captured ammonia with time in different pH was used to obtain the captured ratio (see Figure 6-5A). The values of CR in different pH and relevant ammonia flux are measured to calculate the ammonia flux. The results show that the ammonia

capture ratio and ammonia flux increased with pH, which complies with the free ammonia correlation (equation 4). A comparison of single and dual in-series MD results shows that the dual in-series MD setup has a higher regression line slope, which derives greater ammonia flux. Moreover, the results show that by increasing the pH over 9.5, the capture ratio significantly increased and reached about 150 mg/h at pH = 10.5 and 480 mg/h at pH>13. The present results demonstrated that the CR of the dual in-series MD setup is over twice the single one used in other studies (40-90 mg/h) [278].

The rise in capture ratio as pH increases, leading to greater ammonia flux, is ascribed to the conversion of more ammonium to ammonia gases. Equation 2 reveals that as pH rises, the concentration of OH^- also increases, which facilitates the consumption of NH_4^+ and the production of more NH_3. The higher levels of accessible ammonia on the membrane surface enhance the potential for ammonia transfer and consequently improve the ammonia flux of the membrane. Nevertheless, the elevation of pH results in greater consumption of alkali, and the addition of alkali is anticipated to be the primary cost factor for ammonia recovery [270]. Therefore, there is a need to strike a balance between achieving high ammonia flux and minimizing the cost of alkali consumption for ammonia recovery. This can be achieved through optimization of operating conditions such as pH and concentration of ammonia in the feed solution.

The ammonia flux also increased from 2.34 g/m^2h (pH = 6) to over 29 g/m^2h (pH = 10) and 112 g/m^2h (pH>13) (see Figure 6-5B). Similar ammonia flux range was achieved in a study by McCartney; however, their initial pH was lower than in our present study [279]. The results show that the ammonia capture in a dual in-series MD setup is about 50% higher than that in a single MD setup. This difference can be attributed as result of the

constant H^+ ion concentrations maintained in the acid collector due to the nature of the in-series MD setup, where, the excess water is continuously removed from the acid collector, and the concentration of ions in the acid collector is constantly maintained high. A higher concentration of available ions increases the reaction rate of transferred ammonia with ions and enhances the ammonia capture rate. Moreover, the ammonia flux could be kept constant during the process and prevent the drop of ammonia flux with time [272, 280]. When comparing the ammonia flux in this study to those of previous studies, it was found that the ammonia flux is strongly influenced by various factors, including the initial concentration of ammonia in the feed, membrane thickness and pore sizes, and the characteristics of the permeate [274, 280]. What sets this study apart from others is that it modifies the process by utilizing a series of MD modules, thus increasing the acid collector's potential to harvest a higher percentage of ammonia. As a result of this modification, there was an improvement in the ammonia flux observed.

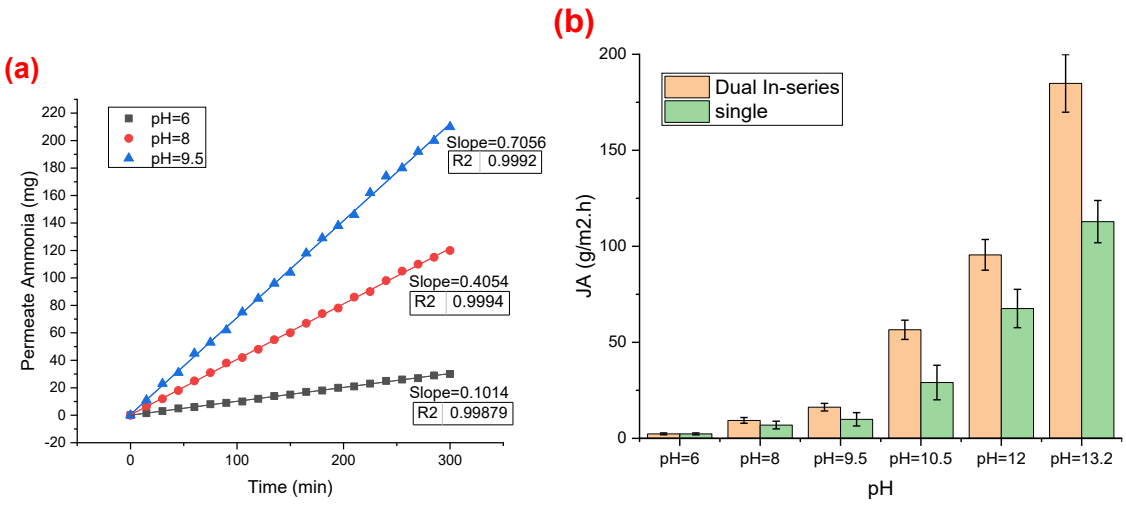

Figure 6-5. Linear regression of ammonia in the permeate vs time for measurement of ammonia capture ratio for the (a) dual in-series-designed MD setup and (b) ammonia flux for both single and in-series MD setups (Single MD: Feed temperature = 60 °C, Permeate temperature = 40 °C, acid collector initial pH = 3, feed and permeate flow rate = 400 mL/min. Dual in-series MD: feed temperature = 60 °C, permeate

temperature = 40 °C, DI water collector temperature = 20 °C, acid collector initial pH = 3, DI water collector pH = 7, Feed and permeate flow rate = 400 mL/min).

6.3.2 Effect of feed temperature

The effect of feed temperature on the system's performance has been studied, and the results are shown in Figure 6-6. The trend indicates that the dual in-series MD obtained higher ammonia concentration and kept its difference over time. Additionally, with an increase in feed temperature, a higher value of ammonia concentration is achieved in a shorter period of time. In other words, higher feed temperatures result in a higher ammonia transfer rate. The increase in the feed temperature obtained higher water and ammonia flux in all setups, which are attributed to the increased driving force of the process. In this study, the permeate temperature was kept constant, while only the feed temperature was varied. Temperature serves as the primary driving force in MD systems, and to ensure a reliable interpretation of the impact of feed temperature on system performance, it is crucial to maintain a constant permeate temperature while varying only the feed temperature. Higher feed temperature and constant permeate temperature (T_p) caused the enhancement in driving force and a greater amount of transfer for both water and ammonia. Other research studies have also investigated the impact of temperature on water flux and ammonia capture, and their findings have consistently shown that capturing ammonia can triple when the temperature rises from 50°C to 75°C [280]. Furthermore, the equilibrium of urea conversion to ammonium ions directly depends on the temperature, in which higher ammonia concentration is available in the feed solution at elevated temperature. A comparison of the single and dual in-series MD setups shows that the rises in water flux and ammonia concentration ratio are almost identical, while the direction of SAT is different in elevated temperatures. Although ammonia transfer is higher in elevated temperatures, the water

flux is more affected by temperature and causes greater rate of water transfer than ammonia transfer. Therefore, the ratio of transferred ammonia to water dropped with temperature [158, 261]. Other scientific studies have corroborated the decrease in saturation (SAT) value with increasing temperature. For example, Yu et al's research findings revealed that the SAT value dropped to more than one fourth of its initial value when the temperature was raised from 40°C to 70°C [281]. Furthermore, other research studies have also calculated saturation (SAT) values for a basic DCMD setup, which fell within the range of the SAT values obtained in the current study for a single MD setup. However, notably, the SAT value for the dual in-series setup in the current study was found to be significantly higher at 0.05, compared to the values reported in other studies for basic DCMD, which was 0.02 [158]. Moreover, the dual in-series MD setup showed a higher drop in SAT with temperature compared to the single setup. This trend is attributed to the decline of ion concentration in the acid collector due to a higher water input and the decrease in the SAT value.

At higher feed temperatures, the feed ammonia concentration decreased more rapidly. This positive effect of increasing feed temperatures on K_{ov} is demonstrated in Figure 6-6c.

As the temperature increases, the rate of ammonia dissociation in urine generally increases. This leads to a higher concentration of ammonium ions in the urine solution. The increase in dissociated ions affects the chemical equilibrium between ammonia and ammonium ions. The mass transfer coefficient, on the other hand, is a measure of how efficiently ammonia molecules are transported across a membrane or interface. It is influenced by various factors, including temperature. Generally, an increase in

temperature can increase the concentration of ammonia on the feed side, which enhances the driving force for ammonia transfer across the membrane. On the other hand, temperature enhances the mass transfer coefficient due to the increased kinetic energy of the molecules, resulting in more rapid diffusion or movement of ammonia through the urine solution or across a membrane [160, 282].

Comparing single and dual in-series systems shows that dual in-series systems kept their distance from the single module in all temperatures. The increased NH_3 diffusion in both the bulk solution and membrane pores, attributed to the higher feed temperature, resulted in a higher mass transfer coefficient. Additionally, the feed solution contained more volatile ammonia due to the endothermic nature of ammonium ion dissociation. As a result, the higher mass transfer coefficient facilitated faster ammonia removal from the feed solution, leading to improved separation efficiency in the membrane process. On the other hand, in dual in-series systems, the acid collector with constant pH preserved its capacity for capturing more ammonia and derived higher mass transfer. Specifically, K_{ov} increased from 1.79 to 8.24 × 10^{-6} m/s as the feed temperature rose from 40 to 70 °C [283-285]. The mass transfer coefficient for a single MD module obtained in this study is within the range of values reported in previous studies [273-275]. However, the coefficient is greatly influenced by the membrane's characteristics, as well as the specifications of the feed and permeate. The notable aspect of this study is that it enhances the coefficient by modifying the acid collector's characteristics and extending the duration of ammonia capturing in the permeate. This results in a higher value of the mass transfer coefficient.

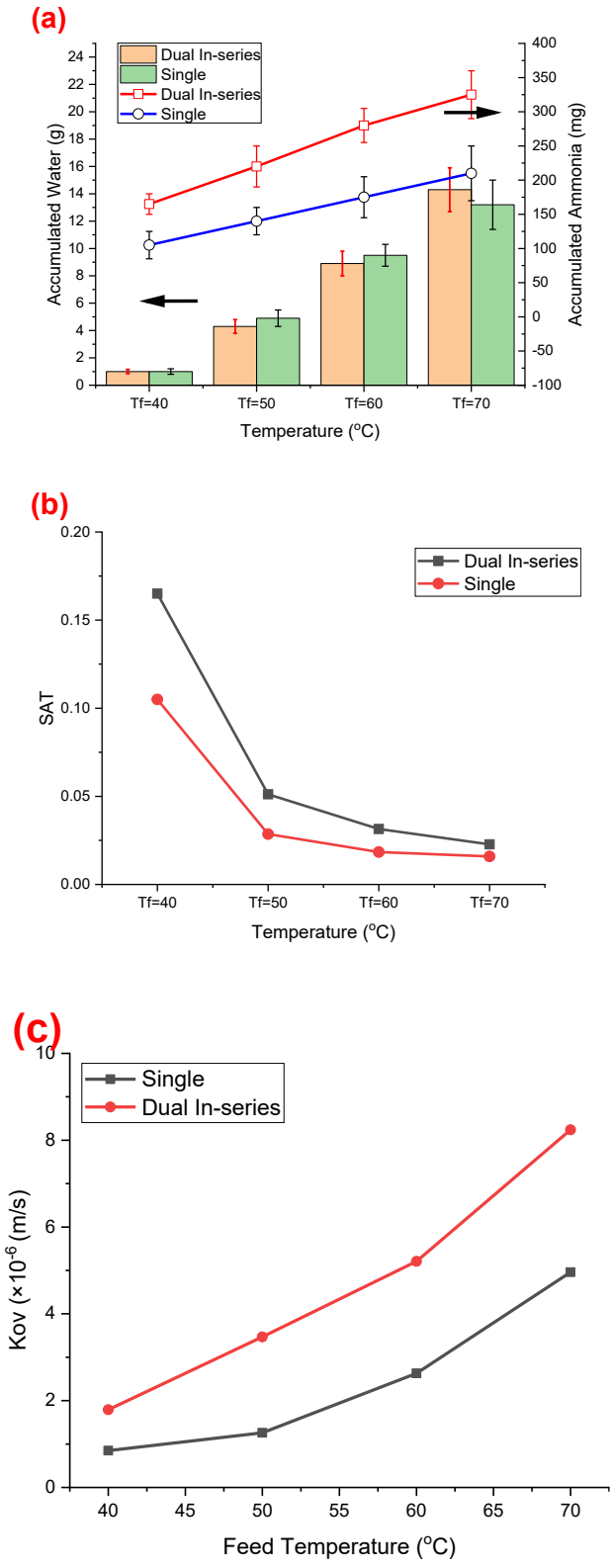

Figure 6-6. (a) Accumulated water and ammonia measurements in the acid collector for both single and in-series MD setups and, (b) the variation of SAT for both single and in-series setups in different feed temperatures (T_f), (c) the mass transfer coefficient change in different temperatures (Single MD: Permeate temperature = 40 °C, feed pH = 12, acid collector initial pH = 3, feed and permeate flow rate = 400 mL/min. Dual in-

series MD: permeate temperature = 40 °C, DI water collector temperature = 20 °C, feed pH = 12, acid collector initial pH = 3, DI water collector pH = 7, Feed and permeate flow rate = 400 mL/min).

6.3.3 Effect of pH

The conversion rate of ammonium to ammonia in hydrolyzed urine directly depends on the temperature and pH [272]. Therefore, the change in pH causes a difference in the availability of free ammonium for transferring to the permeate side [286]. Figure 6-7 shows the ammonium concentration in the acid collector in both single and dual in-series MD setups. The results demonstrated that pH greatly influences the rate of ammonia capturing. In pH equivalent to acidic or neutral conditions, the ammonium concentration in the acid collector is negligible, and the system's efficiency is very low. By increasing the pH, the ammonium concentration rose dramatically in the feed, which is attributed to the conversion of equilibrium reaction towards forming more ammonium. Consequently, more ammonia is produced and increases the driving force of ammonia from the feed side to the acid collector and more ammonia is transferred via the membrane pores. This behaviour causes an increase in mass transfer coefficient, as shown in Figure 6-7b [158, 265, 286]. These results indicate that running the process at a slightly higher pH than the natural pH of hydrolysed urine enhances the performance of the process. However, it is worth mentioning that the change of pH to values greater than 11 needs a higher volume of caustic soda and makes additional waste, which is not favourable. Therefore, an optimum pH value could be reached to create a balance between the amount of added basic source and captured ammonium.

Figure 6-7a shows that approximately no ammonium was captured in pH around 6 in both single and dual in-series MD setups [143]. However, the ammonium concentration in pH = 9.5 rose to over 200 mg/l in the dual in-series MD setup, which is twice higher

than the single one. Then after just one grade increase in pH (pH =10.5), the ammonia captured soared to over two times for both single and dual in-series MD setups. These results demonstrate that although an increase in pH causes an increment in the ammonia capture and can reach up to 700 mg/L at pH = 13.2, the high volume of basic source added to the feed decreases its efficiency [275]. In other investigations, it has been observed that there is an increase in ammonia capture with higher pH levels. Yu et al. conducted a study where they found that an increase in pH significantly influenced the transfer of ammonia, primarily due to the rise in free ammonia concentration on the feed side of the membrane under a constant driving force condition [158].

Figure 6-7b illustrates the relationship between K_{ov} and feed pH values for both single and dual in-series systems. The results show that the dual in-series module has a higher mass transfer coefficient, especially in higher pH, mainly due to higher ammonia capture by time in the dual in-series system. The continuous dewatering of the first module provides the proper conditions for transferring of ammonia to the acid collector. It can be observed that K_{ov} increased significantly from 0.03 to 7.24×10^{-6} m/s as the pH value increased from 6 to 12 for the dual in-series set-sup. However, when the pH value further increased to 13.2, the ammonia transfer coefficient rate dropped. This suggests that there may be an upper and lower limit to the effect of pH on the ammonia transfer coefficient [283-285].

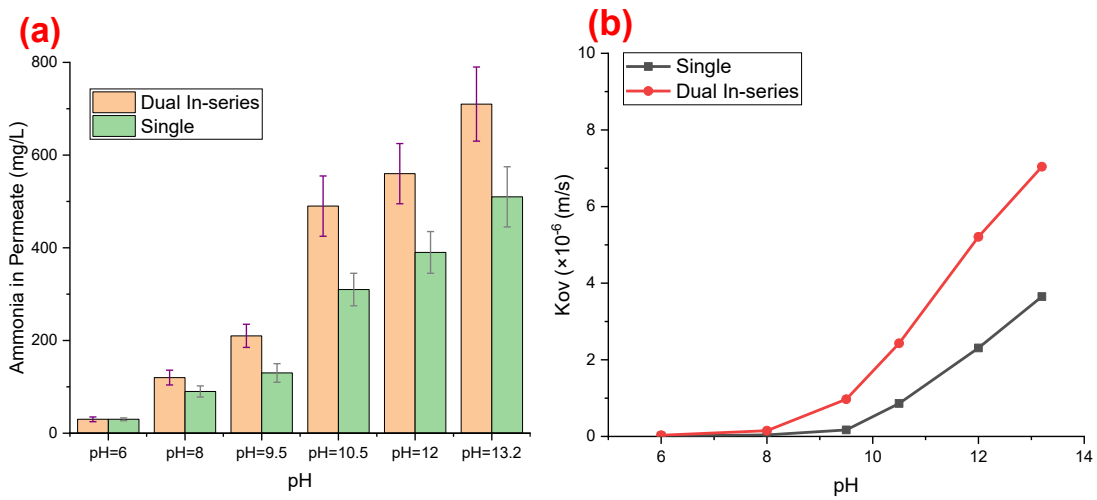

Figure 6-7. a) Ammonia concentration in the acid collector at various pH values for both single and Dual In-series MD configuration, b) the change in mass transfer coefficient with the pH (Single MD: Feed temperature = 60 °C, Permeate temperature = 40 °C, acid collector initial pH = 3, feed and permeate flow rate = 400 mL/min. Dual in-series MD: feed temperature = 60 °C, permeate temperature = 40 °C, DI water collector temperature = 20 °C, acid collector initial pH = 3, DI water collector pH = 7, Feed and permeate flow rate = 400 mL/min).

The advancement of membrane technologies and the advantages of the MD process have drawn attention to its potential use in utilizing human urine resources. Table 6-2 provides an overview of some studies that have utilized the MD process and compares their outcomes. Our results indicate good ammonia flux and robust ammonia recovery in comparison with others through our dual in-series design. Although the MD process has demonstrated significant success in separating and recovering nutrients from source-separated human urine, further research is necessary to fully comprehend the benefits and drawbacks of this system. Nonetheless, applying the MD process to recover nutrients from source-separated human urine directly presents an appealing solution to mitigate the environmental impact of nutrient waste and meet the demand for fertilizers.

Table 6-2 Application of the membrane distillation process in nutrient recovery and comparison of their performance with the present study

Type of Feed	Module	Performance	Ref.

Simulated urine feed solution composed of 250 mM ammonium hydroxide and 250 mM ammonium bicarbonate	Isothermal membrane distillation	Ammonia Flux: 14 mol/m^2h SAT: -3 (mol H_2O/mol NH_3)	[279]
Anaerobic digestion effluent from a large-scale biogas plant using pig manure	Isothermal membrane distillation	Removal efficiency over 98% in 12 h Ammonia flux 8 g/m^2h Mass transfer coefficient: 7×10^{-7}	[274]
Source-separated human urine	Membrane Distillation	SAT: 0.01 g-N/g-H_2O	[158]
Digester centre from Aaby wastewater treatment plant in Aarhus	Vacuum and Direct contact membrane distillation	Recovery factor: 80% Ammonia flux: 18 g/m^2.h	[287]
Fresh urine, acidic urine, and hydrolysed urine	Membrane distillation	SAT: 0.001 g-N/g-H_2O Removal factor: 90% Higher ammonia recovery for the hydrolyzed urine Higher fouling of the hydrolysed urine	[143]
Synthetic urine	Direct contact membrane distillation	Mass transfer coefficient: 8×10^{-5} Ammonia flux: 10 g/m^2.h The ammonia removal efficiency of DCMD, HMC and MDCMD was 52%, 88% and 99.5%, respectively	[275]
Aerobic effluent	Direct contact membrane distillation	Mass transfer coefficient: 1.0×10^{-6} ammonia removal efficiency over 99.95% High fouling of the membrane	[285]
Hydrolyzed urine	Direct contact membrane distillation	31% ammonia rejection Urine concentration about 18 times 97% rejection of P and K	[265]
Source-separated human urine	Direct contact membrane distillation	Removal rate 81.8% Doing a hybrid system of nitrificatino and distillation	[288]
Source-separated human urine	Direct contact membrane distillation	SAT= 0.17 (Max) Ammonia flux= 180 g/m^2h Mass transfer coefficient = 11×10^{-6}	Present study

6.3.4 Effect of flow rate

The variation of the ammonia in the acid collector at different feed flow rates is shown in Figure 6-8. It can be seen that a rise in flow rate increased the ammonia capture. The ammonia concentration increased from 360 mg/L to 490 mg/L when the feed flow rate rose from 100 mL/min to 400 mL/min. Since dissolved agents require a specific time for transferring from the bulk fluid to the membrane boundary layer, changes in feed velocity affect the amount of the transferred water and ammonia. On the other hand,

rises in flow rate enhance the turbulence of the fluid and decrease the mass transfer boundary layer and improve the mass transfer coefficient [275]. A higher mass transfer coefficient yields enhancement in transferring ammonia, which is in gaseous form in the feed flow, and, as shown in Figure 6-8, derives higher ammonia transfer. Meanwhile, a higher flow rate also decreases the heat transfer boundary layer and affects the driving force for water vapour transfer. However, the results show that ammonia transferring is more affected by flow rate, and a higher flow rate is more desirable. The effect of flow rate on the performance of the MD process was also studied by Xie et al. and results showed the same trend for the ammonia flux and permeate flux, which rose about 100% by doubling the flow rate [280].

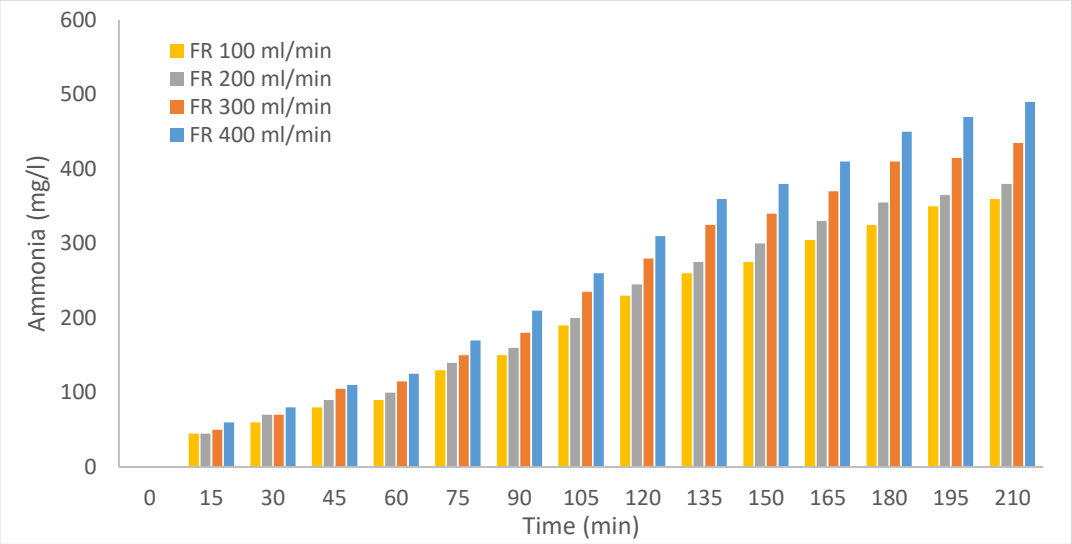

Figure 6-8. Variation of the ammonia concentration in the acid collector at different feed flow rate in a dual, in-series MD module (Dual in-series MD: feed temperature = 60 ^{o}C, permeate temperature = 40 ^{o}C, DI water collector temperature = 20 ^{o}C, feed pH = 12, acid collector initial pH = 3, DI water collector pH = 7).

6.4 Conclusion

The harvesting of ammonia from hydrolyzed human urine in an acid collector via a dual, in-series MD process was proven to be technically feasible for nutrient recovery and potential fertilizer production. Controlling the acid collector pH has been observed to be an important parameter in retaining the efficiency of the process. In the designed dual in-series MD module setup, the dewatering of the acid collector can provide two simultaneous benefits: it increases the concentration of H^+ ions and, consequently, the permeate pH, and it also increases the concentration of produced fertilizer. The results revealed that the dual in-series-designed MD modules produced higher transfer rate and ammonia capture compared to a single MD set up. While the water flux was comparable between the single and dual in-series setups, the ammonia flux in the in-series MD reached over 180 g/m^{2}h, which was approximately 80% higher than the single setup. Moreover, higher specific ammonia transfer (SAT) values were achieved at the normal pH of hydrolyzed urine in the dual in-series setup. The results also demonstrated that at low feed temperatures, the SAT value of the dual in-series setup was significantly higher than the single setup (0.17 for dual and 0.1 for single), and these values tended to converge as the temperature increased (0.025 for dual and 0.02 for single). However, both flux and accumulated ammonia values showed a significant increase with temperature increment. The utilization of a dual in-series MD setup proved to be effective in maintaining a constant acid collector pH during the test, in contrast to the single MD setup where pH continuously rose to over 9, resulting in decreased process efficiency. Furthermore, increasing the feed flow rate from 100 mL/min to 400 mL/min resulted in an increase in ammonia capture from 360 mg/L to 490 mg/L. These findings

highlight that modifying the regular setup and designing MD modules specifically to enhance process efficiency is a promising approach for increasing nutrient recovery from urine. Overall, the findings suggest that the dual MD in-series module process has the potential to improve nutrient recovery from human urine, and further research could focus on optimizing the operational conditions for enhanced performance.

Chapter 7

Application of Inkjet Printing in Nutrient Recovery for Sustainable Circular Economy

7.1 Introduction

According to estimates, the cost of poor sanitation and water outflow in developing nations exceeds $260 billion, highlighting the urgent need for funding infrastructure improvements [289].

Sustainable wastewater management must include the treatment of human urine. Each person excretes an average of 1.2 L/day of urine, which is mostly water (95%) but also includes a variety of organic and inorganic chemicals and minute amounts of pathogenic and therapeutic molecules. The existence of these contaminants emphasises how crucial it is to manage waste properly to avoid any potential risks to human health and the environment. Additionally, a large portion of the nitrogen, phosphorus, and potassium contamination of domestic wastewater is caused by human urine. The environment may be negatively affected by the release of wastewater containing urine into the ecosystem. As a result, eliminating these contaminants from wastewater results in high financial costs for wastewater treatment plants [141, 290, 291].

Contrarily, a variety of useful substances found in human urine can be used to make fertiliser. In reality, recovering human urine has the potential to supply about 25% of the commercial fertilisers needed to address the existing problems with animal and human food production. As a result, recycling human urine is turning into a crucial component of the circular economy and the safety of the food chain [159, 288]. Research on the source separation of human urine has increased as a result, with two main goals being pursued: lowering the costs associated with wastewater treatment plants and recovering valuable nutrients from human urine for the production of fertilisers. Overall, the results point to urine source separation as having substantial

potential for wastewater treatment and nutrient recovery that is both affordable and sustainable [141, 288]

Due to the unique properties of urine, such as its low volume, stability of compounds in the hydrolyzed state, and hygienic care, commonly used methods cannot be used directly for urine recovery despite the high importance of nutrient recovery in protecting the environment and food cycle. Recent urine purification techniques include distillation [292], biological process [293], oxidation process [294], and so on.

In this approach, the Bill & Melinda Gates Foundation launched the "Reinvent the Toilet Challenge" project, which focuses on recovering nutrients and energy through source separation of human waste, in-situ generation of water and electricity, and harvesting of priceless materials like phosphorus and potassium. As a result, urine-diverting dry toilets (UDDTs) are used to separate human wastes, including urine and faeces. The source-separated urine is kept in storage until the hydrolysis and urea-to-ammonia conversion are finished [295].

There are numerous methods for using source-separated urine to extract important nutrients and create N, P, or K-based fertilisers. However, the production of healthy fertilisers is significantly hampered by the presence of pharmaceutical compounds and other dangerous chemicals in urine. As a result, focus has switched to creating cutting-edge techniques that allow for the direct synthesis of pure fertilisers [156, 160, 260].

Furthermore, landfill leachate is a complicated mixture made up of a number of elements, including organic and inorganic chemicals that are suspended and dissolved. The presence of nutrients in landfill leachate is one of these elements that significantly

affect the ecological and environmental dynamics of the area. These components are necessary for both microbial activity and plant growth.

Nutrients are essential for natural processes, but too much of them in landfill leachate can have negative effects on the environment. Leachate can lead to eutrophication if it leaks into nearby soil or water bodies. This problem happens when algae and other aquatic plants develop excessively due to high nitrogen concentrations. As a result, the water's oxygen levels drop, killing aquatic life and upsetting the ecosystem's equilibrium. We can maintain water quality, defend ecosystems, and reduce possible threats to human health by managing nutrient concentrations in leachate.

It's crucial to comprehend the presence of nutrients in landfill leachate while creating sustainable waste management plans. We can strive for environmentally acceptable waste disposal practises and guarantee the preservation of our natural resources by concentrating on minimising nutrient loads and developing efficient treatment procedures.

The recovery of nutrients from urine and leachate using membrane distillation (MD) is one such technique. While pollutants and dangerous substances are left behind, MD has the ability to selectively separate and concentrate nutrients from the urine, such as nitrogen [261, 271]. Membrane technology is a strong candidate for in-situ nutrient recovery in small- or medium-scale setups and has demonstrated excellent performance for off-grid treatment applications. MD is a thermal-based membrane technique that can separate volatile compounds from non-volatile components using low-grade or wasted thermal energy. The vapour pressure gradient across the membrane brought on by variations in temperature and concentration is what propels the MD process.

Desalination, wastewater treatment, and the concentration of food and pharmaceutical goods are all areas where MD has demonstrated significant potential. The procedure provides an energy-efficient replacement for conventional separation techniques since it can run at low pressures [145, 166]. The separation of nitrogen-based molecules from other components and the synthesis of fertilisers with high concentrations of nitrogen, potassium, and phosphorus are two capabilities that the MD technology makes possible for the treatment and recovery of nutrients from human urine. Gaseous ammonia is collected on the permeate side of a microporous membrane in an MD system after passing through the membrane. Ammonia can be harvested using an acid collector system, which uses an acid solution to react quickly with ammonia to produce nitrogen-enriched molecules. Most of the time, these substances can be used directly as liquid fertilisers [270, 296].

Vacuum membrane distillation (VMD), which has good selectivity and achieves over 99% COD separation, was employed in a study to dewater human urine [163]. In another work, ammonia from human urine was concentrated using direct contact membrane distillation (DCMD). However, the normal operation of the urine treatment process is disrupted by fouling brought on by organic and scaling chemicals [158].

Numerous research teams have concentrated on developing underwater oleophobic surfaces that can significantly reduce fouling issues brought on by microorganisms or organic fouling in MD applications. These surfaces were inspired by nature, specifically sea creatures like clamshells and sharkskin. The Janus membrane, which has a multilayer hydrophilic/hydrophobic structure, is one of the many strategies that have been suggested and is a potential one for MD systems. Most fouling substances can be

repelled and kept from adhering to the surface by a Janus membrane with one hydrophilic and one hydrophobic side. By serving as both a fouling barrier and a heat barrier, the hydrophilic layer of the Janus membrane lowers overall heat transmission while maintaining the mass transfer coefficient [148, 166].

Furthermore, inkjet printing provides a flexible method for the uniform deposition of interlayers based on nanomaterials in a variety of applications. It enables quick and accurate deposition of organic, polymeric, and nanomaterials with tight control over the properties of the resultant membrane. Inkjet printing allows for the high-speed deposition of ink droplets onto a substrate with specific precision in location and volume [244, 245, 297]. In Chapter 5, we employed inkjet printing to increase the membranes' resistance to fouling. The study's findings gave us knowledge of both the procedure' benefits and drawbacks. For instance, mixing PEI with PDA might clog the pores in printer cartridges and reduce their effectiveness. We also had to deal with some membrane surface unintegrity brought on by a delay in the polymerisation of the polymeric mixture. As a result, we changed the polymer and printed the polymeric solutions individually in this chapter using the lessons learned from those experiences.

In order to change the surface of commercial polyvinylidene fluoride (PVDF) membranes and create Janus membranes, this work used inkjet printing, taking into account the fouling propensity induced by human urine or landfill leachate during the MD-assisted treatment process. To examine the impact of multilayer printing on the effectiveness of membranes, the inkjet printing cycles were repeated. The modified membranes were then applied directly to the recovery of nutrients from landfill leachate and human urine. In order to examine the changes in the ammonia flow and capture ratio of each system,

this study investigated two different types of permeates (DI water and acid collector system).

7.2 Materials and methods

7.2.1 Materials

A commercial PVDF membrane with a nominal pore size of 220 nm was used as the base membrane and bought from Milipore. Poly(sodium 4-styrenesulfonate) PSS (Mw=70000) and polyethyleneimine (PEI) (Mw=25000) were used as the polymers for inkjet printing and purchased from Sigma Aldrich. Milli-Q water was used as a solvent, and all chemicals were directly used without further purification. A commercial Deskjet 2130 HP printer was used for the printing process, and the printing resolution was set to a maximum (1200 x 1200 dpi). The hydrolysed urine was collected from the basement of the University of Technology Sydney's building 11, which collected all urine from the dry male toilets in all building stores. The urine was stored in special storage tanks to complete the hydrolysis process.

7.2.2 Janus membrane fabrication

This study used different solutions as inks during the inkjet printing process for membrane surface modification. 3 wt% PEI and 3 wt% PSS aqueous solutions were separately prepared by adding the polymers to Milli-Q water. The polymer solutions were stirred for 4 hrs to prepare homogenous solutions.

To start the printing process, a 4 cm × 6 cm black pattern was created in PowerPoint and printed onto polymer as the pattern for printing. A commercial PVDF membrane was cut to the same size as the pattern and taped onto an A4-sized PET film in the same position.

Cartridges were washed, dried, filled with the prepared solutions, and placed in the printer to print the solution onto the PVDF membrane surface. Afterwards, the printing was carried out to deposit a thin layer of polymer solution on the taped PVDF membrane surface.

The Janus composite membrane was fabricated using a layer-by-layer assembly method by alternately depositing polycation PEI and polyanion PSS onto the prepared PVDF substrate. The PEI aqueous solution was printed onto the surface and left to dry for 15 minutes, and then the substrate was printed with PSS aqueous solution. The number of PEI/PSS cycles was studied by repeating the printing process. The commercial membrane was named Com-PVDF, and the modified Janus membrane was named Janus-1 for one cycle of modification and Janus-3 for three PEI/PSS inkjet printing cycles. The resulting membrane was cross-linked in a 0.5 g/L glutaraldehyde (GA) solution at 40 °C for 8 hours and rinsed with deionised water to remove any residual GA. Finally, the membrane was dried thoroughly in the air.

7.2.3 Membrane Characterisations

The attenuated total reflectance Fourier transform infrared (ATR-FTIR, Affinity-1 Shimadzu) spectrometer was used to characterise the functional groups on the membrane surface and to evaluate the integrity of the different layers based on the charges. Understanding the presence of various functional groups determines the potential of layers in the adsorption or repulsion of fouling agents.

The field emission scanning electron microscopy (FESEM, Zeiss Supra 55VP, Carl Zeiss AG) was used to image the membrane surface and investigate the effect of fouling

agents on membrane. The contact angle of the PVDF membrane was changed after the modification of inkjet printed polyelectrolytes. Therefore, Theta Kite 100, Biolin Scientific equipment, and a sessile drop method were used to characterise the membrane surface wettability and measure the contact angles.

7.2.4 Membrane performance evaluation

To assess the performance of the commercial PVDF and Janus membranes, a laboratory-made DCMD setup was utilised in this study. A detailed explanation of the process and setup can be found in Chapter 6. Hydrolysed urine was employed as the feed water, which was recirculated over the membrane through a gear pump drive (Cole-Parmer Instrument, USA). The permeate was collected in an acid collector containing a solution of sulfuric acid to harvest transferred ammonia. The change in weight of the acid collector was monitored using a digital balance (ADAM PGL 8001). A water bath (WiseCircu, Digital Circulated Water Bath) was employed to heat the feed, while a lab-scale chiller was used to cool down the permeate. The feed and permeate flow rate was set to 400 mL/min using a rotameter, and the inlet and outlet temperatures were continually recorded with a digital thermometer (Vernier Go Temp USB Temperature Thermometer Probe). The pH and conductivity of the process were measured using a pH meter probe (Tris-Compatible Flat pH Sensor) and a conductivity meter probe (HQ40d Portable Conductivity Meter). The feed and permeate samples were collected regularly to measure their ammonia concentrations. In addition, the reaction equilibriums and equations for harvesting ammonium are described in the previous chapter (Chapter 6)

7.3 Results and Discussions

7.3.1 SEM images

The morphology of fabricated membranes is an important parameter that can significantly affect membrane performance. As shown in Figure 7-1A the pristine PVDF membrane displayed irregular pores on its surface. The surface was found to be highly porous, containing numerous uneven structures.

However, the non-homogeneity in pore size and porosity distribution on the membrane surface can result in uneven flow of the fluid through the membrane, thereby reducing the separation efficiency of the membrane [44, 298].

To address this issue, we employed inkjet printing technology to fabricate Janus membranes with controlled surface properties. Proper printing of a membrane active layer is crucial for preventing fouling, as membrane fouling can lead to membrane failure and reduced separation efficiency [240, 297]. Figure 7-1B shows the SEM image of the membrane coated with one layer of PEI/PSS solution. The image analysis revealed that some parts of the printed surface were not properly coated. The improper coating can create points for the accumulation of hydrophobic fouling agents, which can easily adhere to the hydrophobic surface of the membrane and cause fouling. Over time, these foulants can penetrate through the membrane, leading to the wetting and subsequent failure of the membrane [9, 35]. As shown in Figure 7-1C, after coating polyelectrolytes via layer-by-layer inkjet printing, the surface of the PVDF substrate was thoroughly covered. With an increase in the number of deposited layers, the observable pores or cracks on the surface of the membrane became less pronounced. After three deposition

cycles, the membrane surface became uniform and compact, achieving complete and defect-free coverage of the membrane surface, which could provide a strong barrier against fouling agents. This result indicates that the inkjet-printed layers effectively fill in the pores on the surface of the PVDF membrane, resulting in a smooth and uniform surface [243].

Furthermore, the binding between the deposited multilayer and substrate was robust, as evidenced by the lack of change in surface morphology after subjecting the membrane to 10 min ultrasonic treatment. This result indicates that the inkjet-printed Janus membrane forms a strong bond with the substrate, which is critical for the long-term stability and performance of the fabricated membranes.

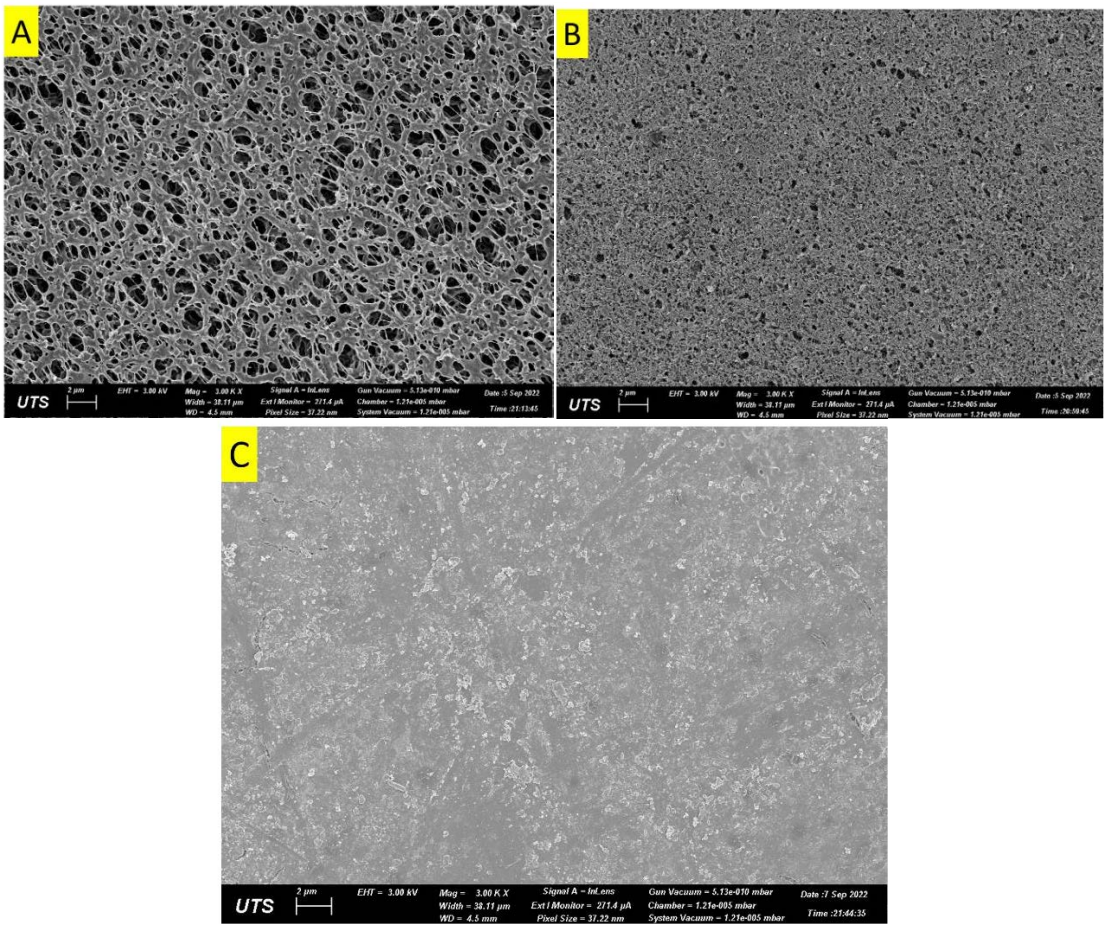

Figure 7-1. SEM images of the commercial PVDF membrane- (A), Janus-1 membrane (B), and Janus-3 membrane (C).

7.3.2 FTIR

The FTIR analysis has the capability to determine the attachment of different layers onto membranes. This is achieved by identifying the functional groups present on the membrane surface to evaluate the presence of different agents. Figure 7-2 displays the FTIR spectra of the membranes before and after the deposition process. After printing of PEI solution, the membrane exhibits absorption peaks at 1270 and 1169 cm^{-1} associated with C-N stretching vibration, indicating the successful deposition of PEI on the membrane [299].

Additionally, the appearance of characteristic peaks of the $-SO_3$ group at 1118, 1091, and 1017 cm^{-1} in the FTIR spectrum confirms the deposition of PSS on the PEI-coated membrane. This further verifies the successful deposition of both polycation and polyanion on the pristine PVDF membrane.

Furthermore, after crosslinking with GA, a slight increase in intensity at 1625 cm^{-1} was observed. This suggests the formation of the imine carbon-nitrogen linkage, confirming the occurrence of a crosslinking reaction between $-CHO$ groups of GA and $-NH_2$ sites of PEI [299].

Overall, the FTIR spectra analysis provides strong evidence of the successful depositions of PEI and PSS on a PVDF membrane and subsequent crosslinking with GA.

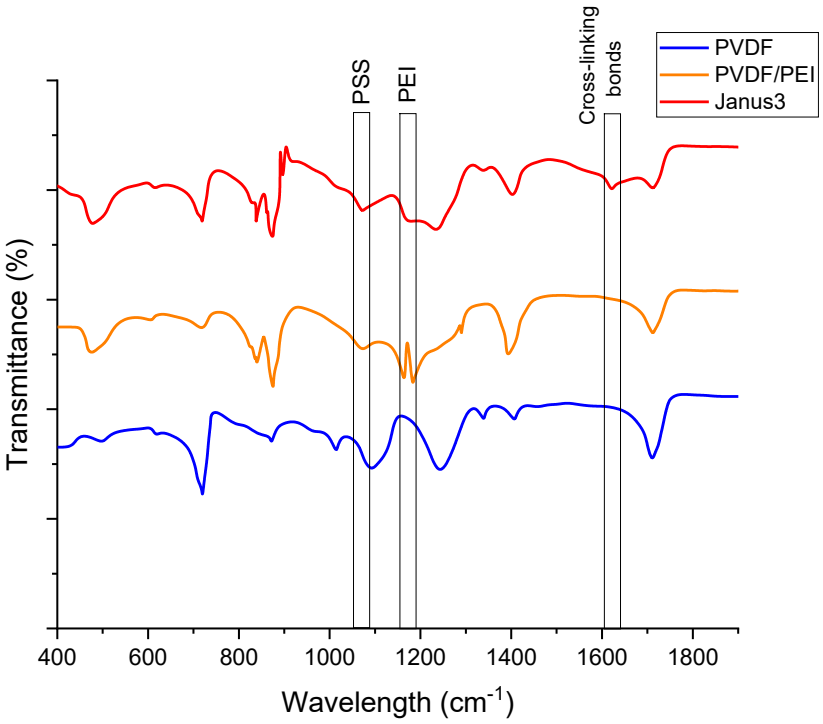

Figure 7-2. FTIR spectra of the commercial PVDF and the inkjet-modified membranes

7.3.3 Contact Angle

A sessile drop contact angle was used to analyse the water and oil wettability of the commercial and modified membranes. As depicted in Figure 7-3, the in-air water contact angle (WCA) of the commercial PVDF membrane was 125°, indicating its hydrophobicity.

The Janus membranes, on the other hand, possessed relatively low CAs due to the presence of polyelectrolyte multilayers. The values are 47° and 29° for Janus-1 and Janus-3, respectively, indicating their hydrophilic property. This change in the hydrophilicity of the membrane is essential for the antifouling performance of the Janus membrane. The Janus-3 membrane showed a lower WCA (29°) compared to Janus-1, indicating an increase in hydrophilicity due to the increment in coating layers.

To analyse the fouling tendency of the modified membrane, the under-water contact angle (OCA) was measured. This was achieved by immersing the membranes in DI water and placing oil drops on the membrane. As shown in Figure 7-3, the commercial membrane exhibited oleophilic behaviour, even in underwater conditions, as evidenced by the spread of the oil droplet on its surface. However, the modified membranes exhibited different behaviours, with the underwater OCA for Janus-1 and Janus-3 membranes reaching 85^{o} and 132^{o}, respectively. This demonstrates acceptable oleophobicity of the modified membrane. In other words, the hydrophilic characteristic of the coated layer increased the interaction between water and membrane, thereby preventing the attachment of oil droplets onto the membrane surface. This interaction was derived from the presence of hydrophilic functional groups, which provide strong hydrogen bonding with water droplets and increase the oleophobicity of the modified surface. The results also indicate that increasing the thickness of the hydrophilic layer enhances the hydrophilic performance of the membrane and, consequently, increases its antifouling characteristics. The hydrogen bonding is strong and requires a high energy demand to destruct, which hydrophobic foulant agents cannot afford, leading to the inability of hydrophobic fouling agents to adsorb on the surface and foul the membrane [101, 161, 166].

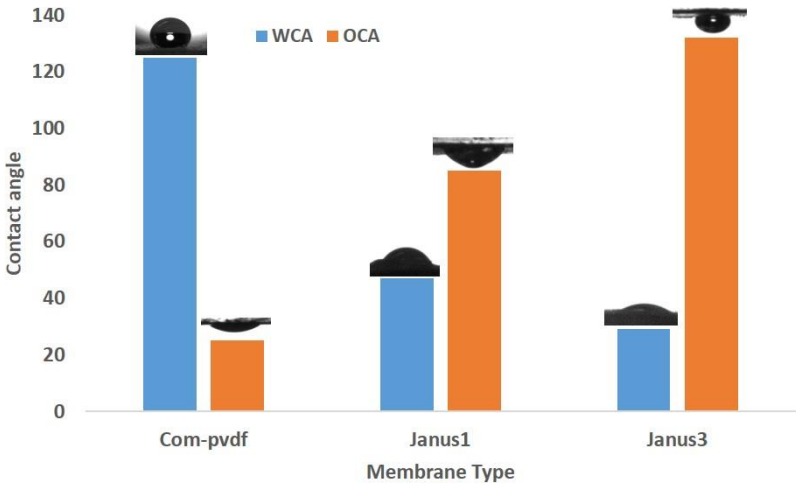

Figure 7-3. Water contact angle and oil contact angle of commercial and inkjet-modified membranes

7.3.4 Antifouling Test and Nutrient Recovery from Human Urine

The gas stripping process is highly dependent on several parameters, with permeate pH being one of the most crucial. This study examined the impact of an acid solution on ammonia capture in the gas stripping process for both pristine and inkjet-printed membranes. The ammonia capture process involved using a MD module to treat hydrolysed urine, with either DI water or sulphuric acid solution used on the permeate side. In this experiment, the feed and permeate temperatures remained constant at 60 and 20 ^{o}C, respectively, with 400 mL/min flowrates.

Figure 7-4A illustrated the trend of pH changes in the permeate, with results indicating that DI water as the permeate led to a rapid rise in pH, rapidly exceeding 9 and reaching over 12 after about 4 hrs of test for both pristine and Janus-3 membrane. Afterwards, it remained approximately constant, demonstrating drops in the rate of ammonia transfer. This trend can be explained by the process of harvesting of ammonia in permeate that consumes hydrogen ions, thereby increasing the pH over time. The trend also displays that pH increase rate around 7 was higher, primarily due to the logarithmic

effect of hydrogen concentration on pH values. This outcome aligns with the correlation between hydrogen ion concentration and pH. Compared to the Janus-3 membrane, the Com-PVDF membrane exhibited greater pH variation, which could be attributed to higher membrane flux and ammonia transfer during the initial hours of the test. However, over time, the rate of pH change for both membranes tended to be similar. This was primarily due to the fouling of the Com-PVDF membrane, which led to a drop in flux.

Furthermore, the impact of using an acid solution versus DI water on the rate of pH increase in the gas stripping process was also investigated, and the result is shown in Figure 7-4B. The results demonstrated that during the initial hours of the process, the rate of pH increase for the acid solution was significantly lower than that of DI water. Specifically, within the first hour, the pH of the acid solution increased from 3 to 4, whereas for DI water, it rose from 6.5 to over 10. This indicates that the presence of hydrogen ions and cations that absorb ammonia gas effectively mitigates the pH rise rate. These findings have important implications for optimising the gas stripping process and improving its performance in various applications [138, 152]. In addition, the results demonstrated that the Com-PVDF membrane had a higher pH compared to Janus-3, mainly due to its higher flux. However, in last hours of test the pH for both membranes tended to be equal due to drop in flux of Com-PVDF membrane.

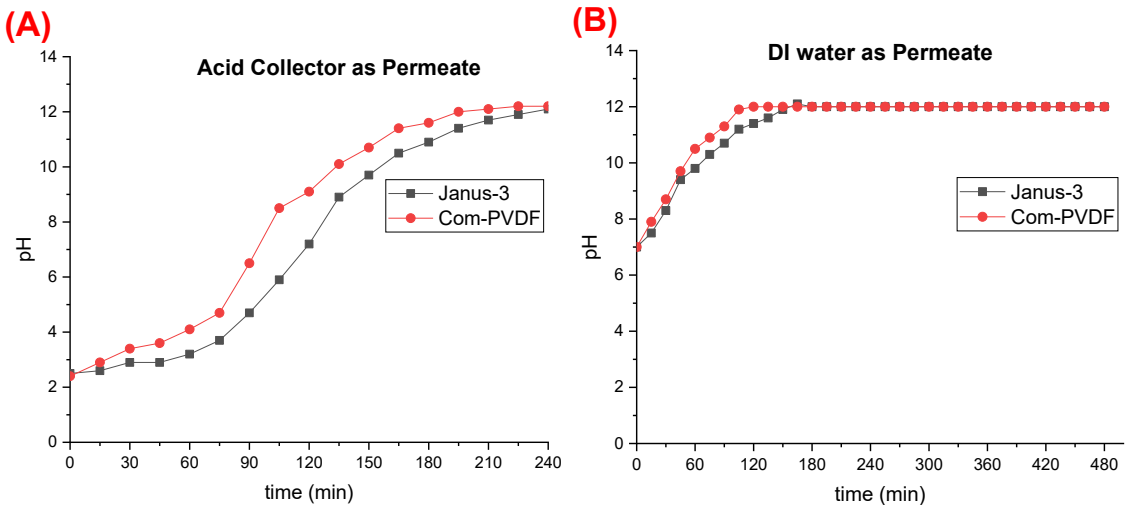

Figure 7-4. Change of pH vs time for commercial and Janus-3 membrane in DI water (left) and acid solution (right)

Furthermore, the experimental results indicate that the conductivity of DI water increases with time for both Com-PVDF and Janus-3 membranes (Figure 7-5A). The conductivity of Com-PVDF and Janus-3 membrane were 4500 µS/cm and 3800 µS/cm, respectively, indicating the transfer of ammonia from the feed to the permeate. In conventional MD systems, an increase in conductivity indicates membrane wetting, whereas in urine recovery, it indicates ammonia transfer.

In the acid collector system, the conductivity trend shown in Figure 7-5B is different story, and the acid solution exhibited high conductivity, about 7000 µS/cm. Upon transferring ammonia, the transferred ammonia reacted with the acid solution and formed NH_4SO_4 electrolyte solution. A comparison of the conductivity of the initial solution with the formed compound showed that the reaction product had lower conductivity than the initial solution and caused a drop in the conductivity during the process. The graph showed that the conductivity of the permeate dropped from an initial conductivity of 6700 µS/cm to approximately 2300 µS/cm after 4 hrs of test. However, the trends suggested that the rate of change in conductivity dropped with

time. The shift in the trend was primarily attributed to the dilution of the acid solution, which decreased the rate of ammonia capture, and therefore, a part of the transferred ammonia was absorbed by the permeate solution without undergoing any reaction with acid solution. Consequently, the absorption of ammonia without the reaction caused an increase in the conductivity, which decelerated the rate of conductivity drop in permeate [300].

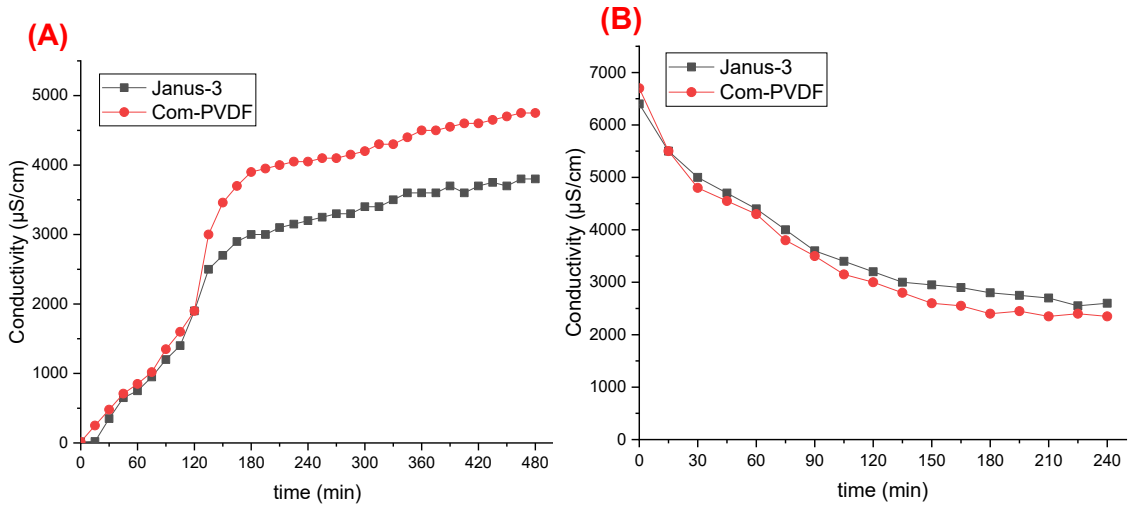

Figure 7-5. Change of conductivity vs time for commercial and Janus-3 membrane in DI permeate (left) and acid collector (right)

The net accumulated water flux of the Com-PVDF, Janus-1 and Janus-3 membranes in a DCMD setup is presented in Figure 7-6. The experimental findings revealed that the commercial PVDF membrane experienced a continual decrease in flux over time. The presence of organic agents in the hydrolysed urine amplified the fouling issue in the hydrophobic membranes, primarily due to the hydrophobic-hydrophobic interaction between the fouling agents present in the hydrolysed urine, like organic matter and the PVDF membrane. In comparison to the commercial PVDF membrane, the Janus-1 membrane exhibited greater tolerance against fouling agents but still experienced a gradual decrease in flux. Although the Janus-1 membrane was coated with one cycle of

PEI/PSS layers, some uncovered points remained that may act as fouling-prone areas. Consequently, the decrease in flux may be attributed to the attachment of fouling agents to some defects on the membrane surface. In contrast, the Janus-3 membrane, which is coated with three cycles of PEI/PSS inkjet-printed layers, acted as a robust barrier against foulant and demonstrated complete flux throughout the experiment. However, the initial flux of the Janus-3 membrane was partially lower than that of the commercial and Janus-1 membranes, mainly due to the presence of a hydrophilic layer that affects the system's driving force.

The study findings indicated that there were comparable trends for both DI water and acid collectors in terms of their impact on water flux behaviour in the DCMD process (Figure 7-6A and B). Specifically, the type of solution present in the permeate stream does not appear to affect water flux behaviour significantly. The membrane flux in the DCMD process is primarily determined by the driving force, which is influenced by factors such as temperature and composition of the feed and permeate. The research showed that the low concentration of acid solution (1 mg/L) used in the acid collector system has a minimal effect on the vapour pressure of the permeate. Consequently, this has a low impact on the driving force of the system and, ultimately, on the flux of water. These results suggest that the DCMD process is adaptable to different types of feed solutions without a significant impact on water flux behaviour [143].

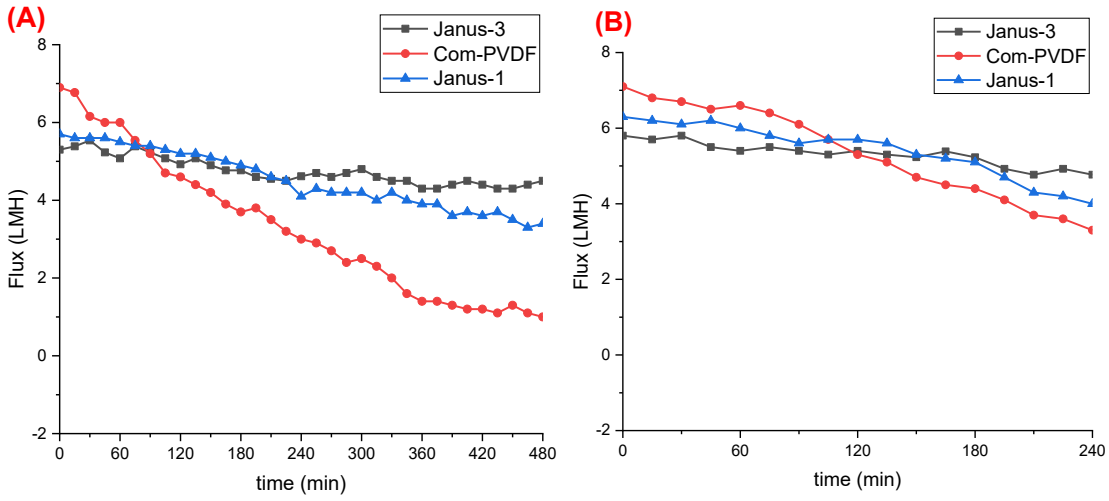

Figure 7-6. Performance of commercial and inkjet-printed membrane for direct nutrient recovery using DCMD and DI water as permeate (left) and acid collector as permeate (right)

The captured ratio (CR), which represents the change in the amount of captured ammonia over time (mg/hr), was used to determine the ammonia flux. Different operating conditions were examined, and the corresponding CR values were measured to calculate the ammonia flux. Figure 7-7 illustrates the ammonia capture and ammonia flux for the Com-PVDF, Janus-1 and Janus-3 membranes during the test. It also illustrates the change of ammonia harvesting rate with time in systems with DI water as permeate (Figure 7-7A) and acid collector (Figure 7-7B). Moreover, the comparison of ammonia flux for modified membranes in the initial and last hours of test is shown in Figure 7-7C. The results show that the rate of ammonia capturing in the initial hours of the test is higher than in the last hours of the experiment. The change in the rate of ammonia capture can be attributed to increasing the concentration of ammonia in permeate and a drop in the driving force of ammonia transfer. Initially, during the early hours of testing, the Com-PVDF membrane exhibited a higher capture ratio and consequently achieved a greater ammonia flux compared to the two modified membranes. The initial CR values for Com-PVDF, Janus-1, and Janus-3 were 29.31, 27.46, and 25.85,

respectively. However, after approximately 2 hours, the capture ratio of the commercial membrane dropped to 3.81, 4.15, and 4.89, respectively, and its slope became lower than that of the inkjet-printed membranes. As a result, the derived ammonia flux for the Com-PVDF membrane decreased, while the modified membranes demonstrated better performance. A comparison between Janus-1 and Janus-3 in Figure 7-7 revealed that in long-term applications, the Janus-3 membrane maintained a persistent ammonia capture ratio and exhibited a higher ammonia flux. The fouling of the membrane surface by fouling agents reduces the availability of pores for ammonia transfer, resulting in a decrease in ammonia flux for the commercial membrane and, to some extent, the Janus-1 membrane [301].

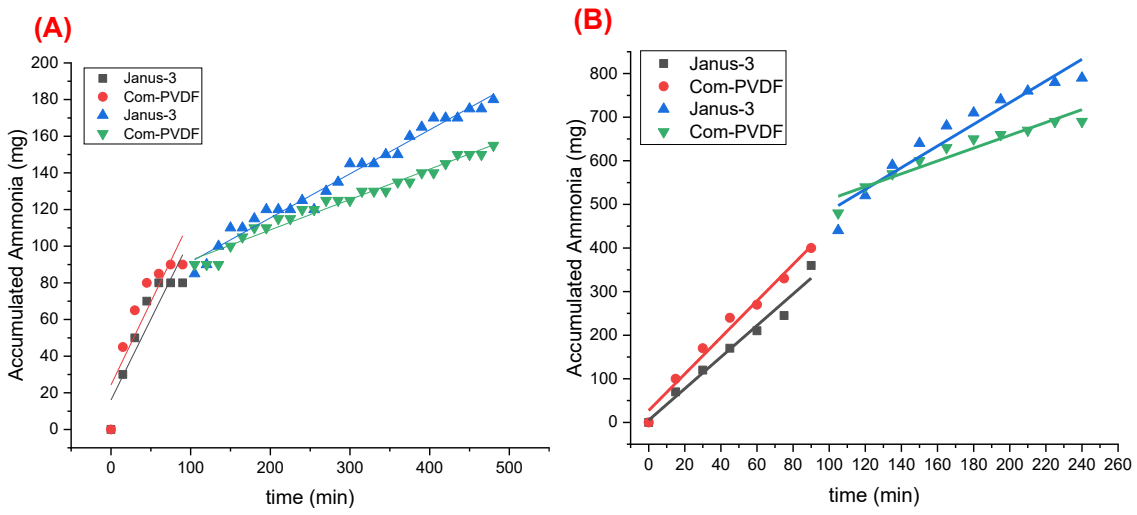

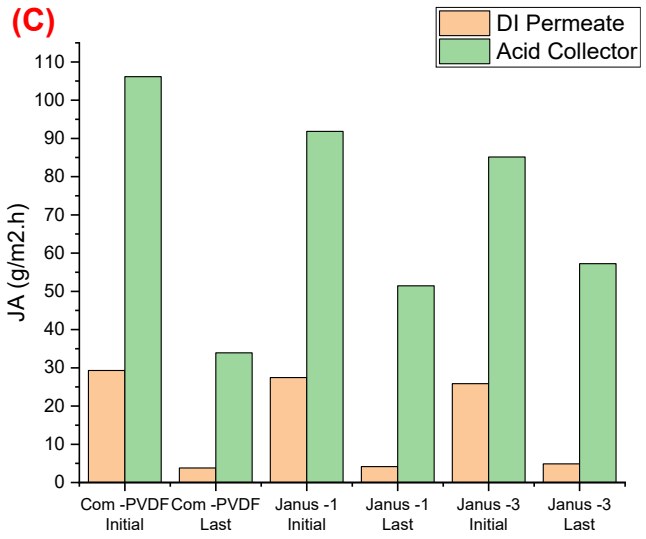

Figure 7-7. Linear regression of ammonia in the permeate vs time for measurement of ammonia capture ratio for the commercial and inkjet-printed membranes in DCMD system having DI water a permeate (a), acid collector as permeate (b), and ammonia flux for both systems (c)

7.3.5 Treatment of landfill leachate in Dual-in series MD system using inkjet-printed membrane

Following the successful application of the new MD configuration for harvesting ammonia from human urine and the demonstrated resistance of the inkjet-printed membrane against fouling issues, we proceeded to utilise a combination of two previous studies to evaluate the performance of the new setup for treating and recovering nutrients from landfill leachate.

Additionally, insights gained from the preceding two studies were applied to establish a dual in-series membrane distillation (MD) setup, incorporating inkjet printed membranes for the treatment of landfill leachate and analysing the performance of the designed setup and modified membrane to address critical objectives of treatment of landfill leachate and the recovery of nitrogen.

In Chapter 5, inkjet printing was employed to enhance the fouling resistivity of the membranes. The outcomes from this investigation provided valuable insights into the advantages and disadvantages of the technique. For instance, the combination of PEI and PDA led to blockages in the pores of the printer cartridges, resulting in reduced performance. Furthermore, challenges related to the integrity of the membrane surface arose due to delayed polymerisation of the polymeric mixture. Drawing from these lessons, this chapter utilises these experiences to modify the polymer selection and implement individual printing of the polymeric solutions.

For this investigation, we manufactured two types of inkjet-printed membranes: Janus-3 and Janus-5. These membranes were coated with three and five layers, respectively, of PSS/PEI solutions. The modified membranes were immersed in an aqueous glutaraldehyde (GA, 25 wt%) solution to complete the crosslinking process. Subsequently, the membranes were thoroughly rinsed with DI water and left to dry in an oven overnight.

Furthermore, more studies were conducted to study the effect of permeate solution on harvesting nutrients from landfill leachate. In one study, DI water was used as the first module's permeate; in another study, the acid solution containing 1 g/l of sulphuric acid was used as the acid collector. The results are shown in Figure 7-8.

The research findings revealed comparable trends for both DI water and acid collectors regarding their influence on water flux behaviour in the DCMD process, as shown in Figure 7-8, A and B. The results demonstrated that the type of solution present in the permeate stream did not demonstrate a significant effect on water flux behaviour. The primary determinant of membrane flux in the DCMD process is the driving force, which

low concertation of the acid solution in the permeate doesn't influence it. While the vapour pressure on the permeate side may be influenced by the composition of the permeate, the experimental data indicated a minimal variation in vapour pressure when the concentration of sulphuric acid was low. These findings suggest that the DCMD process possesses adaptability to accommodate different types of feed solutions without causing a substantial influence on water flux [258].

Furthermore, when comparing the ammonia harvesting performance between the two systems, it becomes evident that employing an acid collector as the permeate solution greatly enhances the rate of ammonia capture. The concentration of ammonia in the acid collector exceeded 200 mg/l, whereas in the system using DI water as the permeate, the concentration reached only 50 mg/l. As explained in earlier sections, the presence of harvesting ions in the acid collector, along with the reactions between these ions and ammonia, substantially increases the rate of ammonia capture.

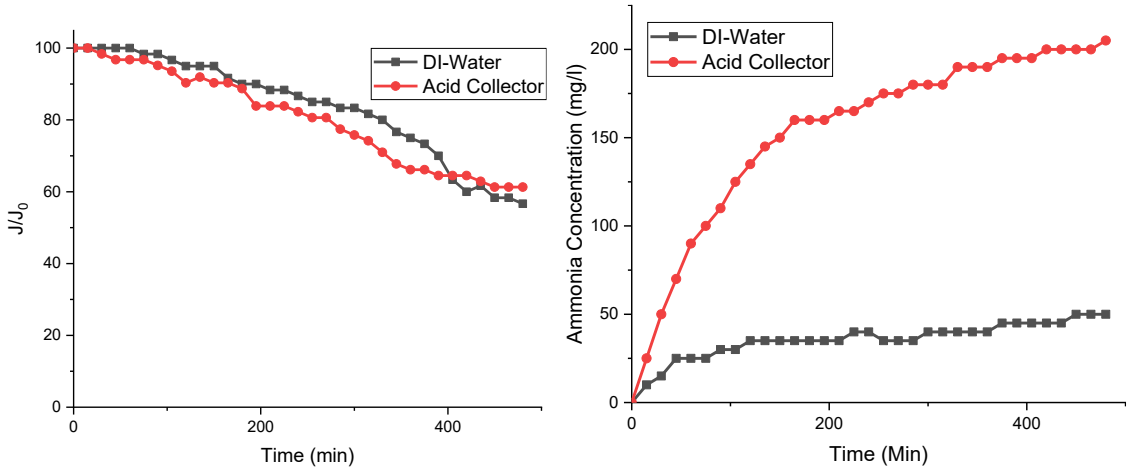

Figure 7-8 Impact of Permeate Solution on Membrane Flux (left) and Ammonia Harvesting (right) from Landfill Leachate for commercial PVDF membrane: DI Water vs. Acid Solution with 1 g/l Sulphuric Acid

The cumulative water flux of the Com-PVDF, Janus-3, and Janus-5 membranes was assessed in a DCMD configuration, and the results are illustrated in Figure 7-9. Observations from the experimental investigation revealed a progressive decline in flux for the commercial PVDF membrane. The introduction of organic materials in the landfill leachate intensified fouling concerns, specifically in the hydrophobic membranes. This can be primarily attributed to the interactions between the fouling agents, such as organic substances, and the PVDF membrane [151, 153, 302]. In contrast, the Janus-3 membrane displayed enhanced resistance against fouling agents; however, it still exhibited a small decrease in flux. The comparison of Janus-3 and Janus-5 membranes shows that the initial flux of Janus-5 membrane is smaller than Janus-3. However, the results show that at the end of the test, the flux of Janus-3 is lower than Janus-3. This small decrease in the flux can be attributed to the presence of some defects on the Janus-3 membrane, which showed small fouling and decreased the flux of membrane.

On the other hand, the Janus-5 membrane, benefiting from five cycles of PEI/PSS inkjet-printed layers, effectively acted as a robust barrier against fouling and maintained a consistent flux throughout the entire experiment. Nonetheless, the initial flux of the Janus-5 membrane was marginally lower compared to that of the commercial and Janus-3 membranes, primarily due to the presence of a hydrophilic layer that impacted the driving force of the system.

Figure 7-9 also depicts the ammonia flux observed in three different membranes during the experiment: Com-PVDF, Janus-3, and Janus-5. The findings indicate that the rate of ammonia capture was higher during the initial hours of the experiment, and its rate dropped by time. This change in the capture rate can be attributed to an increase in the

concentration of ammonia in the permeate and a decline in the driving force for ammonia transfer. Initially, the Com-PVDF membrane exhibited a higher ammonia harvesting, resulting in a greater ammonia flux compared to the two modified membranes. The initial ammonia harvesting for Com-PVDF is higher than two modified membranes (Janus-3, and Janus-5). However, after approximately 1.5 hours, the rate of ammonia harvesting for the commercial membrane dropped, and its slope became lower than that of the inkjet-printed membranes. Consequently, the ammonia flux derived from the Com-PVDF membrane decreased, while the modified membranes showcased improved performance.

The results demonstrate that Janus-3 membrane shows a higher amount of ammonia capture over time. The concentration of ammonia in the acid collector from Janus 3 reached to over 250 mg/l, while Janus 5 could reach just 225 mg/l. This difference can be attributed to more coatings on the Janus-5 membrane, which hampered the transfer of the ammonia by clogging some pores and decreasing the effective surface pore size. However, the flux results show that the printing process doesn't affect the water flux and it just affects on the flux of ammonia. The presence of a hydrophilic layer on the modified membranes doesn't show a barrier against water transfer.

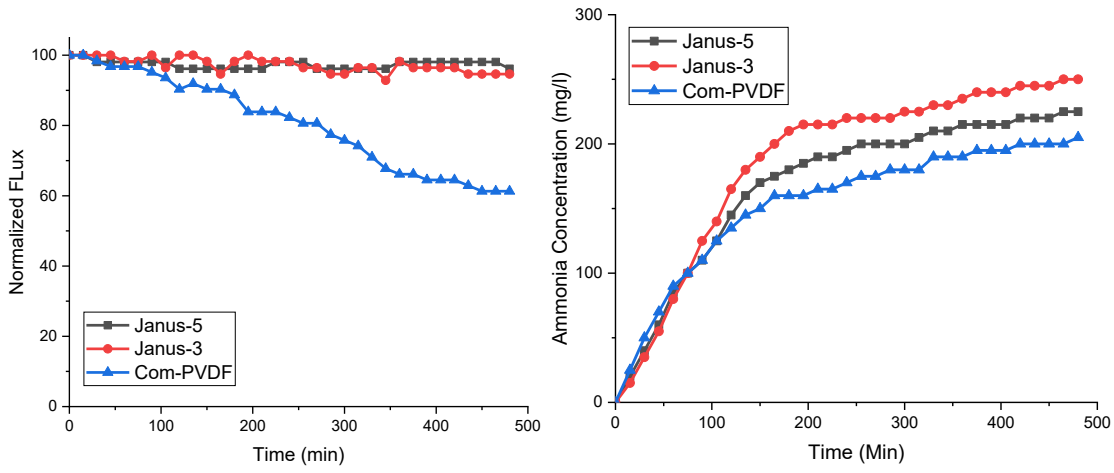

Figure 7-9 Cumulative Water Flux (Left) and Ammonia Concentration (Right) Comparison in Com-PVDF, Janus-3, and Janus-5 Membranes during the Experiment in a DCMD Configuration

In Figure 7-10, a comparison between Janus-3 and Janus-5 revealed that in long-term applications, the Janus-5 membrane exhibited a persistent ammonia harvesting derived from a higher ammonia flux. The fouling of the membrane surface by fouling agents led to a reduction in available pores for ammonia transfer, causing a decrease in the ammonia flux for both the commercial membrane and, to some extent, the Janus-3 membrane [245, 297].

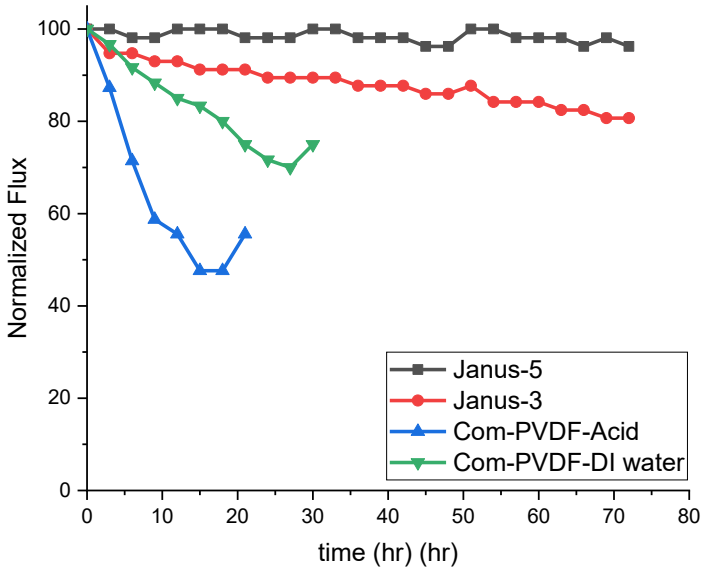

Figure 7-10 Long-term Comparison of Janus-3 and Janus-5 Membranes: Persistent Ammonia Harvesting and Higher Ammonia Flux in Janus-5 Membrane

Moreover, the experimental findings reveal a time-dependent increase in conductivity for both Com-PVDF and Janus-3 membranes, indicating that the conductivity of DI water rises over time (as depicted in Figure 7-11A). The Com-PVDF membrane exhibits a conductivity of 1500 µS/cm after 8 hrs. These values indicate the transfer of ammonia from the feed to the permeate.

However, as described in the previous sections, in the acid collector system, the conductivity trend is different compared to the DI system, as illustrated in Figure 7-11. Initially, the conductivity of the acid solution was around 6300 µS/cm. After starting the experiments, the ammonia is transferred to the acid solution and reacts with the ions present in the permeate, resulting in the formation of a different electrolyte solution. The reaction products have lower conductivity than the initial solution, leading to a drop in conductivity during the process. The conductivity of the permeate decreases from an initial value of 6300 µS/cm to approximately 3100 µS/cm after 8 hours of testing for modified membranes. Comparing the commercial and modified membranes, it is observed that the commercial membrane exhibits a higher rate of conductivity drop compared to the modified membrane. However, after approximately one hour of experimentation, the commercial membrane experiences a decrease in the rate of ammonia transfer and consequently in the rate of conductivity drop, while the modified membrane demonstrates a higher drop in conductivity. This change can be attributed to membrane fouling, which diminishes the rate of ammonia transfer and the subsequent reaction of ammonia in the acid collector [142].

The trends suggest that the rate of change in conductivity is time-dependent, and the change in the trend primarily arises from the consumption of the ions in the acid solution, which reduces the rate of ammonia capture.

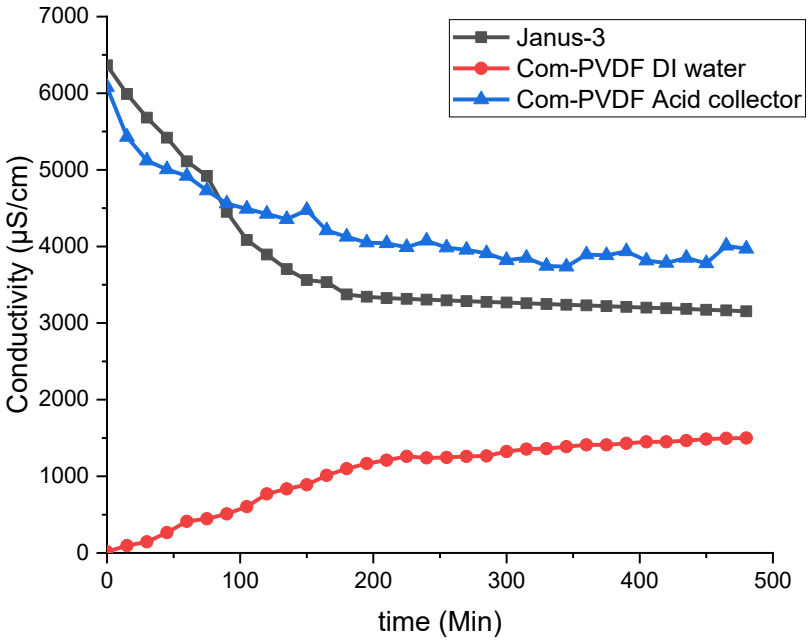

Figure 7-11 Conductivity change over time for commercial and Janus-3 membrane in DI permeate and acid collector

7.4 Conclusion

This paper discussed the fabrication of composite Janus membranes by polyelectrolyte inkjet printing on a hydrophobic substrate. Characterisation and investigation were done on the impact of multiple printing on the antifouling capabilities of the membranes. For the purpose of recovering nutrients from human urine, the modified membranes were evaluated in a DCMD system. The outcomes demonstrated that inkjet printing generated a uniform hydrophilic coating with enhanced antifouling properties. The potential of inkjet printing as a method of surface modification to enhance membrane performance was highlighted in this work. The results show that inkjet printing may provide a uniform hydrophilic layer, which enhances membrane function.

The Com-PVDF, Janus-1, and Janus-3 had initial capture ratio (CR) values of 29.31, 27.46, and 25.85, respectively. However, after about 2 hours, the capture ratio of the commercial membrane decreased to 3.81, 4.15, and 4.89, respectively. Despite a slight decrease in ammonia flux, the inkjet-printed membranes sustained their flux during the entire test, outperforming commercial membranes. In addition, despite the slight decrease in ammonia flux observed after the modification process, the inkjet-printed membrane showcased the ability to sustain its flux during the entire test. While the ammonia flux of 10% dropped after inkjet printing, the membrane reached from 5.8 LMH to 4.8 LMH. In contrast, the flux of the commercial membrane decreased by half. These results underscore the potential of inkjet printing as a convenient surface modification strategy for enhancing MD membrane performance. Inkjet printing can be used to modify the surface of MD membranes, leading to improved performance. This technique could be a cost-effective and efficient way to enhance the flux of MD membranes in various industrial applications.

Chapter 8
Conclusions and Recommendations

8.1 Conclusion

The PhD research helps create cutting-edge solutions for the membrane distillation method's present problems.

For generating freshwater from saltwater or contaminated wastewater, membrane distillation (MD) has emerged as a promising hybrid separation process. MD's long-term applicability limitations include poor flux, fouling, and problems with wetting agents in the feed solution. Potential answers to these problems can be found in Janus membranes, a novel kind of membrane that layers a hydrophilic membrane on top of a hydrophobic membrane (or the other way around). Janus membranes have demonstrated the potential to reduce wetting and fouling issues that are frequently present in MD systems while also enhancing flux performance. The present study thoroughly examined various Janus membrane preparation production, modification, and novel design methodologies. In order to get insight into these membranes' prospective applications, the performance of these membranes in desalination and wastewater treatment utilising MD is carefully assessed and analysed.

The physical properties and operating conditions of membranes employed in membrane distillation (MD) were the main subjects of this investigation. The aim of this study was to establish the ideal values for various feed types for factors including thickness, porosity, and membrane qualities. In order to understand the primary phenomena in the MD system, the behaviour of the system was first simulated using Comsol Software, taking into account variables like temperature differential, flow velocity, membrane characteristics, and feedwater salinity. This phase showed that one of the key challenges faced by MD systems when treating challenging waters is heat loss. In order to increase

energy economy while preserving high flux and rejection capacities for desalination of hypersaline water, a triple-layer membrane with low thermal conductivity was developed. The outcomes demonstrated improved energy efficiency. The findings of the experiment, however, indicated that electrospun nanofiber membrane modification is not simple. In order to build Janus membranes with a hydrophilic layer on a hydrophobic membrane surface that provides resistance to oil fouling, the next stage was using inkjet printing. The outcomes demonstrated enhanced antifouling performance with constant water flux. The inkjet-printed membranes demonstrated an excellent MD process modification approach. As a result, in the subsequent stage, membranes with inkjet printing were employed to treat two more types of wastewater: landfill leachate and human urine. This step involved the development of a dual in-series MD arrangement, which offered a promising method for recovering nutrients from human urine. An inkjet-printed membrane was also used to improve the separation performance. This study makes a valuable contribution to advancing nutrient recovery methods based on MD and promoting sustainable resource utilisation. In conclusion, the present investigation has yielded the following findings:

- The review of the Janus Membrane demonstrated the potential of utilising this membrane to boost the capabilities of a MD system in addressing prevalent difficulties such as wetting and fouling. This study aimed to evaluate and compare the antiwetting and antifouling capabilities of Janus membranes and hydrophobic membranes across various types of feed water. The findings of this investigation revealed that Janus membranes exhibited superior performance in treating heavily contaminated water. Nevertheless, there are still obstacles that

need to be addressed in order to advance the field. These issues encompass the requirement to create a membrane specifically designed for membrane distillation, as well as the careful selection of modification materials that are both economically viable and environmentally sustainable. Further enquiry and modelling are necessary to explore the mechanical stability of Janus membranes, as well as to gain a comprehensive understanding of the transport process through the hydrophilic layer and the phase transition to vapour. Notwithstanding the encouraging outcomes shown in experiments, there exist areas of knowledge that necessitate attention, including the resolution of delamination challenges encountered during the production of flawless Janus membranes, as well as the investigation of alternative layer arrangements to surmount prevailing constraints.

- In light of the notable potential exhibited by Janus membranes in molecular dynamics systems, a triple-layer electrospun nanofiber membrane was fabricated for the purpose of desalinating hypersaline feedwater. The implementation of an intermediate layer characterised by a low thermal conductivity has enhanced energy efficiency through the mitigation of heat dissipation. The research revealed that the intermediate layer exhibited a more pronounced influence on the process of desalinating highly saline feedwater, resulting in an augmentation of both permeate flux and energy efficiency. The suitability of the membrane for treating feedwater with high salt levels was proven by computational fluid dynamics (CFD) models that were validated using experimental data. The determination of the optimal membrane thickness was conducted by considering multiple characteristics. It was shown that thicker

membranes are better suited for hypersaline desalination due to their lower thermal conduction properties. The study additionally emphasised the impact of salinity on both vapour pressure and flow, as well as the compensatory influence of reduced thermal conductivity on flux. In general, the results of this study enhance our comprehension of membrane architecture in relation to the effective desalination of hypersaline feedwater.

- The utilisation of inkjet printing to coat commercial PVDF membranes with a hydrophilic solution resulted in enhanced resistance to fouling in comparison to conventional commercial membranes. Notably, the presence of a thicker hydrophilic coating on the membranes contributed to a better level of fouling resistance, even when exposed to higher concentrations of oil. The Janus membranes, which were printed on both sides or had three layers, exhibited the most significant fluxes and sustained high rates of rejection. This study showcases the efficacy of inkjet printing as a straightforward and efficient technique for fabricating Janus membranes capable of enduring oil fouling in membrane distillation applications. Consequently, this research expands the potential utilisation of these membranes in demanding wastewater treatment and desalination procedures.
- The dual in-series MD module has successfully exhibited the technological viability of extracting ammonia from hydrolysed human urine. This configuration has shown improved rates of transfer and enhanced ammonia capture in comparison to the conventional MD setup. Although the water flux exhibited similarities across the settings, it is noteworthy that the ammonia flux in the in-series MD configuration demonstrated a substantial increase, surpassing 180

g/m2h. The implementation of the dual in-series configuration ensured a consistent pH level in the acid collector, in contrast to the single configuration, where pH fluctuations resulted in reduced process efficiency. The augmentation of the feed flow rate resulted in a corresponding rise in the efficiency of ammonia capture.

- The utilisation of inkjet printing to fabricate composite Janus membranes exhibited enhanced resistance to fouling. The utilisation of inkjet printing has been identified as a convenient and effective method for surface modification, with the aim of boosting the performance of MD membranes. Despite a modest drop in ammonia flow following inkjet printing, the modified membranes exhibited consistent flux throughout the duration of the test, in contrast to the commercial membranes. This observation underscores the potential of inkjet printing as a means to enhance the performance of MD membranes in many industrial applications.

Hence, the utilisation of Janus membranes holds significant promise in enhancing MD modules to address challenges associated with the treatment of complex feedwater sources such as hypersaline feedwater, human urine, or landfill leachate. The utilisation of a three-layer inkjet printing technique exhibits considerable potential as a viable solution for the treatment of feedwater that contains fouling agents while simultaneously maintaining the membrane's flux efficiency. The incorporation of modified layers in inkjet-printed membranes guarantees their sustained resilience when exposed to challenging environments such as landfill leachate or human urine.

8.2 Recommendations

This PhD study focused on the development of various classes of Janus membranes with the aim of attaining enhanced anti-fouling capabilities. Despite the commendable performances, additional research is necessary to facilitate the integration of this distinctive technology into practical, real-world scenarios. In order to advance the application of Janus Membranes in the membrane distillation process, the following areas of research are suggested:

- Studying the effect of the thickness of the hydrophilic layer on heat resistivity of the Janus membranes
- Exploring the effect of viscosity on the performance of inkjet-printed membranes
- Fabrication of trilayer membrane that has a hydrophilic affinity in both sides but hydrophobic affinity in the middle, which theoretically shows an attractive configuration for enhancement of both heat and mass transfer efficiency
- Fabrication of Janus membranes using economic and non-fluorinated materials that have low environmental issues and low cost
- Focusing on one-step fabrication methods to ease the fabrication process and decrease the processing costs like improvement of SMM-based Janus membranes
- Studying the mechanism of nutrient harvesting and evaluation of energy balance in the acid collector
- Investigation of the effect of the hydrophobic and hydrophilic regions on heat and mass transfer rates, flux, and selectivity. Explore the mechanisms governing

transport phenomena in Janus membranes and optimize their design for enhanced performance.

- Investigation of the feasibility and scalability of Janus membrane MD systems for large-scale applications. Evaluate the performance of Janus membranes on a pilot scale and assess their potential for commercialization. Study the challenges associated with upscaling, including module design, system operation, and cost considerations.
- Investigate the fabrication of Janus membranes in MD processes using innovative materials like graphene oxide, nanocomposites, or functional polymers. Examine their effect on the stability, selectivity, and flow of the membrane.
- For the development of hybrid MD systems, look into combining Janus membranes with other separation techniques, such as forwards osmosis or membrane nanofiltration. Analyse the overall effectiveness and efficiency of these hybrid systems and examine the synergistic benefits of integrating various separation techniques.

References

[1] C. Copeland, N. T. Carter. Energy-water nexus: The water sector's energy use, Congressional Research Service Washington, DC, USA, 2014.

[2] A. A. Najafpoor, A. Sadeghi, H. Alidadi, M. Davoudi, B. Mohebrad, A. Hosseinzadeh, S. Jafarpour, A. Zarei, *Environmental Health Engineering and Management Journal*, **2015***, 2 (2),* 79-86.

[3] Z. Wang, D. Hou, S. Lin, *Environ. Sci. Technol.*, **2016***, 50 (7),* 3866-3874.

[4] H. C. Yang, Y. Xie, J. Hou, A. K. Cheetham, V. Chen, S. B. Darling, *Adv. Mater.*, **2018***, 30 (43),* e1801495. DOI: 10.1002/adma.201801495

[5] S. Kheirieh, M. Asghari, M. Afsari, *Rev. Chem. Eng.*, **2018***, 34 (5),* 657-693.

[6] A. Hosseinzadeh, J. L. Zhou, A. Altaee, M. Baziar, X. Li, *Bioresour. Technol.*, **2020***,* 123391.

[7] L. N. Nthunya, L. Gutierrez, S. Derese, E. N. Nxumalo, A. R. Verliefde, B. B. Mamba, S. D. Mhlanga, *J. Chem. Technol. Biotechnol.*, **2019***, 94 (9),* 2757-2771.

[8] T. Bao, M. M. Damtie, A. Hosseinzadeh, W. Wei, J. Jin, H. N. P. Vo, J. S. Ye, Y. Liu, X. F. Wang, Z. M. Yu, *J Environ Manage*, **2020***, 260,* 110105.

[9] N. G. P. Chew, S. Zhao, R. Wang, *Adv. Colloid Interface Sci.*, **2019***, 273,* 102022. DOI: 10.1016/j.cis.2019.102022

[10] T. Bao, M. M. Damtie, A. Hosseinzadeh, R. L. Frost, Z. M. Yu, J. Jin, K. Wu, *Applied Clay Science*, **2020***, 195,* 105735.

[11] Y. Zhao, H. Wang, H. Zhou, T. Lin, *Small*, **2017***, 13 (4)*. DOI: 10.1002/smll.201601070

[12] H. Zhou, Z. Guo, *Journal of Materials Chemistry A*, **2019***, 7 (21),* 12921-12950. DOI: 10.1039/c9ta02682g

[13] M. Sheikh, M. Asghari, M. Afsari, *Alexandria engineering journal*, **2018***, 57 (4),* 3661-3669.

[14] X. Li, X. Yu, C. Cheng, L. Deng, M. Wang, X. Wang, *ACS Appl Mater Interfaces*, **2015***, 7 (39),* 21919-30. DOI: 10.1021/acsami.5b06509

[15] E. J. Lee, B. J. Deka, J. Guo, Y. C. Woo, H. K. Shon, A. K. An, *Environ Sci Technol*, **2017***, 51 (17),* 10117-10126. DOI: 10.1021/acs.est.7b01108

[16] C. Li, X. Li, X. Du, T. Tong, T. Y. Cath, J. Lee, *ACS Appl Mater Interfaces*, **2019***, 11 (20),* 18456-18465. DOI: 10.1021/acsami.9b04212

[17] Y. Chen, K. J. Lu, T.-S. Chung, *J. Membr. Sci.*, **2020***, 595,* 117572.

[18] Z. Zhu, Y. Liu, H. Hou, W. Shi, F. Qu, F. Cui, W. Wang, *Environ Sci Technol*, **2018***, 52 (5),* 3027-3036. DOI: 10.1021/acs.est.7b06227

[19] S. Lin, S. Nejati, C. Boo, Y. Hu, C. O. Osuji, M. Elimelech, *Environmental Science & Technology Letters*, **2014***, 1 (11),* 443-447. DOI: 10.1021/ez500267p

[20] C. Boo, J. Lee, M. Elimelech, *Environ Sci Technol*, **2016***, 50 (22),* 12275-12282. DOI: 10.1021/acs.est.6b03882

[21] B. J. Deka, E. J. Lee, J. Guo, J. Kharraz, A. K. An, *Environ Sci Technol*, **2019***, 53 (9),* 4948-4958. DOI: 10.1021/acs.est.8b07254

[22] T. Li, F. Liu, S. Zhang, H. Lin, J. Wang, C. Y. Tang, *ACS Appl Mater Interfaces*, **2018***, 10 (29),* 24947-24954. DOI: 10.1021/acsami.8b08278

[23] B. J. Deka, J. Guo, N. K. Khanzada, A. K. An, *Water Res*, **2019***, 165,* 114982.

[24] S. Bonyadi, T. S. Chung, *J. Membr. Sci.*, **2007***, 306 (1-2),* 134-146. DOI: 10.1016/j.memsci.2007.08.034
[25] M. Khayet, T. Matsuura, *Desalination*, **2003***, 158 (1-3),* 51-56.
[26] C. Fornaguera, A. Dols-Perez, G. Caldero, M. J. Garcia-Celma, J. Camarasa, C. Solans, *J. Control. Release*, **2015***, 211,* 134-43. DOI: 10.1016/j.jconrel.2015.06.002
[27] J. H. Roque-Ruiz, N. A. Medellín-Castillo, S. Y. Reyes-López, *Results in Physics*, **2019***, 12,* 193-204. DOI: 10.1016/j.rinp.2018.11.068
[28] B. S. Chapman, S. R. Mishra, J. B. Tracy, *Dalton Trans*, **2019***, 48 (34),* 12822-12827. DOI: 10.1039/c9dt01872g
[29] J. A. Kharraz, M. U. Farid, N. K. Khanzada, B. J. Deka, H. A. Arafat, A. K. An, *Water Res*, **2020***, 174,* 115600.
[30] B. Bhushan, Y. C. Jung, in *Nanotribology and Nanomechanics II*, **2011**, 533-699.
[31] A. Kyoungjin An, E. J. Lee, J. Guo, S. Jeong, J. G. Lee, N. Ghaffour, *Sci. Rep.*, **2017***, 7,* 41562. DOI: 10.1038/srep41562
[32] H.-M. Song, C. Chen, X.-X. Shui, H. Yang, L.-J. Zhu, Z.-X. Zeng, Q.-J. Xue, *J. Membr. Sci.*, **2019***, 573,* 126-134. DOI: 10.1016/j.memsci.2018.11.063
[33] M. Cao, J. Xiao, C. Yu, K. Li, L. Jiang, *Small*, **2015***, 11 (34),* 4379-84. DOI: 10.1002/smll.201500647
[34] Z. Zhu, Z. Liu, L. Zhong, C. Song, W. Shi, F. Cui, W. Wang, *J. Membr. Sci.*, **2018***, 563,* 602-609. DOI: 10.1016/j.memsci.2018.06.028
[35] H. C. Yang, J. Hou, V. Chen, Z. K. Xu, *Angew. Chem. Int. Ed. Engl.*, **2016***, 55 (43),* 13398-13407. DOI: 10.1002/anie.201601589
[36] B. Wang, B. Li, B. Dong, B. Zhao, C. Y. Li, *Macromolecules*, **2010***, 43 (22),* 9234-9238.
[37] D. Y. Cheng, S. J. Wiersma. Composite membrane for a membrane distillation system, Google Patents, 1982.
[38] D. Miao, Z. Huang, X. Wang, J. Yu, B. Ding, *Small*, **2018***, 14 (32),* 1801527.
[39] M. Nosonovsky, B. Bhushan, *Langmuir*, **2008***, 24 (4),* 1525-1533.
[40] J. Lee, C. Boo, W.-H. Ryu, A. D. Taylor, M. Elimelech, *ACS applied materials & interfaces*, **2016***, 8 (17),* 11154-11161.
[41] P. Wang, T.-S. Chung, *J. Membr. Sci.*, **2015***, 474,* 39-56.
[42] J. A. Kharraz, A. K. An, *J. Membr. Sci.*, **2020***, 595,* 117596.
[43] N. G. P. Chew, Y. Zhang, K. Goh, J. S. Ho, R. Xu, R. Wang, *ACS Appl Mater Interfaces*, **2019***, 11 (28),* 25524-25534. DOI: 10.1021/acsami.9b05967
[44] M. Yao, L. D. Tijing, G. Naidu, S.-H. Kim, H. Matsuyama, A. G. Fane, H. K. Shon, *Desalination*, **2020***, 479,* 114312.
[45] F. Huang, B. Motealleh, W. Zheng, M. T. Janish, C. B. Carter, C. J. Cornelius, *Ceram. Int.*, **2018***, 44 (5),* 4577-4585. DOI: 10.1016/j.ceramint.2017.10.134
[46] Y. X. Huang, Z. Wang, J. Jin, S. Lin, *Environ Sci Technol*, **2017***, 51 (22),* 13304-13310. DOI: 10.1021/acs.est.7b02848
[47] M.-B. Wu, H.-C. Yang, J.-J. Wang, G.-P. Wu, Z.-K. Xu, *ACS applied materials & interfaces*, **2017***, 9 (6),* 5062-5066.
[48] A. M. Pornea, J. M. C. Puguan, V. G. Deonikar, H. Kim, *Sep. Purif. Technol.*, **2020***, 236,* 116297.
[49] M. Mohammadi Ghaleni, A. Al Balushi, S. Kaviani, E. Tavakoli, M. Bavarian, S. Nejati, *ACS Appl Mater Interfaces*, **2018***, 10 (51),* 44871-44879. DOI: 10.1021/acsami.8b16621

[50] V. Zargar, M. Asghari, M. Afsari, *Int. J. Environ. Sci. Technol. (Tehran)*, **2019***, 16 (1),* 37-46.
[51] M. Han, T. Dong, D. Hou, J. Yao, L. Han, *J. Membr. Sci.*, **2020**. DOI: 10.1016/j.memsci.2020.118078
[52] M. Li, K. J. Lu, L. Wang, X. Zhang, T.-S. Chung, *J. Membr. Sci.*, **2020***, 603*. DOI: 10.1016/j.memsci.2020.118031
[53] L. Eykens, I. Hitsov, K. De Sitter, C. Dotremont, L. Pinoy, I. Nopens, B. Van der Bruggen, *J. Membr. Sci.*, **2016***, 498,* 353-364.
[54] P.-J. Lin, M.-C. Yang, Y.-L. Li, J.-H. Chen, *J. Membr. Sci.*, **2015***, 475,* 511-520.
[55] N. G. P. Chew, S. Zhao, C. Malde, R. Wang, *J. Membr. Sci.*, **2017***, 541,* 162-173.
[56] Z. Zhang, X. Du, K. H. Carlson, C. A. Robbins, T. Tong, *Desalination*, **2019***, 454,* 82-90.
[57] R. Z. Waldman, H.-C. Yang, D. J. Mandia, P. F. Nealey, J. W. Elam, S. B. Darling, *Advanced Materials Interfaces*, **2018***, 5 (15)*. DOI: 10.1002/admi.201800658
[58] M. B. Wu, H. C. Yang, J. J. Wang, G. P. Wu, Z. K. Xu, *ACS Appl Mater Interfaces*, **2017***, 9 (6),* 5062-5066. DOI: 10.1021/acsami.7b00017
[59] *The effect of different process parameters on polyamide 66 nano fibre by force spinning method*, AIP Publishing LLC.
[60] F. Ardeshiri, A. Akbari, M. Peyravi, M. Jahanshahi, *Journal of Industrial and Engineering Chemistry*, **2019***, 74,* 14-25.
[61] J. Meng, J. Zhong, H. Xiao, J. Ou, *AIP Advances*, **2019***, 9 (6),* 065108.
[62] J.-G. Lee, E.-J. Lee, S. Jeong, J. Guo, A. K. An, H. Guo, J. Kim, T. Leiknes, N. Ghaffour, *J. Membr. Sci.*, **2017***, 526,* 395-408. DOI: 10.1016/j.memsci.2016.12.045
[63] M. Afsari, M. Asghari, P. Mohammadi Moghaddam, *International Journal of Nano Dimension*, **2017***, 8 (4),* 316-328.
[64] Y. Liu, T. Xiao, C. Bao, Y. Fu, X. Yang, *J. Membr. Sci.*, **2018***, 563,* 298-308. DOI: 10.1016/j.memsci.2018.05.067
[65] L. Zou, P. Gusnawan, G. Zhang, J. Yu, *Journal of Membrane Science*, **2020***, 597,* 117756.
[66] M. Asghari, M. Sheikh, M. Afsari, M. Dehghani, *J. Mol. Liq.*, **2017***, 246,* 7-16. DOI: https://doi.org/10.1016/j.molliq.2017.09.045
[67] R. Kardani, M. Asghari, N. F. Hamedani, M. Afsari, *Journal of Industrial and Engineering Chemistry*, **2019**.
[68] J. E. Efome, D. Rana, T. Matsuura, C. Q. Lan, *Water Res*, **2016***, 89,* 39-49. DOI: 10.1016/j.watres.2015.11.040
[69] H. N. Li, J. Yang, Z. K. Xu, *Advanced Materials Interfaces*, **2020***, 7 (7)*. DOI: 10.1002/admi.201902064
[70] F. Ren, G. Li, Z. Zhang, X. Zhang, H. Fan, C. Zhou, Y. Wang, Y. Zhang, C. Wang, K. Mu, Y. Su, D. Wu, *Journal of Materials Chemistry A*, **2017***, 5 (35),* 18403-18408. DOI: 10.1039/c7ta04392a
[71] H.-C. Yang, J. Hou, L.-S. Wan, V. Chen, Z.-K. Xu, *Advanced Materials Interfaces*, **2016***, 3 (9)*. DOI: 10.1002/admi.201500774
[72] K. Wang, D. Hou, P. Qi, K. Li, Z. Yuan, J. Wang, *J. Colloid Interface Sci.*, **2019***, 537,* 375-383. DOI: 10.1016/j.jcis.2018.11.040
[73] Z. Wang, X. Yang, Z. Cheng, Y. Liu, L. Shao, L. Jiang, *Materials Horizons*, **2017***, 4 (4),* 701-708. DOI: 10.1039/c7mh00216e

[74] A. Ghaee, M. Karimi, M. Lotfi-Sarvestani, B. Sadatnia, V. Hoseinpour, *Materials Science and Engineering: C*, **2019***, 103,* 109767.
[75] Z. S. Tai, M. H. A. Aziz, M. H. D. Othman, A. F. Ismail, M. A. Rahman, J. Jaafar, in *Membrane Separation Principles and Applications*, Elsevier, **2019**, 251-281.
[76] M. Essalhi, M. Khayet, *J. Membr. Sci.*, **2012***, 417,* 163-173.
[77] Y. Zhang, M. Barboiu, *Chem. Commun.*, **2015***, 51 (88),* 15925-15927.
[78] M. Khayet, M. C. García-Payo, L. García-Fernández, J. Contreras-Martínez, *Desalination*, **2018***, 426,* 174-184. DOI: 10.1016/j.desal.2017.10.036
[79] M. Khayet, T. Matsuura, M. R. Qtaishat, J. I. Mengual, *Desalination*, **2006***, 199 (1-3),* 180-181. DOI: 10.1016/j.desal.2006.03.039
[80] J. Chen, Y. Liu, D. Guo, M. Cao, L. Jiang, *Chem. Commun.*, **2015***, 51 (59),* 11872-11875.
[81] X. Li, W. Zhang, R. Qu, Y. Liu, Y. Wei, L. Feng, *Journal of Materials Chemistry A*, **2019***, 7 (16),* 10047-10057. DOI: 10.1039/c9ta01686d
[82] Z. Wang, Y. Wang, G. Liu, *Angew. Chem. Int. Ed. Engl.*, **2016***, 55 (4),* 1291-4. DOI: 10.1002/anie.201507451
[83] E.-J. Lee, A. K. An, P. Hadi, S. Lee, Y. C. Woo, H. K. Shon, *J. Membr. Sci.*, **2017***, 524,* 712-720. DOI: 10.1016/j.memsci.2016.11.069
[84] L. N. Nthunya, L. Gutierrez, A. R. Verliefde, S. D. Mhlanga, *J. Chem. Technol. Biotechnol.*, **2019***, 94 (9),* 2826-2837.
[85] M. R. S. Kebria, A. Rahimpour, S. K. Salestan, S. F. Seyedpour, A. Jafari, F. Banisheykholeslami, N. Tavajohi Hassan Kiadeh, *Desalination*, **2020***, 479*. DOI: 10.1016/j.desal.2019.114307
[86] S. Zhou, Z. Xiong, F. Liu, H. Lin, J. Wang, T. Li, Q. Han, Q. Fang, *Journal of Materials Chemistry A*, **2019***, 7 (2),* 632-638. DOI: 10.1039/c8ta08541b
[87] A. Figoli, C. Ursino, F. Galiano, E. Di Nicolò, P. Campanelli, M. C. Carnevale, A. Criscuoli, *J. Membr. Sci.*, **2017***, 522,* 192-201. DOI: 10.1016/j.memsci.2016.08.066
[88] X. Yang, L. Yan, F. Ran, A. Pal, J. Long, L. Shao, *J. Membr. Sci.*, **2019***, 576,* 9-16. DOI: 10.1016/j.memsci.2019.01.014
[89] A. Vanangamudi, L. F. Dumée, M. C. Duke, X. Yang, *ACS applied materials & interfaces*, **2017***, 9 (21),* 18328-18337.
[90] L. Yan, X. Yang, J. Long, X. Cheng, D. Pan, Y. Huang, L. Shao, *Chem. Commun. (Camb.)*, **2020***, 56 (3),* 478-481. DOI: 10.1039/c9cc08088k
[91] L. D. Tijing, Y. C. Woo, M. A. H. Johir, J.-S. Choi, H. K. Shon, *Chemical Engineering Journal*, **2014***, 256,* 155-159.
[92] X. Yue, T. Zhang, D. Yang, F. Qiu, Z. Li, *Cellu*, **2018***, 25 (10),* 5951-5965. DOI: 10.1007/s10570-018-1996-8
[93] Y. C. Woo, Y. Chen, L. D. Tijing, S. Phuntsho, T. He, J.-S. Choi, S.-H. Kim, H. K. Shon, *Journal of Membrane Science*, **2017***, 529,* 234-242.
[94] A. A. Najafpoor, A. J. Jafari, A. Hosseinzadeh, R. K. Jazani, H. Bargozin, *Environmental Science and Pollution Research*, **2018***, 25 (1),* 233-241.
[95] A. Hosseinzadeh, A. A. Najafpoor, A. J. Jafari, R. K. Jazani, M. Baziar, H. Bargozin, F. G. Piranloo, *Process Saf. Environ. Prot.*, **2018***, 119,* 261-270.
[96] G. Toskas, C. Cherif, R. D. Hund, E. Laourine, B. Mahltig, A. Fahmi, C. Heinemann, T. Hanke, *Carbohydr. Polym.*, **2013***, 94 (2),* 713-22. DOI: 10.1016/j.carbpol.2013.01.068
[97] H. Ye, J. Zhu, D. Deng, S. Jin, J. Li, Y. Man, *J. Biomater. Sci. Polym. Ed.*, **2019***, 30 (16),* 1505-1522. DOI: 10.1080/09205063.2019.1646628

[98] Y. Yin, W. Wang, A. K. Kota, S. Zhao, T. Tong, *Environmental Science: Water Research & Technology*, **2019***, 5 (11),* 2004-2014. DOI: 10.1039/c9ew00626e
[99] C. Wang, J. Wang, L. Zeng, Z. Qiao, X. Liu, H. Liu, J. Zhang, J. Ding, *Molecules*, **2019***, 24 (5)*. DOI: 10.3390/molecules24050834
[100] H.-C. Yang, W. Zhong, J. Hou, V. Chen, Z.-K. Xu, *J. Membr. Sci.*, **2017***, 523,* 1-7. DOI: 10.1016/j.memsci.2016.09.044
[101] L. Zou, P. Gusnawan, G. Zhang, J. Yu, *J. Membr. Sci.*, **2020***, 597*. DOI: 10.1016/j.memsci.2019.117756
[102] C. Su, Y. Li, H. Cao, C. Lu, Y. Li, J. Chang, F. Duan, *J. Membr. Sci.*, **2019***, 583,* 200-208. DOI: 10.1016/j.memsci.2019.04.037
[103] K. J. Lu, J. Zuo, J. Chang, H. N. Kuan, T.-S. Chung, *Environ. Sci. Technol.*, **2018***, 52 (7),* 4472-4480.
[104] J. Zuo, T.-S. Chung, G. S. O'Brien, W. Kosar, *J. Membr. Sci.*, **2017***, 523,* 103-110. DOI: 10.1016/j.memsci.2016.09.030
[105] A. Naderi, T.-S. Chung, M. Weber, C. Maletzko, *J. Membr. Sci.*, **2019***, 591,* 117292.
[106] E. Virga, J. de Grooth, K. Žvab, W. M. de Vos, *ACS Applied Polymer Materials*, **2019***, 1 (8),* 2230-2239.
[107] L. D. Tijing, J.-S. Choi, S. Lee, S.-H. Kim, H. K. Shon, *J. Membr. Sci.*, **2014***, 453,* 435-462.
[108] L. D. Tijing, Y. C. Woo, W.-G. Shim, T. He, J.-S. Choi, S.-H. Kim, H. K. Shon, *Journal of Membrane Science*, **2016***, 502,* 158-170.
[109] Y. C. Woo, L. D. Tijing, M. J. Park, M. Yao, J.-S. Choi, S. Lee, S.-H. Kim, K.-J. An, H. K. Shon, *Desalination*, **2017***, 403,* 187-198.
[110] B. Yue, B. Zhang, J. You, Y. Li, L. Li, J. Li, *RSC Advances*, **2016***, 6 (21),* 17215-17221. DOI: 10.1039/c5ra24632f
[111] C. Boo, J. Lee, M. Elimelech, *Environ. Sci. Technol.*, **2016***, 50 (15),* 8112-8119.
[112] L. D. Tijing, Y. C. Woo, M. Yao, J. Ren, H. K. Shon, in *Comprehensive Membrane Science and Engineering*, **2017**, 418-444.
[113] J. Xue, T. Wu, Y. Dai, Y. Xia, *Chem. Rev.*, **2019***, 119 (8),* 5298-5415. DOI: 10.1021/acs.chemrev.8b00593
[114] M. R. Elmarghany, A. H. El-Shazly, S. Rajabzadeh, M. S. Salem, M. A. Shouman, M. N. Sabry, H. Matsuyama, N. Nady, *Membranes*, **2020***, 10 (1),* 15.
[115] E.-J. Lee, B. J. Deka, A. K. An, *J. Membr. Sci.*, **2019***, 573,* 570-578. DOI: 10.1016/j.memsci.2018.12.019
[116] J. L. Wang, M. Hassan, J. W. Liu, S. H. Yu, *Adv. Mater.*, **2018***, 30 (48),* 1803430.
[117] J. Wu, N. Wang, L. Wang, H. Dong, Y. Zhao, L. Jiang, *Soft Matter*, **2012***, 8 (22),* 5996-5999.
[118] W. Sun, F. Shen, Z. Wang, Y. Zhang, Y. Wan, *Desalination*, **2018***, 445,* 40-50.
[119] D. Hou, Z. Wang, K. Wang, J. Wang, S. Lin, *J. Membr. Sci.*, **2018***, 546,* 179-187.
[120] H. Qiu, Y. Peng, L. Ge, B. V. Hernandez, Z. Zhu, *Appl. Surf. Sci.*, **2018***, 443,* 217-226.
[121] D. Cheng, J. Zhang, N. Li, D. Ng, S. R. Gray, Z. Xie, *Ind. Eng. Chem. Res.*, **2018***, 57 (28),* 9313-9322.
[122] Y. Zhan, X. Wan, S. He, Q. Yang, Y. He, *Chem. Eng. J.*, **2018***, 333,* 132--145.
[123] W. Xu, X. Hu, S. Zhuang, Y. Wang, X. Li, L. Zhou, S. Zhu, J. Zhu, *Advanced Energy Materials*, **2018***, 8 (14)*. DOI: 10.1002/aenm.201702884
[124] L. Shi, X. Liu, W. Wang, L. Jiang, S. Wang, *Adv. Mater.*, **2019***, 31 (5),* 1804187.

[125] Y. Dong, J. Kong, C. Mu, C. Zhao, N. L. Thomas, X. Lu, *Materials & Design*, **2015**, *88,* 82-87.
[126] C. Mendoza, Z. Gonzlez, Y. Castro, E. Gordo, B. Ferrari, *J. Eur. Ceram. Soc.*, **2016**, *36 (2),* 307--317.
[127] J. A. Prince, D. Rana, T. Matsuura, N. Ayyanar, T. S. Shanmugasundaram, G. Singh, *Sci. Rep.*, **2014**, *4,* 6949. DOI: 10.1038/srep06949
[128] C. Ursino, E. Di Nicolò, B. Gabriele, A. Criscuoli, A. Figoli, *J. Membr. Sci.*, **2019**, *581,* 58-71.
[129] J. Kim, J. Kim, S. Hong, *Water Res*, **2018**, *129,* 447-459. DOI: 10.1016/j.watres.2017.11.017
[130] L. D. Tijing, Y. C. Woo, J.-S. Choi, S. Lee, S.-H. Kim, H. K. Shon, *J. Membr. Sci.*, **2015**, *475,* 215-244.
[131] J. A. Bush, J. Vanneste, E. M. Gustafson, C. A. Waechter, D. Jassby, C. S. Turchi, T. Y. Cath, *J. Membr. Sci.*, **2018**, *554,* 366-377.
[132] T. Tong, A. F. Wallace, S. Zhao, Z. Wang, *J. Membr. Sci.*, **2019**.
[133] Y. Liao, R. Wang, M. Tian, C. Qiu, A. G. Fane, *J. Membr. Sci.*, **2013**, *425,* 30-39.
[134] Z. Xiao, R. Zheng, Y. Liu, H. He, X. Yuan, Y. Ji, D. Li, H. Yin, Y. Zhang, X.-M. Li, *Water Res*, **2019**, *155,* 152-161.
[135] Z. Xiao, Z. Li, H. Guo, Y. Liu, Y. Wang, H. Yin, X. Li, J. Song, L. D. Nghiem, T. He, *Desalination*, **2019**, *466,* 36-43.
[136] Y. Wang, X. Liu, J. Ge, J. Li, Y. Jin, *Chem. Eng. J.*, **2023**, *462,* 142335. DOI: https://doi.org/10.1016/j.cej.2023.142335
[137] L. Francis, F. E. Ahmed, N. Hilal, *Membranes*, **2022**, *12 (1),* 81.
[138] G. Naidu, L. Tijing, M. A. H. Johir, H. Shon, S. Vigneswaran, *J. Membr. Sci.*, **2020**, *599,* 117832. DOI: https://doi.org/10.1016/j.memsci.2020.117832
[139] A. Patel, A. A. Mungray, A. K. Mungray, *Chemosphere*, **2020**, *259,* 127372.
[140] P. Simha, M. Ganesapillai, *Sustainable Environment Research*, **2017**, *27 (3),* 107-116.
[141] M. Maurer, W. Pronk, T. A. Larsen, *Water Res*, **2006**, *40 (17),* 3151-3166. DOI: https://doi.org/10.1016/j.watres.2006.07.012
[142] L. He, Y. Wang, T. Zhou, Y. Zhao, *Chem. Eng. J.*, **2020**, *400,* 125338. DOI: https://doi.org/10.1016/j.cej.2020.125338
[143] H. Yao, Z. Hu, W. Qing, S. Sun, W. Zhang, *Journal of Environmental Chemical Engineering*, **2022**, *10 (2),* 107176.
[144] U. Badeti, N. K. Pathak, F. Volpin, U. Dorji, S. Freguia, H. K. Shon, S. Phuntsho, *Process Saf. Environ. Prot.*, **2021**, *150,* 298-304.
[145] M. Afsari, A. H. Ghorbani, M. Asghari, H. K. Shon, L. D. Tijing, *Chemosphere*, **2022**, *305,* 135294. DOI: https://doi.org/10.1016/j.chemosphere.2022.135294
[146] J. Wang, Y. Liu, U. Rao, M. Dudley, N. D. Ebrahimi, J. Lou, F. Han, E. M. V. Hoek, N. Tilton, T. Y. Cath, C. S. Turchi, M. B. Heeley, Y. S. Ju, D. Jassby, *J. Membr. Sci.*, **2021**, *626,* 119188. DOI: https://doi.org/10.1016/j.memsci.2021.119188
[147] G. Guan, C. Yao, S. Lu, Y. Jiang, H. Yu, X. Yang, *Desalination*, **2018**, *445,* 123-137. DOI: https://doi.org/10.1016/j.desal.2018.07.031
[148] M. Zhang, Q. Yang, M. Gao, N. Zhou, J. Shi, W. Jiang, *Journal of Environmental Chemical Engineering*, **2021**, 106016.
[149] M. Afsari, H. K. Shon, L. D. Tijing, *Adv. Colloid Interface Sci.*, **2021**, *289,* 102362. DOI: https://doi.org/10.1016/j.cis.2021.102362

[150] M. Tang, L. Zheng, D. Hou, X. Jia, J. Wang, *Chem. Eng. J.*, **2022**, *430,* 132973.
[151] H. Yang, Q. Liu, X. Shu, H. Yu, H. Rong, F. Qu, H. Liang, *Water Res*, **2023**, *240,* 120080.
[152] M. E. Ersahin, B. Cicekalan, A. I. Cengiz, X. Zhang, H. Ozgun, *J Environ Manage*, **2023**, *335,* 117518.
[153] Z. Yan, Y. Jiang, X. Chen, Z. Lu, Z. Wei, G. Fan, H. Liang, F. Qu, *Desalination*, **2021**, *520,* 115358.
[154] M. T. T. Ngo, X.-T. Bui, T.-K.-Q. Vo, P. V. M. Doan, H. N. M. Nguyen, T. H. Nguyen, T.-L. Ha, H.-V. Nguyen, T.-D.-H. Vo, *Current Pollution Reports*, **2023**, 1-19.
[155] N. A. Oz, C. C. Yarimtepe, *Waste Manage. (Oxford)*, **2014**, *34 (7),* 1165-1170.
[156] T. M. Martin, F. Esculier, F. Levavasseur, S. Houot, *Crit. Rev. Environ. Sci. Technol.*, **2022**, *52 (6),* 890-936.
[157] J. Zhang, M. Xie, X. Tong, D. Yang, S. Liu, D. Qu, L. Feng, L. Zhang, *Sci Total Environ*, **2021**, *768,* 144478.
[158] L. L. Tun, D. Jeong, S. Jeong, K. Cho, S. Lee, H. Bae, *J. Membr. Sci.*, **2016**, *512,* 13-20.
[159] P. Kuntke, K. M. Śmiech, H. Bruning, G. Zeeman, M. Saakes, T. H. J. A. Sleutels, H. V. M. Hamelers, C. J. N. Buisman, *Water Res*, **2012**, *46 (8),* 2627-2636. DOI: https://doi.org/10.1016/j.watres.2012.02.025
[160] A. Almuntashiri, A. Hosseinzadeh, F. Volpin, S. M. Ali, U. Dorji, H. Shon, S. Phuntsho, *Chemosphere*, **2021**, *280,* 130870. DOI: https://doi.org/10.1016/j.chemosphere.2021.130870
[161] L. Meng, W. Shi, Y. Li, X. Li, X. Tong, Z. Wang, *Adv. Colloid Interface Sci.*, **2023**, 102937.
[162] Q. Liu, C. Liu, L. Zhao, W. Ma, H. Liu, J. Ma, *Water Res*, **2016**, *91,* 45-54.
[163] Z.-P. Zhao, L. Xu, X. Shang, K. Chen, *Sep. Purif. Technol.*, **2013**, *118,* 369-376.
[164] L. D. Tijing, M. Yao, J. Ren, C.-H. Park, C. S. Kim, H. K. Shon, in *Water and Wastewater Treatment Technologies*, **2019**, 431-468.
[165] A. Hosseinzadeh, J. L. Zhou, A. H. Navidpour, A. Altaee, *Bioresour. Technol.*, **2021**, *330,* 124998. DOI: https://doi.org/10.1016/j.biortech.2021.124998
[166] M. Afsari, H. K. Shon, L. D. Tijing, *Adv. Colloid Interface Sci.*, **2021**, 102362. DOI: https://doi.org/10.1016/j.cis.2021.102362
[167] M. Yao, J. Ren, N. Akther, Y. C. Woo, L. D. Tijing, S.-H. Kim, H. K. Shon, *Chemosphere*, **2019**, *230,* 117-126. DOI: https://doi.org/10.1016/j.chemosphere.2019.05.049
[168] M. Asghari, M. Raji, *Journal of Modeling in Engineering*, **2018**, *16 (55),* 41-49.
[169] S. G. Lovineh, M. Asghari, B. Rajaei, *Desalination*, **2013**, *314,* 59-66. DOI: https://doi.org/10.1016/j.desal.2013.01.005
[170] A. Hosseinzadeh, J. L. Zhou, A. Altaee, D. Li, *Bioresour. Technol.*, **2022**, *343,* 126111. DOI: https://doi.org/10.1016/j.biortech.2021.126111
[171] A. Ali, C. A. Quist-Jensen, F. Macedonio, E. Drioli, *Chemical Engineering and Processing: Process Intensification*, **2016**, *110,* 188-200.
[172] A. Deshmukh, C. Boo, V. Karanikola, S. Lin, A. P. Straub, T. Tong, D. M. Warsinger, M. Elimelech, *Energy Environ. Sci.*, **2018**, *11 (5),* 1177-1196.
[173] A. Anvari, A. A. Yancheshme, K. M. Kekre, A. Ronen, *J. Membr. Sci.*, **2020**, 118413.
[174] D. J. Park, E. Norouzi, C. Park, *Int. J. Heat Mass Transfer*, **2019**, *129,* 1031-1042.
[175] V. Perfilov, A. Ali, V. Fila, *Desalination*, **2018**, *445,* 181-196.

[176] A. Esfandiari, A. H. Monjezi, M. Rezakazemi, M. Younas, *Appl. Therm. Eng.*, **2019***, 163,* 114391.
[177] L. Ding, P. Radfar, M. Rezaei, M. E. Warkiani, *Microchimica Acta*, **2021***, 188 (8),* 242. DOI: 10.1007/s00604-021-04897-9
[178] J. Lou, J. Vanneste, S. C. DeCaluwe, T. Y. Cath, N. Tilton, *J. Membr. Sci.*, **2019***, 591,* 117150.
[179] I. Hitsov, T. Maere, K. De Sitter, C. Dotremont, I. Nopens, *Sep. Purif. Technol.*, **2015***, 142,* 48-64. DOI: https://doi.org/10.1016/j.seppur.2014.12.026
[180] W. Ni, Y. Li, J. Zhao, G. Zhang, X. Du, Y. Dong, *Membranes*, **2020***, 10 (8)*. DOI: 10.3390/membranes10080179
[181] S. Al-Sharif, M. Albeirutty, A. Cipollina, G. Micale, *Desalination*, **2013***, 311,* 103-112.
[182] H. Chang, C.-D. Ho, J.-A. Hsu, *Journal of Applied Science and Engineering*, **2016***, 19 (2),* 197-206.
[183] H. Chang, J.-A. Hsu, C.-L. Chang, C.-D. Ho, T.-W. Cheng, *ApEn*, **2017***, 185,* 2045-2057.
[184] M. S. Salem, A. H. El-shazly, N. Nady, M. R. Elmarghany, M. A. Shouman, M. N. Sabry, *Case Studies in Thermal Engineering*, **2019***, 13,* 100396.
[185] Y. Taamneh, K. Bataineh, *Desalination*, **2017***, 408,* 25-35.
[186] I. Janajreh, M. N. Hussain, R. Hashaikeh, R. Ahmed, *ApEn*, **2018***, 227,* 7-17.
[187] H. Yu, X. Yang, R. Wang, A. G. Fane, *J. Membr. Sci.*, **2011***, 384 (1-2),* 107-116.
[188] M. Ghadiri, S. Fakhri, S. Shirazian, *Polymer Engineering & Science*, **2014***, 54 (3),* 660-666.
[189] B. S. Lalia, I. Janajreh, R. Hashaikeh, *J. Membr. Sci.*, **2017***, 539,* 144-151.
[190] H. Hayer, O. Bakhtiari, T. Mohammadi, *Journal of Industrial and Engineering Chemistry*, **2015***, 21,* 1379-1382.
[191] N. Loussif, J. Orfi, *Membr. Water Treat*, **2016***, 7 (1),* 71-86.
[192] J. Seo, Y. M. Kim, J. H. Kim, *Desalination*, **2017***, 417,* 9-18.
[193] S. Soukane, M. W. Naceur, L. Francis, A. Alsaadi, N. Ghaffour, *Desalination*, **2017***, 418,* 43-59.
[194] R. Schofield, A. Fane, C. Fell, *J. Membr. Sci.*, **1990***, 53 (1-2),* 159-171.
[195] J. Phattaranawik, R. Jiraratananon, A. G. Fane, *J. Membr. Sci.*, **2003***, 215 (1),* 75-85. DOI: https://doi.org/10.1016/S0376-7388(02)00603-8
[196] H. L. Chiang, P. C. Chiang, Y. C. Chiang, E. E. Chang, *Chemosphere*, **1999***, 38 (12),* 2733-2746. DOI: https://doi.org/10.1016/S0045-6535(98)00475-5
[197] M. R. S. Kebria, A. Rahimpour, in *Advances in membrane technologies*, IntechOpen, **2020**.
[198] J. Phattaranawik, R. Jiraratananon, A. G. Fane, *J. Membr. Sci.*, **2003***, 212 (1),* 177-193. DOI: https://doi.org/10.1016/S0376-7388(02)00498-2
[199] F. Y. Huang, R. Reprogle, *Environ. Eng. Sci.*, **2019***, 36 (4),* 420-430.
[200] H. B. Harandi, A. Asadi, H. Fathi, P.-C. Sui, *Desalination*, **2021***, 514,* 115171.
[201] S. S. Ibrahim, Q. F. Alsalhy, *AlChE J.*, https://doi.org/10.1002/aic.13845, **2013***, 59 (2),* 589-603. DOI: https://doi.org/10.1002/aic.13845
[202] L. G. Leal, *Advanced transport phenomena: fluid mechanics and convective transport processes*, Cambridge University Press, **2007**.
[203] T. L. Bergman, F. P. Incropera, D. P. DeWitt, A. S. Lavine, *Fundamentals of heat and mass transfer*, John Wiley & Sons, **2011**.

[204] A. Muhammad, M. Younas, M. Rezakazemi, *Chem. Eng. Res. Des.*, **2017**, *127,* 52-61. DOI: https://doi.org/10.1016/j.cherd.2017.09.007
[205] M. Jafarizave, A. Khaleghi, M. Rezakazemi, *Chem. Eng. Res. Des.*, **2019**, *145,* 226-234. DOI: https://doi.org/10.1016/j.cherd.2019.03.019
[206] M. Ahmadlou, M. Rezakazemi, *Journal of Porous Media*, **2018**, *21 (6)*.
[207] J. Lou, Colorado School of Mines **2020**.
[208] S. Al-Obaidani, E. Curcio, F. Macedonio, G. Di Profio, H. Al-Hinai, E. Drioli, *J. Membr. Sci.*, **2008**, *323 (1),* 85-98. DOI: https://doi.org/10.1016/j.memsci.2008.06.006
[209] G. Guan, H. Lou, C. Yao, J. Li, X. Yang, *Desalination*, **2021**, *499,* 114833. DOI: https://doi.org/10.1016/j.desal.2020.114833
[210] J. A. Sanmartino, M. Khayet, M. C. García-Payo, in *Emerging Membrane Technology for Sustainable Water Treatment*, (Eds: N. P. Hankins, R. Singh), Elsevier, Boston, **2016**, 77-109.
[211] D. Winter, J. Koschikowski, M. Wieghaus, *J. Membr. Sci.*, **2011**, *375 (1),* 104-112. DOI: https://doi.org/10.1016/j.memsci.2011.03.030
[212] N. Tang, H. Zhang, W. Wang, *Desalination*, **2011**, *274 (1-3),* 120-129.
[213] A. Ali, C. Quist-Jensen, F. Macedonio, E. Drioli, *Journal of Membrane Science and Research*, **2016**, *2 (4),* 179-185.
[214] H. Y. Wu, R. Wang, R. W. Field, *J. Membr. Sci.*, **2014**, *470,* 257-265. DOI: https://doi.org/10.1016/j.memsci.2014.06.002
[215] L. Martinez, J. M. Rodriguez-Maroto, *J. Membr. Sci.*, **2008**, *312 (1-2),* 143-156.
[216] L. Eykens, T. Reyns, K. De Sitter, C. Dotremont, L. Pinoy, B. Van der Bruggen, *Desalination*, **2016**, *399,* 105-115.
[217] M. Essalhi, M. Khayet, *J. Membr. Sci.*, **2013**, *433,* 180-191.
[218] A. A. Najafpoor, S. Dousti, A. Joneidi Jafari, A. Hosseinzadeh, *Environmental Health Engineering and Management Journal*, **2016**, *3 (1),* 41-46.
[219] R. Ullah, M. Khraisheh, R. J. Esteves, J. T. McLeskey Jr, M. AlGhouti, M. Gad-el-Hak, H. V. Tafreshi, *Desalination*, **2018**, *433,* 56-67.
[220] M. M. A. Shirazi, A. Kargari, A. F. Ismail, T. Matsuura, *Desalination*, **2016**, *377,* 73-90.
[221] M. Khayet, *Adv. Colloid Interface Sci.*, **2011**, *164 (1-2),* 56-88.
[222] L. Eykens, K. De Sitter, C. Dotremont, L. Pinoy, B. Van der Bruggen, *Sep. Purif. Technol.*, **2017**, *182,* 36-51.
[223] L. Francis, F. E. Ahmed, N. Hilal, *Desalination*, **2022**, *526,* 115511. DOI: https://doi.org/10.1016/j.desal.2021.115511
[224] C.-Y. Pan, G.-R. Xu, K. Xu, H.-L. Zhao, Y.-Q. Wu, H.-C. Su, J.-M. Xu, R. Das, *Sep. Purif. Technol.*, **2019**, *221,* 44-63.
[225] M. Essalhi, M. Khayet, *J. Membr. Sci.*, **2013**, *433,* 167-179.
[226] Y. Si, C. Sun, D. Li, F. Yang, C. Y. Tang, X. Quan, Y. Dong, M. D. Guiver, *Environ. Sci. Technol.*, **2020**, *54 (14),* 9074-9082.
[227] C. Sun, Q. Lyu, Y. Si, T. Tong, L.-C. Lin, F. Yang, C. Y. Tang, Y. Dong, *Environ. Sci. Technol.*, **2022**, *56 (9),* 5775-5785.
[228] Y. Dong, L. Ma, C. Y. Tang, F. Yang, X. Quan, D. Jassby, M. J. Zaworotko, M. D. Guiver, *Nano Lett.*, **2018**, *18 (9),* 5514-5521.
[229] M. M. A. Shirazi, S. Bazgir, F. Meshkani, *Chem. Eng. Res. Des.*, **2020**, *164,* 125-146.

[230] H. Sanaeepur, A. E. Amooghin, M. M. A. Shirazi, M. Pishnamazi, S. Shirazian, *Desalination*, **2022**, *521,* 115350.
[231] M. Yao, Y. C. Woo, L. D. Tijing, W.-G. Shim, J.-S. Choi, S.-H. Kim, H. K. Shon, *Desalination*, **2016**, *378,* 80-91.
[232] M. Khayet, A. Velázquez, J. I. Mengual, *J. Membr. Sci.*, **2004**, *240 (1),* 123-128. DOI: https://doi.org/10.1016/j.memsci.2004.04.018
[233] J. Phattaranawik, R. Jiraratananon, A. Fane, *J. Membr. Sci.*, **2003**, *215 (1-2),* 75-85.
[234] M. Fouladivanda, J. Karimi-Sabet, F. Abbasi, M. A. Moosavian, *Sep. Purif. Technol.*, **2021**, *256,* 117809.
[235] P. Nuamcharoen, T. Kobayashi, P. Potiyaraj, *Polym. Int.*, **2021**, *70 (10),* 1465-1477.
[236] M. Qasim, I. U. Samad, N. A. Darwish, N. Hilal, *Desalination*, **2021**, *518,* 115168.
[237] J. Cui, F. Li, Y. Wang, Q. Zhang, W. Ma, C. Huang, *Sep. Purif. Technol.*, **2020**, *250,* 117116.
[238] M. Toriello, M. Afsari, H. K. Shon, L. D. Tijing, *Membranes*, **2020**, *10 (9),* 204.
[239] A. Anvari, A. Azimi Yancheshme, K. M. Kekre, A. Ronen, *J. Membr. Sci.*, **2020**, *616*. DOI: 10.1016/j.memsci.2020.118413
[240] R. Li, H. Fan, L. Shen, L. Rao, J. Tang, S. Hu, H. Lin, *Chemosphere*, **2020**, *250,* 126236.
[241] L. Rao, J. Tang, S. Hu, L. Shen, Y. Xu, R. Li, H. Lin, *J. Colloid Interface Sci.*, **2020**, *565,* 546-554.
[242] Z. Wang, Y. Nagao, *Electrochim. Acta*, **2014**, *129,* 343-347.
[243] Y. Zhang, T. Ren, J. He, *ACS applied materials & interfaces*, **2018**, *10 (13),* 11343-11349.
[244] M. J. Park, C. Wang, D. H. Seo, R. R. Gonzales, H. Matsuyama, H. K. Shon, *J. Membr. Sci.*, **2021**, *620,* 118901.
[245] C. Wang, M. J. Park, D. H. Seo, H. K. Shon, *Sep. Purif. Technol.*, **2021**, *254,* 117604.
[246] T. Bao, M. M. Damtie, W. Wei, H. N. P. Vo, K. H. Nguyen, A. Hosseinzadeh, K. Cho, Z. M. Yu, J. Jin, X. L. Wei, *Journal of Cleaner Production*, **2021**, *287,* 125068.
[247] X. Li, H. Shan, M. Cao, B. Li, *J. Membr. Sci.*, **2019**, *589,* 117262.
[248] Y. Xu, Y. Yang, X. Fan, Z. Liu, Y. Song, Y. Wang, P. Tao, C. Song, M. Shao, *Desalination*, **2021**, *499,* 114832. DOI: https://doi.org/10.1016/j.desal.2020.114832
[249] M. Han, T. Dong, D. Hou, J. Yao, L. Han, *J. Membr. Sci.*, **2020**, 118078.
[250] J. Chen, J. Li, H. Jiang, J. Yu, H. Wang, N. Wang, S. Chen, W. Mo, P. Wang, R. L. Tanguay, *Ecotoxicol. Environ. Saf.*, **2021**, *215,* 112176.
[251] H. J. Dyson, P. E. Wright, H. A. Scheraga, *Proceedings of the National Academy of Sciences*, **2006**, *103 (35),* 13057-13061.
[252] J. A. Howarter, K. L. Genson, J. P. Youngblood, *ACS applied materials & interfaces*, **2011**, *3 (6),* 2022-2030.
[253] X. Zhu, H.-E. Loo, R. Bai, *J. Membr. Sci.*, **2013**, *436,* 47-56.
[254] M. Yao, Y. C. Woo, L. D. Tijing, C. Cesarini, H. K. Shon, *Applied Sciences*, **2017**, *7 (1),* 78.
[255] D. Feng, Y. Chen, Z. Wang, S. Lin, *Environ. Sci. Technol.*, **2021**, *55 (20),* 14156-14164.

[256] S. Guida, L. Van Peteghem, B. Luqmani, M. Sakarika, A. McLeod, E. J. McAdam, B. Jefferson, K. Rabaey, A. Soares, *Chem. Eng. J.*, **2022**, *427,* 130896. DOI: https://doi.org/10.1016/j.cej.2021.130896
[257] Á. Robles, D. Aguado, R. Barat, L. Borrás, A. Bouzas, J. B. Giménez, N. Martí, J. Ribes, M. V. Ruano, J. Serralta, *Bioresour. Technol.*, **2020**, *300,* 122673.
[258] T. Yan, Y. Ye, H. Ma, Y. Zhang, W. Guo, B. Du, Q. Wei, D. Wei, H. H. Ngo, *Chem. Eng. J.*, **2018**, *348,* 143-156.
[259] L. Wooram, A. Seonyoung, C. Yongju, *Chem. Eng. J.*, **2021**, *405,* 126662. DOI: https://doi.org/10.1016/j.cej.2020.126662
[260] J. Ren, D. Hao, J. Jiang, S. Phuntsho, S. Freguia, B.-J. Ni, P. Dai, J. Guan, H. K. Shon, *Water Res*, **2021**, *207,* 117810.
[261] *Dewatering of source-separated human urine for nitrogen and water recovery using air gap membrane distillation (AGMD)*.
[262] A. N. Petukhov, A. A. Atlaskin, S. S. Kryuchkov, K. A. Smorodin, D. M. Zarubin, A. N. Petukhova, M. E. Atlaskina, A. V. Nyuchev, A. V. Vorotyntsev, M. M. Trubyanov, I. V. Vorotyntsev, V. M. Vorotynstev, *Chem. Eng. J.*, **2021**, *421,* 127726. DOI: https://doi.org/10.1016/j.cej.2020.127726
[263] M. Asghari, M. Afsari, *Journal of Membrane Science and Research*, **2018**, *4 (1),* 34-40.
[264] M. Yao, Y. C. Woo, L. D. Tijing, J.-S. Choi, H. K. Shon, *Desalination*, **2018**, *440,* 146-155. DOI: https://doi.org/10.1016/j.desal.2017.11.012
[265] K. Xu, D. Qu, M. Zheng, X. Guo, C. Wang, *J. Environ. Eng.*, **2019**, *145 (3),* 04018144.
[266] F. Volpin, J. Jiang, I. El Saliby, M. Preire, S. Lim, M. A. H. Johir, J. Cho, D. S. Han, S. Phuntsho, H. K. Shon, *Journal of Cleaner Production*, **2020**, *270,* 122390.
[267] S. Kartohardjono, G. M. Damaiati, C. T. Rama, *Journal of Environmental Science and Technology*, **2015**, *8 (5),* 225.
[268] E. E. Licon Bernal, A. Alcaraz, S. Casas, C. Valderrama, J. L. Cortina, *J. Chem. Technol. Biotechnol.*, **2016**, *91 (12),* 2983-2993.
[269] C.-L. Lai, S.-h. Chen, R.-M. Liou, *Desalination and Water Treatment*, **2013**, *51 (25-27),* 5307-5310.
[270] J. Zhang, M. Xie, X. Tong, S. Liu, D. Qu, S. Xiao, *Sep. Purif. Technol.*, **2020**, *239,* 116579.
[271] M. M. Damtie, F. Volpin, M. Yao, L. D. Tijing, R. H. Hailemariam, T. Bao, K.-D. Park, H. K. Shon, J.-S. Choi, *Environmental Engineering Research*, **2020**.
[272] M. Fillingham, A. C. VanderZaag, J. Singh, S. Burtt, A. Crolla, C. Kinsley, J. D. MacDonald, *Membranes*, **2017**, *7 (4),* 59.
[273] M. Xiao, Y. Shang, L. Ji, M. Yan, F. Chen, Q. He, S. Yan, *Membranes*, **2022**, *12 (11),* 1164.
[274] M. Shi, M. Xiao, L. Feng, T. Tu, Q. He, S. Yan, *Journal of Water Process Engineering*, **2022**, *49,* 102949.
[275] D. Qu, D. Sun, H. Wang, Y. Yun, *Desalination*, **2013**, *326,* 135-140.
[276] N. Coote, B. Kirsop, *Journal of the Institute of Brewing*, **1976**, *82 (3),* 149-153.
[277] Z. Ding, L. Liu, Z. Li, R. Ma, Z. Yang, *J. Membr. Sci.*, **2006**, *286 (1-2),* 93-103.
[278] M. Fillingham, A. VanderZaag, J. Singh, S. Burtt, A. Crolla, C. Kinsley, J. D. MacDonald, *Membranes*, **2017**, *7 (4),* 59.
[279] S. N. McCartney, N. A. Williams, C. Boo, X. Chen, N. Y. Yip, *ACS Sustainable Chemistry & Engineering*, **2020**, *8 (19),* 7324-7334.

[280] Z. Xie, T. Duong, M. Hoang, C. Nguyen, B. Bolto, *Water Res*, **2009**, *43 (6),* 1693-1699.
[281] C. Yu, W. Yin, Z. Yu, J. Chen, R. Huang, X. Zhou, *RSC advances*, **2021**, *11 (56),* 35525-35535.
[282] A. Almuntashiri, A. Hosseinzadeh, U. Badeti, H. Shon, S. Freguia, U. Dorji, S. Phuntsho, *Journal of Water Process Engineering*, **2022**, *45,* 102480. DOI: https://doi.org/10.1016/j.jwpe.2021.102480
[283] A. Hasanoğlu, J. Romero, B. Pérez, A. Plaza, *Chem. Eng. J.*, **2010**, *160 (2),* 530-537.
[284] M. J. Semmens, D. Foster, E. Cussler, *J. Membr. Sci.*, **1990**, *51 (1-2),* 127-140.
[285] P. Jacob, P. Phungsai, K. Fukushi, C. Visvanathan, *J. Membr. Sci.*, **2015**, *475,* 330-339.
[286] Y. Ahn, Y.-H. Hwang, H.-S. Shin, *Water Sci Technol*, **2011**, *63 (12),* 2944-2948.
[287] G. Simoni, B. S. Kirkebæk, C. A. Quist-Jensen, M. L. Christensen, A. Ali, *Journal of Water Process Engineering*, **2021**, *44,* 102350.
[288] K. M. Udert, M. Wächter, *Water Res*, **2012**, *46 (2),* 453-464. DOI: https://doi.org/10.1016/j.watres.2011.11.020
[289] G. Hulton, W. H. Organization. Global costs and benefits of drinking-water supply and sanitation interventions to reach the MDG target and universal coverage, World Health Organization, 2012.
[290] L. Bo-Bertil, B. Zsófia, B. Stefan, *Ecol. Eng.*, **2001**, *16 (4),* 561-566. DOI: https://doi.org/10.1016/S0925-8574(00)00107-5
[291] F. Imke, H. H. Hermann, *Water Sci Technol*, **1998**, *38 (6),* 9-16. DOI: https://doi.org/10.1016/S0273-1223(98)00562-9
[292] J. L. Cartinella, T. Y. Cath, M. T. Flynn, G. C. Miller, K. W. Hunter, A. E. Childress, *Environ. Sci. Technol.*, **2006**, *40 (23),* 7381-7386. DOI: 10.1021/es060550i
[293] G. A. Ekama, J. A. Wilsenach, G. H. Chen, *Water Sci Technol*, **2011**, *64 (6),* 1307-1316. DOI: 10.2166/wst.2011.403
[294] M. N. Chong, A. K. Sharma, S. Burn, C. P. Saint, *Journal of Cleaner Production*, **2012**, *35,* 230-238. DOI: https://doi.org/10.1016/j.jclepro.2012.06.003
[295] E. Tilley, *Compendium of sanitation systems and technologies*, Eawag, **2014**.
[296] Z. Li, B. Cheng, J. Ju, W. Kang, Y. Liu, *Desalination*, **2021**, *501,* 114834. DOI: https://doi.org/10.1016/j.desal.2020.114834
[297] C. Wang, M. J. Park, R. R. Gonzales, H. Matsuyama, E. Drioli, H. K. Shon, *Desalination*, **2023**, *549,* 116357. DOI: https://doi.org/10.1016/j.desal.2022.116357
[298] Y. Dong, X. Dai, L. Zhao, L. Gao, Z. Xie, J. Zhang, *Membranes*, **2021**, *11 (2),* 122.
[299] A. Ananth, G. Arthanareeswaran, H. Wang, *Desalination*, **2012**, *287,* 61-70.
[300] M. M. Damtie, F. Volpin, M. Yao, L. D. Tijing, R. H. Hailemariam, T. Bao, K. D. Park, H. K. Shon, J. S. Choi, *Environmental Engineering Research*, **2020**, *26*. DOI: 10.4491/eer.2019.523
[301] F. Kamranvand, C. Davey, H. Sakar, O. Autin, E. Mercer, M. Collins, L. Williams, A. Kolios, A. Parker, S. Tyrrel, *Sep. Sci. Technol.*, **2018**, *53 (9),* 1372-1382.
[302] A. Ramos, C. A. Teixeira, A. Rouboa, *Energies*, **2019**, *12 (1)*. DOI: 10.3390/en12010137